

AD-A102 794

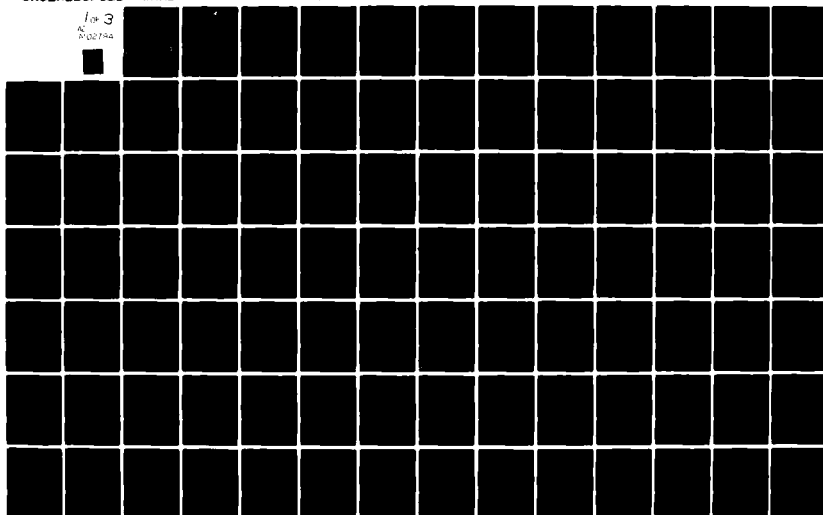
WESTINGHOUSE ELECTRIC CORP MADISON PA ADVANCED REACT--ETC F/6 13/13
EVALUATION OF THE STA0SC-1 SHELL ANALYSIS COMPUTER PROGRAM.(U)
AUG 81 K THOMAS, L H SOBEL
WARD-10881

N00014-79-C-0825

NL

UNCLASSIFIED

1 of 3
D-02794



LEVEL

(12)

Report No. WARD-10881

EVALUATION OF THE STAGSC-1 SHELL ANALYSIS COMPUTER PROGRAM

AD A102794

**Kevin Thomas
L. H. Sobel**

**Westinghouse Electric Corporation
Advanced Reactors Division
P.O. Box 158, Madison, PA 15663**

August 1981

**DTIC
SELECTED
AUG 11 1981**

DTIC FILE COPY

**Prepared for
Office of Naval Research
Department of the Navy**

Contract N00014-79-C-0825

DISTRIBUTION STATEMENT A
Approved for public release;
Distribution Unlimited

81 8 11 018

Report No. WARD-10881

EVALUATION OF THE SIAGSC-1
SHELL ANALYSIS COMPUTER PROGRAM

Final report of 77-12 511 81

10

Kevin Thomas
~~Person Engineer~~

L. H. Sobel
Fellow Engineer

Westinghouse Electric Corporation
Advanced Reactors Division
P.O. Box 158, Madison, PA 15663

11

Aug 1981

DTIC
ELECTE

1981 1981

12 269

Prepared for
Office of Naval Research
Department of the Navy

15
Contract N00014-79-C-0825

391-11

STAGSC-1 EVALUATION REPORT

TABLE OF CONTENTS

	<u>Page</u>
1.0 INTRODUCTION	1
2.0 STAGS DOCUMENTATION	5
3.0 PROGRAM ARCHITECTURE	19
4.0 FUNCTIONAL DESCRIPTION	36
4.1 Analysis Options	36
4.2 Surface and Mesh Geometry	41
4.3 Finite Element Library	43
4.4 Constitutive Relationships	45
4.5 Linear and Non-Linear Analysis	46
4.6 Solution of Equations	49
4.7 Eigenvalue Analysis	50
4.8 Transient Integration	52
4.9 User Coded Subroutines	54
4.10 Restart Capability	55
4.11 Input and Output	56
4.12 Post-Processing and Plotting	58
4.13 Special STAGS Features	59
5.0 VERIFICATION EXERCISES	72
6.0 ADVANCED EVALUATION	79
6.1 Element Convergence	79
6.2 Eigensolution Performance	88
6.3 Transient Integration Performance	94
6.4 Non-Linear Collapse Analysis	101
6.5 Program Efficiency	116
7.0 OVERALL CONCLUSIONS AND RECOMMENDATIONS	195
8.0 REFERENCES	207
9.0 APPENDIX	211

09178-848:2
(S3034) 1

Accession For	
NTIS GRA&I	<input checked="" type="checkbox"/>
DTIC TAB	<input type="checkbox"/>
Unannounced	<input type="checkbox"/>
Justification	
By _____	
Distribution/	
Availability Codes	
Dist	Avail and/or Special
A	

LIST OF FIGURES

<u>Figure</u>	<u>Title</u>	<u>Page</u>
3.1	Primary Overlay Structure of STAGS1	32
3.2	Secondary Overlay Structure of STAGS1	33
3.3	Primary Overlay Structure of STAGS2	34
3.4	Secondary Overlays in STAGS2	35
4.1 (a)	Linear Pre-buckling	68
4.1 (b)	Nonlinear Pre-buckling -- Softening	68
4.1 (c)	Nonlinear Pre-buckling -- Stiffening	68
4.2	Nonlinear Solution Procedure	69
4.3	Subspace Iteration Algorithm	70
4.4	Time Integration Methods	71
5.1	Shallow Arch Problem	74
5.2	Shallow Arch Problem -- Results	75
5.3	Buckling of an Anisotropic Plate	76
5.4	Circular Ring with Initial Velocity	77
5.5	Ring with Initial Velocity -- Results	78
6.1	Simply Supported Cylindrical Roof -- Gravity Load	142
6.2	Cylindrical Shell Roof -- Element Convergence (1)	143
6.3	Cylindrical Shell Roof -- Element Convergence (2)	144
6.4	Flat Plate Problem	145
6.5	Flat Plate with Clamped Edges -- Roark Solution	146
6.6	Flat Plate with Clamped Edges Under Uniform Pressure Loading -- Linear Element Convergence	147
6.7	Flat Plate with Clamped Edges Under Uniform Pressure -- Nonlinear Solution	148

LIST OF FIGURES (Continued)

Figure	Title	Page
6.8	Flat Plate with Clamped Edges Under Uniform Pressure -- Nonlinear Element Convergence	149
6.9	Flat Plate with Clamped Edges Under Uniform Pressure -- Percent Error in Nonlinear Solution	150
6.10	Single Element Load Cases	151
6.11	Nodal Forces for Single Element Load Cases	152
6.12 (a)	Stiffness Eigenmodes -- QUAF410	153
6.12 (b)		154
6.12 (c)		155
6.13	3-D Beam Model for Modal Analysis	156
6.14	Flat Plate Cantilever	157
6.15	Flat Cantilever Plate Vibrations	158
6.16	Simply Supported Cylinder	159
6.17	Simply Supported Cylinder Flexural Vibration Modes	160
6.18	1/8 Cylinder Model -- Mode Shapes - 16 x 4 Mesh	161
6.19	1/2 Cylinder Model -- Mode Shapes (1)	162
6.20	1/2 Cylinder Model -- Mode Shapes (2)	163
6.21	1/2 Cylinder Model -- Mode Shapes (3)	164
6.22	1/2 Cylinder Model -- Mode Shapes (4)	165
6.23	Cantilever Beam -- Pressure Pulse	166
6.24	Cantilever Plate Under Transient Pressure Loading -- Tip Displacement History	167
6.25	Cantilever Plate Under Transient Pressure Loading -- Tip Velocity History	168
6.26	Impulsively Loaded Ring	169

LIST OF FIGURES (Continued)

<u>Figure</u>	<u>Title</u>	<u>Page</u>
6.27	Impulsively Loaded Ring -- Nonlinear Elastic Plastic Response -- Deflection	170
6.28	Impulsively Loaded Ring -- Nonlinear Elastic Plastic Response -- Circumferential Strain	171
6.29	Impulsively Loaded Ring -- Deformed Shape at about 0.0008 Seconds	172
6.30	Impulsively Loaded Ring -- Rotation at 0.0010 Seconds	173
6.31	Impulsively Loaded Ring -- Nonlinear Elastic Response -- Park Operator	174
6.32	Impulsively Loaded Ring -- Nonlinear Elastic Response -- Trapezoidal Operator	175
6.33	Impulsively Loaded Ring -- Nonlinear Elastic Response -- Gear's Operator	176
6.34	Comparison of Load-Displacement Results for the Venetian Blind	177
6.35	Comparison of Load-Displacement Results for the Pinched Cylinder	178
6.36	Hoop Variation of Radial Displacement at Midlength. Linear Results for Poked Cylinder. $R/t = 638$, $L/R = .892$	179
6.37	Hoop Variation of Hoop Bending Moment at $x = 3.5" \approx (1/40)(L/2)$. Linear Results for Poked Cylinder. $R/t = 638$, $L/R = .892$	180
6.38	Axial Variation of Radial Displacement Along the Loaded Generator. Linear Results for Poked Cylinder. $R/t = 638$, $L/R = .892$	181
6.39	Axial Variation of Hoop Bending Moment Along $\phi = 1/2^\circ$. Linear Results for Poked Cylinder. $R/t = 638$, $L/R = .892$	182
6.40	Load-Displacement Results for Poked Cylinder	183-184

LIST OF FIGURES (Continued)

Figure	Title	Page
6.41	Initially Compressive Membrane Forces Near Load ($x = 3.5"$, $\phi = 1/2^\circ$) Become Tensile Due to Geometry Changes. Poked Cylinder	185
6.42	Hoop Variation at Midlength of Radial Displacement at Collapse. Poked Cylinder	186
6.43	Hoop Variation Along $x = 3.5"$ of Hoop Bending Moment at Collapse. Poked Cylinder	187
6.44	Axial Variation Along Loaded Generator of Radial Displacement at Collapse. Poked Cylinder	188
6.45	Axial Variation Along $\phi = 1/2^\circ$ of Hoop Bending Moment at Collapse. Poked Cylinder	189
6.46	Hoop Variation Along $x = 3.5"$ of Change in Hoop Curvature at Collapse. Poked Cylinder	190
6.47	Load vs. Change in Hoop Curvature at $x = 3.5"$, $\phi = 22.95"$. Poked Cylinder	191
6.48	Progressive Deformation of Scaled Down Model Under Increasing Load. Poked Cylinder	192-193
6.49	Comparison of Three Solutions for Region I of Figure 6.40. Poked Cylinder	194
9.1	Main Pre-processing Program	216
9.2	User Subroutine Loader	217
9.3	Main Pre-processing Program	218
9.4	Shell Unit Generation Overlay	219
9.5	Element Table Generation	220
9.6	Node Table Generation	221
9.7	Element Unit Generation	222
9.8	Model Input Summary	223
9.9	Element Stiffness Pre-processor	224

LIST OF FIGURES (Continued)

<u>Figure</u>	<u>Title</u>	<u>Page</u>
9.10	Beam Element Overlay	225
9.11	Formulation and Update of Constitutive Matrices	226
9.12	Quadrilateral Plate Element Generation	227
9.13	Nodal Coordinates and Integration Points	228
9.14	Triangular Plate Element Generation	229
9.15	Data Base Preservation Overlay	230
9.16	Shell Unit Intersection Overlay	231
9.17	Shell Unit Loads Overlay	232
9.18	Element Unit Loads Overlay	233
9.19	Main Execution Program	234
9.20	User Subroutine Loader	235
9.21	STAGS2 Data Statements	236
9.22	Data Transfer from STAGS1	237
9.23	Analysis Restart Control	238
9.24	Stiffness Matrix Decomposition	239
9.25	Eigenvalue Solver	240
9.26	Eigensolution for Subspace	241
9.27	Stiffness Matrix Formulation	242
9.28	Element Stiffness Data	243
9.29	Element Stiffness Computation	244
9.30	Overlay for 1st Variation of Strain Energy	245
9.31	1st Variation of Strain Energy	246
9.32	Plasticity Overlay	247

LIST OF FIGURES (Continued)

Figure	Title	Page
9.33	Dynamic Response Overlay	248
9.34	General Ordinary Differential Equation Solver	249
9.35	Plasticity Overlay (Dynamic)	250
9.36	Overlay for Solution Strategy and Output Control	251
9.37	Overlay for Stress Computation and Output	252
9.38	Overlay for Stress and Strain Computation -- 1D Elements	253
9.39	Overlay for Stress and Strain Computation -- 2D Elements	254

LIST OF TABLES

<u>Table</u>	<u>Title</u>	<u>Page</u>
1.1	STAGS Development	4
4.1	Shell Surface Geometries	62
4.2	Summary of Element Library	63-65
4.3	Characteristics of Time Integration Operators in STAGSC-1	66-67
6.1	Linear Convergence of Elements 410 and 420 for the Clamped, Pressure Loaded Square Plate	119
6.2	Nonlinear Convergence of Elements 410, 411, 420, 422 for the Clamped, Pressure Loaded Square Plate	119
6.3	Nonlinear Flat Plate Analysis: Execution Statistics	120-121
6.4	QUAF 410 - Stiffness Eigenmodes	122-123
6.5	Single Element Load Cases - Modal Energy Distribution	124
6.6	Flexural Frequencies in XZ-Plane	125
6.7	Closely Spaced and Equal Modes	126
6.8	Flat Plate Cantilever Frequencies	127
6.9	1/4 Wave Model Frequencies	127
6.10	1/8 Cylinder Model Frequencies	128
6.11	1/2 Cylinder Model Frequencies	128
6.12	1/2 Cylinder Model Frequencies	129
6.13	Critical Time Step Estimates - Explicit Integration	129
6.14	Summary of Ring Transient Analyses	130
6.15	Nonlinear Transient Execution Statistics	131
6.16	Dimensions, Material Properties and Collapse Loads	132
6.17	Particulars of Finite Element Analyses	133

LIST OF TABLES (Continued)

<u>Table</u>	<u>Title</u>	<u>Page</u>
6.18	Comparison of Linear Solutions for Venetian Blind and Pinched Cylinder Problems	134
6.19	Variable Meshes Used in Pinched and Poked Cylinder Analyses	135
6.20	Comparison of Linear Results for the Poked Cylinder	136
6.21	Comaprison of Three Solutions for Region I	137
6.22	STAGSC-1 Execution Statistics - 1	138-139
6.23	STAGSC-1 Execution Statistics - 2	140
6.24	Comparative Program Statistics	141
7.1	Evaluation Ratings	206
9.1	ELMOD Listing	214-215

ACKNOWLEDGMENTS

This work was sponsored by the Office of Naval Research under Contract N00014-79-C-0825. The authors would like to acknowledge the support given by Dr. Nicholas Perrone, Director of the Structural Mechanics Program at ONR. Thanks are due in particular to Dr. Robert E. Nickell for his overall guidance in the project and many fruitful technical suggestions. We would also like to acknowledge the help obtained throughout the evaluation from the staff at Lockheed Palo Alto Research Laboratories, especially Mr. Frank Brogan and Dr. Bo Almroth. Finally, thanks are due to the following persons who provided technical consultation and technical support:

Dr. R. Dunham, Pacifica Technology, Del Mar, CA

Mr. D. B. Vogtman, Westinghouse Advanced Reactors Division

1.0 INTRODUCTION

The series of programs, known generally by the name STAGS, has been under development at the Lockheed Palo Alto Research Laboratory for roughly fifteen years. The first version of STAGS was operational in about 1967 and was a finite difference based program for the nonlinear analysis of cylindrical shells with cutouts. This initial development was sponsored by LMSC (Lockheed). It was followed in about 1968 by a special linear version restricted to shells of revolution. Buckling and thermal effects were added in 1970 followed by inelastic capability, some finite elements and more general shell geometry by 1972. These programs were funded by a number of government agencies, but all went by the name STAGS. A new version, STAGS2 (ca. 1974), included transient response, dynamic buckling and could analyze branched or segmented shells. The first version to be used by the structural analysis community, STAGSA, was released in 1973 and included dynamic eigenvalue analysis. The final version to be based on the finite difference method was released in 1976 (STAGSC). Since that time, the program has undergone a major re-writing and the latest version, STAGSC-1, was released in 1979. This version of the program is now entirely based on finite elements and future development will be along the same lines. The development since the earlier STAGS version (STAGS2 and on) has been under the sponsorship of NASA, Langley. Table 1.1 summarizes this brief historical survey.

The present report deals only with the finite element version, STAGSC-1. The evaluation study, described in the body of this report, follows the general methodology described by Nickell [1] and is intended to provide a potential user of STAGSC-1 with an in-depth description and critique of the program. On the other hand, it is not intended to be a "consumer report" by rating the program against other similar programs. In fact, this would probably be a very difficult, if not impossible, task since STAGSC-1 has many unique features which set it apart from most other finite element programs.

To begin with, STAGSC-1 is a special purpose program in the respect that its primary function is shell analysis (although a structure composed entirely of beams can also be analyzed). Secondly, it is fundamentally developed for nonlinear geometric and inelastic analysis. Thirdly, bifurcation buckling and dynamic analysis are very strong features in STAGSC-1. Bearing this in mind, it is to be anticipated that the majority of users will be interested mainly in the more sophisticated and less common analysis problems and will also be aware of the capabilities of other candidate programs in these areas. For this reason, the evaluation study performed for STAGSC-1 has done little comparison with other programs and has concentrated on the program features, algorithms, structure and performance.

The specific tasks which were performed can be summarized as follows:

- A. Review of program documentation (theoretical and users manuals)
- B. Program architecture description
- C. Program functional description
- D. Advanced evaluation topics;
 - (1) mesh convergence
 - (2) eigenvalue extraction
 - (3) transient integration
 - (4) large scale nonlinear collapse

The advanced evaluation provides some direct evidence of the performance of STAGSC-1 for shell structural models which vary in complexity from the simplest single element model up to models with more than 4000 degrees of freedom for the study on nonlinear collapse. The mesh convergence study was performed with models up to 630 d.o.f., while the eigenvalue and transient integration studies used up to about 1500 d.o.f. Not all capabilities which are available were exercised but the objective was to examine, in depth, those features which it is felt are of most significance for the program in general. No specific study was made on the performance of the modified Newton-Raphson nonlinear equation solver. The reason for this is simply that since the solver is used in most of the problems analyzed, sufficient evidence of its performance would be generated automatically.

The criteria for evaluating a structural analysis computer program will depend to some extent on the nature of the program itself and hence on the community of potential users. In the case of STAGSC-1, as has already been pointed out, the user community will be relatively sophisticated and will expect more than a "black box" capability. Thus, program and theory documentation must be accorded substantial weighting. Of course, the most important considerations are still the ability of the program to perform the types of analysis for which it was written, accurately and as economically as possible. For a program which performs mainly nonlinear analysis, relative economy is particularly important, since such analyses tend to be expensive in any case. Ease of input is always desirable but for a program which is less routinely used it is not an overriding factor. More important for nonlinear analysis is the ability to post-process the results with as much freedom as possible.

This report is organized into seven major sections plus an Appendix. Section 2 discusses the documentation of STAGSC-1; Sections 3 and 4 describe the program architecture and functions; Section 5 describes program verification and Section 6 presents the advanced evaluation studies. Conclusions and recommendations are presented in Section 7. The Appendix contains reference diagrams for the program structure and also details of the element stiffness matrix modal energy spectrum method used in the evaluation of element convergence.

This evaluation was performed as part of the ISEG program [1] under ONR Contract No. N00014-79-C0825 with Westinghouse Advanced Reactors Division.

TABLE 1.1
STAGS DEVELOPMENT

Version and Date	General and Added Capabilities	Sponsor	Comments
STAGS (ca. 1967)	Nonlinear Finite Difference Code for Cylindrical Shells with Cut- Outs.	LMSC	Initial Version.
STAGS (ca. 1968/9)	Linear Version for Shells of Revolution.	NSRDC	
STAGS (ca. 1970)	Bifurcation Buckling; Thermal Effects.	SAMSO	
STAGS (ca. 1970/2)	Inelastic Analysis; Finite Elements; Extension to More General Shell Properties (Grid Spacing).	AFFDL	First Introduction of Finite Elements.
STAGS2 (ca. 1972/4)	Transient Response; Dynamic Buckling; Branched and Segmented Shells.	NASA Langley	Versions for CDC 6600 and UNIVAC 1108
STAGSA 1973	Dynamic Eigenvalue Analysis.	NASA Langley	Used by Structural Analysis Community.
STAGSC 1976	Improved Convergence with Gridsize for Nonlinear Analysis.	NASA Langley	Increased Inaccuracy Due to Rigid Body Motions.
STAGSC1 1979	Completely Revised Input; F.E. Library Updated to Include Springs, Beams, Shells (Triangle, Quadrilateral and Transition). Plotting Available for Geometry, Deformations, Stresses, Strains, etc.	NASA Langley	Program now Entirely Finite Element Based.

2.0 PROGRAM DOCUMENTATION

The documentation pertaining directly to STAGSC-1 is at present confined to a users manual [2] describing the input and strategy required to execute a given problem. A theoretical manual also exists [3] which is not specific to the STAGSC-1 version. A third manual, of example cases for STAGSC, is available in draft form and is described as preliminary and incomplete. No programmer's manual has so far been written.

Therefore, the situation with respect to documentation appears, at least superficially, to be not entirely satisfactory. However, this is in part made up for by the overall high quality of the documentation which is available. A user, quite unfamiliar with STAGSC-1, can progress to the point of successful execution of a problem on the basis of the user instructions (Vol. II) alone [2]. Moreover, he can do this with some fair understanding of the basis of the program provided that he is reasonably knowledgeable on the subject of nonlinear finite element analysis. This is because there are sections in this volume which deal with the important questions of modeling and solution strategy. The theoretical manual was written when STAGS (STAGSC) was based on finite difference theory and therefore a significant part of its content (20-25%) is no longer applicable. It clearly needs to be extensively rewritten to bring it up to date with the program but, nevertheless, the greater part of it still provides valuable insight into the content and philosophy of STAGSC-1. The draft of example problems is not useful for STAGSC-1 since the input of the problems described was written for the previous version STAGSC and can no longer be used. This section will describe and comment on the user's and theoretical manuals.

2.1 STAGSC-1 USER INSTRUCTIONS MANUAL

As already noted, the user input manual is largely self-contained and provides the analyst with explicit instructions for problem execution together with enough background material to provide a reasonable understanding of the theoretical basis for the program.

The manual itself has ten sections of which two minor ones are, as yet, not issued. After a short introductory section there is a section describing the general capabilities of STAGSC-1 together with some basic concepts on the description of shell surfaces. The third section provides a detailed description of each input data card and groups of cards. There are nine such groups as follows:

- o Summary and Control Parameters
- o Computational Strategy Parameters
- o Data Tables
- o Geometry
- o Discretization
- o Boundary Conditions
- o Loads
- o Output Control
- o Element Unit

All input is free format and allows the insertion of comments which is a valuable feature from the archival viewpoint. Each input variable is assigned a name which is usually the same as the internal variable name used in the program. Branching to the next input card is governed by values of variables previously set or is unconditional. This is unambiguous (at least as far as the present evaluation is concerned--not all paths have been investigated) and makes for reasonably trouble free input provided that the user takes sufficient care. At the end of each input card description there are a number of conditional "go to's" which lead to the next card or card group. This kind of programming logic for input preparation is somewhat unusual but in the opinion of the reviewer has much to recommend it. At this point it is appropriate to mention a special concept in defining shell geometry which is a basic feature of STAGSC-1. A shell structure may often be conveniently described in terms of one or more distinct types of surface geometry (e.g., cylinder, cone, torus, etc.). Each such type can be defined in STAGSC-1 as a "shell unit" with its own local coordinate system. Shell units may then be connected to form the complete structure. Each shell unit has its own surface coordinate grid (rows and columns) the nodes of which are employed (selectively or otherwise) to define element connectivity. If a region of the

shell has a geometry which does not lend itself to this treatment, nodes and elements may be specified directly to form, what is referred to in STAGSC-1 terminology, as an element unit. Further details are discussed in Section 4.2.

The summary and control parameter group provide a title and define the analysis type. The next group, computational strategy parameters, define the following: load incrementation; eigenvalue extraction strategy (spectral shift, eigenvalue range); time history forcing function input and integration method; basic mesh summary for each shell unit (rows and columns); shell unit interconnections; element unit summary (element types and number). The third group (data tables) specifies all material properties, cross-sections of beam elements, shell wall construction (multilayer, composite, etc.) and a table of real and integer constants for use in user coded subroutines if required.

Shell unit surface geometry is defined in the fourth group. This may be chosen from a library of standard forms (11 surfaces) or generated by a user subroutine. A thirteenth option, to fit a surface to defined points by spline functions, is indicated but not currently available. Shell wall type is also specified in this group together with the type of strain-displacement relationships (linear or nonlinear), elastic or elastic-plastic material behavior and initial imperfections (if of trigonometric form).

The next major input group controls the finite element discretization. The analyst may use the mesh defined in the shell geometry or specify an overlying mesh of elements which picks shell mesh nodes selectively for element connectivity. Patches of elements can be defined which allow changes in element type; also segments of the mesh can be defined with different spacing. In addition, the user may define the element connectivity through a user subroutine. Also specified in this group are the location of discrete stiffeners which may be eccentric with respect to the shell surface and can be skewed with respect to the shell surface mesh.

Boundary conditions for shell units are specified in the sixth group. These can be of a standard type (simple support, clamped, etc.) along a specified edge of the shell or they may be selected degree of freedom types along the edge which can be designated fixed or free. An additional distinction may be

drawn between boundary conditions applicable to incremental displacements or basic displacements (pre-buckling, prestress). The seventh group controls the applied loads, displacements and initial conditions (for dynamic analysis). A concept is introduced here which is unusual in structural analysis programs, i.e., the specification of loads, displacements or initial conditions in two categories, A and B, which are independent. They are scaled by two independent load factors P_A and P_B . The purpose of this is specifically the determination of bifurcation buckling behavior for systems where there is a fixed load, or prestress, defined by System B and an increasing load defined by System A. At bifurcation the total stress is obtained from the sum of System B stresses and System A multiplied by the eigenvalue. For non-buckling analysis it is not necessary to specify both A and B systems. For a new user, reading the documentation unaided, this concept can be rather puzzling at first and the documentation should provide a little more discussion than it does. However, in all other respects the description of loads input is quite satisfactory.

Output control is input on the eighth group of data cards. Basically, the user can control the frequency of printing displacements, stress resultants, strains, stresses and point forces. The frequencies for each of the above quantities are independently specified. These controls govern printout for all elements in a given unit and must be specified separately for each unit. In addition, certain selected stress or displacement components may be printed at every step. Apart from this control, the manual recommends the use of the post-processor STAPL. This, however, is geared mainly to the generation of contour plots and does not currently fulfill many post-processing needs, e.g., time history of stresses or displacements or spatial distribution of stresses or displacements. A significant aid in this respect would be detailed descriptions of the model and solution data files (MØD and SØD) so that the data may be processed according to the user's needs in a separate program. Such descriptions are not given in the documentation. All of the preceeding input pertaining to the shell unit must be repeated for each shell unit in the structure. Each shell unit, being independently defined, may be totally different with regard to each section of the input data which is part of the shell unit (geometry, elements, wall, material, etc.)

The final input group is for definition of an element unit. This group specifies user point coordinates, element connectivity, point forces at nodes and distributed forces on elements. This part of the input is rather unsophisticated since input by cards requires specification of each and every node point and its coordinates and each element and its nodes. The only alternative to this is to define node geometry and element connectivity by means of user subroutines.

The fourth section of the manual describes the function and format of each of the thirteen available user subroutines. The descriptions are reasonably complete and each one provides a coded example.

Section five describes the input for the post-processor STAPL. The input required is in free format, as in STAGS, and is straightforward. Currently inoperational features are marked by an asterisk.

Section 6, dealing with modeling and strategy, is one of the most important sections in the manual. It provides the user with valuable background information with regard to the type of analysis which should be performed to solve a particular problem. It is in this section that one may discern the basic philosophy of the STAGS series of programs. Put concisely, the fundamental viewpoint is that the purpose of shell analysis is determination of the structural failure modes. For thin shells, this usually means either static or dynamic collapse of the shell wall rather than a straightforward exceeding of material stress or strain limits. Thus, STAGSC-1 is the result of an evolution of a basic nonlinear shell analysis capability with strong emphasis on bifurcation buckling. The dynamic counterpart has also been developed and plastic material behavior included.

An indication of the degree of development of the nonlinear capability is provided by the statement (in Section 6) ". . . it is suggested that nonlinear static analysis be used as a matter of course. . ." on the grounds that if nonlinear effects are insignificant, the nonlinear solution will converge in one or two iterations and the extra cost will be negligible. General reasons are discussed for the non-convergence of a problem. A few paragraphs are also devoted to the problems of bifurcation buckling analysis.

The next subsection discusses modeling with STAGSC-1 using the shell unit concept for geometry description and also the use of the capability to incorporate either discrete or "smeared" stiffeners. Discretization is discussed next and is basically a description of the element library available in STAGSC-1. This is of vital importance since it is the only place in the documentation where the elements are described. It is adequate for general information but does not provide the depth of detail which should be contained in a proper theoretical description.

The final subsection deals with computational strategy. First, eigenvalue analysis for both bifurcation buckling and vibration frequencies is discussed. The subtleties of bifurcation buckling are highlighted (existence of negative as well as positive eigenvalues) and also the choice of spectral shift values. The general strategy of nonlinear analysis is covered next. The user specified parameters NCUT (total number of times the load increment may be halved) and NEWT (total number of times the factored matrix may be computed) are also dealt with in some detail since they are quite subtle in their effect on the modified Newton-Raphson procedure. Also, the internal logic of the solution algorithm is quite complex in the way it makes decisions with regard to refactoring or cutting the load step. As a result, even given a careful reading of this section, the user may feel that he can exert more control over the solution procedure than is actually the case. The parameters DELX (tolerance criterion for displacement increments) and WUND (relaxation factor) are also user specified and their use discussed.

Finally, the use of the transient integration operators is covered. Most of the discussion deals with the central difference (explicit) operator and the question of its conditional stability and how to estimate the critical time step. The discussion of the implicit operators is less thorough and more guidance on the appropriate choice for a given problem would be useful. Surprisingly, there is hardly any reference to plasticity calculations in this section. Given that plasticity is certain to enter into most nonlinear calculations the omission is serious. It is, however, true that there is not much opportunity for the user to exert control over the plasticity

computations (other than via the specification of the uniaxial stress-strain curve) and that the program handles them automatically. Some discussion on limitations should be provided.

Section 7 of the manual attempts to provide user guidance on the interpretation of output from STAGSC-1. Special problems which may arise during linear, eigenvalue, nonlinear and transient analyses are presented and appropriate actions suggested. While such a list can never be complete, the situations presented are basic and provide general guidance on how the user should handle difficulties in execution.

Section 8 (Index to Volumes 1 and 2) and 9 (Execution Control) are in preparation. An index to the users' manual (Vol. 2) is definitely a necessity. A disadvantage of the way the input is structured is that it is not easy to locate the place in the manual where a specific item is discussed. For example, in order to determine what actions are required to create a restart file it is necessary to trace through some of the input groups in detail. A well constructed index would help the user of only moderate experience very considerably. The proposed section on execution control is perhaps of lesser importance since this must be different for each system on which STAGSC-1 is installed.

Finally, Section 10 (Minimanual) provides a useful summary of all the input records and the associated variable names. This can be also used as a stop-gap until a proper index is available.

2.2 THEORETICAL MANUAL

As indicated previously, the currently available theoretical manual was not written in the context of the STAGSC-1 program. The latest version of the program to which it truly applies is STAGSC, which is a finite difference program whereas STAGSC-1 is wholly finite element. Thus, there are parts of this volume which are still valid and others which are irrelevant and it is part of the purpose of this subsection to identify the portions which remain valid. The manual is organized into ten sections plus an appendix as follows:

- o Introduction
- o Summary of Theory
- o Constitutive Relations (Elastic)
- o The Theory of Plasticity
- o Geometric Nonlinearities
- o Discretization Procedures
- o Beams and Stiffeners
- o Constraints and Transformations
- o Solution Procedures
- o Program Organization
- Appendix

The current version of the manual is incomplete; Sections 7, 8, 10 and two subsections of the Appendix are not yet available.

The introductory section starts off with some general observations on computer-based structural analysis and goes on to list the basic approximations inherent in the STAGS program. It must again be emphasized that many comments, observations and whole sections of this volume are not appropriate to the STAGSC-1 version. This is already apparent in the limitations described for first order shell theory. Since STAGSC-1 is finite element based and there are no curved shell elements available in the program, shell theory cannot be a part of the element formulation.*

Section 2 provides a summary of the basic theoretical principles embodied in STAGS. First, there is a short discussion on variational principles in terms of Hamilton's principle for dynamics which is shown to degenerate to the principle of minimum potential energy for static systems. A point of interest is that the conditions under which "live" pressure loads are conservative are delineated. Thus, it is possible to include these in an analysis based in the variational approach which is necessarily confined to conservative systems. The basic theory of elasticity constitutive equations are presented and the

*The elements are all flat plate triangles or quadrilateral in which there is no coupling of membrane and bending behavior within the element.

point made that the STAGS formulation is based on engineering strain. Kinematic strain displacement relationships are developed for small strains but with moderate rotations (<0.3 radians). These are Green's strain in Lagrangian coordinates.

The third section presents a development of generalized elastic constitutive relationships for combinations of shell wall and stiffeners.

Section 4 provides a reasonably up-to-date discussion of plasticity. First, the classical development of plasticity theory is considered, incremental and deformation theories are discussed with deformation theory being discarded for general non-monotonic loading. Reverse plasticity and the Bauschinger effect are also treated. On the basis of improved correlations with experiment (compared with isotropic or kinematic hardening), the White-Besseling (mechanical sublayer) theory is selected as being representative of more modern theories of plastic work hardening behavior. It is, however, pointed out that for complex loading (non-monotonic and non-proportional), little is known about the applicability of currently available theories. The solution of plasticity problems using the pseudo-force and the tangential stiffness methods is discussed. It is also indicated that STAGS uses a combined approach by normally using the pseudo-force technique and updating the stiffness matrix for plasticity effects whenever convergence behavior indicates reformulation of the stiffness is required. This, however, is quite misleading since the STAGSC-1 program does not include plasticity corrections when formulating the stiffness. An additional feature of the plasticity computations is the so-called subincrement approach. This is discussed later in this report in Section 4.5 of the functional description.

Section 5 is entitled "Geometric Nonlinearities" but concentrates entirely on the question of structural stability. Nevertheless, the discussion is very thorough and reveals where the greatest depth of expertise, applied to the development of STAGS, lies. The concept of structural stability is developed in terms of primary and secondary loading paths and the bifurcation point. Various criteria for instability are discussed followed by the consequences of instability and pre- and post-buckling behavior.

The rest of the section discusses static stability analysis with a large amount of qualitative detail. A short historical survey of analysis methods is followed by a dissertation on flat plate buckling including post-buckling behavior. This is followed by analysis of shells of revolution and general shell buckling. For the user who is mainly preoccupied with shell stability problems this section provides an excellent background.

The next section (Section 6) is a major discussion on discretization procedures. Unfortunately, much of it is no longer of direct consequence to STAGSC-1 since it discusses finite difference procedures in some depth.

Also, the discussion on finite elements is somewhat out-of-date with respect to the specific elements available in STAGSC-1. Nevertheless, the material presented is of high quality and the contents of the section will be reviewed here, at least in part.

The first three subsections give an overview of standard methods for numerical differentiation and integration. This is followed by a discussion in some depth of numerical solution procedures with considerable emphasis on finite difference methods. Finite element procedures in general are discussed mainly from the standpoint of continuity requirements for convergence. Topics covered are C_0 , C_1 continuity requirements, conforming and non-conforming elements, order of convergence and the patch test. The presentation is general and not specific to the STAGSC-1 program. With regard to the finite difference versus the finite element approach, the point of view of the developers is, to quote verbatim;

"There is no clear distinction between the finite element method and the finite difference energy method. It seems reasonable to define as a finite element method a discretization scheme in which the displacement pattern inside the element is determined without the use of nodal freedoms outside the closed domain of the element."

In the opinion of the reviewer, this perspective sheds some light on the reasons for the choice of program architecture in STAGSC-1. This will be described in some detail in Section 3 but it can be said at this point that it

is quite different from conventional finite element programs. Under the heading of "Special Problems", the following topics are discussed briefly; effects of reduced integration in producing spurious mechanisms; strains produced by rigid body motion (super-parametric elements); the undesirability of convergence from "below" for buckling analysis.

Finite difference schemes and some finite elements are discussed next. A so-called "curved" finite element (STAGC) with incompatible ("bubble") modes is discussed but does not appear to have been included in any available version of the program. A flat plate quadrilateral element (STAGF) is introduced next and the compatibility problems associated with modeling curved shell surfaces with flat elements is discussed in some detail. It is concluded that for displacement continuity, cubic variation of in-plane displacement components normal to an edge is required in order to match the cubic variation of transverse (bending) displacements. In addition, degrees of freedom corresponding to average in-plane shear strain and rotation about the surface normal are required at corner nodes. Thus, the complete element is specified with seven freedoms at corner nodes and four at midside nodes (32 total). No derivation is provided.

The merits of Ahmad type elements for thin shell analysis are discussed and finally the Clough-Felippa triangular and quadrilateral elements. The section concludes by listing elements to be included in STAGS as follows:

- o Flat quadrilateral STAGF
- o Ahmad type elements
- o Clough-Felippa triangle and quadrilateral

As will be detailed in Section 4, these are not the elements that are in the STAGSC-1 program, but it is clear that they are derivative versions of the Clough-Felippa series. Ahmad elements are not yet available.

Section 7 (Beams and Stiffeners) and 8 (Constraints and Transformations) are described as being in preparation.

Section 9, entitled "Solution Procedures", is again one of the major parts of the theoretical manual. Topics discussed are as follows:

- o Expressions for strain, kinetic and total potential energies
- o Linear equation systems
- o Nonlinear equation systems
- o Eigenvalue analysis
- o Transient analysis

This section is probably the most mathematically detailed part of the theoretical manual; it begins with statements of strain, kinetic and potential energies and introduces the concept of a stiffness operator $L(x)$ which is defined as the first variation of the total potential energy. $L(x)$ is defined as generally nonlinear, thus, there is a departure from the more familiar ideas of linear and nonlinear stiffness matrices in the subsequent developments. The solution of linear systems of equations is presented in terms of conventional triangular decomposition followed by forward and backward substitution. There is also an important discussion of problems encountered in the solution process due to ill-conditioning. This gives valuable insight into the meaning of the various diagnostic messages which may be output during STAGS execution.

The solution of nonlinear equation systems is also discussed in depth, beginning with a discussion of the relative merits of regular and modified Newton-Raphson; successive substitution with nonlinearities on the right hand side only; tangent stiffness incremental method with residual load correction; dynamic relaxation and, finally, energy search methods. It is concluded that the Newton-Raphson methods include the tangent stiffness methods as special cases and that dynamic relaxation is not competitive. The discussion then goes on to develop equations for regular and modified Newton-Raphson in terms of the operator $L(x)$ (there are, unfortunately, two errors in the equations which require correction). It is stated that the user can involve either regular or modified Newton-Raphson but this does not appear to be operational in the version evaluated (see Section 4.5). It is also stated that the user

can choose to include material nonlinearities in reformulation of the stiffness but, again, this is not available in STAGSC-1. Plastic nonlinearities are included as pseudo-force contributions to the loads vector.

Eigenvalue analysis is introduced in very general terms through use of the nonlinear stiffness operator $L(x)$. While concise, this treatment tends to be somewhat obscure to the less mathematically inclined structural analyst. Having stated the linear eigenvalue problem, the generation of the associated matrices is developed in terms of second derivatives ("second variation") of the potential energy. This step is revealing with respect to the programming of STAGS since it appears that this is the basis of the algorithms implemented. The solution of the eigenvalue problem is described in terms of the inverse power method including a spectral shift. However, the actual method employed in STAGS is not described in detail. This is unfortunate, since the detailed treatment, which was to be included in the Appendix to the theory manual, has not been written. As is described in Section 4.7, the actual method used is a variation on the subspace iteration method, which is a relatively recent development.

The final topic is transient integration, which is one of the strong features of STAGSC-1. The treatment is good and is substantially more clear than some of the preceding sections. Again, the subject is introduced in general terms with a discussion of the solution of initial and boundary value problems. Explicit and implicit integration methods are defined. The explicit (central difference) algorithm is presented and its conditional stability discussed. There is also a lengthy discussion of implicit methods and their stability. Data are presented for the stability boundaries (applicable to a linear analysis) for a number of schemes, viz. Park, Wilson- θ , Houbolt, Gear's 2nd and 3rd order and the trapezoidal method. With regard to their stability for nonlinear analyses it is pointed out that the criteria are not exactly valid and that no method exists which is unconditionally stable.* It may be difficult, therefore, to distinguish between physical and numerical instability in the nonlinear case. It is concluded that energy balance checks are advisable; however, STAGSC-1 is not, as yet, provided with this capability.

*See further discussion in Section 4.8.

The Appendix section is incomplete, since it contains only a section on shell theory, which is not required for STAGSC-1. There should also be more detailed information on the handling of plasticity, element formulations, the eigensolver and transient integration operators.

2.3 CONCLUSIONS

It may be concluded from the foregoing that there are some serious deficiencies in the documentation for STAGSC-1. These are:

- o lack of any program description
- o partial obsolescence of the theoretical manual
- o lack of a problem demonstration manual

On the positive side, it may be fairly stated that the quality of the existing manuals is high and that they are written with the sophisticated user in mind. Since STAGSC-1 is basically a nonlinear program, this is the right approach. However, the availability of a complete set of manuals cannot be predicted at the time of writing and it is to be hoped that some greater priority will be given by the developers to this highly important aspect of the program.

3.0 PROGRAM ARCHITECTURE

STAGSC-1 is the latest version of the STAGS series of programs developed over the last 13 years or so. It is, however, a major departure from previous versions since it is now entirely finite element, rather than finite difference based. The program itself has been completely rewritten and probably bears little resemblance to the earlier versions (although a comparison of the current and earlier source listings has not been made to verify this). However, inspection of the job control deck required for execution shows that there are major differences in organization of the program. The most obvious feature is that STAGSC-1 consists of two programs, referred to as STAGS1 and STAGS2. STAGS1 is a pre-processor which reads the input data, generates the finite element model, derives the nodal forces and creates a file to preserve the data base for execution. STAGS2 then takes over and performs the execution. A new feature is a separate post-processor, STAPL, which provides geometry plots of the model and contour plots of the solution variables. STAPL is not currently fully operational and has been excluded from the evaluation. This section, therefore, will describe in some depth the major features of the architecture of STAGSC-1.

The performance of this part of the evaluation has been hampered by the complete lack of documentation on the programming aspects of STAGSC-1. In addition, the lack of a revised theoretical manual has also made it difficult for the most part to establish the algorithms embedded in the program. This is especially true with respect to the creation of the stiffness and the solution of equations since the procedures involved are unusual.

3.1 GENERAL DESCRIPTION

As already mentioned, the STAGSC-1 program is a system of three separate programs, STAGS1, STAGS2 and STAPL. STAGS1 and STAGS2 are normally executed in tandem with STAPL following or run in a stand-alone mode. The version of STAGSC-1 which was evaluated was configured for the CDC-7600. Both STAGS1 and STAGS2 are highly modularized with primary and secondary overlays. STAGS1 has eight primary and three secondary overlays while STAGS2 has eight primary and four secondary.

The organization of the program for the CDC-7600 using the SCOPE 2 system (Version 2.1.5) utilizes the library file concept. Three files are created; one for routines used in STAGS1, one for STAGS2 and the third for routines used in both STAGS1 and STAGS2.

The source coding is FORTRAN with a few routines written in assembly language (COMPASS). However, equivalent FORTRAN coding is supplied in the form of comment statements. The degree of commenting in the program is somewhat variable. The majority of routines have at least some description of their function; a number of others are rather fully commented while a few have no comments at all. Overall, the commenting is adequate, but is not sufficient to obviate the need for proper programming documentation.

3.2 STAGS1 - PRE-PROCESSOR

The overlay structure of STAGS1 is shown schematically in Figures 3.1 and 3.2. The (0,0) overlay is a short main program which serves to load primary and secondary overlays as required by the input data. As indicated by Figure 3.1, the main program calls overlays (1,0), (2,0) and (7,0) directly and also the other primary overlays through the subroutine PREVU. The direct calls are for the purpose of determining core storage requirements. In addition, the main program saves the model data generated on the file MOT.

Of the eight primary overlays, three are always loaded (6,0), (7,0) and (8,0); these summarize the model input data, prepare the element stiffness data and save the data base. The remaining five primary overlays are loaded selectively depending on whether the model consists of shell units, an element unit or both.

Similarly, the secondary overlays are loaded selectively depending on the class of elements called for at input time (beam, quadrilateral or triangle). A detailed set of diagrams showing the calls made to all subroutines are provided in Section 9 (Appendix). The main program (Figure 9.1) also loads the user subroutines (LUSER1) which may be required for definition of the structural model (Figure 9.2). Major subroutine functions are:

- o PHASE1-controls all pre-processing
- o LOVO-loads overlays from level 0
- o ADATA-sets up data statements
- o BDATA-sets up node number and logical freedom lists

3.2.1 OVERLAY FUNCTIONAL DESCRIPTIONS

The primary and secondary overlays will each be described briefly in this section.

- A. Overlay (1,0) - Program OVSU - Shell Unit Generation. Figure 9.4 shows the schematic representation of the routine calls made in this overlay. The function of this overlay is to generate the underlying mesh for the shell units and the stream of associated elements. Control over the generation is via subroutine GENSU which calls the major routines GINPT, MSHGEN, SUN and SUE. GINPT selects the type of shell unit specified (cylinder, torus, etc. or defined by user subroutine LAME) and defines its global orientation, wall construction and reference surface imperfections (WIMP). MSHGEN generates the underlying mesh when the spacing of the gridlines is non-uniform. The actual nodal coordinates are computed, saved in a node "table" and also printed out by the subroutine SUN; SUN also checks for consistency in the mesh specified by the user. Element connectivity is generated, stored and checked for consistency by SUE. Schematics of calls made by SUN and SUE are given in Figures 9.5 and 9.6. The following routines establish the element data in the shell unit configuration tables:

ATRIA - alternating triangularization for quadrilateral elements
 BEAM - beam elements
 QUAD - quadrilateral elements
 QUIN - transition elements
 STIFIN - discrete stiffeners
 TRI - triangular elements

B. Overlay (2,0) - Program OVEU - Element Unit Generation.

The logic for element unit generation is similar to that for the shell unit but simpler because there are no built in geometries (Figure 9.7). Thus, subroutine EUN reads in node point numbers and coordinates directly or through the user subroutine USRPI. Subroutine EUE generates element connectivity data according to element type.

C. Overlay (6,0) - Program OVIS - Model Input Summary

This overlay creates files which contain all the additional data required for the execution of the analysis. Input data, which is entered in free-format is interpreted by subroutine CARDS and translated into an internal format. The master subroutine, PREMIS, assembles the input data defining the analysis type, loading and solution strategies, structural model definition and provides descriptive output. In addition, PREMIS creates a beam cross-section properties file, material properties file and shell-wall construction file. Data defining the method of time integration (if used) is also loaded and saved (LOADT). The following subroutines perform major functions as follows:

- CARDS - interprets free-form input
- ESPID - generates White-Besseling plasticity data
- RCONST - reads constraint conditions
- TAB - tabulates beam section properties
- TAM - tabulates user materials
- TAP - tabulates user parameters
- TAW - tabulates shell wall properties

Figure 9.8 shows the subroutine calls for this overlay.

D. Overlay (7,0) - Program OVVU - Element Stiffness Preprocessor

The descriptive comments for this overlay use the terminology "unit prevariational overlay" and "prepare variational data for unit". In the context of STAGSC-1 this means that the functions performed are preparatory to formulation of the stiffness matrix during execution with STAGS2. Figure 9.9 indicates that the overlay loads the secondary overlays (7,1), (7,2) and (7,3). The computational flow is controlled mainly by subroutine PREVU. PREVU processes all elements for one shell unit at a time. It calls the element subroutines GSBM, QUAF and TRINC as required. These subroutines perform all necessary geometric calculations, strain-displacement relationships, integration point coordinates, weighting factors and contributions to the mass matrix.

LOV7 - loads overlays from level 7
OVE22 - beam element overlay
GSBM - master routine for beam element generation
MASSE - assembles and transforms beam element mass matrix
MACUP - controls formulation and update of element constitutive matrix
OVE41 - plate element overlay
QUAF - master routine for quadrilateral plate generation
MAPXY - performs bilinear mapping
FDF - finds integration weights and function formulas for bilinear quadrilateral
MSH - finds coordinates and integration points
OVE31 - triangular element overlay
TRINC - master routine for triangular element generation

Figures 9.9 through 9.14 contain full details of the subroutine linkages in this overlay and the secondary overlays.

E. Overlay (10,0) - Program OVSV - Data Base Preservation

This overlay is a data management program to organize the preprocessed information in mass storage in readiness for execution by STAGS2. The subroutine linkages are shown in Figure 9.15.

F. Overlay (12,0) - Program OVSI - Shell Unit Intersection

Overlay (12,0), (Figure 9.16) has the sole purpose of checking the interconnections between shell units for consistency and, where inconsistencies are detected, removing them if possible.

G. Overlay (13,0) - Program OVSL - Shell Unit Loads

Figure 9.17 shows the subroutine calls for this overlay. Program OVSL has a single call to subroutine LOADS which generates a loads file for a given shell unit. LOADS generates consistent nodal forces from applied loads and computes additions to the load vector corresponding to imposed displacements. Output of the load file and mass file is controlled by subroutines LOADOP and MASSOP.

H. Overlay (25,0) - Program OVEL - Element Unit Loads

Program OVEL (Figure 9.18) performs functions similar to OVSL for the element unit. The controlling routine is LOADE with the force vector being determined by FORCEEE. FORCEEE does not currently have as much capability as FORCES in OVSL since it does not process distributed loads.

This completes the description of the major functions in program STAGS1.

3.3 STAGS2 - Execution Phase

The structure of STAGS2 follows the same standard overlaying concept as STAGS1. There are eight primary overlays and four secondary. Figure 3.3 shows the overlay links. The secondary overlays are listed with their functions in Figure 3.4.

STAGS2 functions partly through subroutine CONTRL (Figure 9.19) and partly through direct calls to the overlays. The direct calls are for the purpose of determining storage requirements while CONTRL directs all analysis functions. Also, STAGS2 loads user subroutines required during execution (LUSER2).

Details of the subroutine calls for STAGS2 are contained in the Appendix (Figures 9.19 through 9.39).

A. Overlay (1,0) - Program OV10 - Data Transfer from Pre-processor

This program performs the many complex operations required to start execution, either for a new problem or a restarted problem. Its main functions are performed by three subroutines; ALLOC2, DATAIN, SETPAR, and RSTRT. ALLOC2 is itself a complex routine which determines block sizes, assigns files, sets pointers for various operations (e.g., stiffness matrix computation), determines working space in core and initializes file manager parameters. Subroutine DATAIN initializes parameters. SETPAR also performs parameter initialization, e.g., initial conditions for a transient analysis. RSTRT controls a restart analysis. Subroutine links are shown in Figures 9.22 and 9.23.

B. Overlay (2,0) - Program OV20 - Stiffness Matrix Decomposition

Program OV20 performs one of the crucial stages in the STAGSC-1 analysis, i.e., factorization of the stiffness. It first assembles the total stiffness matrix from the element stiffness file in subroutine ASEM. ASEM calls ASEM2 which adds the element contributions. However, the actual operations are carried out by

calling a COMPASS coded subroutine ASEMA (Figure 9.24) which renders the details somewhat inaccessible to a reviewer. The decomposition into upper and lower triangles is controlled by subroutine FACTOR with the actual reduction occurring in subroutine FACMD.

C. Overlay (3,0) - Program OV30 - Eigenvalue Solution

The eigenvalue solver is probably the most complex program in STAGS2. Figure 9.25 provides details of the subroutine links. The major functions are driven by subroutine SIM1 which controls the computational flow for simultaneous iteration for a cluster of eigenvalues. SIM1 determines the number of eigenvectors required as a subspace for the simultaneous inverse iteration, performs the inverse iteration and solves for the reduced set of eigenvectors using the Householder tridiagonalization and QL method. The major subroutines in which these computations are performed are EIGEN (Figure 9.26) and SOLVE. EIGEN calls subroutines TRED2 and TQL2 which are FORTRAN versions of ALGOL procedures originally developed by Wilkinson, Martin and Reinsch.

D. Overlay (4,0) Program OV40 - Formulation of Stiffness

The comments provided in the subroutines called by this overlay refer to "second variation of strain energy". This terminology refers to all the functions normally associated with the generation of stiffness matrices and this is indeed the function of the overlay. Figures 9.27, 9.28 and 9.29 show the subroutine links for the overlay. The major routines called are VAR2, CVR2, VR2 and VRDATA. VAR2 and CVR2 are the controlling routines which call VRDATA and VR2. VRDATA provides all the necessary information specific to the element type while VR2 performs the actual calculations of the stiffness contributions at a given integration point. Nonlinear terms are handled by VR2 and also effects due to live pressure loads. Brief functional descriptions of significant routines are as follows:

SDBM	- Forms strain-displacement matrix for a beam
FDRV	- finds interpolating polynomials, 1st and 2nd partial derivatives for quadrilateral elements
QUADF	- performs integrations for quadrilaterals
E32LL	- generates shape functions for live pressure loads on triangular elements
TRIDUV	- finds membrane strain-displacement matrix for triangular elements
TRIDW2	- finds curvature-displacement matrix for triangular elements
PENAL	- adds penalty terms to stiffness matrix
VR12D, VR22D	- computes stiffness terms for one and two-dimensional elements

E. Overlay (5,0) - Program OV50 - First Variation of Strain Energy

The form and function of this overlay are geared directly to the method of solution of the nonlinear equations. The modified Newton-Raphson method, as described in Section 4.5, solves the nonlinear system of equations iteratively and obtains the incremental displacement vector by the solution of the equation

$$\{x_{n+1}\} - \{x_n\} = - [K(x_m)]^{-1} (K(x_n) \{x_n\} - \{R\}) \quad 3.1$$

The nonlinear stiffness $K(x_m)$ is determined in overlay (4,0) (second variation of strain energy). This overlay forms the product $K(x_n)\{x_n\}$ directly as the first variation of strain energy and subtracts the contributions from the force vector $\{R\}$. The solution algorithm is discussed more fully in Section 4.5.

Figures 9.30, 9.31 and 9.32 show the subroutine links for OV50. The major subroutines called are ITER, CVR1, VR1 and SOLVE. ITER controls the iterations and checks convergence. The computation of the first variation is controlled by CVR1. This pulls in all the

necessary element information (VRDATA) required for computing the first variation and performs the computation at an integration point in VR1. Plasticity calculations are performed by the secondary overlay (5,1) in program OV51. CVR1 loads program OV51 (Figure 9.31), which has major subroutines as follows:

PLASTC - controls plasticity calculations at each integration point
PLAST - performs plastic stress calculations

Equation solving is performed in subroutines SOLVE and SWEEP.

F. Overlay (6,0) - Program OV60 - Dynamic Response

Program OV60 performs the same function for dynamic response calculations that OV50 does for static analysis. The procedures are necessarily more complex because of the time integration. Figures 9.33 and 9.34 show the subroutine links. The controlling subroutine for OV60 is DYNR which calls CVR1, ODES and EXPLC. CVR1 is the same as OV50 and performs the same function, i.e., sets up the right hand side vector for the nonlinear solution as the first variation of strain energy. The dynamic response obtained using the explicit integration operator does not require the solution of equations and is therefore called directly by DYNR. Solutions using implicit integration operators are performed by subroutine ODES. ODES is a general, multi-step ordinary differential equation solver and is called once per time step. It controls the time step either in the automatic mode or in the "fixed" mode in which it only intervenes if the time step needs to be decreased. It also provides starting procedures and handles damping. ODES calls MSTEP, SOLVE, NITER and NEXT. MSTEP computes the predictor-corrector formulae for the four implicit schemes. There is also a link to a user defined operator by a call to a user written subroutine USTEP. This capability is not currently documented and is not included in LUSER2. NITER controls the iterations for nonlinear equation solving with SOLVE providing the solution procedure. Subroutine NEXT provides the coding for

time step control. OV60 calls a separate overlay for plasticity, OVL61 in dynamic calculations, but this appears to be identical with the plasticity routine used in static analysis OVL51 (Figure 9.32).

G. Overlay (7,0) - Program OV70 - Solution Strategy.

Program OV70 is called by subroutine CONTRL to control the static nonlinear solution strategy. The controlling subroutine within OV70 is DATA1 which controls the output for each load step and calls the major subroutines STRAT, EQCHK, SDATA and OUTSLD. STRAT controls load step size and adjusts it if necessary depending on the rate of convergence. It also controls refactoring of the stiffness and extrapolation of displacements for the next load step. Subroutine EQCHK performs an overall equilibrium check but is disabled in the version evaluated since the programming is not yet complete. SDATA maintains the solution data file (SOD), plastic stress history and also writes TAPE8 for nonlinear analysis in which periodic eigen-solutions may be derived. Thus, estimates of bifurcation buckling loads may be obtained at various points in a nonlinear loading history. Finally, subroutine OUTSLD controls output of selected displacements.

H. Overlay (10,0) - Program OV80 - Stress Computation and Output

Overall control of stress and strain computation and output is exercised through this overlay. A master routine SIGMA calls secondary overlays OV81 and OV82 and major subroutines OUTSLS, SRES, VRDATA and PREFAB. SIGMA controls stress calculations element by element. Element data is brought in by means of VRDATA. SRES controls the actual calculation of strains and stress resultants. The secondary overlays OV81 and OV82 do the element-specific computations; OV81 handles 1-D (beam) elements while OV82 deals with the 2-D elements. Figures 9.37, 9.38 and 9.39 provide the details of the subroutine links.

3.4 DATA MANAGEMENT

The storage and retrieval of data in STAGSC-1 is accomplished by two separate schemes. First, there is the need to transfer large files for vector and matrix operations between core and mass storage. The size of the files may be particularly large when time integration is being performed and vectors must be made available for several time steps. Also, during an eigensolution, twenty or thirty subspace vectors are being manipulated together with mass and stiffness matrices. Second, there is the need to obtain relatively small amounts of data from tables in order to generate element stiffness matrices or calculate element stresses. These tables are themselves lengthy and the mode of retrieval may be described as quasi-random access; this is because transfer of successive sections of data may be from regions of the file which are adjacent.

3.4.1 FILE MANAGER - FMM

FMM is a routine designed to manage working space in blank common for vector and matrix manipulations. When FMM is called, the argument first identifies the number of files to be located simultaneously in core, a list of the file numbers and their lengths and also a priority indication which says whether the file is to be saved or not (in mass storage) when removed from core. FMM provides as output the address in blank common of each file. During execution, FMM checks if a given file is already in core; determines whether the space required by the file is available; adds the file to core and performs other housekeeping functions. The present version does not utilize the LCM (large core memory) feature available on the CDC 7600.

FMM also makes use of a number of other utility routines for performing specific operations. The subroutine calls may be found in the Appendix in Figure 9.3.

3.4.2 VIRTUAL MEMORY OPERATIONS - IOGETR.

The transfer of tabular data from mass storage into core is accomplished using a buffering technique. Such data are used in element matrix generation, stress calculations, etc., and are stored as tables in one lengthy file. On the other hand, the data are needed only in relatively small blocks at any time. The technique used in writing the file is to divide it into a number of records of convenient length. The record length is chosen so that typically 6 to 10 records can be accommodated in core at a given time. This process is reasonably efficient since the required data are often in adjacent blocks if not all in one block. The controlling subroutine is IOGETR, which searches the buffer for the required record and reads it in if it is not already there (having checked for space availability). If the buffer is full, the last record is evicted and written to mass storage. IOGETR calls a few utility subroutines and the links are shown in Figure 9.3.

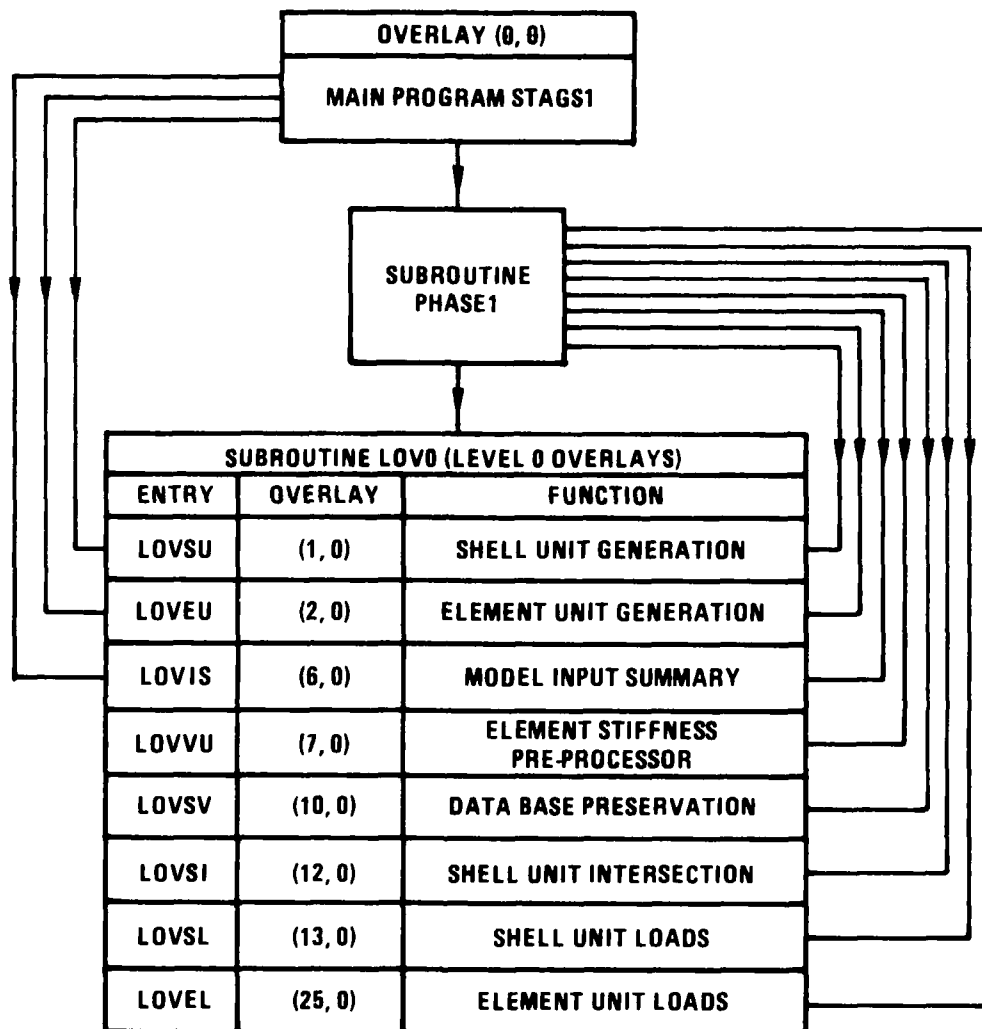


Figure 3.1 Primary Overlay Structure of STAGS1

5407-101

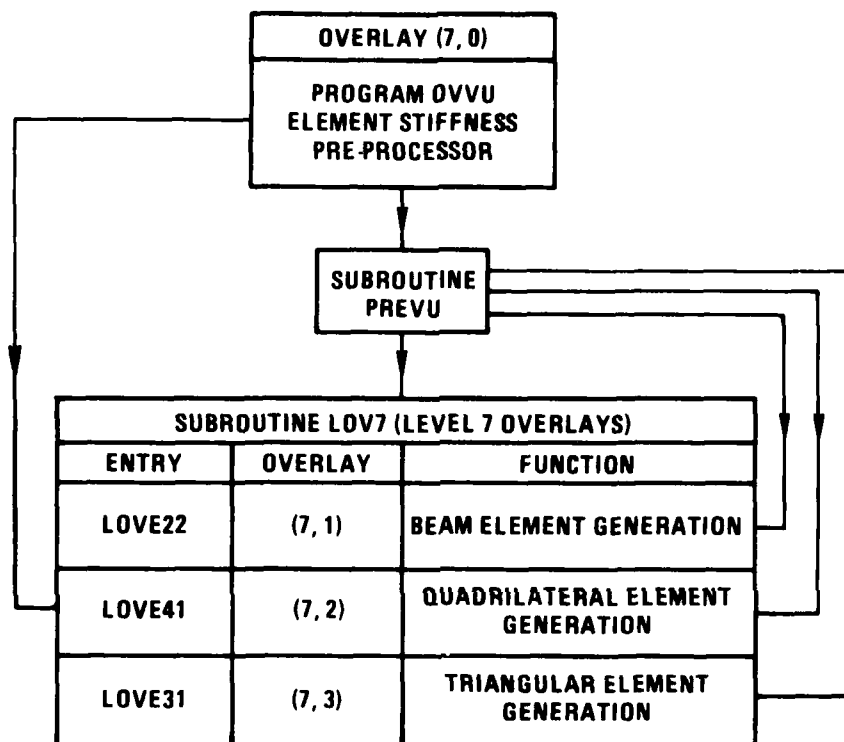


Figure 3.2 Secondary Overlay Structure of STAGS1

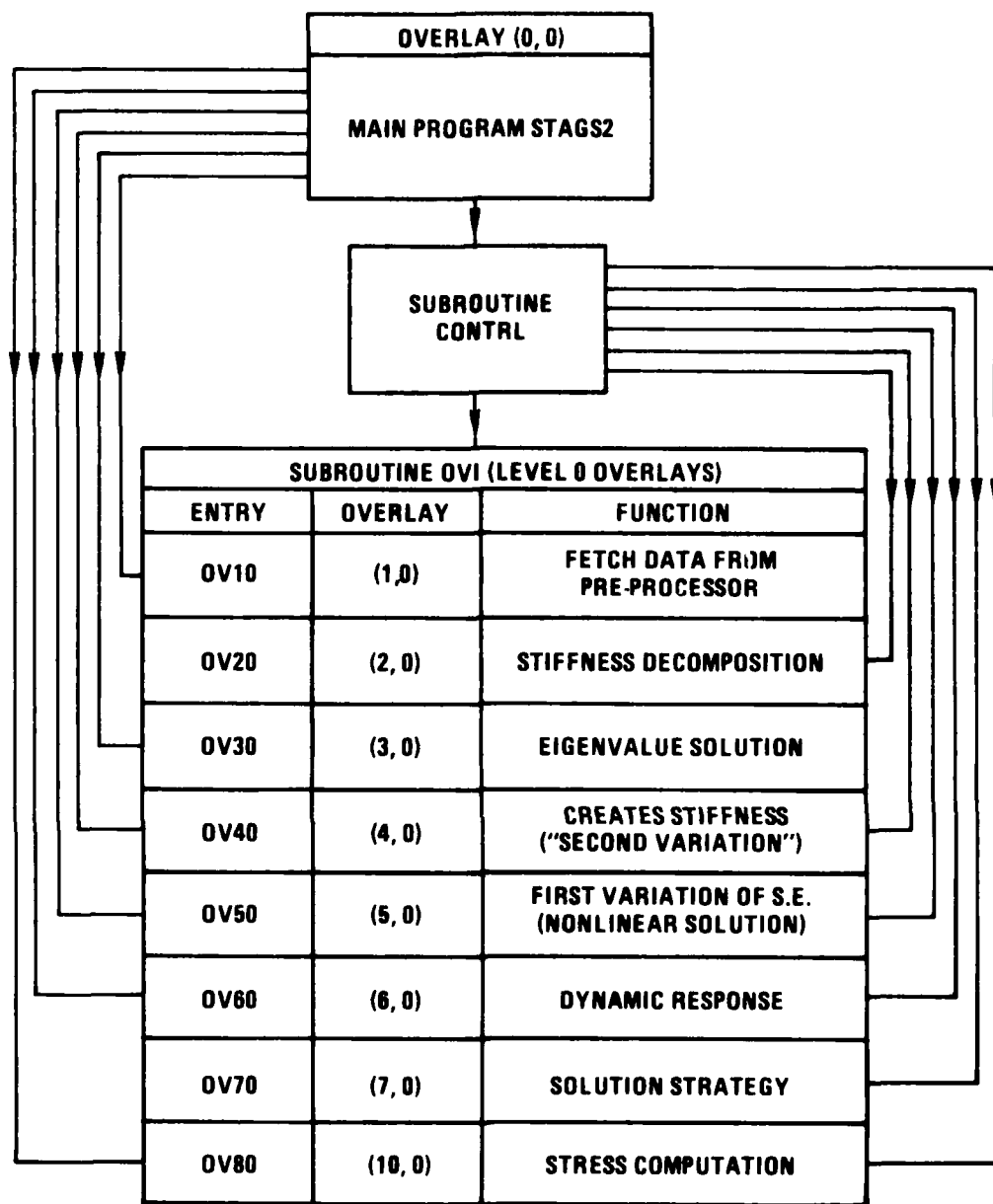


Figure 3.3 Primary Overlay Structure of STAGS2

OVERLAY	ENTRY	CALLED FROM:	FUNCTION
(5, 1)	OV51	OV50	PLASTICITY CALCULATIONS
(6, 1)	OV61	OV60	PLASTICITY CALCULATIONS IN DYNAMICS
(10, 1)	OV81	OV80	STRESS/STRAIN CALCULATIONS FOR 1-D ELEMENTS
(10, 2)	OV82	OV80	STRESS/STRAIN CALCULATIONS FOR 2-D ELEMENTS

Figure 3.4 Secondary Overlays in STAGS2

5407-104

4.0 FUNCTIONAL DESCRIPTION

The purpose of this section is to provide a detailed overview of the major capabilities and analytical methods used in STAGSC-1.

4.1 ANALYSIS OPTIONS

As outlined in the Introduction (Section 1), STAGSC-1 is a general purpose, thin-shell, structural analysis program, designed principally for the nonlinear static and dynamic analysis of thin shells. There are seven different analysis options available to the user.

- o Linear static analysis
- o Bifurcation buckling analysis from a linear stress state
- o Small vibrations (stress free state)
- o Nonlinear static analysis
- o Bifurcation buckling analysis (nonlinear stress state)
- o Small vibrations (linear or nonlinear stress state)
- o Transient response analysis (linear or nonlinear)

4.1.1 LINEAR STATIC ANALYSIS

Although there are numerous general purpose finite element programs which provide thin shell elements for linear static analysis, STAGSC-1 has a number of features which make it an attractive choice for this application. Specifically, these are: (i) built-in geometries for regular shell surfaces such as cylinder, cone, flat plate, torus, sphere, etc.; (ii) user subroutine capability for defining surface deviation with respect to some reference surface; (iii) discrete surface stiffeners (both orthogonal and skewed); and (iv) multilayer shell wall construction. Thus, complex shell geometries can be modeled with relative ease.

Loads may be applied directly at mesh points (defined by "row" and "column" numbers--Section 4.2) as forces and/or moments, as line loads or moments or as surface tractions. Their directions may be specified in global or local surface directions. Thermal loads can also be generated by specifying reference surface temperatures in a user coded subroutine. Temperature variation in a stiffener cross-section may be prescribed (but no variation is permitted through the shell wall thickness). Body forces can be specified by means of acceleration vectors in both translation and rotation. Displacement boundary conditions may be applied as discrete constraints at interior or boundary mesh points or by specialized conditions (e.g., simple supports, clamped, etc.) along shell boundary edges.

The range of basic capabilities for static analysis is therefore quite adequate for simple stress/displacement analysis of thin shells and includes unique features (such as the geometric deviations from a reference surface) which are a definite incentive for its practical use.

4.1.2 BIFURCATION BUCKLING ANALYSIS

The analysis of bifurcation buckling of shells has been an important capability in STAGS since it was introduced in an early version in about 1970 (see Figure 1.1). This part of the program is therefore one of the most highly developed and would probably be a common reason for selection by a potential user.

Bifurcation buckling can be investigated for structures which have linear or nonlinear prebuckling stress states. An example of linear prestress is given by a flat plate with in-plane loading only. Bifurcation buckling is then defined as the value of the load at which a laterally displaced configuration can also be in equilibrium (secondary loading path). A shell of revolution, such as a shallow spherical cap, will exhibit nonlinear prebuckling behavior. Under antisymmetric loading, the shell softens or stiffens depending on the loading direction (e.g., external or internal pressure). Bifurcation buckling may then occur as a nonsymmetric deformation mode. Figure 4.1 shows the characteristic behavior of systems which exhibit linear and nonlinear prebuckling primary load paths.

For a simple linear prebuckling problem, the eigenvalue analysis provides the multiplier by which the basic applied load system must be factored to obtain the critical load level. STAGS allows for the specification of two independent load systems $\{F_A\}$ and $\{F_B\}$ which are characterized by multipliers P_A and P_B . Thus, for example, a cylinder with internal pressure and axial compression will require the axial load to be designated as System A and the pressure as System B. For a given pressure loading, the total magnitude of the two load systems will be

$$\{F\}_{TOTAL} = \lambda P_A \{F_A\} + P_B \{F_B\} \quad 4.1$$

where λ is the eigenvalue at bifurcation.

The case of bifurcation buckling analysis with a nonlinear prebuckling stress state is an option with far less general applicability. However, the more sophisticated user who needs to perform a nonlinear collapse analysis for a general shell can take advantage of a number of subtleties which the nonlinear bifurcation capability provides. The STAGS theoretical manual [3] offers a very detailed and thorough discussion of bifurcation buckling and collapse analysis. Almroth and Brogan [5] give a number of examples in which the nonlinear collapse loads are calculated and compared with bifurcation buckling loads obtained using linear prebuckling analysis. It is shown the linear bifurcation loads may be greater or less than actual nonlinear collapse loads. For example, an elliptic cone undergoing uniform end shortening will collapse at a load over twice that predicted by linear bifurcation, while a cylindrical panel with its ends simply supported ("venetian blind" model) will collapse at a load five times smaller than the bifurcation load. The usefulness of the nonlinear bifurcation analysis appears to be in its application as an adjunct to a full nonlinear collapse analysis. If nonlinear collapse analysis is performed on an imperfection sensitive structure, the analysis may fail due to ill-conditioning of the equations at some load step. A bifurcation buckling analysis carried out at this point will yield a buckling mode which will indicate the type of imperfection which will direct the solution into the secondary path (see Figure 4.1(b)). Another practical

situation is where a nonlinear analysis is carried out only up to a design load. A nonlinear bifurcation analysis at this point will provide an estimate of the remaining margin to collapse.

4.1.3 SMALL VIBRATION ANALYSIS

The capability of STAGSC-1 with respect to vibration mode analysis is very similar to the bifurcation buckling capability. An eigenvalue solution for vibration modes and frequencies may be obtained for a stress-free structure or for a linear or nonlinear stress state. This is particularly relevant for the analysis of shell structures where the presence of pressure loading (internal or external to the shell) is common prior to dynamic loading.

In the case of vibration all eigenvalues will be positive, whereas in the case of bifurcation buckling negative eigenvalues may be obtained (e.g., in a shear loaded plate).

In both the bifurcation and vibration analysis options, it is possible to define by input a uniform stress state directly in terms of direct and shear stress resultants as an alternative to the generation of such stress states by means of applied loads, displacements or temperatures.

STAGSC-1 also permits the user to specify concentrated (lumped) masses directly at node points. It should be noted that lumped rotational inertias cannot be specified.

A further limitation appears to be that vibration modes for unsupported structures ("free-free") cannot be determined because the eigensolver needs to solve the system equations. Rigid body constraints will permit a solution to be obtained.

4.1.4 NONLINEAR STATIC ANALYSIS

Both geometric (large displacements) and material nonlinearities can be included in a STAGSC-1 analysis. The geometrically nonlinear analysis is based on the following;

- A. Small strain based on engineering stress and strain relationships ($\epsilon < 0.1$)
- B. Strain-displacement equations retaining nonlinear rotation terms (moderate rotations < 0.3 radians)
- C. Incremental solution of equations with iterations within each increment using the modified Newton-Raphson method.

Material nonlinearities considered are due to plasticity only. No creep or viscoelastic behavior is incorporated in STAGSC-1. Plasticity is handled according to the White-Besseling theory [7]. This is equivalent to elastic-perfectly plastic behavior, bilinear kinematic hardening or multilinear hardening depending on the number of plastic parameters specified. The theory is outlined in greater detail in Section 4.4.

The plastic strains are computed and used to generate pseudo-force vectors, i.e., an initial strain method is implemented.

4.1.5 TRANSIENT RESPONSE ANALYSIS

This capability represents one of the major strengths of the STAGSC-1 program since, like the bifurcation analysis, it has been under development for a number of years. The program can solve transient problems with a wide range of excitation using one of five different transient integration operators. System damping may be introduced as Rayleigh viscous damping, with constant stiffness and mass matrix multipliers, plus an additional contribution from velocity dependent forces. In addition, the full range of nonlinearities available for static analysis can be utilized in transient response.

Forcing functions may be specified in terms of nodal loading or displacement patterns, with time dependencies either (a) according to certain specified formats or (b) input through a user coded subroutine (FORCET). The specified formats are:

- o piecewise linear function
- o trigonometric function
- o exponential decay

In addition, initial velocities and displacements can be specified for any degrees of freedom.

The integration operators implemented in STAGSC-1 are as follows:

- o explicit (central difference)
- o implicit (trapezoidal, Gear 2nd and 3rd order, and Park's method)

The time step for the central difference method is, of course, fixed and must be selected by the user. For the implicit methods, either a fixed time step may be used or there is an internal algorithm for automatic time step control. The automatic feature is, however, presently regarded as experimental by the developers.

4.2 SURFACE AND MESH GEOMETRY

The STAGSC-1 philosophy for developing the shell geometry and finite element discretization contains some rather unfamiliar concepts and terminology. A central notion is that of the so-called "shell unit". This can refer to the description of a specific portion of the shell surface or to the whole surface. The complete shell may be defined using up to thirty shell units. In addition, or as an alternative, the structure can be defined in terms of an element unit. The basic distinction between these two concepts is that the shell unit defines a geometric surface with a rectangular grid work mapped onto the surface, while the element unit is actually a direct assemblage of elements which may or may not define a shell.

The shell unit grid is then overlaid with a mesh of finite elements which may use all gridpoints of the shell unit or only a subset. This concept allows the use of a library of standard shell geometries (e.g., cylinder, sphere,

torus, etc.) which may then be adapted to model cutouts or stiffened areas by the appropriate omission or addition of elements. Discrete stiffeners may also be attached along arbitrary paths on the shell surface.

4.2.1 SURFACE GEOMETRY LIBRARY

There are eleven standard geometries in STAGSC-1 which are selected using the input key ISHELL. The geometries are listed in Table 4.1

Each geometry has four edges, two of which may be subsequently joined to each other to form a closed surface (except for the rectangle and quadrilateral). Alternatively, edges may be joined to other shell units or may have boundary conditions applied.

4.2.2 USER DEFINED SURFACE GEOMETRY

This may be accomplished using the user-coded subroutine LAME. This subroutine may define global coordinates for the surface and their first order derivatives if flat elements are being used. This is currently the only usable option but, anticipating the introduction of curved elements, the user can define directly the coefficients of the first and second fundamental forms or, alternatively, all the derivatives necessary for internal computation of the coefficients.

4.2.3 SURFACE GRID AND ELEMENT MESH

Given that a reference surface geometry has been defined, a gridwork must be mapped onto the surface. In its simplest form, this is accomplished by specifying numbers of rows and columns which generates a regular gridwork in terms of the surface coordinates. Additional options are:

- o irregular grid spacing by means of definition of different segments
- o grid definition by user subroutine IUGRID

The element mesh is conceptually distinct from the surface grid. This is specified separately and may be defined in a number of ways. In its simplest

form, the element mesh is identical with the surface grid in that all grid points define element nodes. Alternatives are:

- A. Irregular mesh in which cutouts can be defined.
- B. Specialized mesh in which grid points are used selectively and a mesh of varying refinement can be obtained.
- C. Subregion or "patch" concept in which groups of elements are defined within certain row and column boundaries. This allows use of different element types in different regions of the shell surface.

4.2.4 ELEMENT UNITS

An element unit can be defined as a "stand-alone" unit which describes the total structure or it may be used in conjunction with a shell unit. In the latter case, element unit nodes can be nodes on the shell unit or separately defined (auxiliary) nodes or a combination. Thus, parts of the structure which are not shell-like can be connected to the shell. This is in addition to the capability which exists in shell units for specifying stiffeners on the shell surface.

Node geometry for the element unit must be defined individually for each node or by means of the user subroutine USRPT or by a combination of both. No other options are available.

The directions of the degrees of freedom can be separately defined for the auxiliary nodes in the element unit.

4.3 FINITE ELEMENT LIBRARY

The core of the finite element library in STAGSC-1 is the series of triangular and quadrilateral shell elements based on the Clough-Felippa quadrilateral bending element [8]. Since these are all flat elements, the actual curved shell geometry is always approximated by a faceted surface. This has implications for interelement compatibility which will be discussed later.

In addition to the shell elements there are membrane versions of the elements and also a series of beam elements designed to be compatible with the shells. STAGSC-1 also has provision for a series of general linear and nonlinear springs and also transition membrane and plate elements. The latter are designed for regions of changing mesh refinement. Neither the springs nor the transition elements were implemented in the version of the program under evaluation. In total, there are twenty elements currently available in STAGSC-1, of which six are beam elements and fourteen are membrane and shell elements. Table 4.2 provides a summary description of the elements implemented.

The bar and beam elements are fairly standard except for 220 and 221 which have quadratic shape functions for twist. The inclusion of the center node makes them compatible with the majority of the shell elements in STAGSC-1. Also, the center node provides better results when displacements (rotations) are relatively large. For a general thin shell analysis program such as STAGSC-1, the single most important aspect of the program has to be the properties and performance of the shell elements themselves. As has already been mentioned, STAGSC-1 does not, at present, have available a curved shell element and this introduces inevitable incompatibilities. However, considerable effort has been spent by the developers on minimizing these shortcomings.

The basis for both the triangular and quadrilateral elements is the Clough-Felippa triangle (LCCT-12 in Reference 8). This is a triangular bending element consisting of 3 sub-elements with interior nodes condensed out. The lateral displacements have therefore a piecewise cubic distribution. The addition of in-plane degrees of freedom and membrane shape functions gives rise to the quadrilateral element. Reference 8 describes a quadrilateral bending element (Q-19) which is derived from four LCCT-12 elements with the internal freedoms condensed out and the mid-side rotations on the four other edges constrained to be the average of the adjacent nodal components. The 420 (QUARC) elements are variants of the Q-19 element with the addition of translational freedoms at the mid-side nodes parallel and normal to the edges. Table 4.2 gives details of the resulting shape functions.

The 410 (QUAF) elements were specially developed to remove the displacement incompatibility which exists when flat shell elements do not lie in one plane. If edge displacements are to be compatible, then the transverse displacement shape functions must be of the same order as the in-plane functions. The in-plane functions must therefore be cubic. This was accomplished in element 410 by introducing a normal rotation at each of four corners. Element 411 carried this one step further by introducing 2 rotations at each corner, thus permitting individual rotation of each adjacent side and thereby permitting shear strain at the corner. In addition, tangential displacements at mid-side nodes are also included in this element.

4.4 CONSTITUTIVE RELATIONSHIPS

The number of constitutive behavior models available in STAGSC-1 is somewhat limited. Orthotropic elastic behavior and plasticity are the two major options. Creep or viscoelasticity are not available in the present version of STAGSC-1.*

Elastic properties are specified with respect to *principal* material directions for an orthotropic material. Specialization to the isotropic case is trivial. Plasticity is based on the White-Besseling (mechanical sublayer) model. The theoretical manual [3] discusses various types of plastic constitutive behavior and describes the White-Besseling model in some detail. An advantage of the W-B model is that the uniaxial stress-strain curve can be represented with fair accuracy by choosing a sufficient number of components (or "sublayers"). The minimum number of components (2) automatically yields the bilinear kinematic hardening theory.

The input of material properties is based on the specification of a material type number. Up to 30 different material types may be specified. In this way different material properties can be assigned to different regions of the structure (as defined by different shell units). Also, multilayered,

*Development of a creep version is being sponsored by NSRDC. The creep implementation is to be the same as in the BOSOR 4 program [4].

composite-shell-wall construction can be simulated by defining different orthotropic properties for each layer. There is no provision for incorporating temperature dependence of material properties. Although the users manual [2] states otherwise, material properties cannot vary continuously through the wall thickness.

The elastic properties may also be input through a user written subroutine WALL. This gives the user the ability to vary the elastic coefficients continuously over the shell surface. The elastic-plastic stress-strain data, however, can only be input via cards. Any variation throughout the structure must be defined by varying the material type.

In summary, the constitutive capability in STAGSC-1 is adequate for shell structures operating in an environment where temperatures are below the creep range for the material. A simplified approximation to elastic temperature dependence could conceivably be achieved through the user subroutine WALL by correlating temperature, spatial position and elastic properties.

4.5 LINEAR AND NONLINEAR ANALYSIS

STAGSC-1 is primarily a tool for nonlinear analysis although a purely linear analysis option is available and is very economical. Therefore, linear static and dynamic analyses may be appropriately performed for shell problems using STAGSC-1 because of its many features which facilitate the analysis of stiffened or unstiffened shells (see Sections 4.1, 4.2, 4.9 and 4.13). However, the bulk of the developmental effort behind STAGSC-1 has been devoted to its nonlinear solution algorithms and to the implementation of a finite element library. It is in this context that the program must mainly be discussed.

The basic method of equation solving is the modified Newton-Raphson method (MNR), with periodic updating of the stiffness ("refactoring" in STAGSC-1 terminology). The program is self-adaptive to a certain extent in that it can switch to a full Newton-Raphson method (FNR) if indicated by convergence behavior. It must be pointed out, however, that the handling of nonlinearities due to plasticity is by the initial strain method. Thus, the

stiffness matrix is never modified to reflect changes due to the current material state. In these circumstances, the method must be viewed as a hybrid technique.

In order to discuss the solution procedure more specifically, some basic equations will be developed. For a static, nonlinear problem the equations of equilibrium may be written as a Taylor expansion of the total force vector $[F(x)]$ (sum of applied, restoring and residual force vectors) about the currently deformed state;

$$\begin{aligned} \{F(x_{n+1})\} &= \{F(x_n)\} + \left. \frac{\partial \{F\}}{\partial \{x\}} \right|_{\{x\}=\{x_n\}} (\{x_{n+1}\} - \{x_n\}) + \text{terms of higher order} \\ &= \{F(x_n)\} + \left. \frac{\partial \{F\}}{\partial \{x\}} \right|_{\{x\}=\{x_n\}} \{\Delta x\} + \text{terms of higher order} \\ &= 0 \end{aligned} \tag{4.2}$$

In this notation, the derivative $\left. \frac{\partial \{F\}}{\partial \{x\}} \right|_{\{x\}=\{x_n\}}$ is the negative of the nonlinear stiffness matrix $[K(x_n)]$.

A fundamental concept of the STAGSC-1 program is to treat the product vector $[K(x)]\{\Delta x\}$ as a nonlinear operator L acting on the incremental displacements. Thus, equation 4.2 becomes:

$$\{F(x_{n+1})\} = \{L(x_n)\} - \{R\} + (\text{higher order terms}) = 0 \tag{4.3}$$

where the operator L is the first derivative of the strain energy functional. The nonlinear stiffness matrix $[K(x)]$ is then the first derivative of L , $[L'(x)]$. The significance of this goes far beyond the formal statement of the equilibrium conditions because the nonlinear solution algorithm is based on the direct formulation of $\{L'(x)\}$. This has important advantages in the implementation of the Newton-Raphson method. This may be stated in the following terms

$$\begin{aligned} \{x_{n+1}\} &= \{x_n\} - [L'(x_n)]^{-1} \{F(x_n)\} \quad \text{or} \\ \{x_{n+1}\} - \{x_n\} &= [L'(x_n)]^{-1} (\{R\} - \{L(x_n)\}) \end{aligned} \tag{4.4}$$

Equation 4.4 implies a full update of the stiffness matrix and re-solution (refactoring in STAGS terminology) at each iteration. Basically, a modified Newton-Raphson procedure is implemented which performs a refactoring of the stiffness only when indicated by convergence criteria. The MNR algorithm implemented in STAGSC-1 can be written then as

$$\{x_{n+1}\} - \{x_n\} = [L'(x_n)]^{-1} (\{R\} - \{L(x_n)\}) \quad 4.5$$

where $[L(x_n)]$ is represented by the factored stiffness matrix obtained at some previous iteration or step. The operator $L(x_n)$ is, however, defined for the current solution vector $\{x_n\}$ since it is formed directly as a vector.

The nonlinearities included in the computation of $L(x_n)$ are purely geometric and plasticity effects are handled separately as pseudo-force contributions to the loading vector $\{R\}$. Thus, plasticity corrections are computed after each MNR iteration and the modified vector $\{R\}$ is then used in the next iteration.

Figure 4.2 illustrates the MNR algorithm and plasticity solution in an overall sense as implemented in STAGSC-1. It should be pointed out that this is a conceptual flow chart and does not represent the actual program flow.

The parameters over which the user has control at the time of input are

- o total number of times the step size may be cut (NCUT)
- o total number of refactorings allowed (NEWT)
- o initial solution estimate (NSTRAT)
- o convergence tolerance (DELEX)
- o relaxation factor (WUND)

By the use of a negative value of NEWT, refactoring can be enforced at desired load step intervals (including every iteration). Note: the program automatically doubles the load step after two successive steps with single iteration convergence.

Tillerson, Stricklin and Haisler [9] in their excellent survey of numerical methods for solving nonlinear problems, conclude that the MNR method is probably one of the most widely used for general nonlinear problems and that for structural problems it is best suited for those in which geometric nonlinearities predominate. Some doubts are expressed about including material nonlinearities because of the problem of unloading. The situation can arise using MNR where elastic unloading is not correctly handled because the factored stiffness corresponds to a "tangent" stiffness based on a prior loading step. On the other hand, Bushnell [10] describes a subincremental plasticity formulation in which plasticity calculations are performed outside an inner Newton-Raphson loop. The question of plastic unloading was not discussed, however.

The STAGSC-1 method of plasticity calculations between MNR iterations appears therefore to raise some questions about its use in dynamic plastic or static cyclic loading problems.

The STAGSC-1 implementation of MNR seems to be basically efficient in that the direct calculation of the vector $\{L(x)\}$ (eqs. 4.4, 4.5) is analogous to the method of calculating a pseudo-force vector to account for nonlinearities. Moreover, the strategy parameters available to the user provide a degree of control over the MNR procedure which is not available in other programs, e.g., ADINA [11,12].

4.6 SOLUTION OF EQUATIONS

STAGSC-1 employs a conventional Cholesky triangular decomposition with forward and backward substitution for solution of equations. Storage is based on the "skyline" vector concept in which no zero elements beyond the last non-zero element in a row are stored. The skyline vector stores the location of the last non-zero element in a given row. The procedure is outlined in the theoretical manual [3] and discussions may be found in the literature, e.g., Bathe and Wilson [13]. No other solution options are currently available in the program.

4.7 EIGENVALUE ANALYSIS

Eigenvalue analysis is required for both buckling and vibration analyses. In principle, there is no fundamental difference between the two eigenvalue problems. However, in practice, the bifurcation buckling problem requires solution normally only for the smallest buckling load. For certain types of buckling (e.g., pure membrane shear) there can be eigenvalues which are equal but opposite in sign. For vibration problems, the eigenvalues must always be positive and a large set of eigenvalues and eigenvectors may need to be determined. Thus, there is a need to employ a method which is suitable for both types of problem and which is relatively "rugged," i.e., capable of yielding satisfactory solutions for a wide variety of modeling situations. The method implemented in STAGSC-1 is basically the subspace iteration method. This is described in depth by Bathe and Wilson [13] and somewhat sketchily in the theoretical manual [3]. Curiously, the manual does not state explicitly that this is the technique being used.

Subspace iteration, as described in Ref. [13] simultaneously obtains a reduced number of eigenvectors. An initial choice is made of a set of preliminary independent vectors X which are said to span a subspace of the complete set of M eigenvectors. A single inverse iteration step is performed in which a new set \bar{X} is obtained from solution of the equation

$$K\bar{X} = M\bar{X}, \quad 4.6$$

where both K and M are of order $m \times m$ and X and \bar{X} are of order $m \times p$. A new eigenvalue problem is then solved in terms of the reduced matrices \bar{K} and \bar{M} which are obtained from

$$\text{and } \bar{K} = \bar{X}^t K \bar{X} \quad (p \times p) \quad 4.7$$

$$\bar{M} = \bar{X}^t M \bar{X} \quad (p \times p) \quad 4.8$$

$$\text{The reduced eigenvalue problem can be stated as } \bar{K}Q = \Lambda \bar{M}Q \quad 4.9$$

where Λ is the matrix of eigenvalues.

An improved estimate of the subspace vectors X is then obtained as

$$X = \bar{X}Q \quad 4.10$$

at which point the whole process is then repeated.

STAGSC-1 implements this method with some modifications. As is pointed out by Bathe [13], several inverse iteration steps may be performed before solving the reduced eigenvalue problem (in order to reduce the number of eigensolutions performed). This is done in STAGSC-1, with orthonormalization of the subspace vectors with respect to K or M at each step of the iteration. Normally, two inverse iterations are performed at the start and three (per eigensolution) after the first reduced eigensolution. Two other extra features are incorporated. The first is the introduction of a spectral shift parameter σ in the inverse iteration sweep. Thus the solution obtained is for the equations

$$[K - \sigma M] \bar{X} = MX \quad 4.11$$

and the eigenvalues obtained for the reduced system are

$$\Lambda^* = \Lambda - \sigma I \quad 4.12$$

The second modification is to accelerate the convergence of the orthonormalized vectors by means of Chebyshev polynomials. This step is performed before the solution of the reduced eigensystem. According to the developers, this technique has been known to be not always effective, particularly with some computer installations. Its use is controlled internally and depends on the convergence. Figure 4.3 provides a qualitative flow chart of the major functions in the eigensolution system. The method of solving the reduced eigenvalue problem is a combination of Householder's tridiagonalization transformations with the QR method of extracting eigenvalues.

4.8 TRANSIENT INTEGRATION

Transient dynamic analysis for linear and nonlinear shell structures is one of the major capabilities in STAGSC-1. The numerical integration with respect to time of the equations of motion can be accomplished for general time histories of applied load or displacement. The program contains a library of five different algorithms for performing the transient integration which consists of one explicit scheme (central difference) and four implicit methods. The implicit schemes are as follows:

- A. Trapezoidal (Newmark, $\mu = 1/4$)
- B. Gear's second order
- C. Gear's third order
- D. K.C. Park's method

It is clear at the outset, that for such an array of options for implicit time integration to be useful, the program user needs to possess a greater than average level of sophistication in order to make an appropriate choice. The users manual [2] seeks to minimize this difficulty by generally recommending the trapezoidal rule for linear structures and the Park method for nonlinear structures. The theoretical manual [3] discusses the background of the central difference (explicit) method as well as the implicit methods. In order to aid in the discussion of these methods, Figure 4.4 has been provided in an attempt to make clear the basic differences between the methods available in STAGSC-1 and other methods in common use. The characteristics of the STAGSC-1 methods with regard to stability, numerical damping and frequency distortion (dispersion) are summarized in Table 4.3. Although the central difference method has been implemented, it is not particularly well suited to its use in shell problems where lower frequency modes usually dominate the response of the system. The low stability limit requires a very small time step which can largely offset the inherent efficiency of the explicit approach. For the majority of problems therefore, the concern must be with the relative merits of the four implicit methods provided. With the exception of Gear's 3rd order method (G_3), the implicit methods are unconditionally stable for linear conservative systems. This is referred to in the literature as A-stability [15,16]. G_3 has a very small region of instability for a combination of

small time steps, low frequency and low damping. For non-conservative systems, G_2 , G_3 and the K.C. Park method (KCP) are conditionally stable as are the Wilson- θ and Houbolt methods. The trapezoidal method is not stable under these circumstances.

The question of greater interest to a potential user of STAGSC-1 is the performance of these methods in the context of nonlinear response. The stability of time-integration operators for nonlinear structural dynamics problems has also been discussed in the literature (e.g., Refs. 16 and 17). Implicit operators which are unconditionally stable for linear problems have been observed to exhibit instability in some nonlinear problems. The inference has been drawn that the stability properties of the implicit operators are lost or modified in the nonlinear regime. Reference 17 (Belytschko and Schoeberle) presents an energy-based proof of unconditional stability for the Newmark- β method ($\beta=1/4$) for the case of material nonlinearity. The proof is subject to the restriction that the internal energy must increase monotonically with strain and remain positive-definite. The assumption is made that the unconditional stability is preserved when geometric nonlinearities are also present provided that the requirements on the internal energy are still met. It is concluded that the loss of stability in some applications is due to errors accumulated during the solution process and not to the integration operator per se.

A somewhat different conclusion is arrived at in Reference 15 (Park) in which nonlinear stability equations for a number of implicit operators are developed. These criteria apparently include the character of the nonlinearity (e.g., hardening or softening). Stability boundaries are obtained for the Houbolt, Wilson, Park and Newmark- β methods. It is concluded that the approximations inherent in the solution procedures (initial-strain or tangent stiffness methods) are responsible for the departures from unconditional stability.

Thus, in a sense, both evaluations arrive at the same conclusion (i.e., unconditional stability is affected by solution approximations) but the implications are quite different.

It would appear that on the basis of stability the methods provided are probably quite satisfactory for nonlinear analysis, but the user ought to be aware that any given problem should be evaluated with respect to its likely nonlinear behavior when choosing the method of integration. With respect to accuracy, the four implicit methods are comparable. It does appear, for a nonlinear response that the damping and dispersion of KCP are better than the Houbolt method.

4.9 USER CODED SUBROUTINES

As may be expected in a program developed for the solution of nonlinear problems, STAGSC-1 has a significant capability for the user to provide his own coding for problem specification and execution. Thus, there are a total of thirteen dummy subroutines in the program for which the user can provide FORTRAN coding. Some of the subroutines provide additional capability while others are mainly used to reduce the bulk of input data. Each of the subroutines will be briefly described and commented on.

- A. CROSS--This routine defines cross-section dimensions and material properties for beams and stiffeners. Geometry and material type can be specified as functions of spatial coordinates. Used in addition to, or instead of data cards.
- B. FORCET--Describes variation of load factor with time for load system A or B. Used instead of data cards.
- C. UGRID--Allows independent specification of grid coordinates for mesh generation in terms of reference surface geometry. Necessary for quadrilateral elements in a quadrilateral plate.
- D. LAME--Allows definition of a shell unit geometry not included in the twelve built-in options.
- E. SKEWS--Defines orientation on shell surface of the attachment line of a discrete stiffener which does not follow the reference surface gridlines.

- F. TEMP--This is the only means by which temperatures can be specified. Temperatures can vary with surface coordinates and through a stiffener cross-section.
- G. UCONST--Defines linear constraint conditions using Lagrange multipliers. Must not be used with explicit integration.
- H. UPRESS--Defines space and time variation of pressure loads. Pressure may be "follower" or "live" loading.
- I. USRLD--Defines spatial variation of loads including initial displacements and velocities. Saves preparation of bulky sets of data cards.
- J. USRELT--Defines element connectivity for an element unit. Essential when there are more than a few elements.
- K. USRPT--Defines node point geometry for element units. Essential when there are more than a few nodes. May also define additional points in a shell unit.
- L. WALL--Defines shell wall construction (layers, composite material, stiffeners, wall thickness) and material properties which may vary over the reference surface. Material properties may not vary within a layer. Does not apply to plasticity data.
- M. WIMP--Defines small, geometric perturbations of the shell from the reference surface in terms of first spatial derivatives.

4.10 RESTART CAPABILITY

For practical, nonlinear structural analysis, a useful computer program must include a flexible restart capability. Ideally, the user should be able to restart the analysis at any desired point so that a different loading strategy may be used or perhaps an eigenvalue solution obtained. STAGSC-1 has such a capability. At the user's option, three separate files may be saved for

0918B-84B:2
(S3034) 20

restart (TAPE22, 23 and 24). The solution is saved on TAPF22 while TAPE 23 and TAPE24 contains the stiffness matrix and the factored stiffness matrix. Normally, upon restart, refactorization occurs but the user can override this by using TAPE24. The contents of TAPE22 include displacements, velocities and plastic strains, depending on the type of analysis. Additionally, stresses, strains and stress resultants can be saved on the same file for post-processing.

STAGSC-1 provides the option to save data either at every load (time) step or from the final three steps. This could be improved by permitting saving at specified load step intervals as in the MARC program. The advantage of this is that the flexibility to restart at a number of stages is retained but with substantial savings in file space. This can be a significant factor for the analysis of a real nonlinear problem.

4.11 INPUT AND OUTPUT

Input and output are often the basis for user attitudes towards a structural analysis program. Factors which influence these attitudes are many but the major ones are

- o logical input flow
- o input format (free form or otherwise)
- o ability to provide comments
- o ease of generating repetitive data
- o understandability of input instructions
- o control over output
- o format and labeling of output

A user's reaction to the input required for a new program is often influenced by experience with other programs which, of course, may place the new program in a good or bad light depending on the previous experience. Nevertheless, the concept has arisen of "user friendliness" as a measure of the attitude which a program may develop in the user. The meaning of this is obviously subjective, but in such a context STAGSC-1 would probably rate as average. Ease of input depends strongly on the logical flow of the input stream and the

understandability of the input instructions. STAGSC-1 input is quite logical and if the input manual is followed carefully a new user may expect to obtain a set of input which will execute successfully after, perhaps, a couple of tries. However, it is apparent that both the input logic and the input instructions are strongly linked to the programming and are not based on some concept of what might constitute "good" input. This is not necessarily a criticism of the input but more a description of the type of input. Excellent features are the free-form input and the ability to include user commenting. STAGSC-1 input would lend itself easily to the interactive mode since the instructions used in the manual are already in the required form.

If the user selects any of the twelve standard shell units, the input required for the generation of bulk data is minimal. Also, the constraints that provide compatibility between shell units are easily imposed. For other geometries, the user written subroutine LAME may be used to define the reference surface. For element units, the choice is either individual input of each node and element or automatic generation using user subroutines USRPT and USRELT. Individual node and element input is unacceptable for more than a few elements so the use of subroutines is almost always required. An improvement would be the inclusion of simple linear mesh generators and element pattern generators to provide a rapid means of generating meshes for a large class of problems.

For load input, the ability to input both concentrated and distributed loads either individually at mesh points or along specified rows and columns is a good basic feature. This, together with the user subroutines USRLD and UPPRESS for generating loads provide a generally satisfactory capability. For element units, not all load input options are yet operational, e.g., distributed forces and moments.

Output control may be exercised separately on displacements, strains, stresses, stress resultants, stresses and strains at yielded points and forces. The data for each shell unit is output as a block. However, the frequency may be specified differently for each output quantity (displacements, stresses, etc.) and also for each shell unit. Based on some

limited experience, it seems that if different frequencies are specified for say stresses and displacements, both will be printed out at the higher frequency which is contrary to the manual.

In addition, selected stresses and displacements may be output at each load or time step. Thus, if it is desired to output data for a certain portion of the structure at certain load step intervals, the only means of doing this is to specify a special shell unit just for this region of the structure (since all displacements, etc., are output for a shell unit). This may be inconvenient and therefore some additional selectivity is needed to cater for such a situation.

4.12 POST-PROCESSING AND PLOTTING

Currently, post-processing with STAGSC-1 is only partially operational. Its developmental status is not yet comparable with that of the analysis program which is quite a serious disadvantage when performing nonlinear analysis. Moreover, in the case of a nonlinear analysis, the user often needs the ability to access the solution data file and perform his own post-processing directly. A typical requirement would be to extract inelastic strain histories from the solution and post-process them according to design code criteria, e.g., the ASME Boiler and Pressure Vessel Code, Code Case N-47. The necessary descriptions of the structure of the solution files are not available in the documentation however, so this option is unavailable to the user.

The STAGSC-1 post-processing program (STAPL) is executable in tandem with the analysis or separately by saving the post-processing file (TAPE22). STAPL has been developed from routines published by NASA [18] which provide deformed and undeformed geometry plots and also contour plots. The separate routines were merged by Anamet Laboratories [19] and further developed by Lockheed. The current range of capabilities listed in the user's manual [2] are as follows:

- A. geometry plots--deformed, undeformed and exploded (useful for mesh checking)

- B. contour plots--displacements, velocities, force residuals*,
eigenvectors, force resultants, strains, stresses, temperatures*,
masses*, initial conditions and loads.

The items marked with an asterisk are not yet operational according to the manual. Other features advertised which are also not operational are geometry plots showing only shell unit boundaries, solution quantities as vectors emanating from the nodes; and automatic plot scaling. Evaluation of STAGSC-1 plotting is not included in the scope of this report.

Other development work has included the interfacing of the GIFTS* interactive graphics package for mesh generation with STAGSC-1. This combination is currently being evaluated by ONR.

4.13 SPECIAL STAGS FEATURES

This section is intended to highlight those features of the STAGSC-1 program which serve to differentiate it from other finite element nonlinear structural analysis programs. To begin with, STAGSC-1 is the outcome of approximately thirteen years of development effort in an aerospace environment. It is this environment which has stimulated the development of a number of analysis programs for shells of revolution, e.g., BOSOR, DYNAPLAS, SATANS, etc. [20]. STAGSC-1 is an outgrowth of this effort which extends the capabilities to general, three-dimensional thin shells. Other finite element analysis programs (e.g., MARC) have incorporated shell elements in their element libraries but supposedly cannot match the greater efficiency of the special purpose shell programs.

Therefore, the basic advantage of STAGSC-1 is its emphasis on shell analysis. The inclusion of beam and spar type elements does not make it a natural choice for solely beam or truss types of structure, although it certainly is able to

*GIFTS is a finite element mesh generation and analysis program originally developed for the analysis of ship structures and supported by ONR.

perform such analyses. In this context one may pick out a number of features of the program which are probably unique to STAGSC-1. These will be discussed briefly in the remainder of this section.

A. Shell Unit Concept

This has already been introduced and described in Section 4.2. The distinguishing feature is the underlying grid on which the element mesh can be overlaid. This makes it possible to define a library of standard geometries with a minimum of input. Thus the mesh variability which may be required for a specific problem can be divorced from the generation of the surface geometry.

B. Initial Imperfections

The ability to specify an imperfect geometry as small perturbations to a basic reference geometry is a feature of great value in a program oriented towards shell buckling and collapse. To achieve this in a general purpose program, if possible at all, would probably require the writing of a special mesh generator for each problem. In STAGSC-1, even if the reference surface is not part of the library, the writing of the LAME subroutine for the reference surface and WIMP for the initial imperfections is likely to be the most convenient way of generating the data.

C. Layered and Composite Shell Wall Construction

Relatively complicated shell wall designs can be handled by STAGSC-1. The types which may be included are as follows:

- (1) multiple anisotropic layers
- (2) multiple fiberwound layers
- (3) walls reinforced by corrugated skin
- (4) wall properties defined by a shell wall stiffness matrix
- (5) any of the above with "smeared" stiffeners

Multiple anisotropic layers are specified by layer thickness, orthotropic elastic material properties and a principal direction for these properties. This can also be used for fiberwound materials where the layer properties are available. Corrugated skin reinforcement is modeled by trapezoidal shaped corrugations whose cross-section dimensions are input. The shell wall stiffness matrix method is available for layered composite walls whose overall stiffness properties are known.

D. White-Besseling Plasticity Model

This is not a commonly implemented constitutive model of plasticity although the Mroz model, to which it is related, is available in the PLANS program [20]. The user should be aware that although there is some evidence [21] to suggest that methods based on the mechanical sublayer concept model reversed loading behavior well for some materials, there is not as yet a substantial body of testing or analytical experience to validate its use fully. The potential user should therefore be prepared to perform his own validation for his application.

E. Library of Load-Time Histories

STAGSC-1 contains three specific load-time histories for transient integration. These are

- (1) trapezoidal variation
- (2) trigonometric variation--sinusoidal, cosine square impulse or cosine square ramp functions
- (3) linear ramp and exponential decay

These basic ingredients can model a significant variety of transients. However, more general forcing functions may require the user-supplied subroutine FORCET.

TABLE 4.1
SHELL SURFACE GEOMETRIES

ISHELL	Description	No. of Coordinates	Comments
2	Rectangular Plate	4	4 edge coordinates
3	Quadrilateral Plate	8	8 corner coordinates
4	Annular Plate	4	2 radii, 2 subtended angles
5	Cylinder	5	2 axial, 2 subtended angles, 1 radius
6	Cone	6	2 axial, 2 subtended angles, 2 radii
7	Sphere	5	2 meridional and 2 azimuthal angles, 1 radius
8	Torus	6	2 meridional and 2 axial angles, bend radius, cross-section radius
9	Elliptic cone or or Cylinder	7	2 axial, 2 angles, 2 major and 1 minor radii (similar cross- sections)
10	Paraboloid	6	2 axial, 2 angles, distances from apex to focus and to smaller end
11	Ellipsoid	6	2 meridional and 2 azimuthal angles, major and minor radii
12	Hyperboloid	7	2 axial, 2 angles, 3 coordinates to define asymptote

TABLE 4.2
SUMMARY OF ELEMENT LIBRARY

Element	Type	No. of D.o.F.	Type of D.o.F.	Order of Shape Functions	
				In-Plane	Bending
200	Bar	4	Axial displacement and twist at ends.	All linear	-----
201	-----	5	Axial displacement and twist at ends plus axial displacement at center.	Linear twist Quadratic translation	-----
210	Beam	12	3 translations and 3 rotations at each end.	All linear	Cubic
211	-----	13	3 translations and 3 rotations at each end plus axial displacement at center.	Linear twist Quadratic translation	Cubic
220	-----	13	3 translations and 3 rotations at each end plus axial rotation at center.	Quadratic twist Linear translation	Cubic
221	-----	14	3 translations and 3 rotations at each end plus axial translation and rotation at center.	All quadratic	Cubic
300	Triangular Membrane	6	2 translations at each corner.	Linear	-----
301	-----	9	2 translations at each corner plus tangential displacement at midside nodes.	Quadratic * to edge Linear Lr+ to edge	-----
302	-----	12	2 translations at each corner plus normal and tangential displacements at midside nodes.	Quadratic	-----

* || = parallel
+ Lr = perpendicular

TABLE 4.2 (Continued)

Element	Type	No. of D.o.F.	Type of D.o.F.	Order of Shape Functions	
				In-Plane	Bending
320	Triangular Plate	18	3 translations and 2 rotations at each corner plus edge rotations at midside nodes.	Linear	Piecewise cubic
321	-----	21	As for 320 plus tangential displace- ment at midside nodes.	Quadratic to edge Linear Lr to edge	Piecewise cubic
322	-----	24	As for 321 plus normal displacement at midside nodes.	Quadratic	Piecewise cubic
400	Quadrilateral Membrane	8	2 translations at each corner.	Piecewise linear	-----
401	-----	13	2 translations at each corner plus tangential displacements at midside nodes on 4 sides and the diagonal.	Quadratic to edge Linear Lr to edge	-----
402	-----	18	As for 401 plus normal displacements at midside nodes.	Piecewise quadratic	-----
410	Quadrilateral Plate	24	3 translations and 3 rotations (includes normal) at each corner.	Cubic to edge Linear Lr to edge	Cubic
411	-----	32	3 translations, 2 in-plane rotations and 2 independent normal rotations at each corner plus tangential displace- ments at midside nodes.	Cubic to edge Quadratic Lr to edge	Cubic

TABLE 4.2 (Continued)

Element	Type	No. of D.o.F.	Type of D.o.F.	Order of Shape Functions	
				In-Plane	Bending
420	-----"	25	3 translations and 2 in-plane rotations at each corner. Edge rotation at midside nodes on 4 sides and the diagonal.	Piecewise linear	Piecewise cubic
421	-----"	30	Same as 420 plus tangential displacement at midside nodes.	Piecewise linear Lr to edges, piecewise quadratic to edges	Piecewise cubic
422	-----"	35	Same as 421 plus normal displacement at midside nodes.	Piecewise quadratic	Piecewise cubic

TABLE 4.3
CHARACTERISTICS OF TIME INTEGRATION OPERATORS IN STAGSC-1

Method	General Description	Linear Systems	Nonlinear Systems	Numerical Damping	Frequency Distortion
Central Difference (Explicit)	Conventional central difference method (two step, two derivative).	Conditionally stable. Limit given by $\Delta t < 2/\omega$ where ω is Target frequency in ties. system.	Same stability limit as for linear with ω modified for nonlinearities.	-----	Gives increase in frequency with increase in step size.
Trapezoidal (Implicit)	Single step, single derivative method. Equivalent to Newmark's average acceleration method ($\beta = 1/4$).	Unconditionally stable (A-stable) for linear damped and undamped systems.	Conditionally stable for both exact and approximate nonlinear spatial solution procedures.	Zero damping, independent of time step.	Reduction in frequency with increase in Δt .
Gear's 2nd Order (Implicit) (G_2)	Two step, single derivative method.	A-stable for damped and undamped systems. Conditionally stable for non-conservative systems (growing oscillations).	Not documented.	Damping grows with time step.	Similar to trapezoidal but greater magnitude.
Gear's 3rd Order (Implicit) (G_3)	Three step, single derivative method.	Not completely A-stable. Larger unstable region than G_2 (for non-conservative systems).	Not documented.	Negative damping for a frequency component ω up to $\Delta t = 2/\omega$. Positive damping for larger Δt .	Intermediate between G_2 and trapezoidal.

09188-848:2
(S3034) 33

TABLE 4.3 (Continued)

Method	General Description	Linear Systems	Nonlinear Systems	Numerical Damping	Frequency Distortion
K.C. Park (Implicit) (KCP)	Three step, single derivative method. Linear combination of G_2 and G_3 $KCP = \frac{3}{2} G_2 + \frac{1}{2} G_3$.	A-stable stability properties intermediate w.r.t. G_2 and G_3 .	A-stable for exact spatial solution. Conditionally stable for approximate solution. Larger stability limit than for trapezoidal.	Similar properties to G_2 , but smaller magnitude.	Intermediate between G_2 and G_3 .

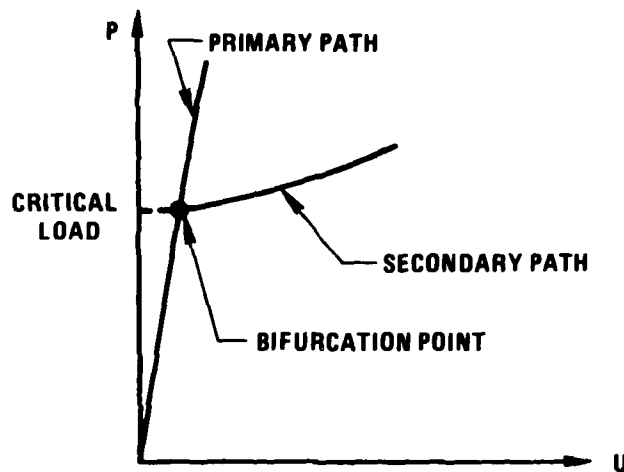


Figure 4.1 (a) Linear Pre-buckling

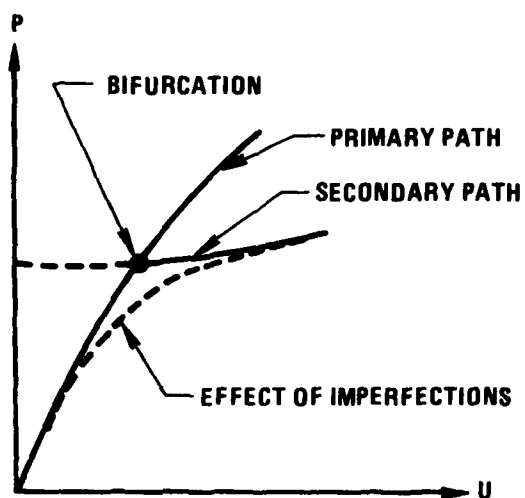


Figure 4.1 (b) Nonlinear Pre-buckling
– Softening

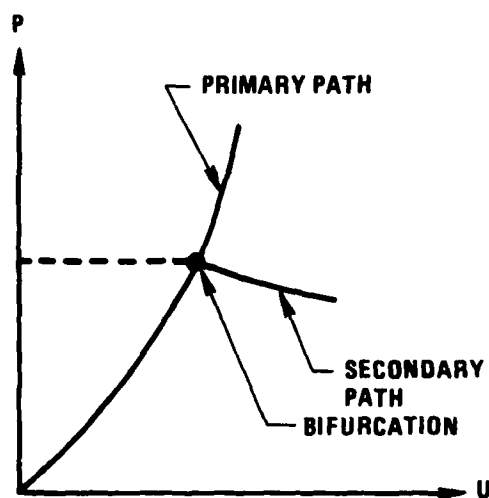


Figure 4.1 (c) Nonlinear Pre-buckling
– Stiffening

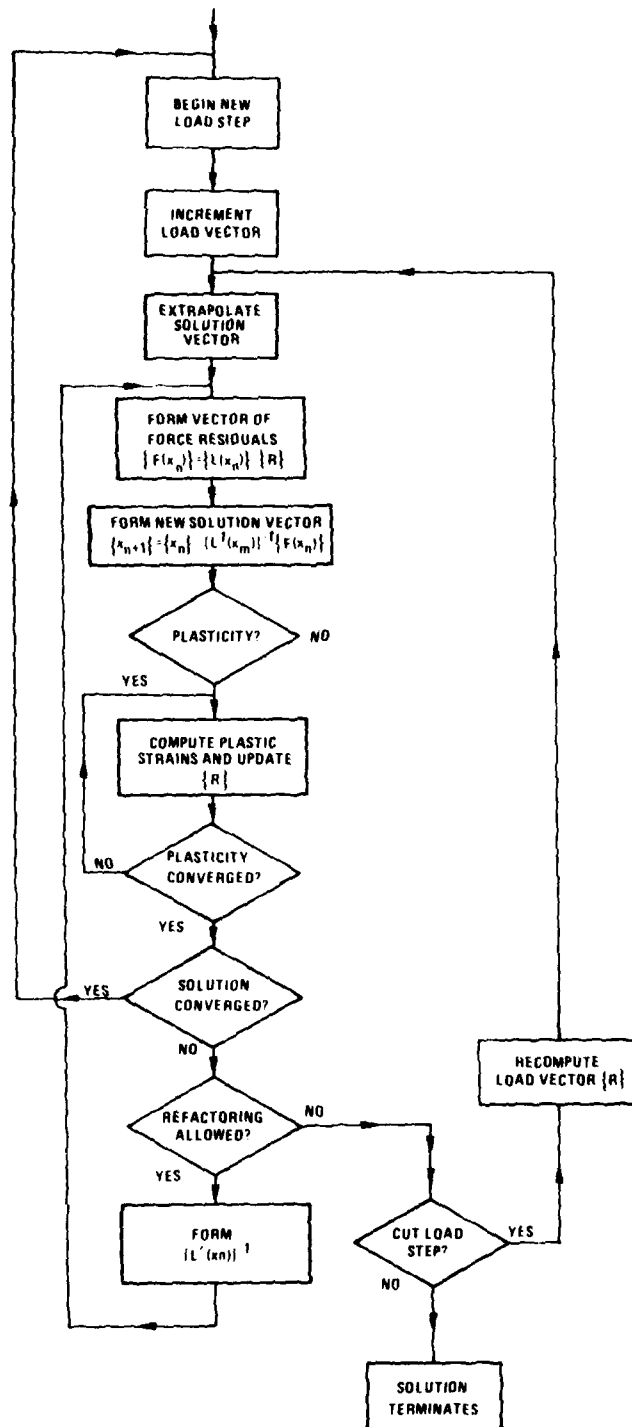


Figure 4.2 Nonlinear Solution Procedure

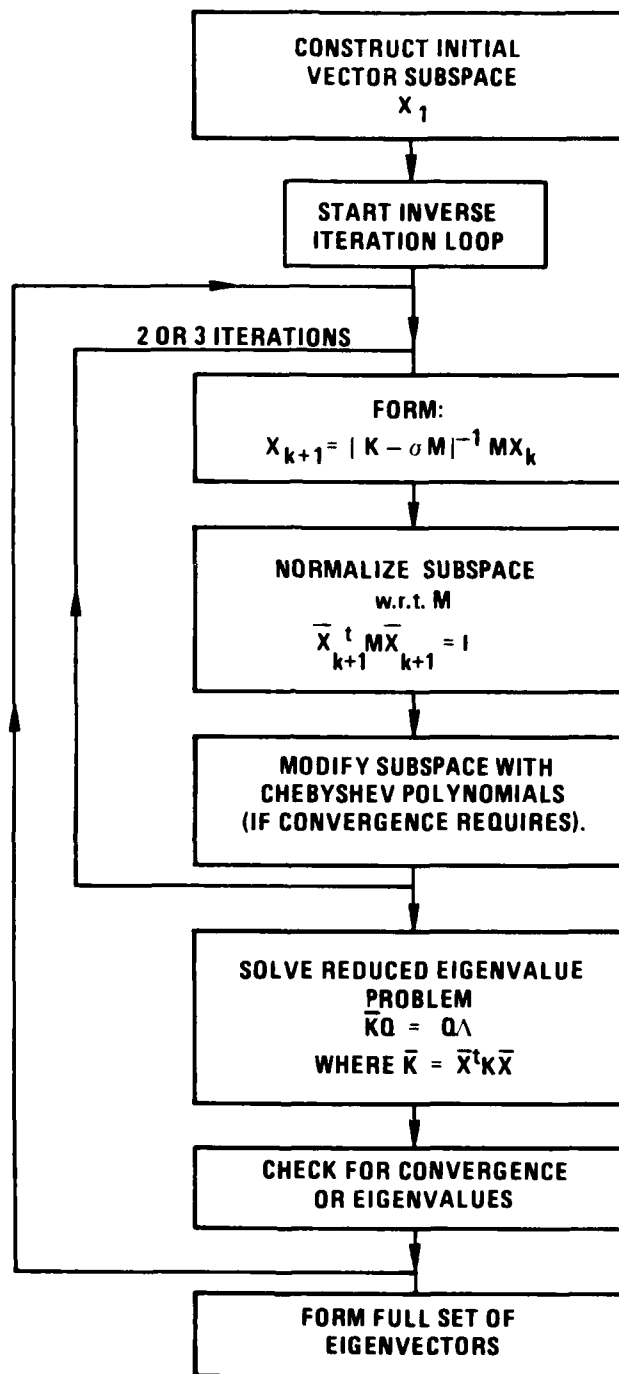


Figure 4.3 Subspace Iteration Algorithm

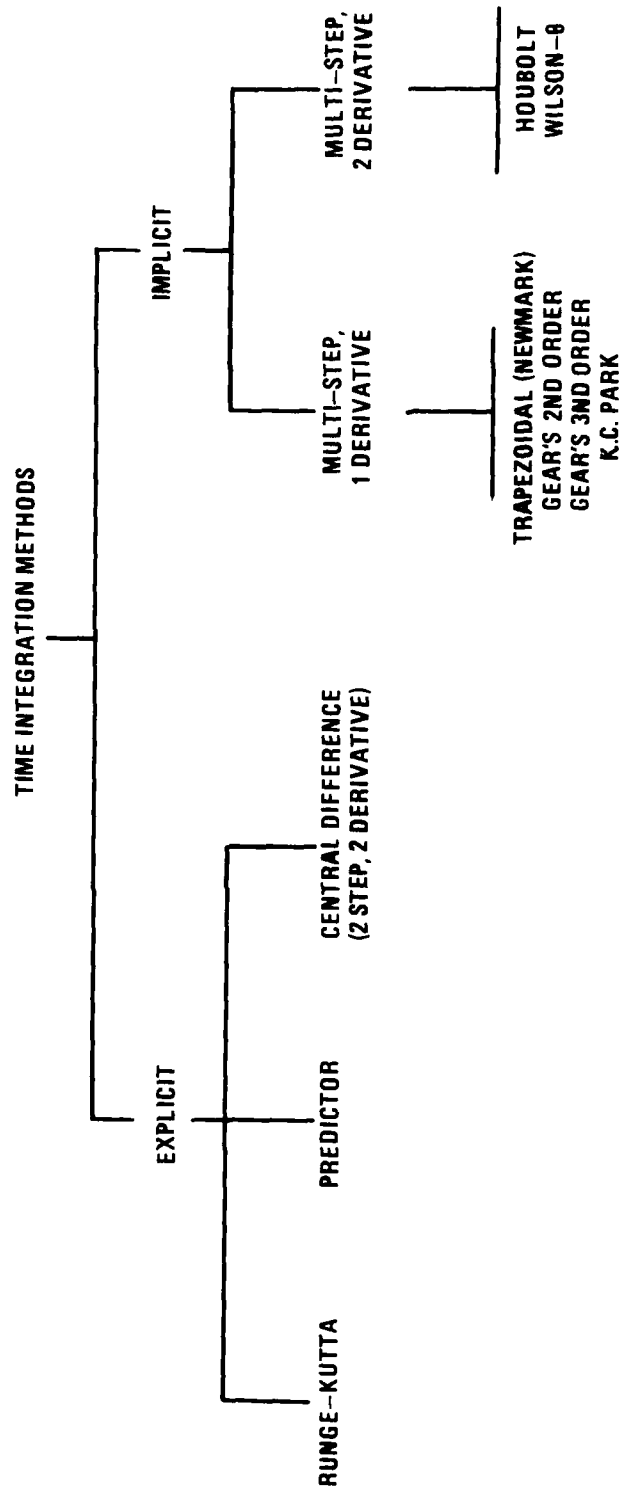


Figure 4.4 Time Integration Methods

5.0 VERIFICATION EXERCISES

The verification procedure followed for the purposes of this evaluation was simply to execute three different problems which were part of the STAGSC-1 program file supplied by Lockheed. The purpose of the verification was solely to ensure that the version, as modified for the CDC 7600, was, in fact, functioning correctly on the Westinghouse system. This does not constitute verification in the normal sense*, but was considered to be sufficient in view of the fact that the problems to be run in the course of the evaluation would themselves provide substantial verification. The verification problems and their solutions will be described in this section.

5.1 SHALLOW ARCH PROBLEM

The first verification exercise was a static, nonlinear analysis of a shallow arch with a uniform, radially inward pressure loading. Figure 5.1 shows the model data. The boundary conditions are simple supports at each end of the arch. The solution converged using three load increments with 6 to 8 iterations required for each increment. One refactoring occurred during the final increment. Figure 5.2 shows the center displacement plotted against pressure. The solution obtained agreed identically with the output generated by Lockheed. No analytically based solution for this problem was available for purposes of comparison.

5.2 BUCKLING OF AN ANISOTROPIC FLAT PLATE

The program options involved in this problem include an eigenvalue analysis for buckling, with material axes rotated with respect to the global axes by 45°. The bifurcation buckling load is 124.6 lb/in. Figure 5.3 shows the plate geometry, the applied loading and the buckling mode. No analytically-based solution was available, but the results agreed with the Lockheed output.

*Verification is nominally the responsibility of the developer, and is intended to ensure that the capabilities provided by the developer are, in an isolated sense, functioning.

5.3 CIRCULAR RING WITH INITIAL VELOCITY

Figure 5.4 shows the geometry for a circular ring segment with a uniform, radially-inward initial velocity. Radially symmetric boundary conditions give rise to a solution which predicts purely radial motion uniform along the segment. Figure 5.5 shows the time history of the radial deflection response. The measured period yields a frequency of 952.4 Hz which compares with the exact value of 1000 Hz [36] (-4.8% error). The results agreed identically with the Lockheed output.

These three checks, when first attempted, failed to execute and identified a coding error which was corrected after consultation with Lockheed. The subsequent successful executions confirmed that the program was performing correctly on the Westinghouse system.

$$E = 76900 \text{ lb/in}^2$$

CROSS-SECTION:

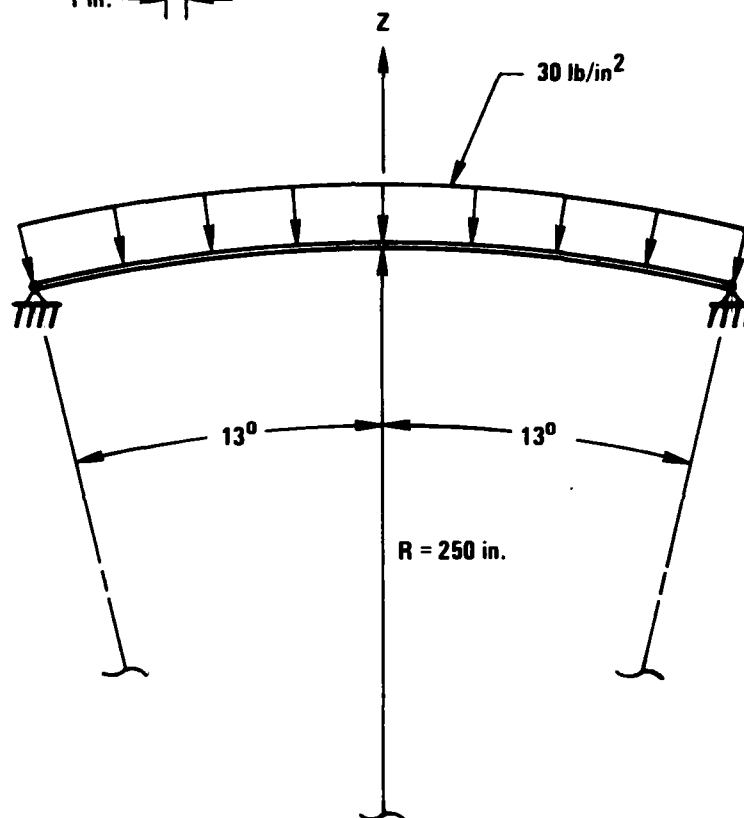
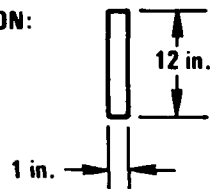


Figure 5.1 Shallow Arch Problem

5407-4

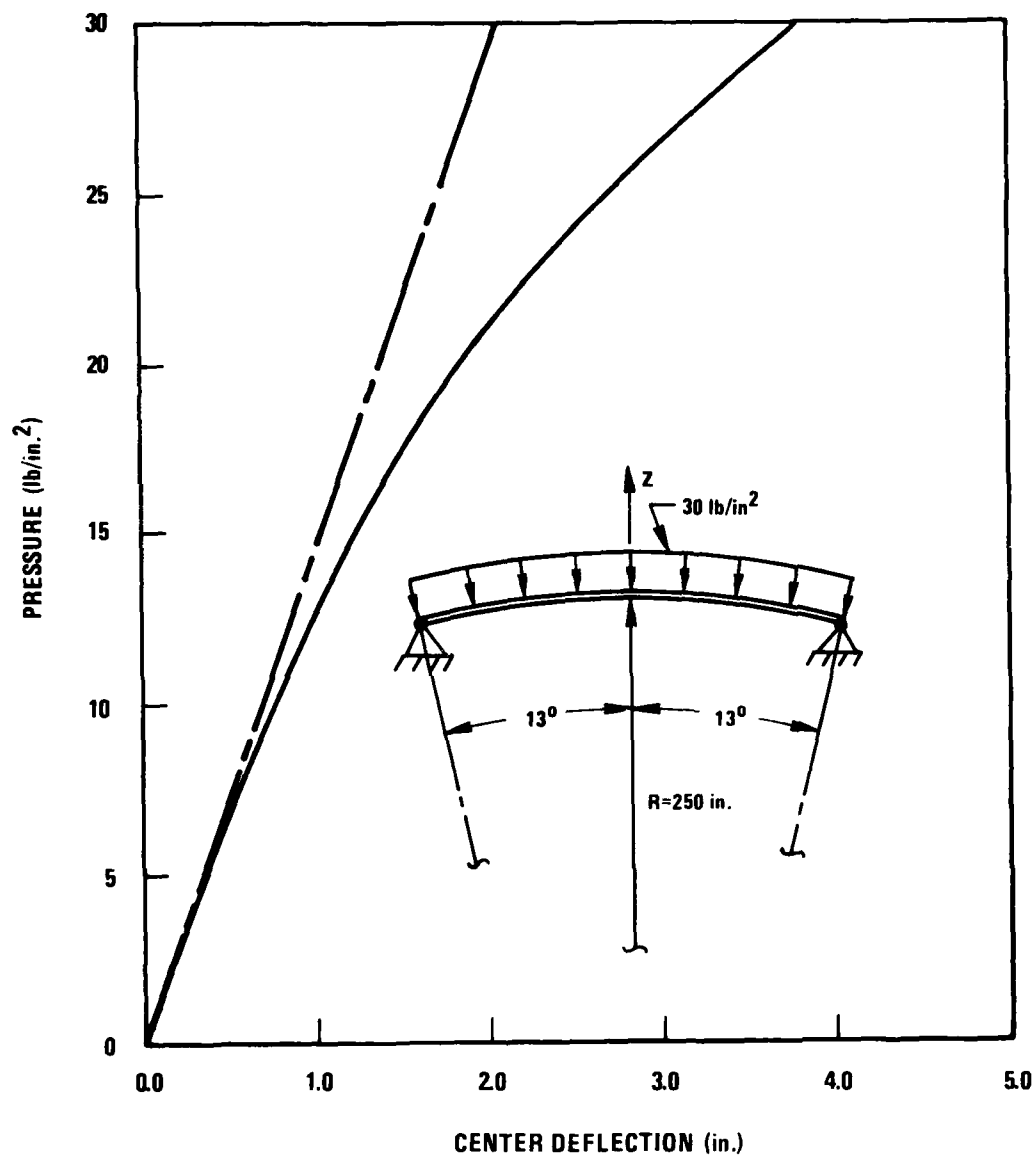


Figure 5.2 Shallow Arch Problem
— Results

5407-5

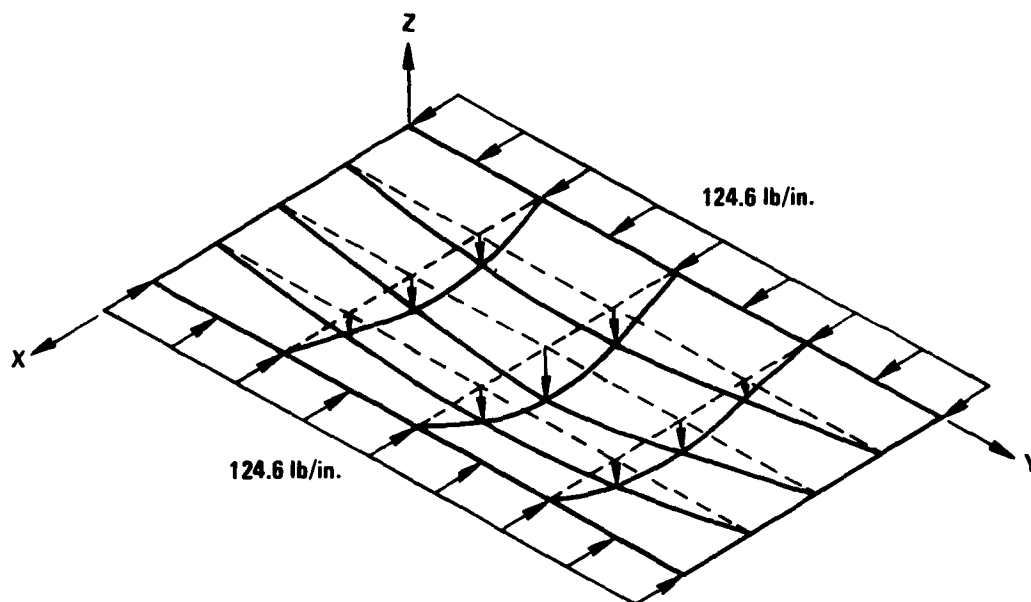


Figure 5.3 Buckling of an Anisotropic Plate

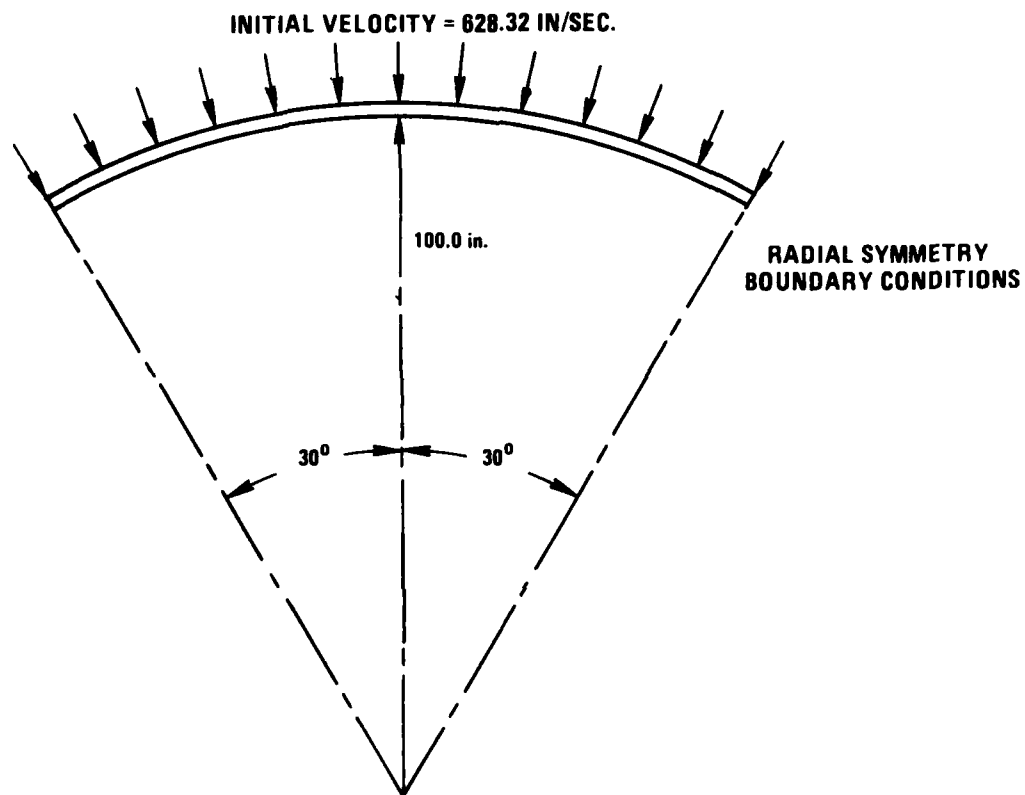


Figure 5.4 Circular Ring With Initial Velocity

5407-7

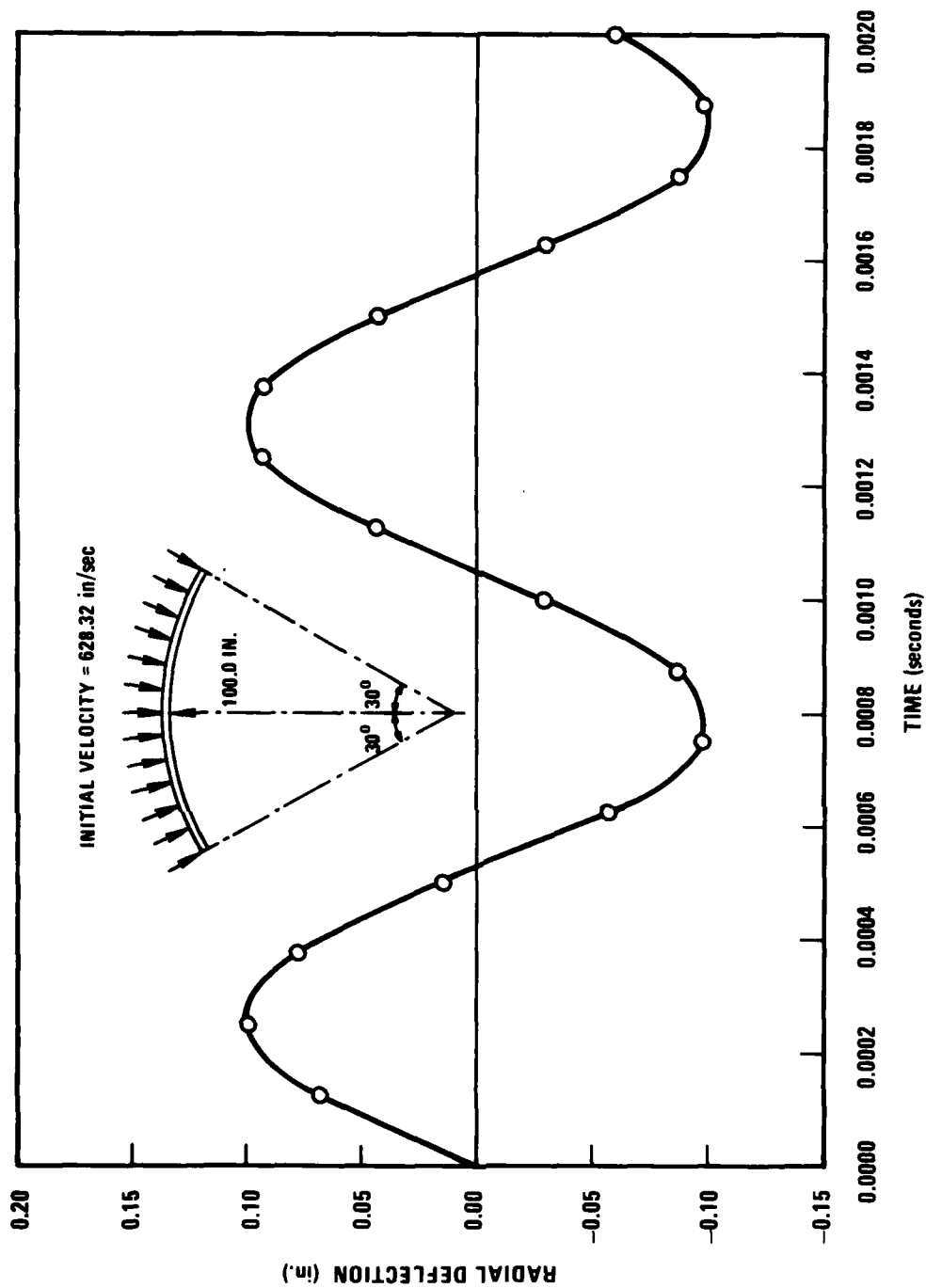


Figure 5.5 Ring with Initial Velocity -- Results

6.0 ADVANCED EVALUATION EXERCISES

The most effective and convincing form of evaluation of a structural analysis computer program is the obtaining of results from the execution of special problems designed to test in-depth the various options of the program both individually and in combination. This basic idea was developed in considerable detail by Nickell [1]. It was made clear in that discussion that these are not conventional verification exercises but problems chosen and executed in order to study specific aspects of the behavior of the elements in the program library together with the solution algorithms. The rigorous evaluation of a sophisticated program such as STAGSC-1 based on these guidelines is a very large task. The scope of the present work is therefore limited to provide an in-depth study of some, but not all, of the capabilities of the program. The areas selected for the advanced evaluation are as follows;

- o Element convergence
- o Eigenvalue extraction
- o Transient integration
- o Nonlinear solution algorithm

These will be described and the results presented in the four following subsections.

6.1 ELEMENT CONVERGENCE

A dual approach has been adopted in investigating the convergence of STAGSC-1 elements. First of all, a direct convergence study has been made by grid refinement of two multi-element problems which have well documented solutions. The problems selected are:

- A. a cylindrical roof (or barrel vault) simply supported at each end and subjected to gravity loading.
- B. a square flat plate with clamped edges and uniform pressure (linear and nonlinear).

These have been extensively studied [14, 22, 23] using both analytical and numerical methods of solution. Also the convergence properties of other elements for the cylindrical roof are well known. The second approach is to determine the eigenvector components of the element stiffness matrix and resolve the energy content for simple loading cases into the various eigenmodes. The spectrum of eigenmodes gives insight into the deformation responses which can be obtained using a particular element and can also show whether there are any spurious (zero energy) modes inherent in the element formulation.

In this work, attention has been confined to the quadrilateral shell elements. The reasons for this are:

- A. STAGSC-1 is primarily a shell program;
- B. The triangular shell elements are embodied in the quadrilaterals.

6.1.1 CYLINDRICAL ROOF PROBLEM

The geometry of the roof is shown in Figure 6.1. For gravity loading, there are two vertical planes of symmetry and hence only one quarter of the structure needs to be modeled. The majority of published solutions to this problem assume a zero value for Poisson's ratio.

For the present investigation, the two classes of quadrilateral plate element (410 and 420 series) were tested. Two of the 420 series (420 and 421) were used but both failed to obtain a solution. In each case a message was printed indicating ill-conditioning of the stiffness matrix and termination of the solution because of this. Reasons for this failure are not understood and are being studied by Lockheed. The mesh configurations used for the 1/4 model (see Figure 6.1) ranged from 2×2 (4 elements) to 10×10 (100 elements). Two displacement measures of convergence were used and gave similar results. These were the vertical deflections at the mid-point of the free edge (Point B) and the mid-point of the whole roof (Point C). Figures 6.2 and 6.3 show the deflections W_B and W_C plotted against total number of degrees of freedom. Figure 6.2 shows also the theoretical solution for deflection W_B based on shallow shell and deep shell theories (see Reference 23). Probably the best numerical solutions to this problem have been achieved using the

ABAQUS [25] and the MARC [26] finite element programs and these are included as benchmark comparisons. In addition, the shallow curved shell triangular element of Cowper, Lindberg and Olson [24] is shown as representative of the earlier approaches to shell element formulation based on a shallow shell approximation (Novozhilov theory). The ABAQUS element is the thin shell isoparametric element due to Ahmad, while the MARC element 24 is based on the de Veubeke element and Koiter-Sanders shell theory and is also doubly-curved, isoparametric. Both of these elements give very accurate results using only four elements.

The STAGSC-1 elements, being flat, approximate the geometry relatively crudely for the coarsest mesh (4 elements) and the results are correspondingly inaccurate. The 410 element for the 4 element mesh overestimates the free edge displacement W_B and the center displacement W_C by about 41% in each case. The 411 element performs better for the coarse mesh but uses 99 degrees of freedom instead of 63 (410). However, the convergence properties of the 411 element appear rather worse than the 410 despite the higher order shape functions. Moreover, its initial high convergence rate gives an overshoot with respect to the exact solution which is why, in the end, it does not give any better results than the 410 element. The NASTRAN evaluation study [14] gives a very comprehensive comparison between the NASTRAN element TRSHL and a number of other elements including the Ahmad isoparametric. Comparing the STAGSC-1 results with this data it is obvious that the STAGSC-1 elements perform considerably better than TRSHL but not so well as MSC/NASTRAN's QUAD 4 element.

In summary, it can be stated that the 410 series performs acceptably for a curved shell problem bearing in mind that the element formulation is for a flat plate.

6.1.2 FLAT PLATE PROBLEM

The failure of the 420 series elements to provide a solution to the cylindrical roof problem made it necessary to select a different test case. A flat square plate, simply supported or clamped at the edges was used in the NASTRAN evaluation study by Jones, et. al., [14] to obtain convergence data

for the QDPLT (quadrilateral plate) element. A purely linear solution to this problem will only provide data for the bending behavior of an element.

herefore, in order to test both bending and membrane convergence, the large deflection problem must be solved. Linear solutions are available in Roark [27] for the flat plate subject to a wide variety of loads and boundary conditions. However, for the nonlinear case the only solutions provided are for uniform pressure loading with various edge conditions. The case selected therefore was the square plate, clamped along all four edges and subject to uniform pressure loading. The linear solution to this problem in terms of the deflection at the mid-point of the plate is

$$w_A = 0.01376 \frac{pb^4}{Et^3}, \text{ where } A \text{ denotes the plate center.}$$

Figure 6.4 shows the geometry of the plate. For this geometry and a pressure of 12500 p.s.i., the maximum deflection is given by

$$w_A = 0.2752 \text{ inches}$$

The nonlinear solution is presented as a function of the applied pressure and is shown in Figure 6.5 in dimensionless form. For a pressure of 12500 p.s.i. the maximum deflection is

$$w_A = 0.1380 \text{ inches}$$

which is only 50% of the linear deflection. The 410 and 411 elements yield identical solutions for the linear case as do 420 and 422. The reason is, of course, that the bending shape functions are the same for the different element types in the two series. Therefore, it was only necessary to compare 410 and 420 for the linear case. Figure 6.6 shows the convergence behavior in terms of the maximum displacement for 410 and 420. It is noteworthy that the presence of the mid-side rotations gives rise to a poorer result for the coarsest mesh. Table 6.1 shows the percent error as a function of the number of elements.

Thus, for bending deformations, the 420 series are clearly superior to the 410 series so far as accuracy and rate of convergence is concerned. However, these results are of limited significance in the wider context of nonlinear shell analysis. The nonlinear case brings in the effect of membrane deformation as well as bending and therefore gives a more complete picture of the overall convergence of the elements. Figure 6.7 shows how the nonlinear solutions, obtained using the 410 element (4 elements and 25 elements), compare with the theoretical. Figure 6.8 shows the relative convergence behavior for 410, 411, 420 and 422. Table 6.2 shows the percent errors as a function of mesh size. The 411 element appears to give the best accuracy for the coarsest mesh in the nonlinear case. This appears somewhat anomalous in comparison with the rest of the elements except for the fact that 411 is the only one that has two independent normal rotations at each corner and thus has an added degree of membrane shear flexibility. It is clear that in this problem it is the refinement of the membrane shape function which is responsible for improvements in accuracy for a given mesh size.

However, in comparing the convergence rates of different elements, we must beware of drawing premature conclusions particularly for nonlinear analysis. The ultimate goal of the structural analyst is to produce the best accuracy commensurate with the cost of performing the analysis. The cost for the nonlinear analysis is not only a function of the element complexity but also of the way in which the element affects the performance of the solution algorithm. This is particularly relevant for STAGSC-1 because of the automatic adjustment of load step size and refactoring operations. Table 6.3 provides details of the 17 nonlinear analyses performed for element convergence. It is clear from the table that much depends on whether or not the step size is halved during the analysis. For example, Run No. 12 using 25 410 elements took less CPU time than Run 9 using only 9 elements. The reason was that with the more refined mesh, solution convergence criteria were satisfied without cutting back the load step. A similar situation occurred for Runs 19 and 20 (element 420) except that Run 19 did not need to refactor whereas Run 20 did.

Thus, if the total CPU time for each run is plotted against solution accuracy (Figure 6.9), a somewhat different view of convergence (in the broader sense) is obtained. Element 411 appears to be again the best performer, except that for higher accuracy ($<3\%$ error) a finer mesh using element 410 provides an equally cost-effective solution. Element 420 in this context appears to be the least cost-effective element.

6.1.3 ELEMENT EIGENVALUE ANALYSIS

The specification of assumed displacement fields in terms of polynomial shape functions is the almost universal method for obtaining the stiffness characteristics of finite elements. A subtle disadvantage of this approach is that the fundamental deformational capability of the element becomes almost totally obscured by the algebraic complexity of the functions. The so-called "natural-mode" method of formulating finite elements was developed by Argyris [28] and his co-workers prior to 1965 but did not achieve widespread use as the problem of defining such modes for more complex elements far out-weighed the advantages. However, these prescribed natural modes of deformation are designed to be orthogonal and are therefore eigenvectors of the resultant stiffness matrix. Therefore, if an eigenmode analysis of any stiffness matrix (however it may be generated) is performed, the so-called natural modes are obtained which are often physically much more revealing than the original shape functions. Moreover, as discussed by Gallagher [29], the complete set of stiffness matrix eigenvectors must include the set of rigid body modes which are identified by zero eigenvalues. Since there can be, at most, six rigid body modes any number of zero eigenvalues greater than six indicates the presence of undesired kinematic degrees of freedom. This approach is therefore also a test for anomalous behavior; this could be inherent in the form of the shape functions which have been assumed, or could be a result of the numerical procedures used for integrating the terms in the stiffness matrix.

Two possible methods of performing the eigenvalue analysis can be envisaged. A direct dynamic eigensolution could, in principle, be obtained for a single element by invoking the appropriate option in STAGSC-1. There are two objections to this approach, one theoretical and the other practical. The practical difficulty is decisive since STAGSC-1 is not able to perform any

AD-A102 794

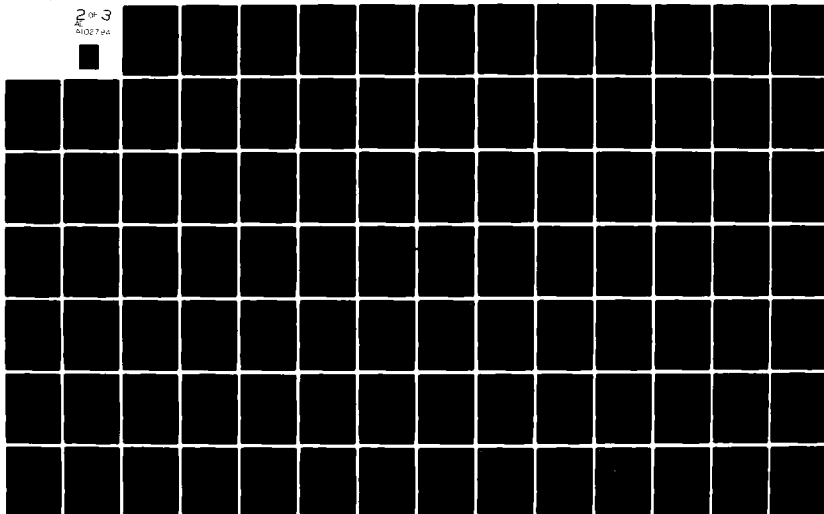
WESTINGHOUSE ELECTRIC CORP MADISON PA ADVANCED REACT--ETC F/8 13/13
EVALUATION OF THE STA0SC-1 SHELL ANALYSIS COMPUTER PROGRAM.(U)
AUG 81 K THOMAS, L H SOBEL
WARD-10881

N00014-79-C-0825

NL

UNCLASSIFIED

2 of 3
AL
A102744



analysis on a system which is totally unsupported. Thus, "free-free" modes of vibration cannot be determined because the solution procedure fails in matrix decomposition. Therefore, the complete set of modes, which must include rigid body modes, cannot be determined in this way. The second objection is, of course, that the vibration mode analysis will obtain the eigensolution for the dynamical matrix and not the stiffness matrix per se.

The second approach (the method adopted for this work) is to obtain the actual stiffness generated by the program for a single element and perform a separate eigenmode analysis on this matrix. STAGSC-1 saves the element stiffness matrix on TAPE23 for a restart or on TAPE8 for an eigenvalue analysis based on a nonlinear stress state (either buckling or vibrations). Since the data on TAPE8 is written as a straightforward unformatted write operation, the latter method was chosen. The eigensolution for the stiffness matrix was then obtained by using a specially written program ELMOD (Appendix). This program reads in the stiffness matrix (written as a lower triangle) and also a solution vector. After the eigenvalues and eigenvectors have been determined, the program computes the strain energy associated with each mode corresponding to the given solution vector. The Appendix provides a description of ELMOD and a listing.

The usefulness of this method depends entirely on the ability to associate the individual terms of the eigenvectors with the corresponding degrees of freedom for the element. This proved to be possible only for the 410 element. All other elements were formed with some degrees of freedom condensed out and the identification of the remaining freedoms could not be performed.

Ten separate load cases were devised for the single element model. Figure 6.10 shows the model geometry and the support conditions (which are sufficient only to eliminate rigid body freedoms). The load cases were chosen so as to excite as many different modes of deformation as possible and also to use as many load options as possible. Figure 6.11 shows the nodal equilibrium forces printed out by STAGSC-1 for each of the cases. Thus, Cases 1 and 2 are identical in distribution (not in magnitude) and have displacement solutions which differ only by a common factor. Cases 3 and 4 are similar but Case 4 (distributed edge load) produces self equilibrating moments about the normal

at the two nodes on the loaded edge. Cases 6 and 7 which are comparable cases (but with the loading in the Y-direction) do not produce moments about the normal. However, as is clear from Figure 6.11, the actual pattern of loads and reactions is different because of the support conditions. Cases 6 and 7 yield identical displacement solutions. Case 5 (uniform tangential shear loading) is very similar to 6 and 7 with respect to nodal force distributions. The displacements in the X-direction are identical with 6 & 7 with only minor (but real) differences in the Y-direction. Cases 8 and 9 (concentrated corner moment) also produce identical displacement patterns. Case 10, with a single concentrated moment about the normal at the free corner produced zero displacements and nodal equilibrium forces; the obvious conclusion for Case 10 is that STAGSC-1 calculates no contributions to the force vector from moment components about the normal.

In order to obtain the modal distribution of strain energy, the stiffness eigenmodes were determined. Figures 6.12-a through 6.12-c provide qualitative sketches of the mode shapes calculated. A total of 24 modes were obtained corresponding to the 24 degrees of freedom of the stiffness matrix. The eigenvalues and mode descriptions are contained in Table 6.4. The most striking observation from Table 6.4 is that there are seven zero eigenvalue modes. Since there can be only six genuine rigid body modes, the existence of an extra mode indicates the presence of some spurious kinematic freedom. This is presumably associated with the inclusion of the rotations about the surface normal at the corners as separate degrees of freedom. Inspection of the eigenvectors shows that for the zero eigenvalue modes, the displacements and rotations are all mutually consistent (and also with all six rigid body freedoms), with the exception of the rotations about the normal. These are an independent set and hence explain the presence of the seventh zero mode. This observation presents difficulties in explaining the declared purpose of the normal rotation [2], which is to provide for cubic variation of in-plane displacements along an edge, i.e., if the rotations are uncoupled in the rigid body modes, how are they coupled to the deformation behavior?

Setting aside this dilemma for the time being, attention will be directed to the deformation modes. The lowest eigenvalue (least stiff) deformation mode (Mode 8) is, somewhat surprisingly, purely membrane. The eigenvector shows

that the dominant freedoms are the corner normal rotations. There is a companion mode (21) in which the translations are the dominant freedoms and for which there is therefore much greater overall stretching. Mode 9 is the essential linear twisting mode. Modes 10 through 13 represent various types of pure bending behavior with Mode 10 being the anticlastic bending mode and Mode 13 spherical bending. Modes 14 and 15 are a combination of bending and twisting. Modes 16 through 22 are various membrane modes which include pure in-plane shear (18) and pure membrane dilation (22). The two remaining modes are doubly antisymmetric diagonal bending and twisting modes. In Mode 23 the diagonals remain straight, while Mode 24 has anticlastic bending along the diagonals.

Table 6.5 shows the results of the modal energy computations. As discussed previously, there are, in reality, only six load cases which provide distinctly different displacement solution vectors; these are Cases 1, 3, 4, 6 and 8.

Case 1, as might be expected, deforms the element almost entirely into a linear twist mode (9); the only other mode involved is 24 but its energy content is so low that it could be attributed to numerical round-off. Load Cases 3, 4, 5 and 6, being all in-plane loadings, excite only membrane modes. The most striking observation is that most of the energy is stored by Modes 8 or 16 with the other modes participating to provide the asymmetric response. Case 4 is outstanding because, although the loading is in the same direction as Case 3, Mode 8 does not participate at all. This may be related to the fact that Case 4 is the only one in which non-zero equilibrium moments are printed out for the normal rotation directions. The response for load Case 8 is mainly provided by Modes 9, 10 and 11.

None of the load cases produced any significant response in the diagonal bending plus twist modes (23 & 24) although it is obvious that a superposition of load Cases 8 and 9 ought to produce a response in which Mode 23 participates more strongly. Accordingly, the solution vectors for Cases 8 and 9 were superposed and the energy distribution calculated. As expected, Mode 23 now provides the dominant response.

It is clear that the only questionable result of the eigenvalue analysis is the existence of the seventh zero eigenvalue mode for element 410. Eigenvalue analyses were performed also for elements 411, 420 and 422 despite the fact that no modal decomposition of the strain energy could be performed. None of these elements had more than six zero eigenvalue modes. The developers recommend that when element 410 is used at least one normal rotation degree of freedom should be constrained.

6.2 EIGENSOLUTION PERFORMANCE

Three particular aspects of performance were chosen for investigation. These were:

- A. ability of the algorithm to discriminate between closely-spaced or multiple eigenvalues, and the orthonormality of the corresponding eigenmodes;
- B. degradation of accuracy with increasing mode number; and
- C. convergence of the solution

Three models, of increasing complexity, were developed to examine these questions. The first was a simple cantilever beam in three dimensions. For equal, or slightly different, principle moments of inertia of the cross-section, multiple or closely-spaced eigenvalues can be easily obtained. The second problem was a cantilever flat plate which is also well documented and therefore provides a further check on accuracy and convergence. Thirdly, a short cylinder with simply supported ends was chosen as an example of a shell structure with closely spaced modes at the lower frequencies.

6.2.1 3-D CANTILEVER BEAM

Figure 6.13 shows the geometry and finite element idealization of the beam. Ten beam elements (Element 210) were used along the length. Element 210 has cubic interpolation for transverse displacement and linear interpolation for axial displacements and twist. The exact solution for flexural frequencies was obtained from Reference 30 and is as follows:

$$f = \frac{(nL)^2}{2\pi} [EI/\rho AL^4]^{1/2} \quad 6.1$$

where

nL is obtained as the solution of

$$\cosh (nL) \cos (nL) + 1 = 0 \quad 6.2$$

and

ρ = density in mass units

A = area of cross-section

The STAGSC-1 analysis consisted of five separate runs. In all cases only lateral motion was permitted. The first two analyses confined vibrations to the XZ plane. The next three permitted motion in both planes but varied the ratio of the principal moments of inertia in order to observe the performance of the algorithm in the presence of closely spaced or multiple frequencies. The only difference between the first two analyses was that five modes were determined in the first case and ten modes in the second. Table 6.6 contains the frequency results for vibrations in the XZ plane.

Comparison of the STAGSC-1 frequencies with the exact results shows that the accuracy begins to degrade significantly after 3 or 4 modes. However, this is probably more a consequence of the mesh than anything else, since there are only 20 active degrees of freedom. The results also indicated that specifying 5 or 10 modes for determination did not affect the accuracy with which they were obtained nor did it affect the number of iterations for convergence (6 in each case).

For the cases of closely spaced and multiple modes, results are presented for the runs made with 1% difference in cross-section dimensions and equal dimensions. Frequencies are tabulated in Table 6.7 for the first six modes in each case.

The determination of the modes and frequencies was performed with accuracy equal to the case where they were not closely spaced. The only noticeable difference is in the solutions for the eigenvectors, where the modes become a

mixture of components in the XZ and XY planes. However, in the case where there is only 1% difference in the frequency pairs, the dominance of one mode over the companion is extremely strong ($1/10^7$). For equal frequencies, this dominance is much less but in this situation no dominance is really to be expected. Convergence of the iterative procedure was the same in all cases.

The comparison with the exact results indicated that STAGSC-1 underestimated all frequencies. The exact solution is based on classical beam theory with no allowance for shear deformation or rotary inertia. These effects are not included in the beam elements so it must be concluded that the lowering of the frequency is associated with the element mass matrix (which is lumped).*

6.2.2 FLAT PLATE CANTILEVER

This problem is well documented, since theoretical and finite element solutions to this problem are available in References 31 (page 550) and 26 (Volume E, page E4, 1-4) and it is therefore well documented. The problem description is contained in Figure 6.14. Table 6.8 shows a comparison between the STAGSC-1 model, using element 410, the MARC solution [26] using MARC element 4, the Zienkiewicz solution [31] using a non-conforming triangular element and the classical solution. In each case the mesh consists of two square regions which gives two elements for STAGSC-1 and MARC and four triangles for the Zienkiewicz solutions.

For two elements, the STAGSC-1 results are very poor. This is not, apparently, a failure of the eigensolver since much better solutions were obtained using more elements.

Figure 6.15 shows the convergence of the first mode frequency for STAGSC-1 as a function of the number of elements. For the purposes of comparison the Zienkiewicz (triangle) solution is plotted as a 2-element mesh because the same basic rectangular grid is used.

*Convergence should be from above. The fact that the frequencies are underestimated indicates a failure to satisfy some equations of mechanics. It may also be the result of numerical integration procedures for stiffness formation.

The eigenvalue solution (4 frequencies requested) required 4 iterations for the 2 element model, 6 iterations for 8 elements and 7 iterations for 32 elements. Thus, the number of iterations required was not strongly dependent on the size of the model.

6.2.3 SIMPLY SUPPORTED CYLINDER

An analytical solution for the free vibrations of a thin-walled cylinder was first documented by Baron & Bleich [34] and their solutions were utilized by other workers [32, 33] for comparison with a finite element solution and also in supersonic flutter calculations. A characteristic of the modal behavior of a thin cylinder is that the lowest frequency is obtained for an axial wavelength of 2 diameters ($m = 1$) and a circumferential wavelength of $\pi/8$ diameters (i.e., 8 circumferential waves; $n = 8$). For numbers of circumferential waves both greater or less than 8, the frequencies are higher. Figure 6.16 shows the geometry selected for the STAGSC-1 analysis, which is the same as that used by Greene, et. al., [32] and Voss [33]. Since the length was chosen to be one diameter and simply supported boundary conditions were imposed at each end, solutions can be obtained for axial wavelengths which are equal to $2D/m$, where m is the number of axial half waves between the ends and D is the diameter. Figure 6.17 shows how the frequencies are distributed with respect to the number of full circumferential waves n . The lowest frequency corresponds to a single axial half wave ($m = 1$), and eight full circumferential waves ($n = 8$). Attention was confined to modes where $m = 1$ and therefore it was possible to impose symmetry boundary conditions at the mid axial section. Some initial runs were made in order to establish a reasonable mesh for the analysis. Greene, et. al., [32] analysed the problem using a mesh based on a quarter wave model, i.e., the model spanned $11\ 1/4^\circ$ circumferentially and half the length, which is $1/4$ wave in both directions for the fundamental mode ($m = 1$, $n = 8$, Figure 6.13). For the present study, two $1/4$ wave meshes were set up, one with a 4×4 mesh (16 elements) and one with a 5×5 mesh. The fundamental frequencies obtained are given in Table 6.9. These results indicate a well-converged solution, at least for the first few modes. However, the $11\ 1/4^\circ$ model is only suitable for the fundamental (or appropriate multiples) because of the boundary conditions imposed on the axial edges. In order to establish a mesh suitable for higher modes, a $1/8$ cylinder model was set up.

Referring to Figure 6.16, the 1/8 model spanned the region ABCD; symmetric boundary conditions were imposed on edges AB, BC and AD. Table 6.10 presents results for four different meshes.

The results show that in order to capture the lowest modes accurately, at least 16 circumferential elements were required (i.e., 2 per quarter wave) and 4 axial (4 per quarter wave).

The larger number per quarter wave in the axial direction is probably due to the poor aspect ratio obtained with the 16 x 2 mesh. This seems to be substantiated by comparing the 16 x 4 and the 16 x 8 meshes. Figure 6.18 shows the corresponding mode shapes and emphasizes the fact that the best accuracy is obtained for Mode 5 ($n = 6$) where the best definition of the mode shape is obtained. Thus, in order to develop reasonable accuracy for a full circumference model, it became clear that 64 circumferential elements would be necessary and at least 2 axial elements for a half cylinder model (using symmetry about the mid-length).

Using the 1/2 cylinder model, some apparently anomalous results were obtained. The first two modes for the cylinder correspond to $n = 8$ and $n = 7$ circumferential waves respectively. STAGSC-1 was executed with the following parameters specified

NEIG = 4, SHIFT = EIGA = EIGB = 0

which instructs the program to determine the four lowest eigenvalues using a zero frequency shift. The frequencies obtained are shown in Table 6.11.

The modes that were isolated by the program consisted of two pairs each with 8 and 7 circumferential waves respectively, but with slightly different frequencies. Such pairs do not exist according to the classical analysis. Figure 6.19 through 6.22 show the mode shapes in terms of the normal displacements plotted around the circumference. It seems clear that modes 1 and 3 (as numbered by STAGSC-1) correspond to the true modes with 8 and 7 circumferential waves whereas modes 2 and 4 are anomalous due to their irregularity in circumferential distribution. The eigensolver obtained converged eigenvalues after a total of 16 iterations, having automatically

selected a frequency shift of 78.53 Hz after 8 iterations. Thus, the algorithm was quite capable of discrimination between the closely-spaced frequencies in each pair. It seems likely, therefore, that the anomalous modes are a result of the finite element discretization. Since the element type and mesh size are the same as for the 1/8 cylinder model (which did not give rise to these paired modes) the most likely source of the anomaly is the juncture of the cylindrical shell unit. This, in effect, introduces an axial "seam" in the structure which probably results in some slight asymmetry.

If this is indeed the situation, then it could be argued that the eigensolver is highly sensitive and discriminatory in identifying modes which are so closely similar. On the other hand, the more practical conclusion is that such powers of discrimination may be a considerable nuisance where, in an unknown situation, the separation of real and spurious modes may not be so easy.

In order to obtain further modes, use was made of the feature whereby the frequencies in the vicinity of a given range can be determined (EIGA, EIGB). The complete set of results is presented in Table 6.12.

6.2.4 CONCLUSIONS

The evaluation exercises performed permit some overall conclusions to be drawn with respect to the performance of the eigensolver. Three aspects were investigated and these can be summarized as follows:

- A. Discrimination between closely spaced or multiple modes is very good for problems of widely varying complexity.
- B. Degradation of accuracy with increasing mode number was observed, but the underlying cause was probably associated more with the adequacy of the mesh and the elements themselves, rather than the eigensolver.
- C. Solution convergence behavior for the problems investigated was satisfactory.

Overall conclusions based on this study are therefore that the eigensolver in STAGSC-1 is highly discriminatory, accurate and efficient. In fact, the quality of the solutions obtained was probably mostly dependent on the elements themselves rather than the eigensolver.

6.3 TRANSIENT INTEGRATION PERFORMANCE

STAGSC-1 is particularly well equipped with transient integration capability having one explicit and four implicit operators. The operators themselves are described in Section 4.8, and it is the purpose of this section to investigate their relative performance. Much has been written about the accuracy, stability, damping and so on of the multitude of numerical operators which have been developed for the integration of ordinary differential equations. Most of the research, however, has dealt with their application to linear problems, presumably because the mathematical proofs involved can be more readily derived. From the practical point of view, use of these algorithms in a program such as STAGSC-1, more often than not, will be for the integration of a non-linear set of equations. The main thrust of the present study was therefore directed towards studying the performance of the operators when applied to a non-linear problem. The properties which are relevant are the same as for a linear problem, i.e., accuracy, stability, artificial damping and frequency distortion (dispersion).

Two problems were selected for the investigation. The first was a benchmark to establish the general validity of the transient integration in STAGSC-1, and was chosen to be the linear elastic response of a thin-cantilever flat plate subjected to a triangular pressure pulse. This example is a demonstration problem used for the MARC program [26] and a comparison solution was therefore available. The second problem was the non-linear response of a circular ring segment subjected to an impulsive pressure loading. The solution to this problem has been reported by Stricklin, et. al., [37] with comparisons between analysis and experiment. All of the candidate integration operators were tested using this problem.

6.3.1 FLAT PLATE MODEL

The basic model and dimensions were the same as were used in the work on the eigensolver performance and details may be found in Figure 6.14. The pressure time history is shown in Figure 6.23 and is a triangular shaped pulse with a peak value of 100 lb/in² applied uniformly over the whole plate. The total duration of the pulse was 0.04 milliseconds.

This problem was analyzed using the explicit and the implicit trapezoidal methods (Newmark - β) in STAGSC-1. The model used element 410 in a mesh with four elements lengthwise and two across the width. The bench mark comparison was obtained using the MARC program. The MARC model was based on element 4 and a mesh consisting of two elements lengthwise.

The explicit method requires the selection of a time step which is below the stability limit. This may be estimated in several different ways which may be summarized as follows:

$$(a) \Delta t \leq \frac{2}{\omega_{\max}}$$

where ω_{\max} is the highest circular frequency which is inherent in the finite element model.

$$(b) \Delta t \leq \text{Min} \left[\left(\left(\frac{C}{\Delta \alpha} \right)^2 + \left(\frac{C_S}{\Delta \beta} \right)^2 \right)^{-1/2} ; \frac{\sqrt{3}}{h c} \left[\left(\frac{1}{\Delta \alpha} \right)^2 + \left(\frac{1}{\Delta \beta} \right)^2 \right]^{-1} \right] \quad 6.3$$

where

$$C^2 = E/\rho (1-\nu^2);$$

$$C_S^2 = G/\rho$$

$\Delta \alpha$ ($\leq \Delta \alpha$) are grid spacings

h = interval in finite difference formulation; in this case the assumption is made that $\Delta\alpha = 2h$
(see [3], page 6-33)

$$\Delta t \leq \frac{\Delta\alpha}{c}$$

6.4

where

$$c^2 = E/\rho (1-\nu^2) = \text{speed of sound}$$

Using the material properties for the flat plate model and the spacing $\Delta\alpha = \Delta\beta = 0.5$ inch (4 x 2 mesh) the following values of Δt were obtained and are tabulated below;

The table shows that a Δt of less than 2×10^{-6} seconds is required for a stable solution. Accordingly a time step of 1×10^{-6} seconds was chosen but the solution diverged after 6 time steps. A tenfold reduction in time step size to 0.1×10^{-6} seconds permitted the solution to progress further but divergence still occurred after 13 time steps. The most probable source of this discrepancy in the assumption used in the critical time step formula 6.3. For high-order finite elements, the values of h (finite difference interval) or $\Delta\alpha$ are difficult to estimate, and these estimates can be seriously affected by inconsistent mass-lumping combined with high-order deformation patterns. As pointed out by Krieg and Key [35], explicit operators do not work effectively with high-order elements for this reason. However, the fact remained that the time step size clearly had to be much smaller, probably by at least an order of magnitude, in order that a stable solution be obtained. The effort was therefore discontinued at this point and attention directed towards the implicit trapezoidal operator.

The MARC solution referred to earlier had used a time step of 20×10^{-6} seconds. Accordingly, for the STAGSC-1 solution values of 10×10^{-6} seconds, 20×10^{-6} seconds and 100×10^{-6} seconds were used and the solutions compared with the MARC response. Solutions were obtained out to a total time of 1000×10^{-6} seconds. Figures 6.24 and 6.25 show the tip

displacement and tip velocity as a function of time for the STAGSC-1 and MARC solutions. First, there was no significant difference in the STAGSC-1 tip displacement time histories for $\Delta t = 10 \times 10^{-6}$ seconds and $\Delta t = 20 \times 10^{-6}$ seconds so results are presented only for $\Delta t = 10 \times 10^{-6}$ seconds. Figure 6.24 shows that there is excellent agreement between the MARC and STAGSC-1 solutions. At first sight there appear to be some dispersive affects in the STAGSC-1 solution as compared with MARC since the fundamental response frequency is about 14% less than the MARC result. However, it is more likely that the "dispersion" is merely underprediction of the frequencies by the STAGSC-1 model (Element 410) as previously demonstrated. The peak-to-peak amplitude of the STAGSC-1 solution is about the same as that predicted by MARC. The solution obtained using a time step of 100×10^{-6} seconds is clearly rather coarse and does not give any resolution of the higher frequency components as might be expected. However, the solution appeared to be on the point of diverging at the final time step. Figure 6.25 shows how the responses in terms of tip velocity compare. The previously observed frequency distortion is rather more pronounced, particularly with regard to the higher frequency components. Thus, it may be inferred from this benchmark case that correct and reasonably accurate results can be obtained using the STAGSC-1 trapezoidal operator for a linear response analysis. The failure to do so with the explicit method could probably be resolved by using a smaller time step, but this was not demonstrated.

6.3.2 IMPULSIVELY LOADED RING

Stricklin, et. al., [37] performed a large deflection elastic-plastic transient dynamic analysis of an impulsively loaded ring using the program DYNAPLAS. The ring problem was initially posed and analyzed by Wu & Witmer [38] who compared their results with experimental data. The geometry of the ring is shown in Figure 6.26. The initial conditions for the problem are zero displacements and a radially inward initial velocity of 4862 inch/second imposed over a central sector of 120° . The STAGSC-1 finite element model assumed symmetry about the plane through the middle of the ring ($\theta = 0^\circ$) and utilized 21 equal elements between $\theta = 0^\circ$ and $\theta = 157.5^\circ$. The element used was element 410.

The original intent was to perform full elastic-plastic large deflection transient analyses for each operator and for various time steps. However, difficulties were encountered with the plasticity solution and this comprehensive approach was discarded in favor of an elastic large displacement solution. This was considered to be sufficiently nonlinear to test the integration operators effectively. Table 6.14 gives a summary of the individual analyses performed.

Runs 10 through 11 were all full non-linear elastic-plastic analyses using the Park integration operator.

A. Park Operator

A time step of 2×10^{-6} seconds was chosen for the first run on the assumption that this would be sufficiently small to permit accurate handling of the plasticity. The results indicated that the first 40 steps required plastic sub-iterations at each step but thereafter the need became only occasional. Solution convergence was obtained with only a single iteration per time step after the first 100 steps. The solution reached a total time of 620×10^{-6} seconds when the execution time limit was reached. Accordingly, the analysis was repeated using the automatic time step control with an initial step of 2×10^{-6} seconds imposed for the first 100 steps. Subsequently, the step was doubled twice during the next 16 steps. A third doubling was attempted but the solution failed because the determinant changed sign. It appears that in the automatic mode STAGSC-1 at present is able only to increase the time step which is obviously unsatisfactory for non-linear analysis in general where the changing character of the nonlinearities as the solution progresses may require successive increases or decreases in the step size.

For the third run (Run 12), a fixed step of 2×10^{-6} seconds was used and a restart file (TAPE22) was saved. The solution was obtained up to a time of 1002×10^{-6} seconds.

The fourth run was an attempted restart which failed giving the message; "Restart tape does not contain plasticity data . . .," notwithstanding the fact that the previous run generating the file confirmed that the plasticity data had been written to tape. At this point, the solution was examined in detail and compared with the published results. Figure 6.27 shows the time history of the deflection at the center of the ring up to 0.001 seconds. The solution compares reasonably well with the DYNAPLAS solution [37] but shows a growing difference. The circumferential strain history (Figure 6.28) at the center of the ring (outer surface) also shows good agreement. Perhaps the most encouraging comparison is with the experimental data presented by Wu and Witmer [38]. The deformed shape at 0.0008 seconds as calculated by STAGSC-1 is compared with the experimental results at 0.00079 seconds in Figure 6.29. Nevertheless, it was concluded that for times greater than this the solution was flawed. Figure 6.30 compares the distribution of bending rotation at 0.001 seconds for STAGSC-1 and DYNAPLAS. STAGSC-1 shows large discontinuities in rotation at three locations ($\theta = 52.5^\circ, 75^\circ$ and 150°) which clearly are unacceptable. This appeared to be traceable to the plasticity solution since the stresses did not lie on the stress-strain curve. Since the emphasis was intended to be on the integration operators, it was decided at this point to avoid the plasticity problems and to perform the evaluation using a purely elastic large displacement model. Thus, runs 14 through 25 (Table 6.14) were confined to the elastic regime. Using the same time step as for the plasticity solution, response was obtained up to the maximum time specified of 0.002 seconds. The solution was considered to be quite accurate since only one or two iterations per time step were required. For the next run, the time step was increased by a factor of ten (20×10^{-6} seconds). This produced an interesting result; after the first step, the time increment was automatically halved and the stiffness matrix refactored, in contrast with run 11 where automatic time step control was used and the time step was not reduced when difficulties were encountered. Since a small time limit had been imposed, the run was repeated with a time step of 10×10^{-6} seconds. This solution

refactored periodically and required from 2 to 8 iterations per time step. Figure 6.31 shows the responses obtained for the two time steps. Increasing the time step eliminated some of the high frequencies and increased the dispersion (about 5%).

B. Trapezoidal Operator

Time steps of 2×10^{-6} seconds and 10×10^{-6} seconds were again chosen. Figure 6.32 shows the responses obtained. There appears to be very little to distinguish the two solutions; dispersion and damping are both unaffected by increasing the time step. Comparison with Figure 6.31 shows that the results are almost identical with those obtained using the Park operator.

C. Gear 2nd and 3rd Order Operators

The Gear 2nd order operator shows about an 8.4% dispersive increase in the fundamental period when the time step is increased (Figure 6.30). In addition, the damping of the higher frequencies is very marked in comparison with the other operators. The Gear 3rd order operator became unstable at about .00035 sec. using the smaller time step. No further runs were attempted.

D. Explicit Operator

Time steps of 1×10^{-6} seconds, 5×10^{-6} seconds and 1×10^{-7} seconds were attempted. The two larger steps both led to divergence after a small number of steps (Figure 33). The run using a step of 1×10^{-7} seconds did not diverge but completed only 1710 steps ($t = .00017$ seconds) when the time limit for the run was reached. Since this was clearly extremely inefficient compared with the other operators, no further runs were attempted. The details of the computer run times and resource usage are presented in Table 6.15.

Examination of the execution times presented in Table 6.12 shows that for the implicit operators there are no obvious grounds for selecting one over another

on the basis of computational efficiency. Comparison of the Park and trapezoidal methods (Runs 14 and 18) shows that when the numbers of iterations are the same and there is no refactoring then the execution times and computer resource usage are also the same. Where differences do occur (e.g., trapezoidal and Gear's 2nd Order - Runs 17 and 19) they can be ascribed to more refactoring in the case of the one method (trapezoidal) compared with the other. Other things being equal, it may be said that this also reflects properties of the integration operator, but such a conclusion would need to be more firmly based than is possible with the present evidence. Such effects as problem dependence would need to be investigated.

Perhaps the most surprising result is the very poor performance of the explicit method which should be far superior on the basis of resources used per time step. This is clearly not the case given the present problem and the low value of the initial time step (0.1×10^{-6} seconds $< \Delta t_{cr} < 0.5 \times 10^{-6}$ seconds) makes it hopelessly uneconomical. For a large problem however, where the cost of refactoring will be much greater, the explicit method should become competitive.

6.3.3 CONCLUSIONS

Overall, the STAGSC-1 integration operators performed satisfactorily for both linear and nonlinear transient response problems. For the relatively small test problems the explicit method did not show to advantage because the size of the critical time step was so small and the number of steps became excessive.

Of the implicit methods, the trapezoidal operator was the most effective and showed the smallest dispersion when the time step was increased. The Gear 2nd and 3rd order operators were the least effective, the 3rd order method becoming unstable even for the smaller time step.

6.4 NONLINEAR COLLAPSE ANALYSIS

This section presents results obtained from a number of elastic nonlinear collapse analyses of point loaded cylindrical shells. The analyses were

performed more or less on a production basis as part of an investigation of the buckling of a nuclear reactor containment vessel due to localized loads, and not as part of the STAGSC-1 evaluation per se. However, because the analyses are for the less frequently considered case of displacement-control, and because of experience gained with certain input strategy parameters, it is fruitful to discuss these aspects of the analyses as they pertain to the STAGSC-1 evaluation. In this respect, it should be pointed out that the analyses might very well have been performed differently, and certainly for simpler and more economical problems, if the objective at the outset had been an evaluation of the nonlinear collapse capability of STAGSC-1.

The problem of interest for the containment vessel buckling investigation is collapse of the so-called "poked cylinder", which is a cylindrical shell subjected to an inward-directed normal point force applied at midlength. Two related and more standard problems were first run on STAGSC-1 to gain familiarity with the program, and to provide check cases. These problems are the point loaded venetian blind and the pinched cylinder. Dimensions and material properties for the three elastic shell problems are given in Table 6.16 along with the STAGSC-1 predictions of the collapse loads. Table 6.16 also serves to define some of the notation.

6.4.1 ANALYSIS CONSIDERATIONS

Either displacement or load can be specified as the controlled variable in STAGSC-1 input. For reasons of economy, and to obtain the post-collapse behavior, displacement-controlled analyses were performed for each of the three shell problems. Specifically, the radial displacement w_0 under the point load P is specified in steps, and the corresponding value of P required to impose the specified displacement is determined from a printout of "equilibrium forces." The nonlinear collapse load is the value of the load at the maximum point (limit point, $dP/dw_0=0$) of the load-displacement ($P-w_0$) curve obtained from the analysis. This load, which is also called the snap-through load or nonlinear buckling load in the literature, should not be confused with the bifurcation buckling load obtained from an eigenvalue type of analysis. For comparison, a load-controlled collapse analysis was also performed for one of the problems. In this case, the collapse load is taken

to be the value of P for which the finite element computations failed to converge within the specified convergence criterion (DELX), specified permissible number of cuts in the load step (NCUT), and the number of times the stiffness matrix can be refactored (NEWT). Because of symmetry conditions, each shell problem is analyzed as a cylindrical panel whose axial length is half the actual length of the shell, and whose circumferential angle is half the actual opening angle of the venetian blind, and 90° and 180° for the pinched and poked cylinders, respectively. Classical simple support (diaphragm) boundary conditions are imposed on the curved edges of all three panels, and free edge conditions are specified on the remaining straight side of the venetian blind panel. The quadrilateral plate element 411 with 2x2 Gaussian integration points⁺ is used in the analyses. Table 6.17 gives the number of mesh points along with computer costs and other details of the analyses.

Analyses of the venetian blind and pinched cylinder were performed in a straightforward manner, with no decisions required for selection of the strategy parameters beyond initial specification of NCUT and NEWT. Specifically, it was not necessary to tighten the convergence criterion DELX from its default value of 10^{-3} , or to force refactoring at each of the higher load steps. In contrast, the poked cylinder analysis required that greater attention be paid to these strategy parameters, with DELX being reduced from 10^{-3} to 10^{-4} and 10^{-5} , and with refactoring forced at consecutive higher load steps (see Table 6.17), as is discussed more completely later.

6.4.2 VENETIAN BLIND & PINCHED CYLINDER RESULTS

A. Comparison With Previous Solutions

Table 6.18 shows that linear STAGSC-1 results appropriate to the meshes of Table 6.17 agree to within 10% with previous solutions [41,42] for $w_0 E t / P$, a dimensionless flexibility coefficient. Use

⁺Use of 2x2 integration points was recommended by the developers of STAGSC-1.

of a finer mesh is seen to reduce the discrepancy in the pinched cylinder results from 10 to 2%. For reasons of economy, the finer mesh was not used in the nonlinear collapse analysis of the pinched cylinder.

With regard to the comparison of nonlinear results for the venetian blind and pinched cylinder, it is noted that the present results are based on the same meshes used in the STAGSA finite difference analyses performed by Brogan and Almroth [41]. The above comparison of linear results indicates that these meshes are not sufficiently fine to render completely converged solutions for w_0 . Furthermore, the rate of convergence with mesh refinement is likely to be different for the STAGSA and STAGSC-1 solutions. Consequently, the STAGSC-1 results for the venetian blind (Figure 6.34) and pinched cylinder (Figure 6.35) agree as well as could be expected with the STAGSA solutions, with respective collapse loads P_c for the venetian blind differing by about 5% (Table 6.16). A similar comparison of collapse loads for the pinched cylinder could not be made because the STAGSA solution in [41] was terminated before collapse.

B. Nonlinear Behavior of Venetian Blind

For comparison, Figure 6.34 shows load-displacement plots obtained from both the displacement-controlled (DC) and load-controlled (LC) analyses. The following observations and comments stem from an examination of this figure and Tables 6.16 and 6.17:

- (1) The collapse loads predicted by the DC and LC analyses agree to three significant figures.
- (2) The LC analysis required over 8 times as many steps to reach the limit point and is 6 times as expensive up to this point.
- (3) The relatively large number of load steps provides a very smooth LC curve at all load levels. The DC curve drifts away from the

more accurate LC curve in a local region and then properly returns to it upon a refactorization at a later displacement step ($w = .02$ "). Since the same (default) value of the convergence criterion is used in both analyses (see Table 6.17), and since there are fewer steps in the DC analysis, it appears that satisfaction of convergence is so much easier in a DC analysis that it sometimes accepts too large a displacement step. This apparently causes a "drift" in the DC solution from the "true" solution (appropriate to the chosen mesh) that is eventually corrected by the Newton-Raphson solution procedure. Such a local drift is generally of little consequence.

- (4) STAGSC-1 has the advantage and convenience of automatically reducing the load or displacement step (as permitted by NCUT) when convergence difficulties are encountered. Thus, it is easier for STAGSC-1 to home-in on the collapse load in a LC analysis than it is for other programs, such as MARC [26], for example, in which input values of the load steps cannot be reduced internally by the program to reflect the increasing ill-conditioning of the stiffness matrix as $P \rightarrow P_c$. Such programs generally require more restarts to obtain the collapse load to the same degree of accuracy.
- (5) The post-collapse curve obtained from the DC analysis shows that the point loaded venetian blind is imperfection-insensitive in the sense that collapse loads for perfect and slightly imperfect venetian blinds are expected to differ by a small amount. Of course, the post-collapse curve cannot be determined from a LC analysis unless special procedures are used.

C. Nonlinear Behavior of Pinched Cylinder

The sketch of the 12×8 variable mesh given in [41] was scaled to provide the axial and hoop intervals given in Table 6.19. The corresponding STAGSC-1 solution is shown by the upper load-displacement plot of Figure 6.35. Inspection of the figure

reveals that collapse of the pinched cylinder is not catastrophic. The load drops off by only 1% from its value at collapse to its minimum post-collapse value, while the corresponding displacement increases by just 4% before stiffening behavior takes place. This portion of the $P-w_0$ plot in the vicinity of the maximum and minimum points was routinely traced out by STAGSC-1, as was the entire $P-w_0$ curve.

These results are useful in a general sense because this is the first time that collapse has been predicted for a pinched cylinder. Hence collapse of the considerably thinner poked cylinder ($R/t = 638$ versus 100) was seen to be a definite possibility, and was therefore investigated. However, specific numerical values and details of the pinched cylinder results may be inaccurate because (1) the mesh is not fine enough to provide converged values of the radial displacement and smooth hoop spatial variations for stresses, (2) computed rotations ($\sim 25^\circ$ at collapse) exceed the range of permissible values for valid application of the theory employed in STAGSC-1, and (3) computed stresses at collapse for this relatively thick cylinder indicate that plasticity effects (not considered here) are significant even at points away from the load.

6.4.3 ANALYSIS OF THE POKED CYLINDER

A. Mesh Considerations

It was decided to use the finest mesh that would not be unduly expensive and that would not exceed the core storage limitation that the total number of nodes mxn could not exceed 528 (on the Westinghouse CDC7600), which was determined by trial and error from linear runs. The chosen variable mesh with $mxn = 16 \times 32 = 512$ nodes (Table 6.19) over the half-length and half-circumference is based on results obtained from two preliminary linear runs in which the mesh spacing was coarse in the axial direction(x) and fine in the hoop direction(y) for the first run, and vice versa for the second. Approximately five elements were then used to span the first half wavelength of the change in axial curvature κ_x in the hoop and

axial directions obtained respectively from the first and second runs.⁺ The size of consecutive axial and hoop intervals was then selected to increase geometrically by 20 and 10%, respectively, as may be deduced from Table 6.19. Linear results appropriate to the finer 16x32 mesh provided about the same wavelengths as those obtained from the preliminary runs, and were found to agree well with available series solutions, as is discussed below. Therefore, the 16x32 mesh was also thought to be adequate to describe the nonlinear behavior of the cylinder because the inward deformation pattern under the load spreads out with increasing load, and this results in an increasingly greater number of nodes spanning the pattern.

B. Linear Behavior & Comparison with Previous Solutions

Figures 6.36 and 6.37 show the hoop variation of the radial displacement w at midlength ($x = 0$) and the hoop bending moment M_y at the axial position $x = 3.5 \approx (1/140)(L/2)$. The rapid decay of the oscillatory hoop variations with increasing circumferential angle $\phi = y/R$ is also typical of the STAGSC-1 results for the axial bending moment M_x and the axial and hoop membrane forces N_x and N_y . In contrast, the axial variations of w and M_y decrease monotonically to zero at the simply supported edge ($x=L/2$), as is shown in Figures 6.38 and 6.39 for the variation of w along the loaded generator ($\phi = 0^\circ$) and M_y along a neighboring generator ($\phi = 1/2^\circ$). For poked shells, note that the slow decay of w in the axial direction is also evident from graphs given in [43] for longer cylinders ($L/R = 4$), and from results for long doubly curved shells presented in [44] where it is mentioned that displacements spread much further in the direction of the smaller curvature than in the direction of the larger one. Also note that the axial attenuation length for w is very large for the closely related case of a pinched cylinder (see [45]).

⁺ κ_x is the response variable with the shortest significant wavelengths in both directions. Therefore, results are more accurate for the more slowly varying and lower order kinematic variable $w(x,y)$, the radial displacement.

The above linear results are in qualitative agreement with series solutions given by Bijlaard [43,46,47] and Mizoguchi [48] for thicker and longer cylinders. Quantitative comparisons are afforded by the series solution presented by Kempner, Sheng, and Pohle [49] for a range of shell geometries that spans the geometry ($R/t = 638$, $L/R = .892$) of the poked cylinder analyzed here. The radial loading considered in [49] is an axial line load distributed uniformly over just 5% of the shell length, and located symmetrically about the midlength of the cylinder. A cylinder with such a short line load provides a good check case for the point loaded cylinder. Tabular results are presented in [49] for w , M_x , M_y , N_x and N_y at the following points: $(x,y) = (0,0)$, the location of the resultant load P ; $(L/4,0)$, the "quarterlength" point on the loaded generator midway between P and one end of the cylinder; and $(0,L/4)$, the corresponding quarterlength point on the circumference through P . Results at the first point for $R/t = 500$ and 800 and $L/R = .2$ and 1 were logarithmically interpolated to provide values of the radial displacement and the stress resultants appropriate to $R/t = 638$ and $L/R = .892$. STAGSC-1 values of the stress resultants at the quarterlength points were determined from known values at neighboring centroidal⁺ points by means of linear interpolation in one direction, and extrapolation to the symmetry plane in the other direction. The extrapolated values were obtained by passing a fourth order polynomial with even terms (because of symmetry considerations) through three points and by evaluating the polynomial at the origin. The series solution [49] and STAGSC-1 results for the three points under consideration are compared in turn in the three horizontal sections of Table 6.20. Stress resultants that are small or which

⁺The option to print out values of the stress resultants (or stresses or strains) at the Gaussian integration points doesn't work. Thus, only centroidal values are printed out.

have very rapid spatial gradients⁺ at the quarterlength points are omitted from the comparison. Examination of the table reveals that the STAGSC-1 results differ from the series solution predictions by an average of only +5.4%, with minimum and maximum deviations of +.4 and +11.1%. Furthermore, each STAGSC-1 result is above the corresponding series solution prediction, and thus properly reflects the more severe nature of the concentrated loading condition. In view of the interpolation and extrapolation procedures employed to arrive at a common basis of comparison, and because slight phase shifts or dispersion in shape at points of moderate spatial gradients may very well lead to percent differences on the order of those given in the table, it seems that the agreement between the STAGSC-1 and series solutions for the two slightly different loading conditions is about as good as can be reasonably expected. This favorable correlation of linear results instills a sense of confidence in the reliability of the STAGSC-1 code in general, and in the adequacy of the particular mesh selected for the poked cylinder analysis, certainly at least with regard to the prediction of linear behavior.

C. Nonlinear Behavior and Collapse

Load-Displacement Behavior

The continuous load-displacement curve in Figure 6.40 represents the "best" solution obtained here by refining values of the strategy parameters in the DC analysis. Regions I and II in the figure represent less accurate solutions that are discussed later. The initial linear portion of the curve is seen to extend over only about 10% of the load range to collapse and over about 4% of the corresponding displacement range. The curve then bends over rapidly

⁺Comparisons at points of rapid spatial gradients can result in deceptively large percent differences, as is exemplified by consideration of two identical shapes that are slightly out-of-phase (shifted relative to one another in the coordinate direction).

for a short range of load levels during which the initially compressive axial and hoop membrane stresses near the load become tensile (see Figure 6.41), due to local geometry changes, and remain tensile thereafter. Figure 6.40 shows that collapse occurs at the limit point of the curve at the following values:

$$\begin{aligned}P_C &= 773,000 \text{ lb} \\w_C &= 65.6''\end{aligned}$$

or

$$w_C/t = 37.5$$

Somewhat suprisingly, the post-collapse behavior could not be determined from the DC analysis. Strategy parameters were then varied in a number of unsuccessful runs, each one being terminated at the same limit point with a message that the stiffness matrix ceased to be positive definite. It is possible that the load-displacement curve is very steep (stiffening behavior) immediately after the limit point, or that it has a sharp maximum there, or both. Another possible explanation is given after consideration of spatial variation plots.

Spatial Variations

Hoop and axial variations of w and M_y at collapse are displayed in Figures 6.42 - 6.45 and are to be compared with the corresponding spatial variations for the case of linear behavior at low load levels (Figures 6.36 - 6.39). Comparison of Figures 6.36 and 6.42 for the hoop variation of w at midlength shows that the inward deformation pattern under the load spreads out with increasing load (as is easily demonstrated by poking at a thin-walled beer can) and that the shapes are similar otherwise. In contrast, Figures 6.43 and 6.37 reveal that the hoop variation of M_y at collapse is markedly different from that at low load levels. The jumpy behavior exhibited in Figure 6.43 near $\phi = 20^\circ$ is due to the development of a sharp hoop

curvature, which is suggested by the displacement results of Figure 6.42, and which is shown directly in the plot of the change of curvature, κ_y , given in Figure 6.46. It is possible that the failure to trace out the post-collapse portion of the $P-w_0$ curve may be due to ill-conditioning associated with this region of sharp curvature. It is interesting to observe from Figure 6.46 that the sharp curvature near $\phi = 20^\circ$ is preceded by a spatial region in which $\kappa_y \approx -1/R$ so that the total curvature ($\kappa_y + 1/R$) is approximately zero, or in other words, the inward displacement ($\phi < 20^\circ$, see Figure 6.42) is circumferentially flat at collapse except, of course, in the immediate neighborhood of the load. Figure 6.44 shows that w is flat also axially for $x > L/20$. Interestingly, comparison of the load-deformation plots of Figures 6.47 and 6.40 for κ_y near $\phi = 20^\circ$ and for w_0 reveals that κ_y starts to grow rapidly at a load level ($P/4 \approx 150,000$ pounds) which corresponds to the beginning of the jog (inflection region) in the $P-w_0$ plot of Figure 6.40.

Scaled Down Model

A scaled down model of the poked cylinder was observed to deform into a spreading diamond shaped pattern with rounded "corners" at midlength (see Figure 6.48). The circumferential corners became increasingly sharper with increasing load until a subtle and noncatastrophic collapse occurred at one and occasionally both of the corners. The collapse mechanism appears to be an asymmetric (about midlength) local snapping, which was sometimes accompanied by a loud ping. Such collapse behavior was noticed at most but not all successively poked points of the model. Regardless of whether collapse was discernible, stiffening behavior was observed to take place at all poked points after the circumferential corners became sufficiently sharp. It is interesting to mention that these corners appear to correspond to the above discussed regions of sharp curvature near $\phi = 20^\circ$ at midlength that are predicted by the STAGSC-1 analysis.

Mesh Considerations in Retrospect

As mentioned earlier, the chosen mesh was thought to be satisfactory for the nonlinear analysis since it provided essentially converged linear results that are in good agreement with available analytical solutions, and because the number of nodes spanning the spreading inward deformation pattern under the load increases with increasing load. Evidently, this mesh (or any finer mesh) is inadequate to describe accurately the corner near $\phi = 20^\circ$ at midlength. However, it is important to point out that the solution for the radial displacement $w(x,y)$ may still be accurate, since displacements converge much more rapidly than higher order derivative variables (M_y or κ_y). If this is the case, and since the $P-w_0$ curve of Figure 6.40 has a limit point (part c of figure), it follows that the above value of the collapse load at this point would also be accurate.

D. Consideration of Strategy Parameters

It has already been shown that the DC solution for the venetian blind drifts away from the more accurate LC solution in a local region of the $P-w_0$ curve. Such drift was also observed in two instances in the DC solution for the poked cylinder, as shown by regions I and II in Figure 6.40. Recall that the continuous curve in the figure represents the "best" solution obtained here by refining values of the strategy parameters governing the convergence criterion (DELX) and the frequency of refactorings (NEWT) so as to eliminate drift. Specifically, drift in region I was eliminated by tightening DELX to 10^{-4} from its default value of 10^{-3} , and drift in region II was smoothed out by forcing refactorings at every step. It is interesting to note that the drift in region II (see Fig. 6.40b) might be interpreted as signifying collapse, which would be spurious.

In view of the improvement brought about by the NEWT=-1 solution in region II, an additional run was made to determine if the drift in region I could similarly be avoided by refactorings at every step, instead of by tightening the condition for convergence. That this happens is evident from inspection of Figure 6.49 for the following

three solutions, which are shown to an expanded scale: (1) default ($\text{DELX} = 10^{-3}$, $\text{NEWT} \neq -1$), (2) tighter convergence (10^{-4} , $\neq -1$) and (3) successive refactoring (10^{-3} , -1). It is significant to observe that the solution based on the more stringent convergence criterion costs 2.25 times as much as does the one which forces refactoring at every step, since it requires more steps (see Table 6.21). Furthermore, it actually requires one more refactoring,* as is also shown in Table 6.21. Indeed, the solution based on successive refactoring turns out to be 26% cheaper than the default solution, since it required roughly half as many steps. Similarly, comparison of run times for both $\text{DELX}=10^{-4}$ solutions for region II of Figure 6.40 shows that the solution with successive refactoring is 23% cheaper. It appears that the savings due to the bigger load steps allowed by successive refactoring more than offsets the cost of the additional refactorings for this size problem.

The foregoing results now make it possible to recommend a simple computational procedure for the economical DC analysis of the nonlinear softening behavior of shells that can be modelled as small or modest size problems on STAGSC-1.

E. Recommended Computational Procedure for Displacement-Controlled Analyses

Step 1: Start the analysis with the default value of $\text{DELX}=10^{-3}$ for the convergence criterion, unless there is a special reason to proceed otherwise, and let the program decide when refactoring should take place ($\text{NEWT}>0$).

*The refactoring that always occurs during the first step of a restart run is excluded from this relative comparison.

Step 2: Require refactoring at every displacement step (NEWT=-1) when convergence difficulties or inaccurate solutions are first encountered. Set NEWT=-1 for the rest of the analysis until stiffening behavior occurs in the post-collapse portion of the load-displacement curve.

Step 3: Reduce DELX each time subsequent computational problems arise.

Note that this computational procedure may not be economical for problems with large bandwidths because of the cost of refactoring. The present results indicate that it is economical for the largest problem considered here, which has 512 mesh points and an average semi-bandwidth of 128. Also note that the procedure does not apply to a load-controlled analysis since such an analysis generally requires smaller steps for satisfaction of convergence than does a displacement-controlled analysis. This is illustrated by the venetian blind results (Figure 6.34).

6.4.4 CONCLUDING REMARKS AND RECOMMENDATIONS

The quadrilateral flat plate element 411 with 2x2 integration points was used in analyses of the geometrically nonlinear behavior and collapse of a point loaded venetian blind and of pinched and poked cylinders. Displacement-controlled analyses were performed for all three shells along with a load-controlled analysis of the venetian blind. Conclusions and recommendations stemming from these analyses are as follows:

- A. The load displacement curves up to the limit point were obtained in a straightforward way for the three problems. Changes in user strategy during the course of the analysis were required only for the poked cylinder due to convergence difficulties or indications that inaccurate solutions had been accepted. In this respect it is worth noting that the user has some control over the sophisticated but flexible strategy in STAGSC-1, and this allows for a more efficient use of the program.

- B. The STAGSC-1 results agree well with linear series solutions and with a limited number of finite difference nonlinear solutions.
- C. A displacement-controlled (DC) analysis is considerably cheaper than a load-controlled (LC) analysis of the same problem, but may require more decisions pertaining to the selection of the strategy parameters governing the convergence criterion (DELX) and the frequency of refactoring (NEWT). Specifically, the DC analysis of the venetian blind was 6 times cheaper than the LC analysis and required 8 times fewer steps to reach the same limit point.
- D. Because satisfaction of the same convergence criterion is so much easier, it appears that too large a step is sometimes accepted in a DC analysis. This may cause the load-displacement curve to drift away from the "true" solution appropriate to the given mesh. For the venetian blind, the DC curve drifted slightly away from the more accurate LC curve in a local region and then properly returned to it when the program decided to refactor at a later step. Drift in the poked cylinder results required a restart from a previous accurate solution with different values selected for the strategy parameters. Thus, drift is either inconsequential or easily corrected, and is a small price to pay for the relatively greater economy of a DC analysis.
- E. For modest size problems, drift can be eliminated at a lower cost by refactoring at each displacement step instead of sharpening the convergence criterion.
- F. Based on these results, a simple computational procedure is recommended for the DC analysis of the nonlinear softening behavior of shells that are run as small or modest size problems on STAGSC-1.
- G. A DC load-displacement curve is smoother if solutions only at refactored steps are plotted.

- H. STAGSC-1 has the advantage of automatically reducing the load or displacement step when convergence difficulties are encountered, such as when the limit point is approached. Thus, in a LC analysis it is easier for STAGSC-1 to home-in on the collapse load to any degree of accuracy than it is for some other programs in which input values of the load step cannot be reduced internally.
- I. Since knowledge of the post-collapse behavior is important, consideration should be given to the implementation of special techniques [50] that allow a limit point to be passed in a LC analysis.
- J. The scope of the post-processor (STAPL) should be expanded to include variable-variable plots or "history" plots to give plots of load vs. displacement, for example, and to include "snapshots" of the spatial variation of the response variable along a selected grid line at a specified load level (or time point).
- K. Finally, it seems appropriate to close by remarking that experience gained here engenders a sense of confidence in the reliability of the elastic nonlinear capability of STAGSC-1.

6.5 PROGRAM EFFICIENCY

The evaluation of the computational efficiency of STAGSC-1 has been based on execution statistics compiled during the course of this study. It is necessarily subjective because all the work has been performed on the Westinghouse Power Systems Computer Centre CDC 7600 installation. This system has a relatively small central core memory (SCM) (151000_8 , 60 bit words) which is augmented by 600000_8 words of large core memory (LCM) and 65_{10} million words of high speed disk storage. The STAGSC-1 version implemented on this system is not configured to use LCM and any data which is not required in core is buffered to and from disk.

The measure of cost on the CDC 7600 is the computer resource unit (CRU) which is determined by means of an algorithm combining the usage of small and large

core memory, mass storage, input/output transfers, number of disk accesses and central processor time. The dayfile output gives a breakdown of the total CRU usage into its individual components thus giving insight into relative costs of computation and data handling. It must of course, be emphasized that this is subjective because of the weighting assigned by the charging algorithm to these various components. Nevertheless, such statistics do shed light on the performance of STAGSC-1 because it becomes apparent where improvements could be made. The most valuable data are direct comparisons between solutions obtained by STAGSC-1 and other programs to the same problem. However, such an in-depth investigation would have exceeded the resources available for this project and therefore only one such comparison was made.

The data presented cover linear and nonlinear static analyses, small and larger size problems, linear and nonlinear dynamic transient and nonlinear collapse analyses. Table 6.22 provides details of the execution statistics for fifteen separate analyses, including one problem using the MARC program. The central processor time (CPU) and the total resources used (CRU) are given for both the pre-processor (STAGS1, MARCPRE) and the execution phases (STAGS2, MARCSTR). For all but the smallest of problems, the resources used by STAGS1 are a very small proportion of the total and will not be discussed further. The final column of Table 6.22 is an index which is the ratio of CRUs to CP hours and is a measure of the execution efficiency (or, more realistically, inefficiency) of the program. Qualitatively, it is the ratio of the total resources used to the resources used solely in computation. The average value is 14.9 with a maximum spread of -5.5 to +6.0. This compares well with the value of 14.5 obtained for the MARC problem. Table 6.24 presents a comparison between several structural analysis programs in use on the Westinghouse system. This shows that STAGS uses the most total resources per central processor hour.*

Returning to the data in Table 6.22, the one point of direct comparison between STAGSC-1 and MARC shows that although, on a relative basis, MARC

*An interesting feature is that the performance of two different versions of ANSYS is apparently very different and is a consequence of the later version (Revision 3) being tailored to run efficiently in the interactive mode.

performed more efficiently than STAGSC-1, MARC used 2.8 times the resources to solve the same problem. Ultimately, it is on such a basis that a program must finally be judged (other things, such as accuracy, being equal). Table 6.23 gives details of the way in which the computer resources were used in a number of STAGSC-1 runs. In all but two cases, the number of disk accesses was the largest contributor to resource usage. Although this is a direct function of the particular charging algorithm employed, it is nevertheless indicative of a potential area for program improvement. On the CDC 7600, this would be reduced by the use of large core memory (LCM).

To sum up, it appears that STAGSC-1 uses a significantly larger amount of total resources for a given computational effort than other structural analysis programs on the Westinghouse system. Much of this resource usage is due to accessing disk storage. On the other hand, an absolute comparison between STAGSC-1 and MARC suggests that STAGSC-1 is much more efficient in its total resource usage for a given problem. This indication is supported by user experience in a qualitative, but undocumented sense.

TABLE 6.1
 LINEAR CONVERGENCE OF ELEMENTS 410 and 420 FOR THE
 CLAMPED, PRESSURE LOADED SQUARE PLATE

No. of Elements	QUAF 410		QUARC 420	
	W_A (in)	% Error	W_A (in)	% Error
4	.25103	-8.78	.24292	-11.73
9	.26461	-3.85	.27104	-1.51
16	.26969	-2.00	.27487	-0.12
25	.27208	-1.13	.27579	+0.21

TABLE 6.2
 NONLINEAR CONVERGENCE OF ELEMENTS 410, 411, 420, 422 FOR THE
 CLAMPED, PRESSURE LOADED SQUARE PLATE

No. of Elements	% Error			
	QUAF 410	QUAF 411	QUARC 420	QUARC 422
4	-13.6	-5.51	-12.60	-6.75
9	-7.16	-4.63	-4.88	-2.46
16	-4.75	-3.38	-3.32	-1.67
25	-3.52	-2.69	-2.54	-1.45
64	-2.19	--	--	--

TABLE 6.3
NONLINEAR FLAT PLATE ANALYSIS: EXECUTION STATISTICS

Run	Element Type	No. of Elements	No. of Steps	Total CPU secs	CPU secs /step	Comments
10	QUAF 410	4	19	1.977	0.1041	Step halved once.
11	QUAF 410	9	19	3.500	0.1842	Step halved once. 1 Refactoring.
9	QUAF 410	16	19	6.275	0.3303	Step halved once. 1 Refactoring.
12	QUAF 410	25	11	6.106	0.5551	1 Refactoring.
13	QUAF 411	4	11	2.018	0.1835	1 Refactoring.
14	QUAF 411	9	11	4.308	0.3916	1 Refactoring.
15	QUAF 411	16	11	6.974	0.6340	1 Refactoring.
16	QUAF 411	25	11	10.171	0.9246	1 Refactoring.
17	QUARC 420	4	18	3.749	0.2083	Step halved once.
18	QUARC 420	9	19	11.389	0.5994	Step halved once.
19	QUARC 420	16	19	17.885	0.9413	Step halved once.
20	QUARC 420	25	11	19.375	1.7614	1 Refactoring.
21	QUARC 422	4	19	5.056	0.2661	Step halved once. 1 Refactoring.
22	QUARC 422	9	11	8.055	0.7323	1 Refactoring.
23	QUARC 422	16	11	14.142	1.2856	1 Refactoring.

TABLE 6.3 (Continued)

Run	Element Type	No. of Elements	No. of Steps	Total CPU secs	CPU secs /step	Comments
24	QUARC 422	25	11	21.934	1.9940	1 Refactoring.
25	QUAF 410	64	11	13.456	1.2232	1 Refactoring.

TABLE 6.4
QUAF 410--STIFFNESS EIGENMODES

Mode	Eigenvalue	Type	Description
1	0.0	Rigid Body	
2	0.0	Rigid Body	All of the "rigid body" modes are linear combinations of the three translational and the three rotational modes. However, the rotations about the normal (Rw) are not consistent in the rigid body sense with the other five d.o.f. There appears to be some kinematic freedom in the shape functions which gives rise to the extra rigid body freedom.
3	0.0	Rigid Body	
4	0.0	Rigid Body	
5	0.0	Rigid Body	
6	0.0	Rigid Body	
7	0.0	Rigid Body	
8	1598	Membrane	Antisymmetric biaxial stretching with quadratic variation normal to each side.
9	1709	Twist	Pure linear twisting.
10	1923	Bending	Anticlastic bending.
11	2111	Bending	Antisymmetric bending with quadratic and cubic variation of normal displacement.
12	2111	Bending	Same as Mode 11 with sides interchanged.
13	3571	Bending	Doubly symmetric spherical bending.
14	41296	Bending + Twist	Cubic displacement along each edge. Diagonal bending at two corners, diagonal twist at the other two.
15	41296	Bending + Twist	Same as Mode 14 with corners interchanged.
16	42260	Membrane	Quadratic displacements along two opposite sides and cubic along the other two.
17	42260	Membrane	Same as Mode 16 with sides interchanged.
18	2338060	Membrane	"Shearing" mode with cubic displacements along all four sides.
19	2370460	Membrane	Biaxial extension/compression with cubic displacement along each side.

TABLE 6.4 (Continued)

Mode	Eigen Value	Type	Description
20	2370460	Membrane	Same as Mode 19 with extension/compression sides interchanged.
21	2435990	Membrane	Similar to Mode 8, but with the emphasis on the corner displacements (as opposed to normal rotations).
22	4285710	Membrane	Pure biaxial compression (no corner rotations).
23	6870160	Bending + Twist	Diagonal twist at each corner. Cubic normal displacements along each side. Straight diagonals.
24	61861600	Bending + Twist	Similar to Mode 23, but with anticlastic bending of the diagonals.

TABLE 6.5
SINGLE ELEMENT LOAD CASES--MODAL ENERGY DISTRIBUTION

Load Case	8	9	10	11	12	13	14	15	16	17	18	19	20	21	22	23	24
1	--	99.98	--	--	--	--	--	--	--	--	--	--	--	--	--	--	0.02
3	91.60	--	--	--	--	--	--	--	2.73	1.67	--	1.23	1.04	1.08	0.65	--	--
4	--	--	--	--	--	--	--	--	2.04	63.76	--	9.60	9.22	9.99	5.38	--	--
5	82.23	--	--	--	--	--	--	--	7.78	0.12	4.26	--	4.06	0.97	0.58	--	--
6	87.46	--	--	--	--	--	--	--	2.61	1.59	4.53	1.17	0.99	1.03	0.62	--	--
8	--	51.01	12.75	22.96	0.48	6.87	0.34	5.59	--	--	--	--	--	--	--	--	--
9	--	51.01	12.75	0.48	22.96	6.87	5.59	0.34	--	--	--	--	--	--	--	--	--
8+9	--	--	3.62	1.86	2.18	--	0.51	1.27	--	--	--	--	--	--	--	90.55	--

TABLE 6.6
FLEXURAL FREQUENCIES IN XZ-PLANE

Mode No.	Frequency (Hz)		% Difference	Comments
	STAGSC-1	Exact		
1	88.3277	88.8164	-0.6	
2	544.409	556.603	-2.2	Motion in the XZ-plane only. All axial and torsional freedoms suppressed.
3	1496.60	1558.20	-4.0	
4	2869.83	3054.05	-6.1	
5	4631.57	5048.56	-8.3	20 active degrees of freedom.
6	6739.66	7541.67	-10.6	
7	9140.57	10533.4	-13.2	
8	11746.7	14023.8	-16.2	
9	14379.4	18012.7	-20.2	
10	16594.3	22500.4	-26.2	

TABLE 6.7
CLOSELY SPACED AND EQUAL MODES

Mode No.	Frequency (Hz)		% Difference	Dispt. Ratio (XZ/XY)	Comments
	STAGSC-1	Exact			
1	80.3059	80.7422	-.54	$\frac{1}{10^7}$	1% difference in cross-section dimensions.
2	81.1081	81.5496	-.54	10^7	
3	495.253	506.003	-2.13	$\frac{1}{10^7}$	
4	500.173	511.063	-2.13	10^7	
5	1362.69	1416.54	-3.8	$\frac{1}{10^7}$	
6	1376.09	1430.71	-3.8	10^7	

1	80.3058	80.7422	-.54	6.66	Equal dimensions.
2	80.3058	80.7422	-.54	$\frac{1}{6.66}$	
3	495.253	506.003	-2.13	1.148	
4	495.253	506.003	-2.13	$\frac{1}{1.148}$	
5	1362.66	1416.54	-3.8	$\frac{1}{1.041}$	
6	1362.66	1416.54	-3.8	1.041	

TABLE 6.8
FLAT PLATE CANTILEVER FREQUENCIES

Mode No.	Mode Type	Frequency (Hz)				% Error		
		Exact	STAGSC-1	MARC	Zienk.	STAGSC-1	MARC	Zienk.
1	First Bending	846	750	845	826	-11.3	-0.12	-2.4
2	First Twist	3638	2172	3651	3728	-40.3	0.36	2.5
3	Second Bending	5266	3784	5280	5157	-28.1	0.27	-2.1
4	Second Twist	11870	6335	12100	12055	-46.6	1.9	1.6

TABLE 6.9
1/4 WAVE MODEL FREQUENCIES

Mesh	Fundamental Frequency (Hz)	% Error
4 x 4	81.58	-2.73
5 x 5	82.45	-1.69

TABLE 6.10
1/8 CYLINDER MODEL FREQUENCIES

Elements	Mode	n	Frequency Hz	% Error	Element Aspect Ratio	Comments
8 Circ.	1	8	75.79	-9.6	2.55	3 modes only requested
2 Axial	4	10	88.37	-13.6		
	5	6	99.77	-4.6		
16 Circ.	1	8	74.81	-10.8	5.09	Circumferential refinement
2 Axial	4	10	84.83	-17.1		
	5	6	99.80	-4.6		
	7	12	108.15	-22.3		
16 Circ.	1	8	82.17	-2.0	2.55	Axial refinement
4 Axial	4	10	99.22	-3.0		
	5	6	103.63	-0.9		
	7	12	133.89	-3.9		
16 Circ.	1	8	84.15	0.33	1.27	Axial refinement
8 Axial	4	10	103.28	0.92		
	5	6	104.55	-0.01		
	7	12	141.69	1.74		

TABLE 6.11
1/2 CYLINDER MODEL FREQUENCIES

STAGSC-1 Mode No.	Frequency Hz			n	Comments
	STAGSC-1	Exact	% Error		
1	82.17	83.87	-2.0	8	
2	82.39	--	--	8	Spurious mode
3	86.35	87.69	-1.5	7	
4	86.63	--	--	7	Spurious mode

TABLE 6.12
1/2 CYLINDER MODEL FREQUENCIES

Actual Mode No.	Frequency - Hz		% Error	n
	STAGSC-1	Exact		
1	82.17	83.87	-2.03	8
2	86.35	87.69	-1.53	7
3	87.75	89.92	-2.41	9
4	99.34	102.3	-2.89	10
5	103.63	104.6	-0.93	6

TABLE 6.13
CRITICAL TIME STEP ESTIMATES - EXPLICIT INTEGRATION

Method	Critical Δt (secs)	Comments
(i)	4.94×10^{-6}	Based on highest frequency.
(ii)	(a) 2.03×10^{-6} (b) 4.08×10^{-6}	Users' Manual formulae.
(iii)	2.36×10^{-6}	Speed of sound.

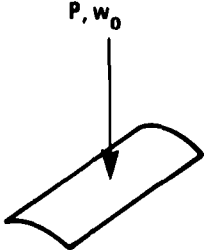
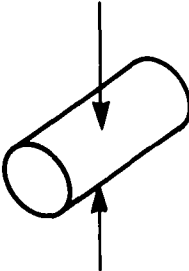
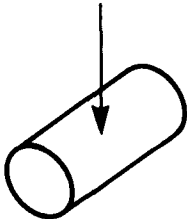
TABLE 6.14
SUMMARY OF RING TRANSIENT ANALYSES

Run	Type	Operator	Time Step Δt (sec)	Comments
10	Elastic- Plastic	Park	2×10^{-6}	Final time reached = 620×10^{-6} sec. Time limit.
11	Elastic- Plastic	Park	Automatic	Initial $\Delta t = 2 \times 10^{-6}$ sec. Increased to 16×10^{-6} sec. Solution breaks down.
12	Elastic- Plastic	Park	2×10^{-6}	Final time reached = 1002×10^{-6} sec. TAPE22 saved for restart.
13	Elastic- Plastic	Park	2×10^{-6}	Attempted restart failed. Message indi- cated plasticity data could not be found.
14	Elastic	Park	2×10^{-6}	Small number of iterations required per time step (2 or 1).
15	Elastic	Park	20×10^{-6}	Δt reduced to 10×10^{-6} sec. at Step 2. Small time limit (8 secs).
16	Elastic	Park	10×10^{-6}	2000×10^{-6} secs. reached. Increased Δt caused periodic refactoring.
17	Elastic	Trapezoidal	10×10^{-6}	Periodic refactoring.
18	Elastic	Trapezoidal	2×10^{-6}	No refactoring. Average of 2 iterations per time step.
19	Elastic	Gear 2nd Order	10×10^{-6}	Periodic refactoring.
20	Elastic	Gear 2nd Order	2×10^{-6}	No refactoring. 1 or 2 iterations per time step.
21	Elastic	Gear 3rd Order	2×10^{-6}	A lot of refactoring after 240×10^{-6} sec. Determinant changed sign at $336 \times$ 10^{-6} sec.
22	Elastic	Explicit	1×10^{-6}	Divergence occurred after 14 steps.
23	Elastic	Explicit	1×10^{-7}	Time limit after 265 steps.
24	Elastic	Explicit	5×10^{-7}	Divergence occurred after 17 steps.
25	Elastic	Explicit	1×10^{-7}	Solution obtained out to 1710 steps. Time limit.

TABLE 6.15
NONLINEAR TRANSIENT EXECUTION STATISTICS

Run	Type	Operator	No. of Steps	CPU secs.	CPU secs/ Step	CRU	CRU/Step	Comments
12	Elastic- Plastic	Park	501	200.45	0.400	0.798	.00159	Approx. 1 iteration/ step. Also plastic sub-iterations.
14	Elastic	Park	1000	139.61	0.140	0.587	.00059	2 iterations/step. No refactoring.
16	Elastic	Park	200	45.88	0.229	0.169	.00085	2 to 7 iterations/ step. Periodic refactoring.
17	Elastic	Trapezoidal	200	63.28	0.316	0.215	.00108	2 to 6 iterations/ step. Frequent refactoring.
18	Elastic	Trapezoidal	1000	141.53	0.142	0.593	.00059	2 iterations/step. No refactoring.
19	Elastic	Gear 2nd Order	200	38.84	0.194	0.148	.00074	2 to 7 iterations/ step. Periodic refactoring.
20	Elastic	Gear 2nd Order	1000	119.04	0.119	0.511	.00051	1 or 2 iterations/ step. No refactoring.
21	Elastic	Gear 3rd Order	167	44.85	0.269	0.156	.00093	2 to 20 iterations/ step. Much refactoring.
25	Elastic	Explicit	1710	316.54	0.185	1.271	.00074	No iterations or refactoring necessary.

Table 6.16 Dimensions, Material Properties and Collapse Loads

	VENETIAN BLIND	PINCHED CYLINDER	POKED CYLINDER
			
GEOMETRY			
R = mid. surface radius (in.)	2.5	.5	1117
L = length (in.)	6	1.0	996
t = thickness (in.)	.01	.005	1.75
ϕ_0 = opening angle	45°	—	—
R/t	250	100	638
L/R	2.4	2	.892
MATERIAL PROPERTIES			
E = Young's modulus (psi)	10 ⁷	10 ⁷	2.79 x 10 ⁷
ν = Poisson's ratio	.3	.3	.3
BOUNDARY CONDITIONS			
curved edges	SS	SS	SS
straight sides	F	—	—
COLLAPSE LOAD P_c (lb)			
STAGSC-1			
DC = disp-cont.	2.35	12.14	773,200
LC = load-cont.	2.35	—	—
STAGSA (Brogan & Almroth)	2.48	—	—
% diff.	5.2	—	—

SS = simply support (classical)

F = free

% diff. is relative to STAGSA collapse load

TABLE 6.17
PARTICULARS OF FINITE ELEMENT

Problem	Mesh			DOF	Average Semi -Bandwidth	Number of Runs	Number of Steps to:		CPS	
	Type	m	n				P_c	P_{end}	P_c	P_{end}
Venetian Blind	unif.	10	8	603	64	DC: 1	19	30	37	6
						LC: 2	157	157	198	19
Pinched Cylinder	var.	12	8	693	61	5	45	59	248	28
Poked Cylinder	var.	16	32	4185	128	11	102	102	3717	3717

m,n = Number of mesh points in axial & circumferential directions, respectively

DOF = Number of active degrees of freedom

P_c = Collapse load at limit point of $P-w_0$ curve

P_{end} = Denotes end of analysis

CPS = Computer processing seconds on the Westinghouse CDC-7600 computer

CRU = Computer Resource Units

\$ Cost is based on in-house rate of \$90/CRU

DELX = Error tolerance for convergence. Default value is 10^{-3}

(Note that the default value of the relaxation factor WUND was used in all anal)

EMENT ANALYSES

	CPS	CRU		\$		DELX	Refactor at Every Step ?
	<u>P_{end}</u>	<u>P_c</u>	<u>P_{end}</u>	<u>P_c</u>	<u>P_{end}</u>		
7	65	.170	.297	15	27	10 ⁻³	No
8	198	1.021	1.021	92	92	10 ⁻³	No
8	289	.940	1.098	85	99	10 ⁻³	No
7	3717	21.367	21.367	1923	1923	10 ⁻³ , 10 ⁻⁴ , 10 ⁻⁵	Yes for P+P _c

ly

all analyses)

TABLE 6.18
COMPARISON OF LINEAR SOLUTIONS FOR VENETIAN BLIND
AND PINCHED CYLINDER PROBLEMS

Problem	Mesh (mxn)	$w_o Et/P$		
		STAGSC-1	Prev. Sol.	% Diff. ^(a)
Venetian Blind	10x8	1091	1156 ^(b)	-5.6
Pinched Cylinder	12x8	148		-9.8
	23x15	160	164 ^(c)	-2.4

- (a) % difference is relative to the previous solution
(b) Brogan & Almroth, 1971
(c) Lindberg, et al., 1969

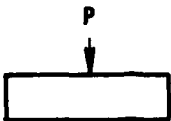
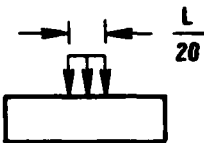
TABLE 6.19
VARIABLE MESHES USED IN PINCHED AND POKED CYLINDER ANALYSES

Row (or Col.) Numbers	Size of Intervals in Axial & Hoop Directions			
	Pinched Cylinder		Poked Cylinder	
	Axial(in.)	Hoop(deg)	Axial(in.)	Hoop(deg)
1-2	.0124	3.481	7	1
2-3	.0170	5.469	8.4	1.1
3-4	.0232	6.96	10.08	1.21
4-5	.0341	10.94	12.096	1.331
5-6	.0449	19.89	14.5152	1.4641
6-7	.0495	21.38	17.4182	1.6105
7-8	.0557	21.88	20.9019	1.7716
8-9	.0651		25.0823	1.9487
9-10	.0650		30.0987	2.1436
10-11	.0665		36.1185	2.3579
11-12	.0666		43.3422	2.5937
12-13			52.0106	2.8531
13-14			62.4127	3.1384
14-15			74.8952	3.4523
15-16			83.6286	3.7975
16-17				4.1172
17-18				4.5950
18-19				5.0545
19-20				5.5599
20-21				6.1159
21-22				6.7275
22-23				7.4002
23-24				8.1403
24-25				8.9543
25-26				9.8497
26-27				10.8347
27-28				11.9182
28-29				13.1100
29-30				14.4210
30-31				15.8631
31-32				15.5060

Load is applied at Row 1 and Column 1.

The size of consecutive axial and hoop intervals for the poked cylinder increase geometrically by 20% and 10%, respectively, except for the last interval.

Table 6.20 Comparison Of Linear Results For The Poked Cylinder

Location	Variable	STAGSC-1	Kempner et al.	% Diff. (a)
				
at load, $x=y=0$	$w_0 Et/P$	1092	1045	4.5
$x=L/4$	$w Et/P$	368	366	.4
$y=0$	M_y/P	.01542	.01492	3.3
	M_x/P	.00405	.00395	2.7
	$N_x R/P$	-15.04	-13.72	9.6
$x=0$	$w Et/P$	346	325	6.5
$y=L/4$	$N_x R/P$	27.50	24.75	11.1
				Average = 5.4%

(a) % Difference is Relative to Previous Solution

TABLE 6.21
COMPARISON OF THREE SOLUTIONS FOR REGION I

	Base Run (Default)	"Tighten Conv." Run	"Refactored" Run
DELX =	10 ⁻³	10 ⁻⁴	10 ⁻³
Refactor at Every Step?	No	No	Yes
CRU =	<u>2.582</u>	<u>4.298</u>	<u>1.908</u>
w ₀ (in.)	$\frac{P}{4}$ (lb)	$\frac{P}{4}$ (lb)	$\frac{P}{4}$ (lb)
18.5		69880 ⁺	69886 ⁺
19	71592 ⁺	71523	
19.5		73453	73319*
20		75364	
20.5		76888	76626*
21	78449	78360*	
21.5		79771	
22	82842*	81538*	
22.5		83104	82933*
23	86392	84742	
23.5	86421*	86113*	
24	88421	87593	
24.5	90249	<u>89106</u>	88592*
25	90539*	90460 ⁺	
25.5	92010	91847*	
26	92873	93289*	
26.5	94222 ⁺	94826	93625*
27		96537*	
27.5	97309	97359	
28		98530	
28.5	102340	99774*	98397*
29		101470	
29.5	99486	<u>102800</u>	
30		103870 ⁺	
30.5		105140*	<u>103020*</u>

⁺Automatic refactoring during first step of restart run

*Refactoring

TABLE 6.22

STAGSC-1 EXECUTION STATISTICS - 1

Run	Description	Element Type	Active D.o.F.	STAGS-1			STAGS-2			Total		
				CPU Secs.	CRU	CPJ Secs.	CPU Secs.	CRU	CPJ Secs.	CPJ	CRU	CP Hours
FLATPLATE 08	Center loaded flatplate. Linear static.	410	96	0.329	0.001	0.456	0.002	0.002	0.785	0.003	13.8	
FLATPLATE 10	Pressure loaded flatplate. Nonlinear static.	410	13	0.220	0.001	1.977	0.006	0.006	2.197	0.007	11.5	
FLATPLATE 21	Pressure loaded flatplate. Nonlinear static.	422	41	0.300	0.001	5.056	0.020	0.020	5.356	0.021	14.1	
FLATPLATE 24	Pressure loaded flatplate. Nonlinear static.	422	326	1.029	0.004	21.934	0.084	0.084	22.963	0.088	13.8	
CYLROOF 01	Gravity loaded cylindrical roof. Linear static.	410	30	0.224	0.001	0.189	0.001	0.001	0.413	0.002	17.4	
CYLROOF 05	Gravity loaded cylindrical roof. Linear static.	410	630	1.229	0.005	3.064	0.009	0.009	4.293	0.014	11.7	
PLATETRAN 06	Linear transient analysis of a flatplate. Trapezoidal integ.	410	72	0.267	0.001	5.249	0.027	0.027	5.516	0.028	18.3	
MARCDemo PRO8401A*	Linear transient analysis of a flatplate. Modal superposition.	MARC Element 4	48	MARCPRE 1.099	MARCPRE 0.003	MARCPRE 18.252	MARCPRE 0.075	MARCPRE 0.075	19.351	0.073	14.5	
RINGSTAT 05	Elastic-plastic, static, large displacement analysis of a center loaded ring.	410	246	0.427	0.001	20.553	0.054	0.054	20.980	0.055	9.4	

TABLE 6.22 (Continued)

Run	Description	Element Type	Active D.o.F.	STAGS-1		STAGS-2		Total	
				CPU Secs.	CRU	CPU Secs.	CRU	CPU Secs.	CRU
RINGTRAN 16	Elastic, large displacement analysis of a ring with initial velocity. Park method.	410	122	0.465	0.002	45.879	0.169	46.344	0.171
									13.3
RINGTRAN 25	Same as above using explicit method.	410	122	0.466	0.002	---	---	327.435	1.271
									14.0
WMSLO3P	Shallow cylinder segment (Venetian blind). Nonlinear collapse.	411	603	0.871	0.003	126.419	0.665	127.290	0.668
									18.9
WMSLOQP	Pinch-loaded cylinder. Nonlinear collapse.	411	2772	5.042	0.017	154.659	0.767	159.701	0.784
									17.7
WMSLOJA	Pinch-loaded cylinder. Nonlinear collapse.	411	693	1.350	0.004	83.382	0.308	84.732	0.312
									13.3
WMSLO7Y	Point-loaded cylinder.	411	4185	8.895	0.038	---	---	514.184	2.991
									20.9

**MARC Demonstration, Problem 401-a

TABLE 6.23
STAGSC-1 EXECUTION STATISTICS - 2

Run	Description	SCM	I/O	Percent of Total CRUs			CP
				I/O Buffers	Disk Storage	Disk Accesses	
CYLROOF 05	Gravity loaded cylindrical roof. Linear static.	13.0	17.4	4.4	0	52.2	13.0
PLATETRAN 06	Linear transient analysis of flatplate. Trapezoidal integration	13.2	2.6	2.6	0	73.7	7.9
MARC DEMO PROB401A	Same as above using MARC and modal superposition.	16.1	4.6	1.1	0	67.8	10.3
RINGSTAT 05	Elastic-plastic, static, large disp. Center loaded ring.	21.0	22.6	4.8	0	37.1	14.5
RINGTRAN 16	Elastic, large disp. Ring with initial velocity. Park method.	15.9	22.5	3.3	0.5	47.3	10.4
RINGTRAN 25	Same as above using explicit method.	15.1	3.1	2.1	1.3	68.4	9.9
WMSLOJA	Pinch-loaded cylinder. Nonlinear collapse.	16.0	35.8	2.8	0.6	34.3	10.5
WMSLO7Y	Point-loaded cylinder Nonlinear collapse.	13.0	42.9	2.1	1.5	33.8	6.6

TABLE 6.24
COMPARATIVE PROGRAM STATISTICS

Program	<u>CRU</u> CP hr.
STAGS	16.6
MARC	11.5
WECAN	9.1
ANSYS Rev. 2	5.8
ANSYS Rev. 3	12.0
PLACRE	10.6

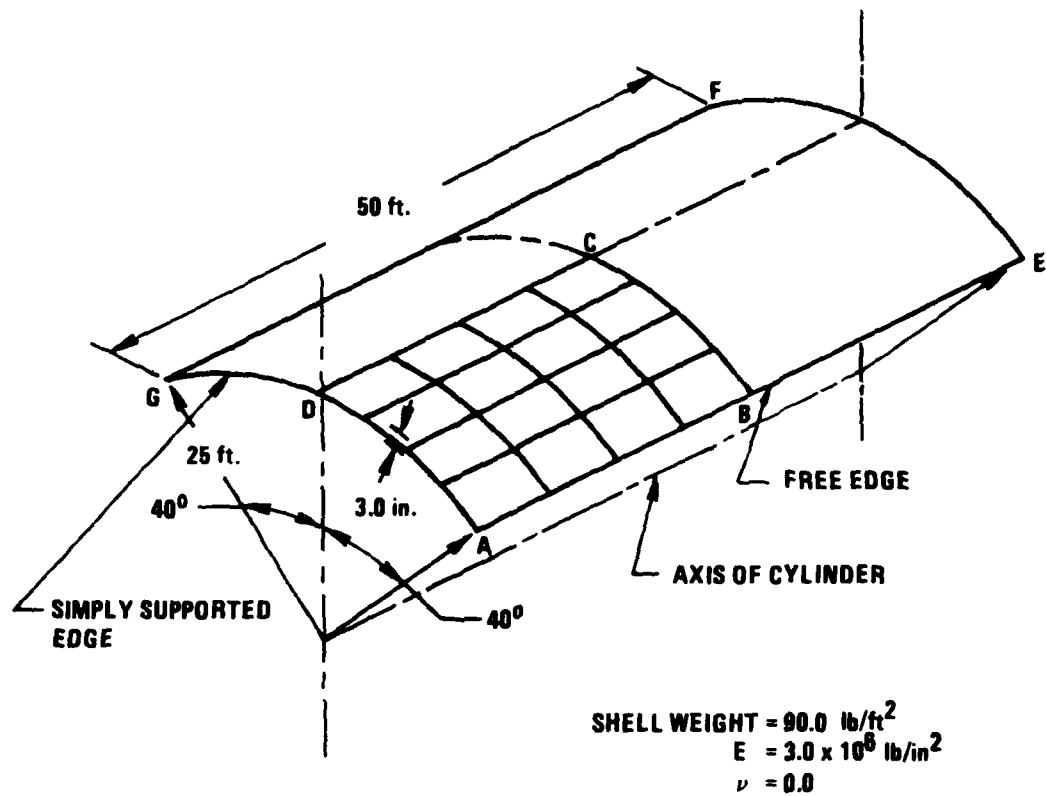


Figure 6.1 Simply Supported Cylindrical Roof
 - Gravity Load

5407-8

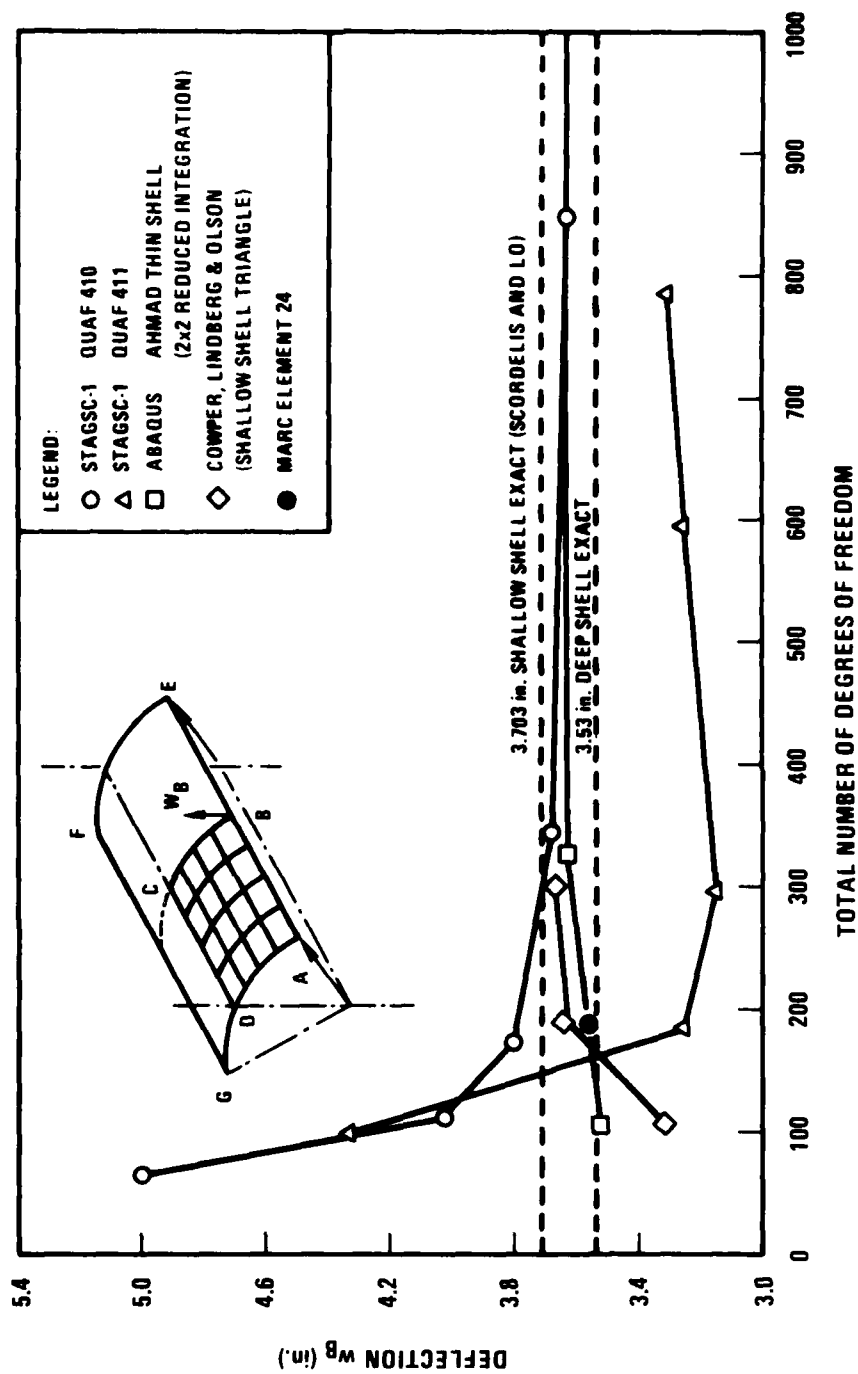


Figure 6.2 Cylindrical Shell Roof - Element Convergence (1)

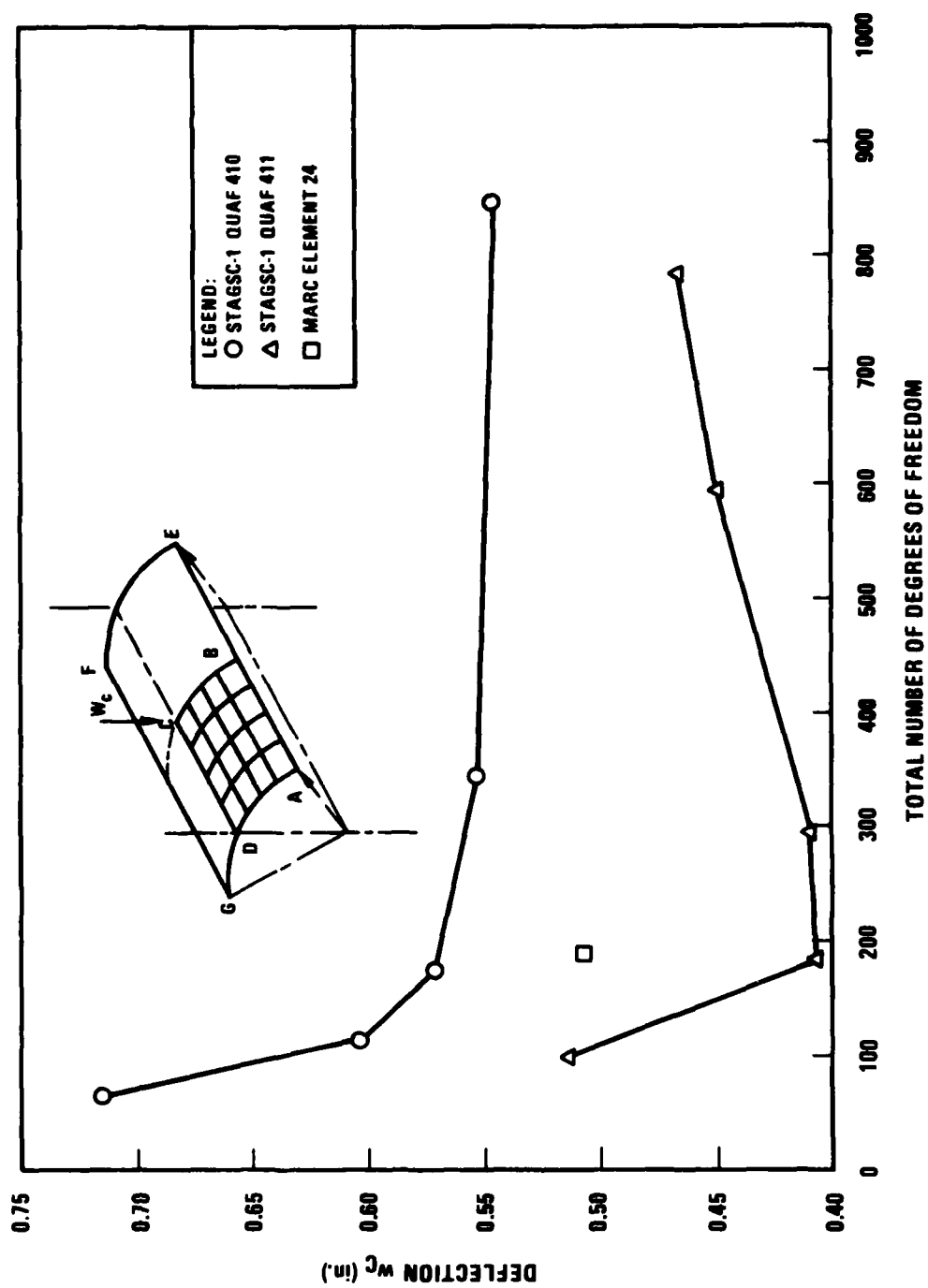


Figure 6.3 Cylindrical Shell Roof - Element Convergence (2)

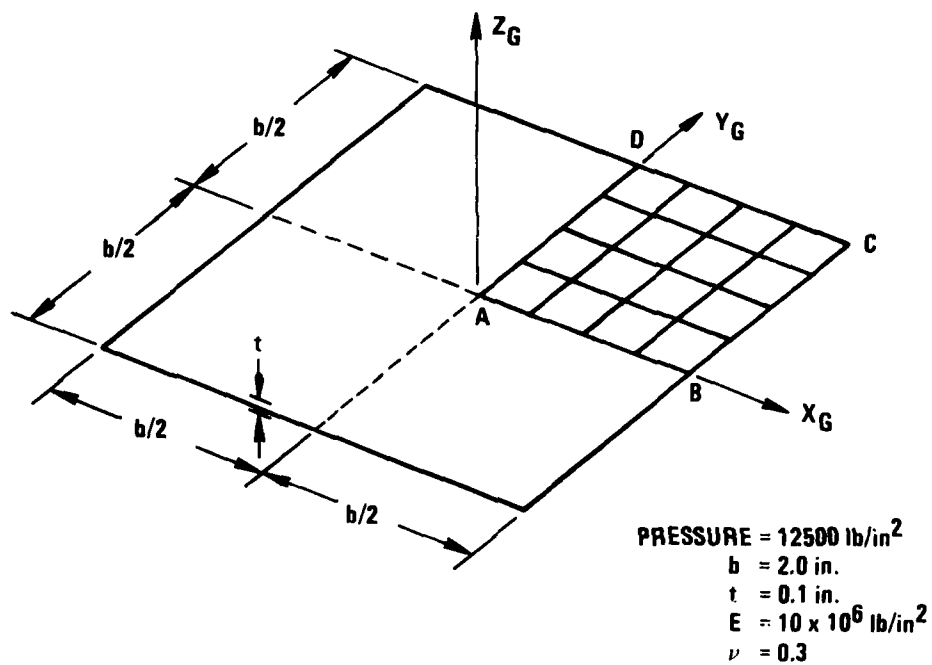


Figure 6.4 Flat Plate Problem

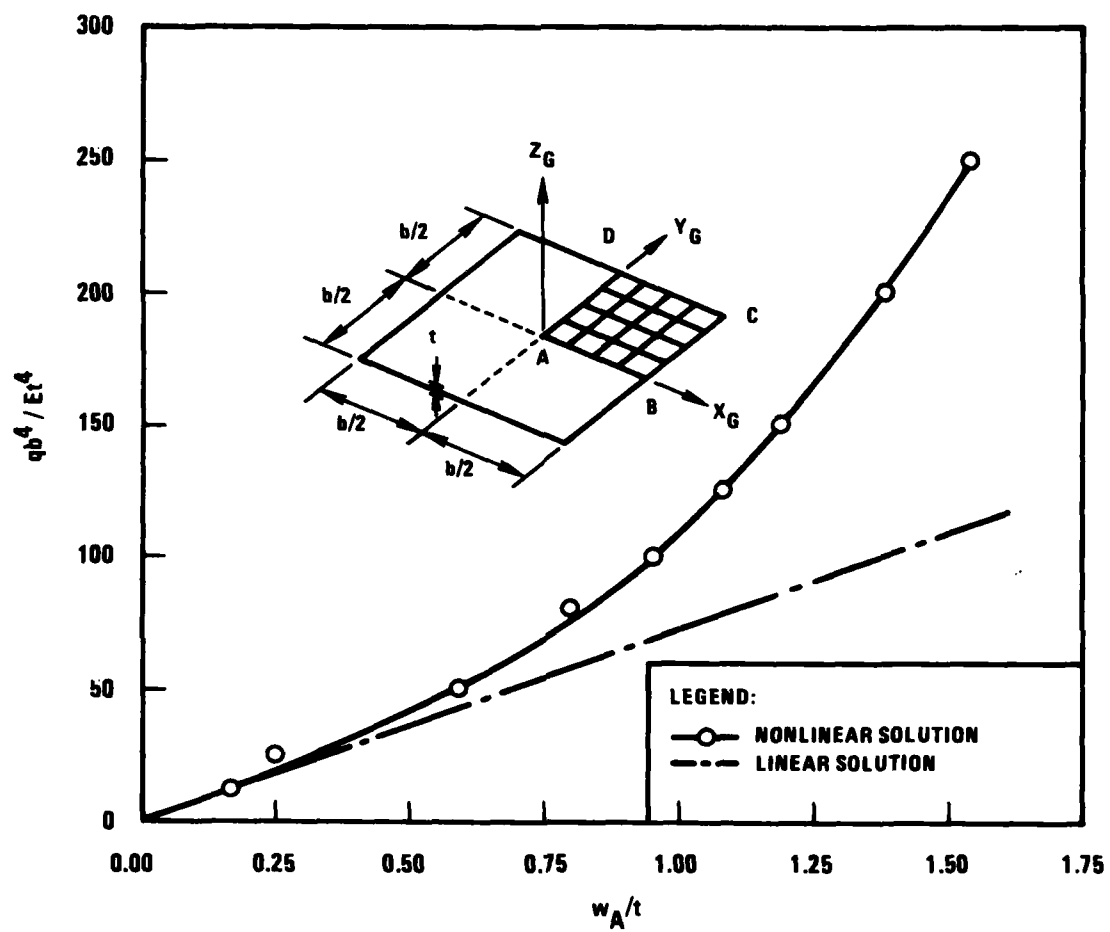


Figure 6.5 Flat Plate with Clamped Edges (Ref: Roark p. 408)

5407-36

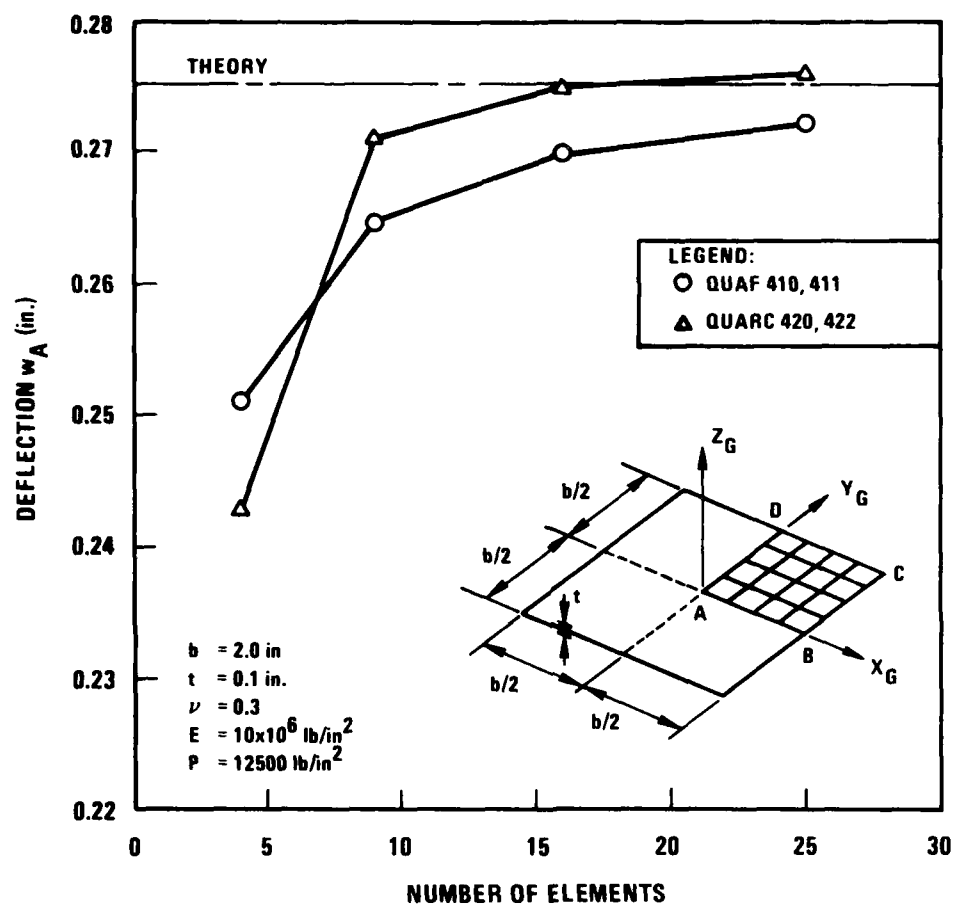


Figure 6.6 Flat Plate with Clamped Edges Under Uniform Pressure Loading
 -- Linear Element Convergence

5407-37

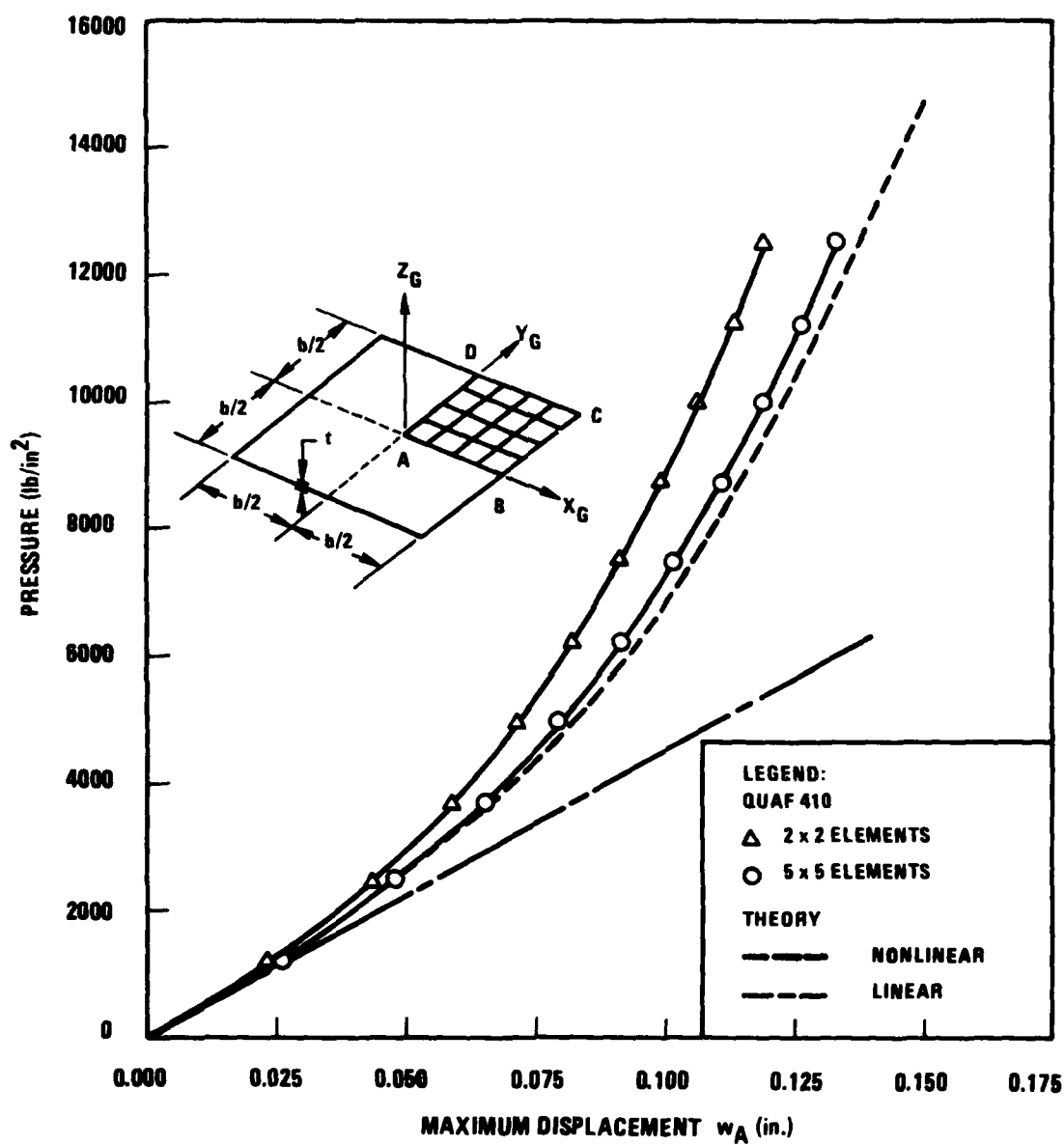


Figure 6.7 Flat Plate With Clamped Edges Under Uniform Pressure
— Nonlinear Solution

5407-35

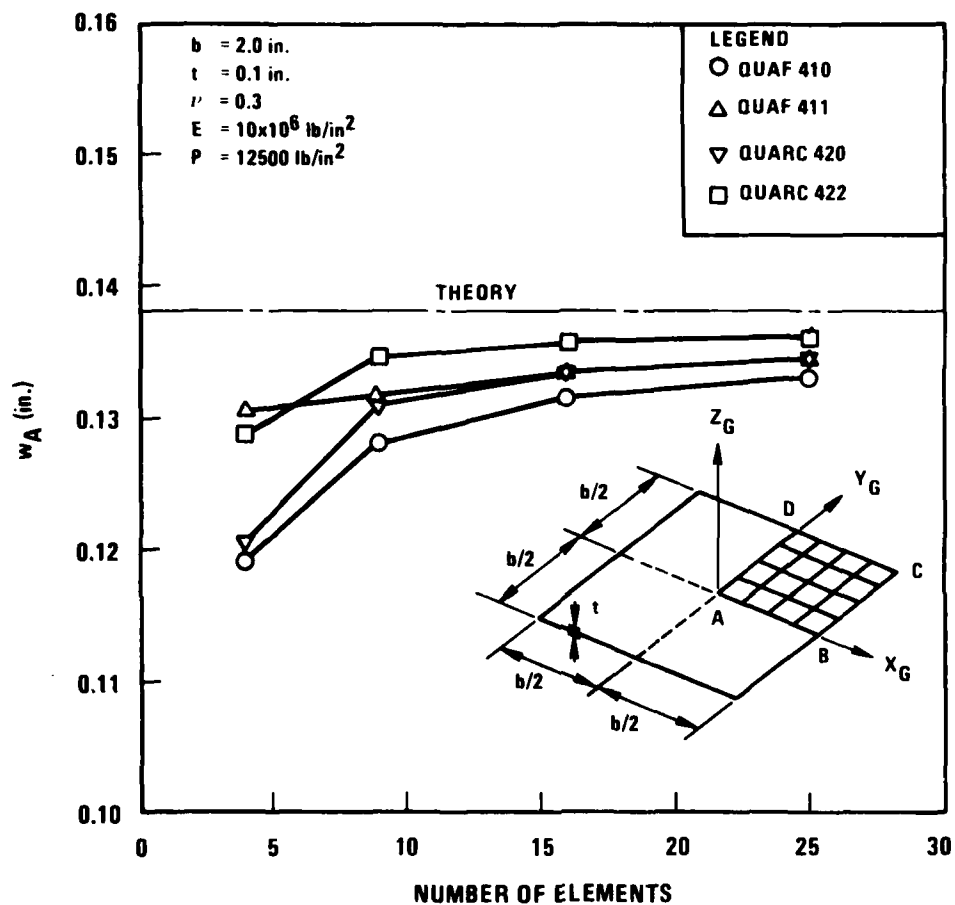


Figure 6.8 Flat Plate with Clamped Edges Under Uniform Pressure Loading – Nonlinear Element Convergence

5407-34

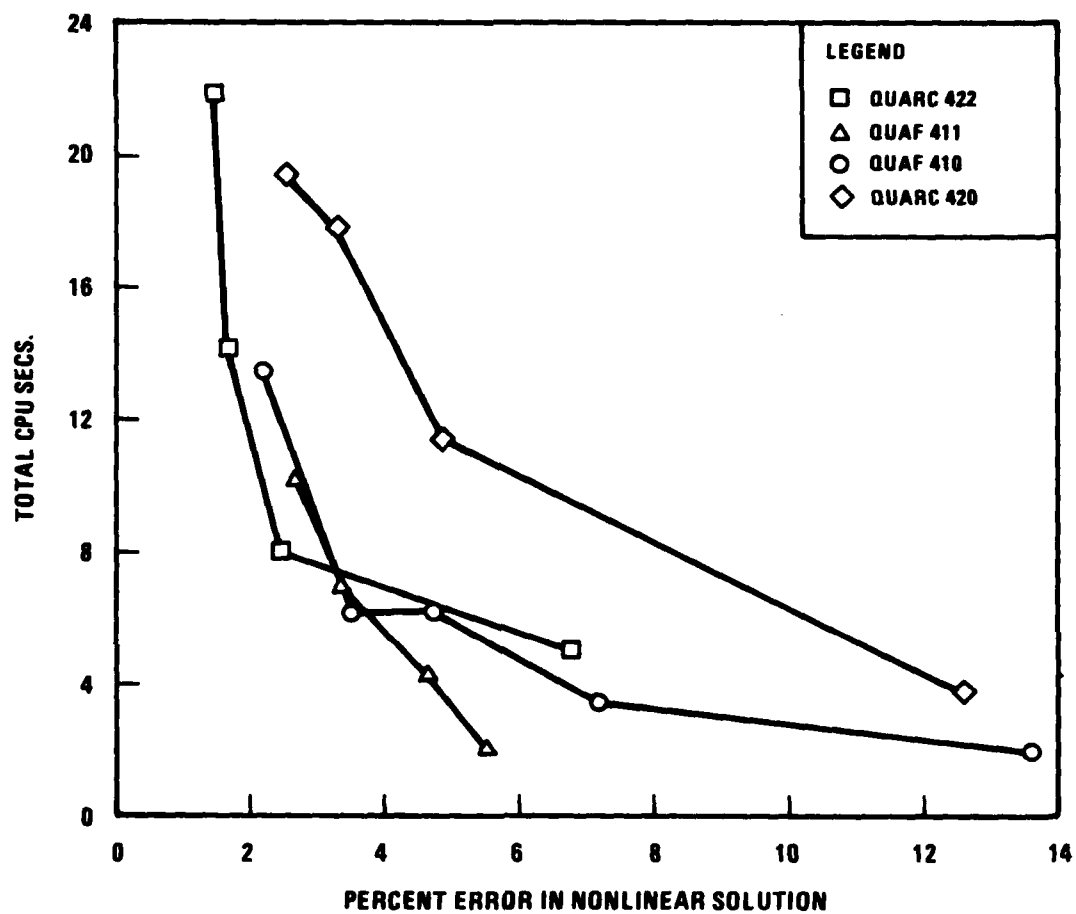


Figure 6.9 Flat Plate with Clamped Edges Under Uniform Pressure
– Percent Error in Nonlinear Solution

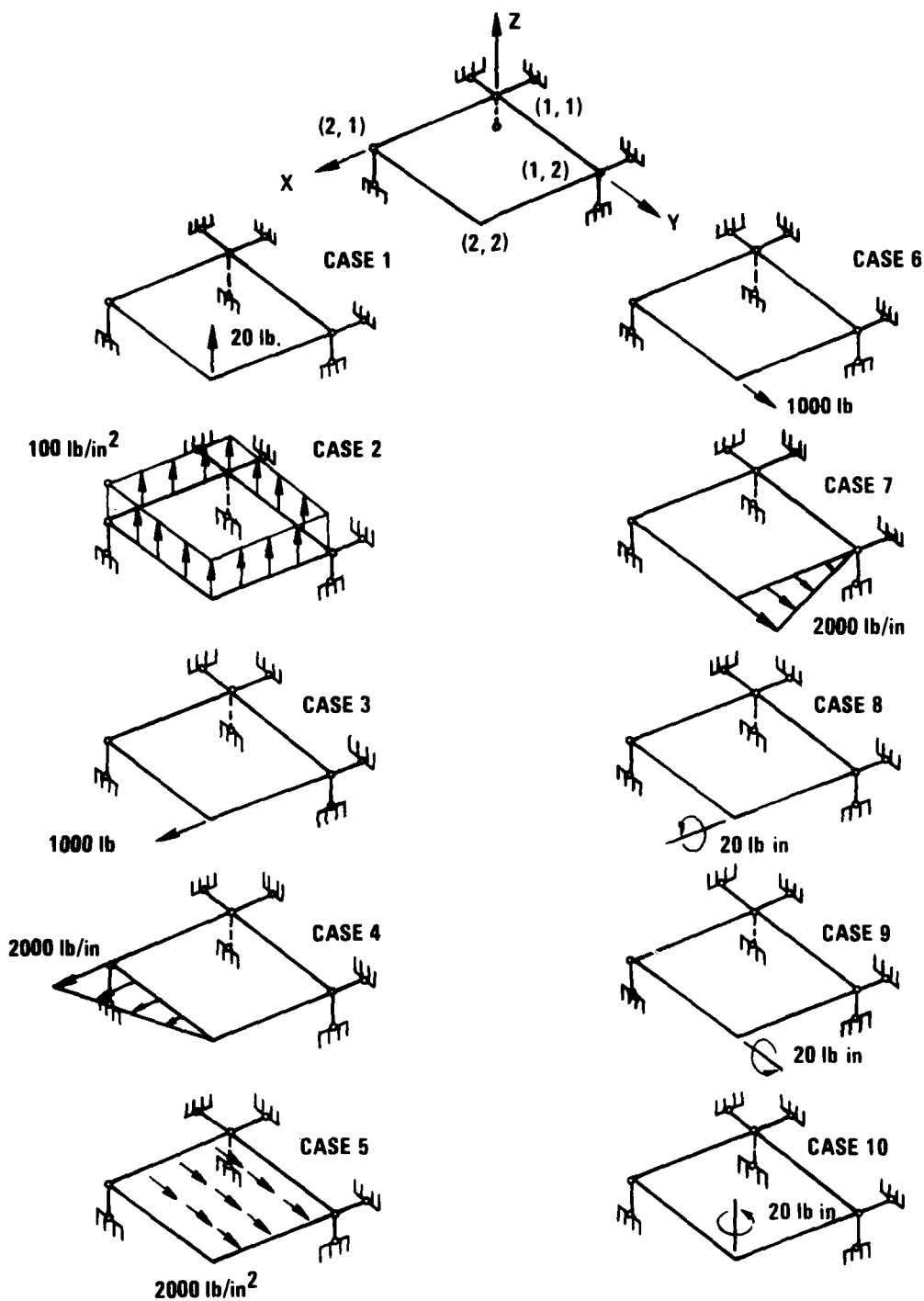


Figure 6.10 Single Element Load Cases

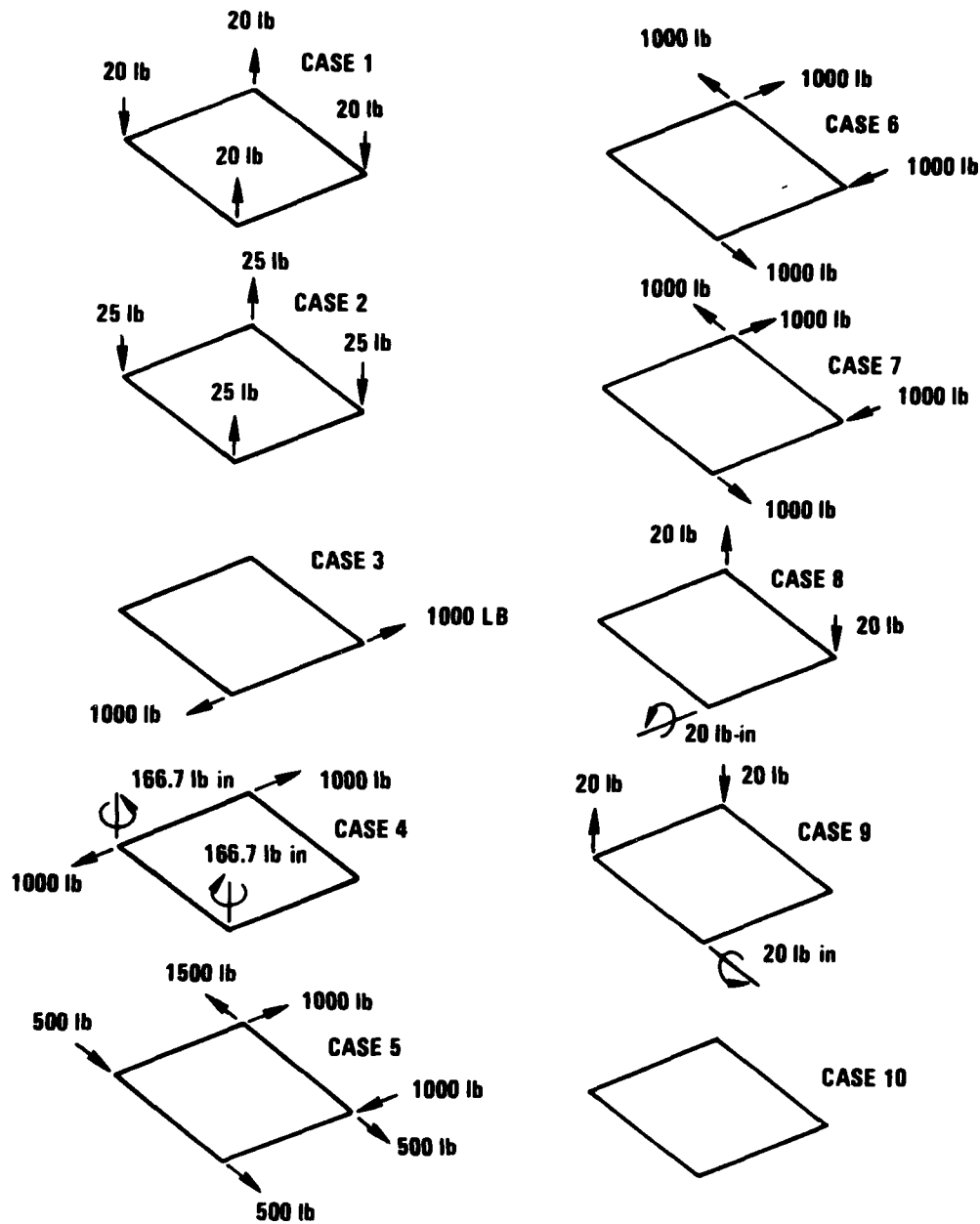


Figure 6.11 Nodal Forces for Single Element Load Cases

5407-11

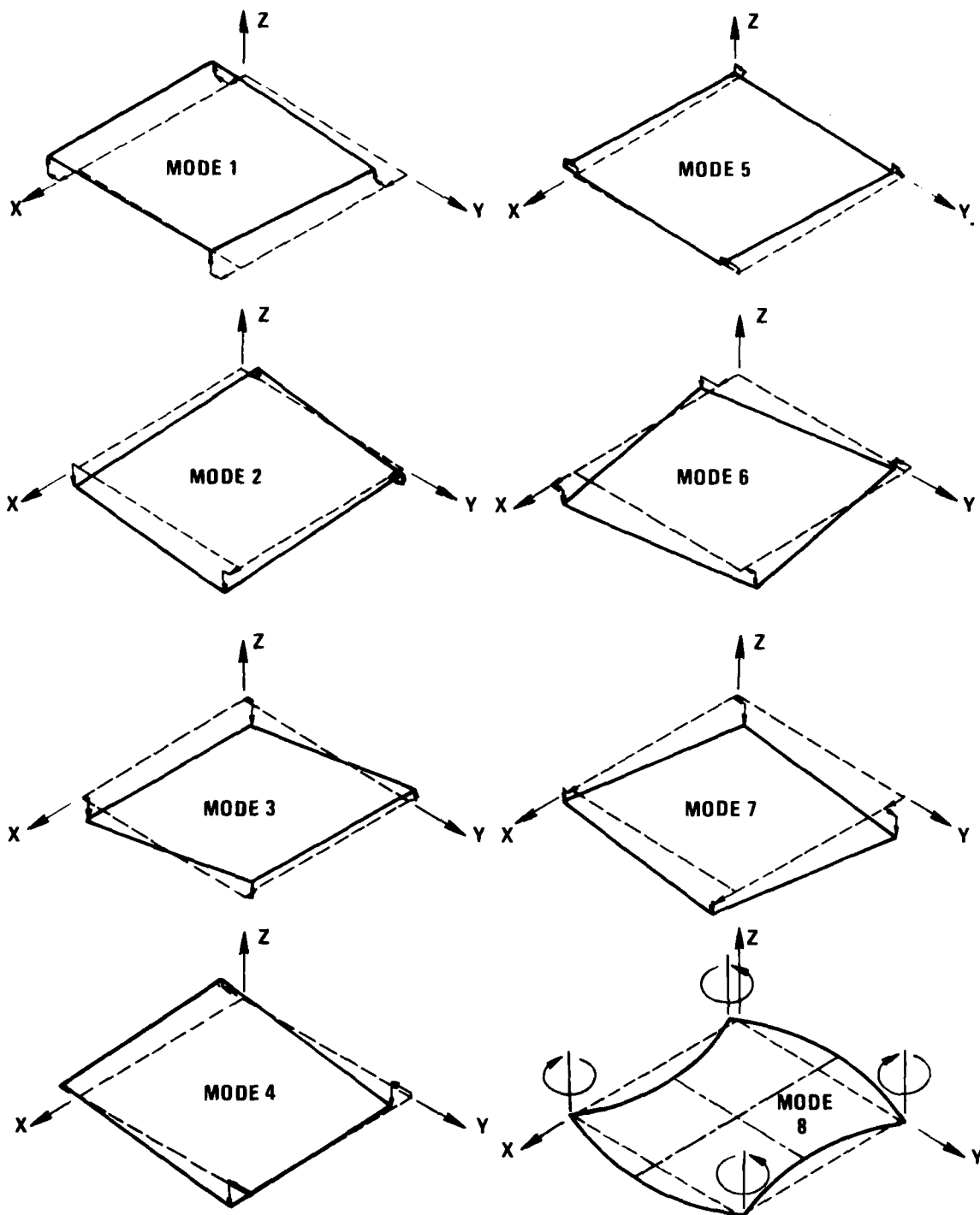


Figure 6.12-a Stiffness Eigenmodes - QUAF 410

5407-32

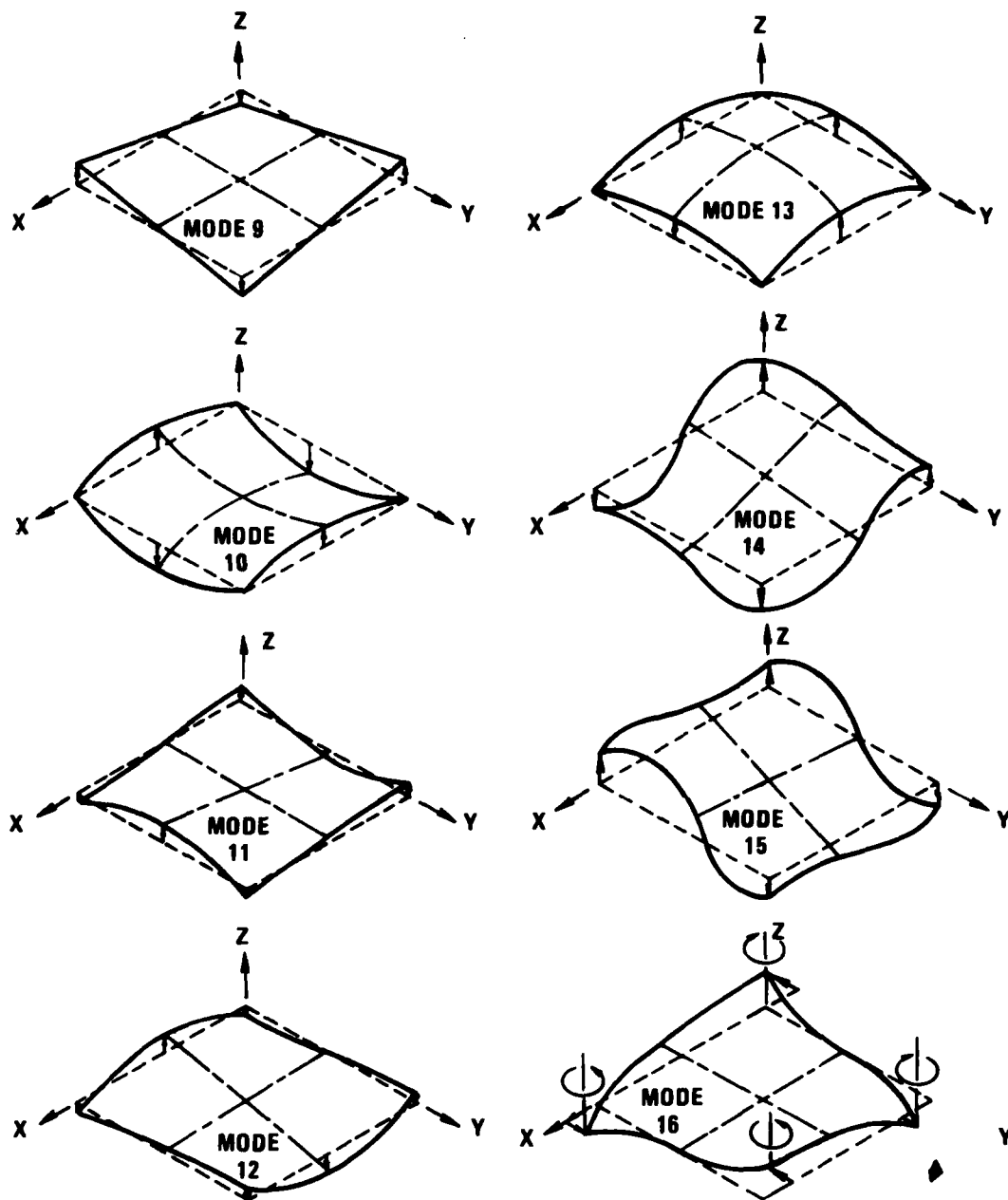


Figure 6.12.b Stiffness Eigenmodes - QUAF 410

5407-30

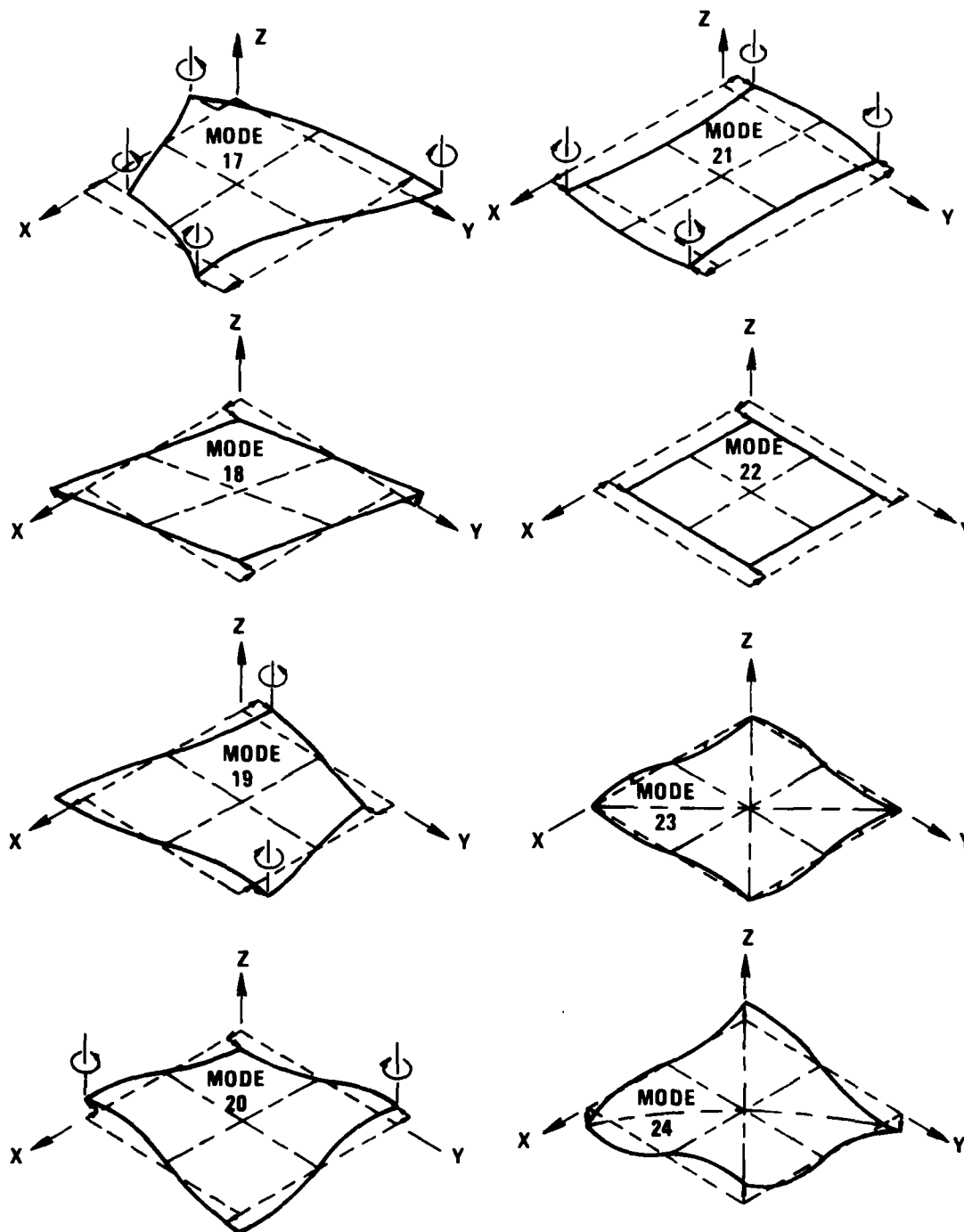
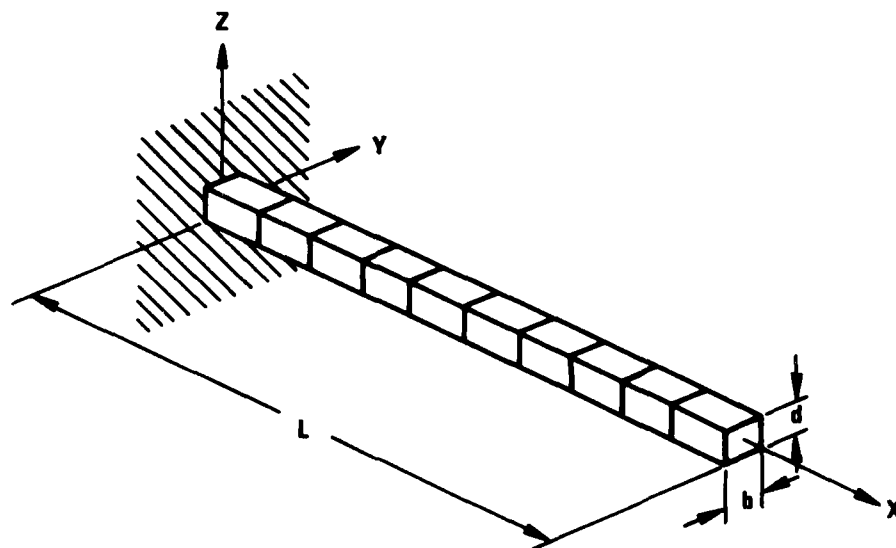


Figure 6.12-c Stiffness Eigenmodes - QUAF 410

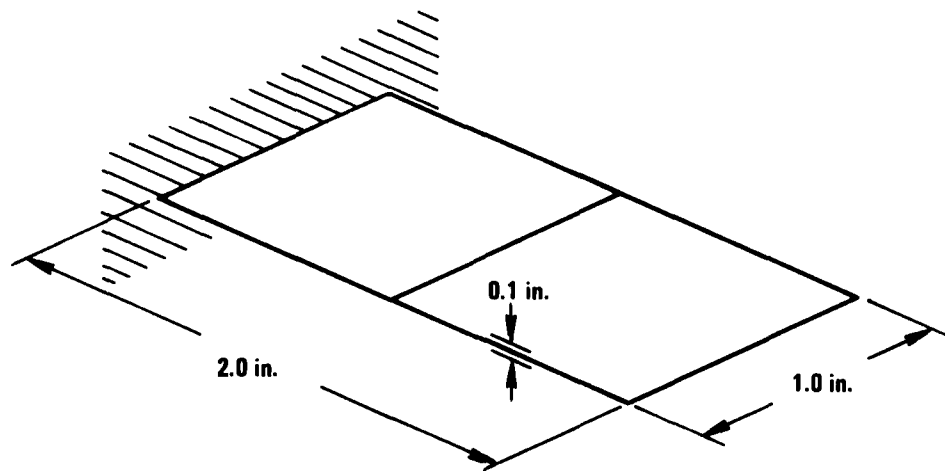
5407-31



$L = 20 \text{ in.}$
 $b = 1.0 \text{ in.}$
 $d = 1.1 \text{ in.}$
 $E = 30 \times 10^6 \text{ lb/in}^2$
 $\rho = 0.29 \text{ lb/in}^3$
 $\nu = 0.25$

BEAM ELEMENT 210

Figure 6.13 3-D Beam Model For Modal Analysis



$$\begin{aligned} E &= 30 \times 10^6 \text{ lb/in}^2 \\ \nu &= 0.3 \\ \rho &= 0.283 \text{ lb/in}^3 \end{aligned}$$

Figure 6.14 Flat Plate Cantilever

5407-13

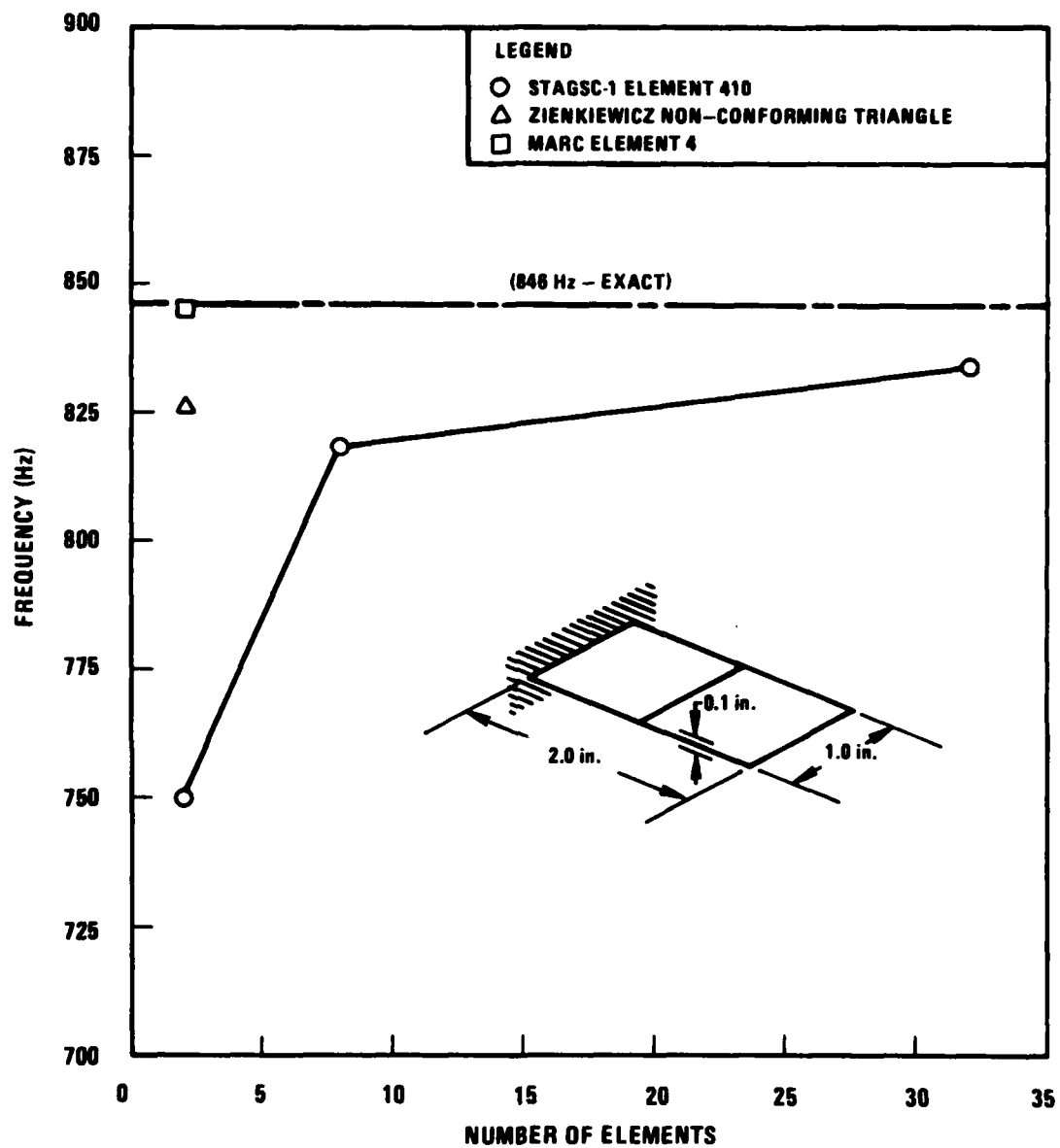


Figure 6.15 Flat Cantilever Plate Vibrations

5407-29

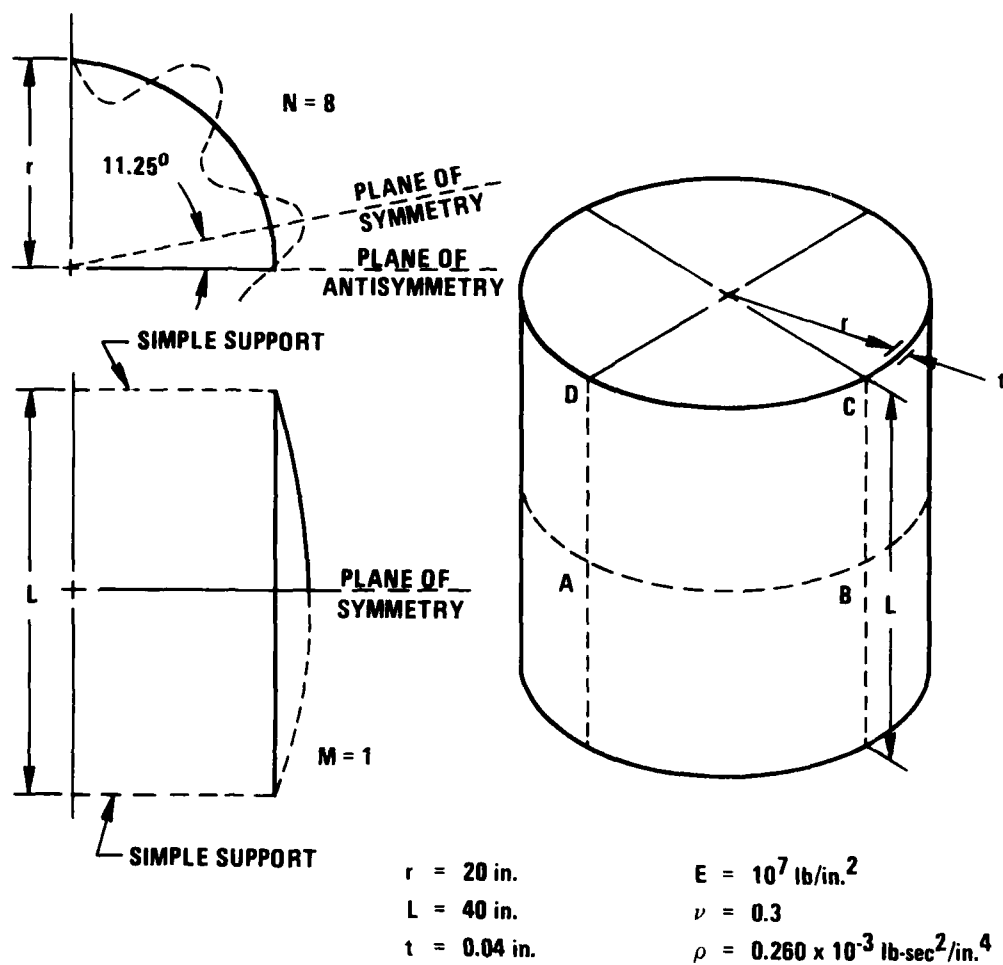


Figure 6.16 Simply Supported Cylinder

5407-14

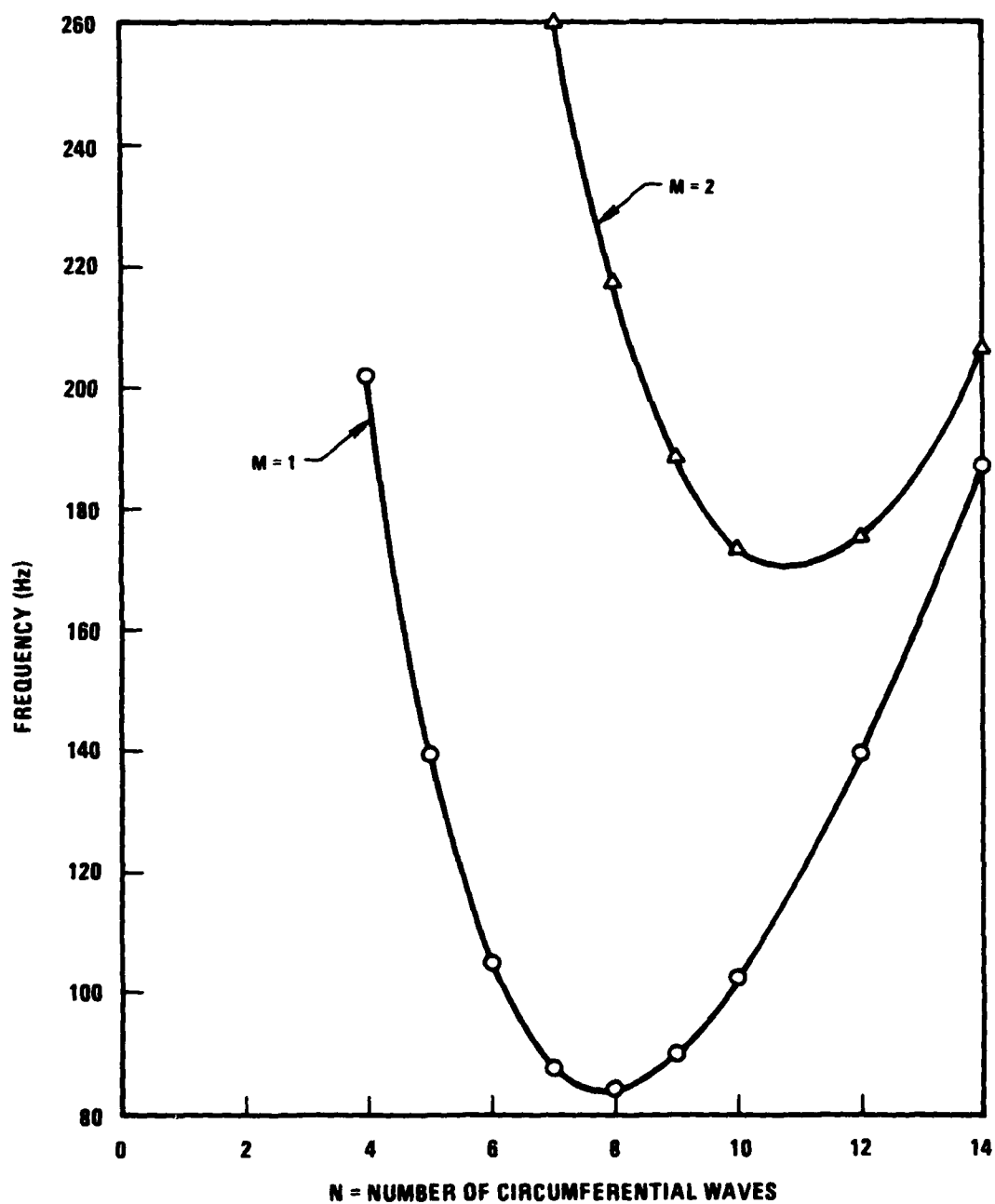


Figure 6.17 Simply Supported Cylinder Flexural Vibration Modes

5407-28

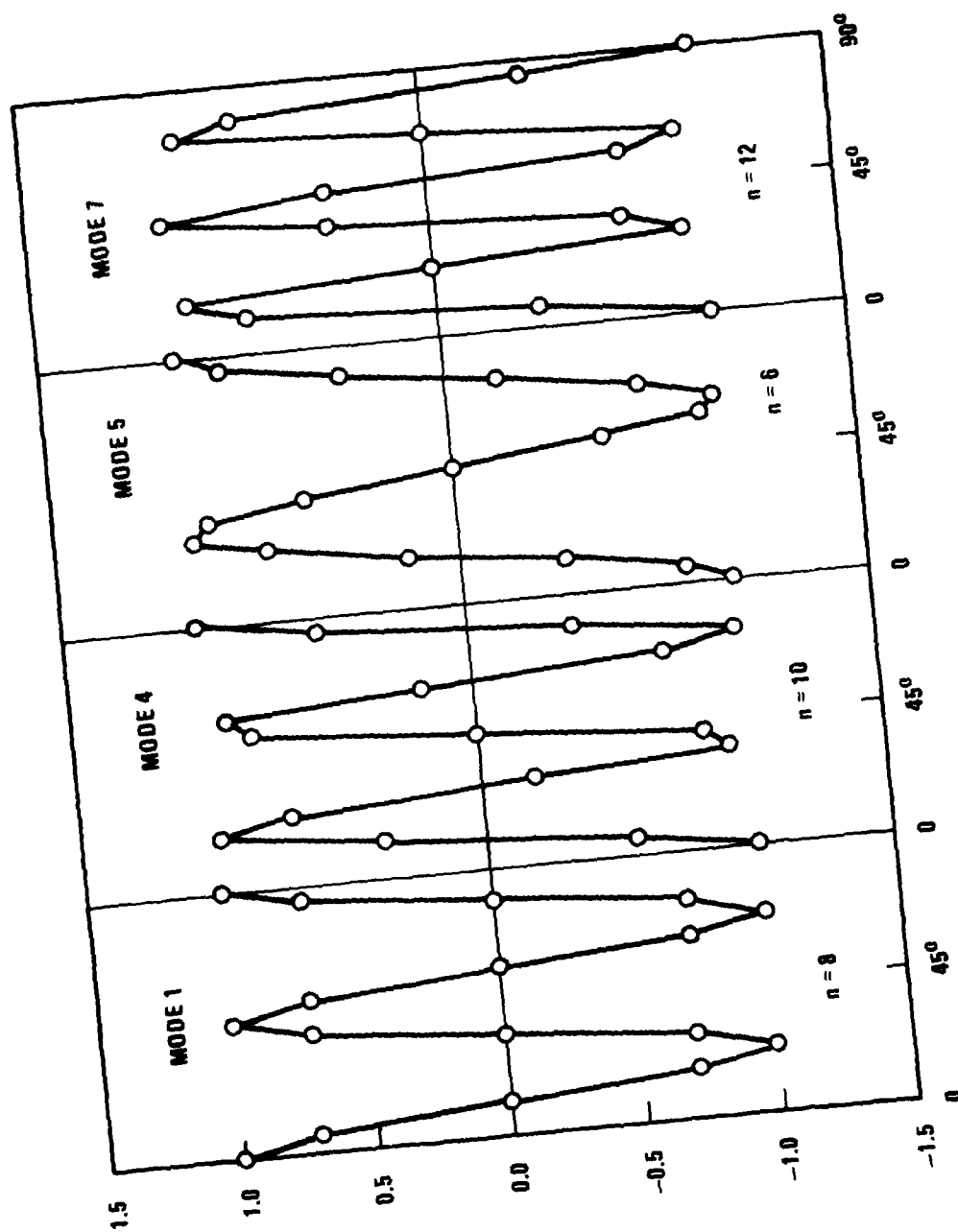


Figure 6.18 1/8 Cylinder Model - Mode Shapes - 16 x 4 Mesh

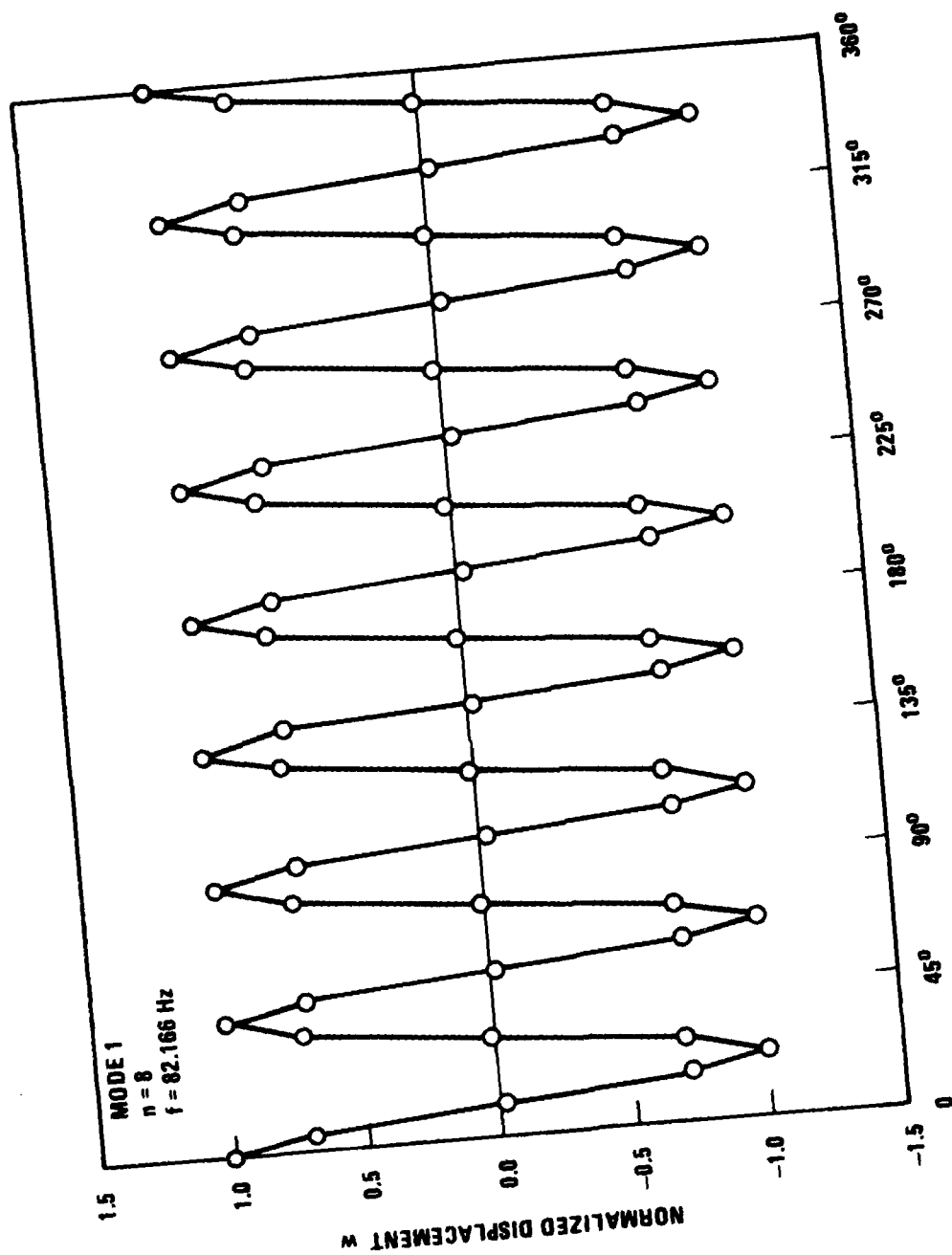


Figure 6.19 1/2 Cylinder Model — Mode Shapes (1)

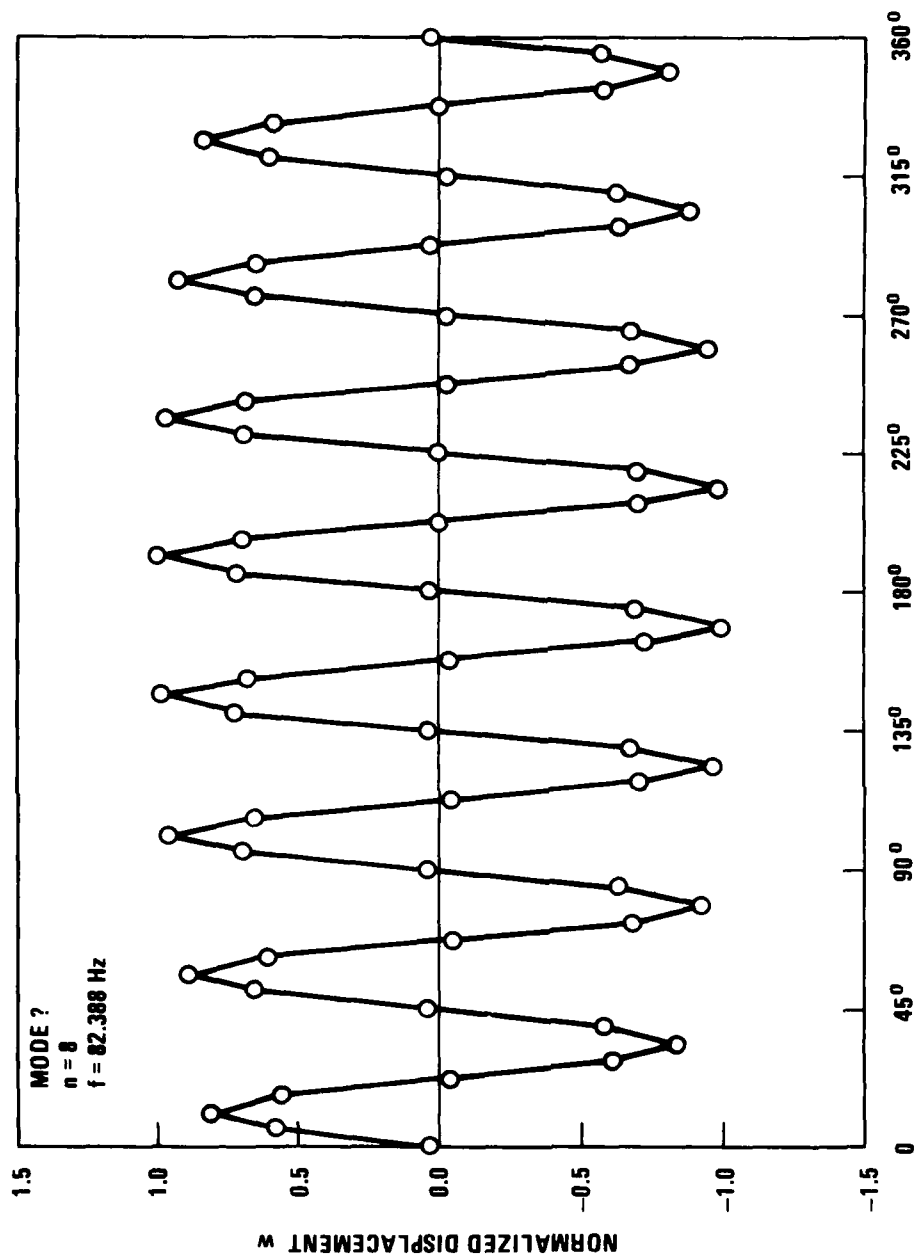


Figure 6.20 1/2 Cylinder Model — Mode Shapes (2)

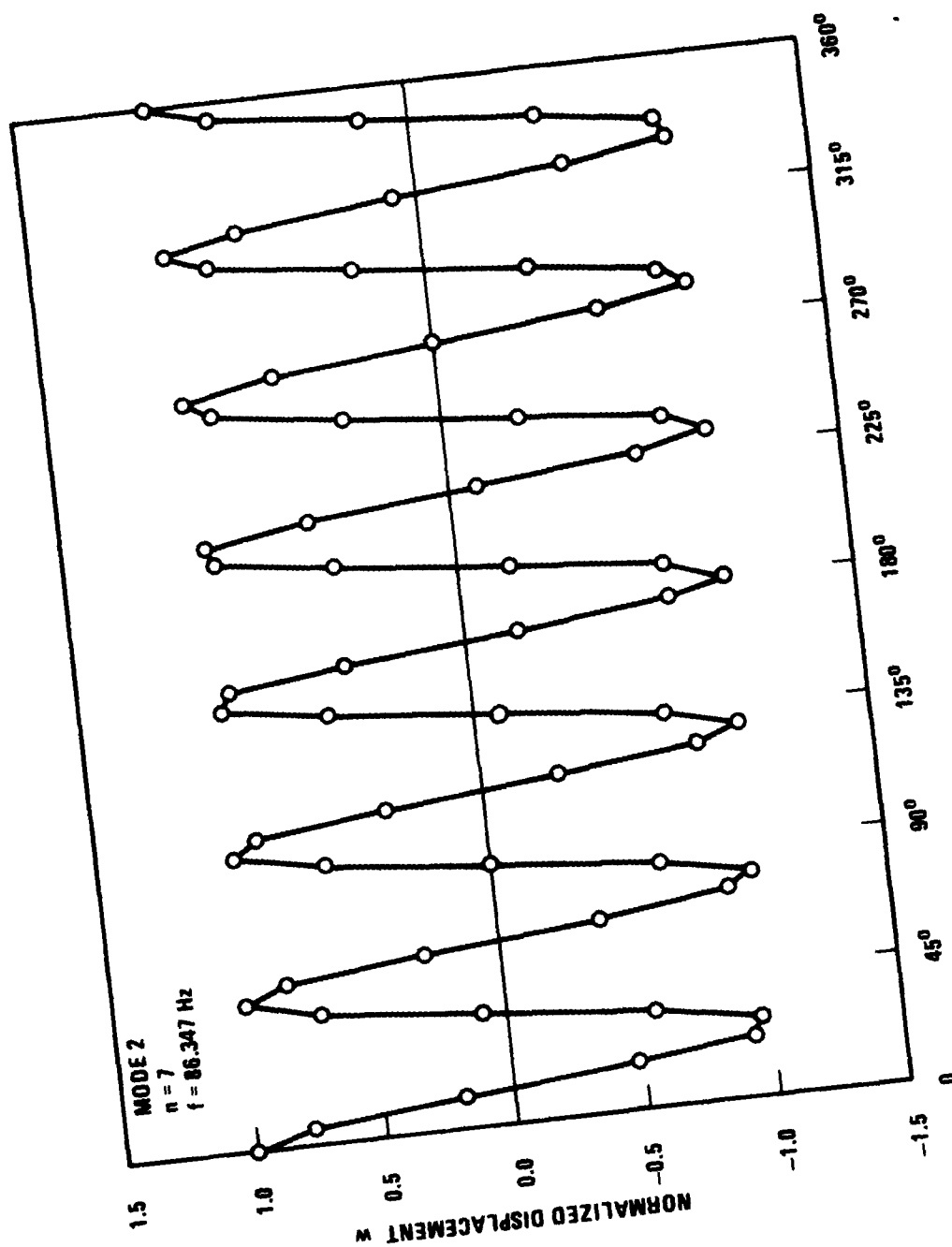


Figure 6.21 1/2 Cylinder Model — Mode Shapes (3)

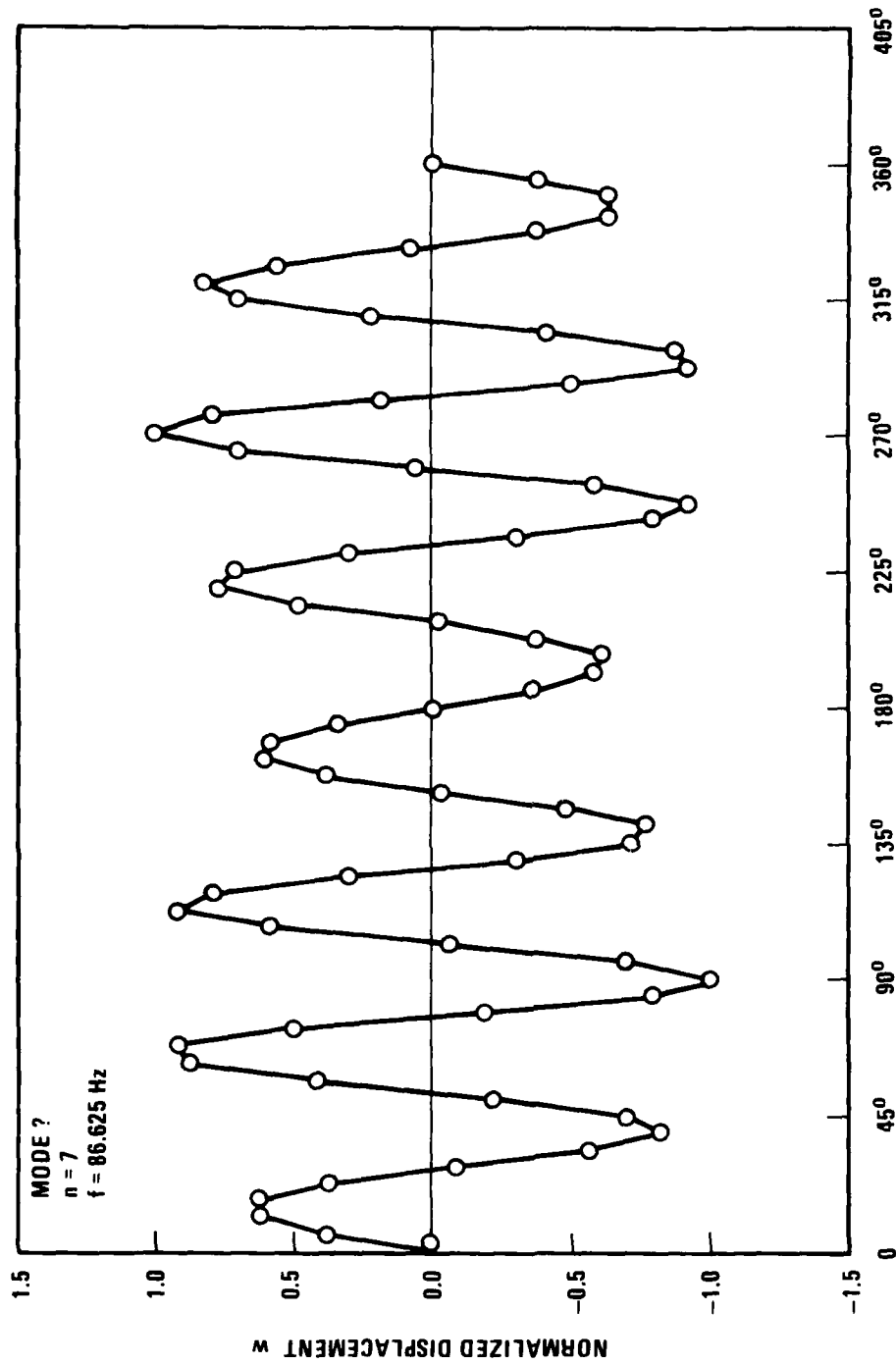


Figure 6.22 1 2 Cylinder Model — Mode Shapes (4)

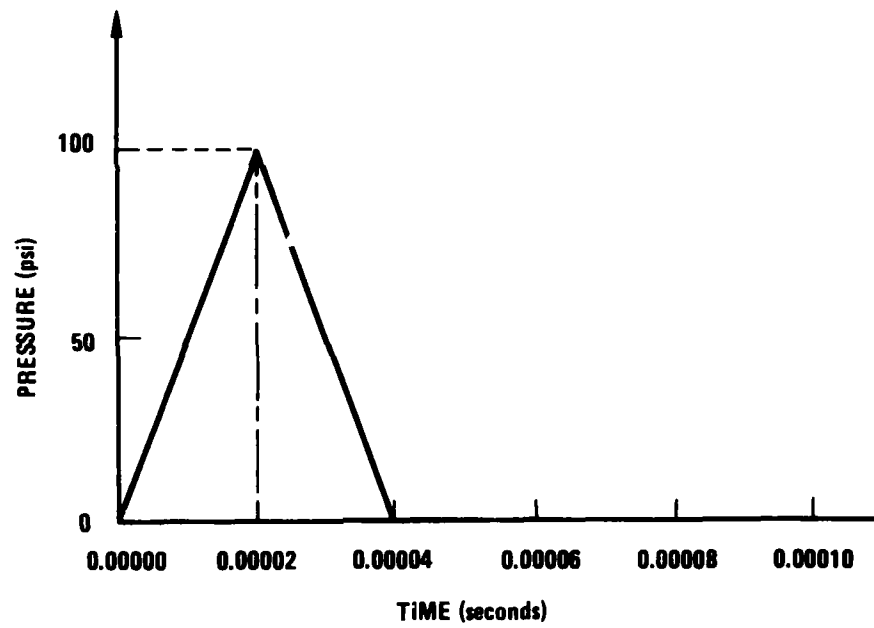


Figure 6.23 Cantilever Beam-Pressure Pulse

5407-15

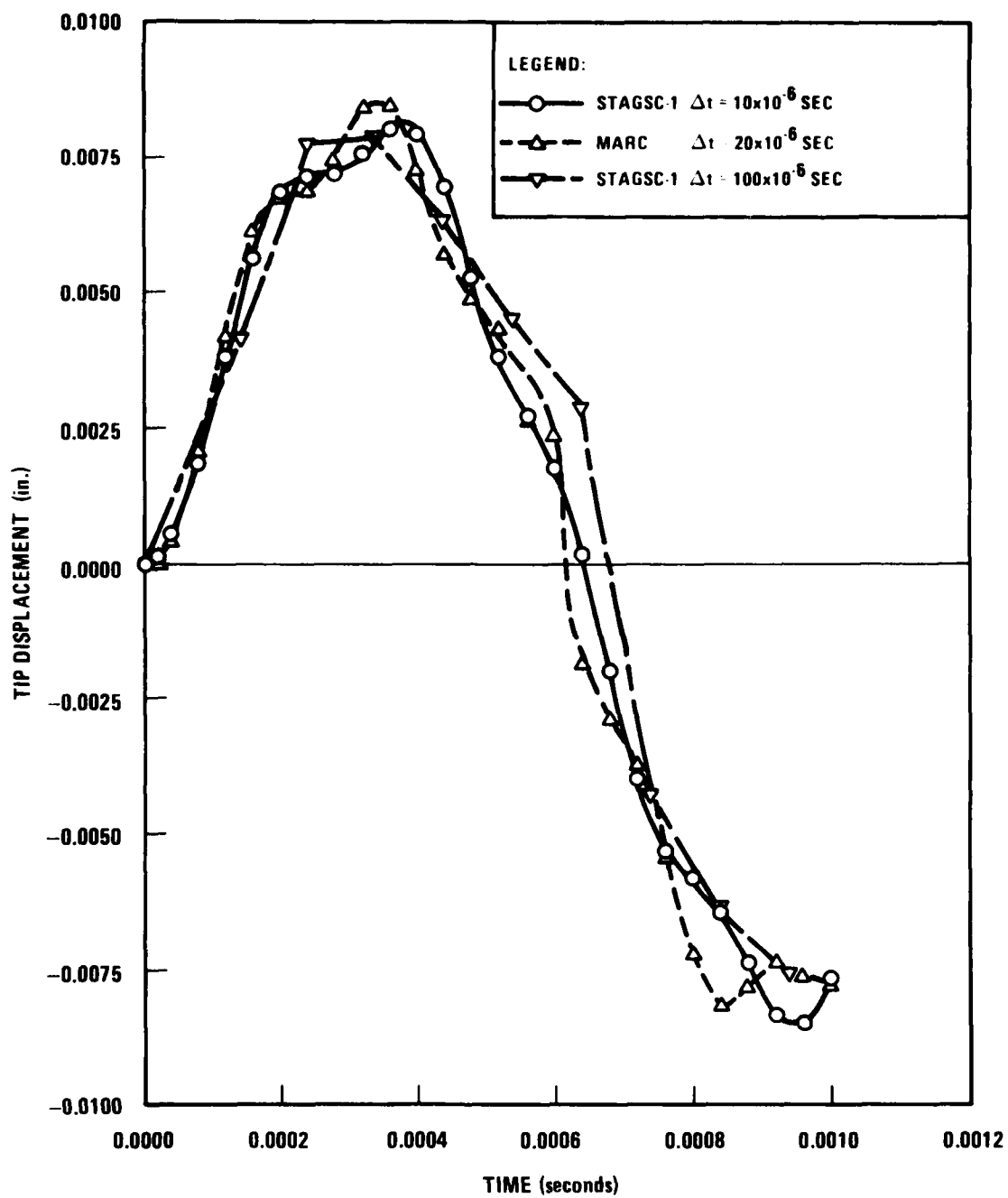


Figure 6.24 Cantilever Plate Under Transient Pressure Loading
— Tip Displacement History

5407-22

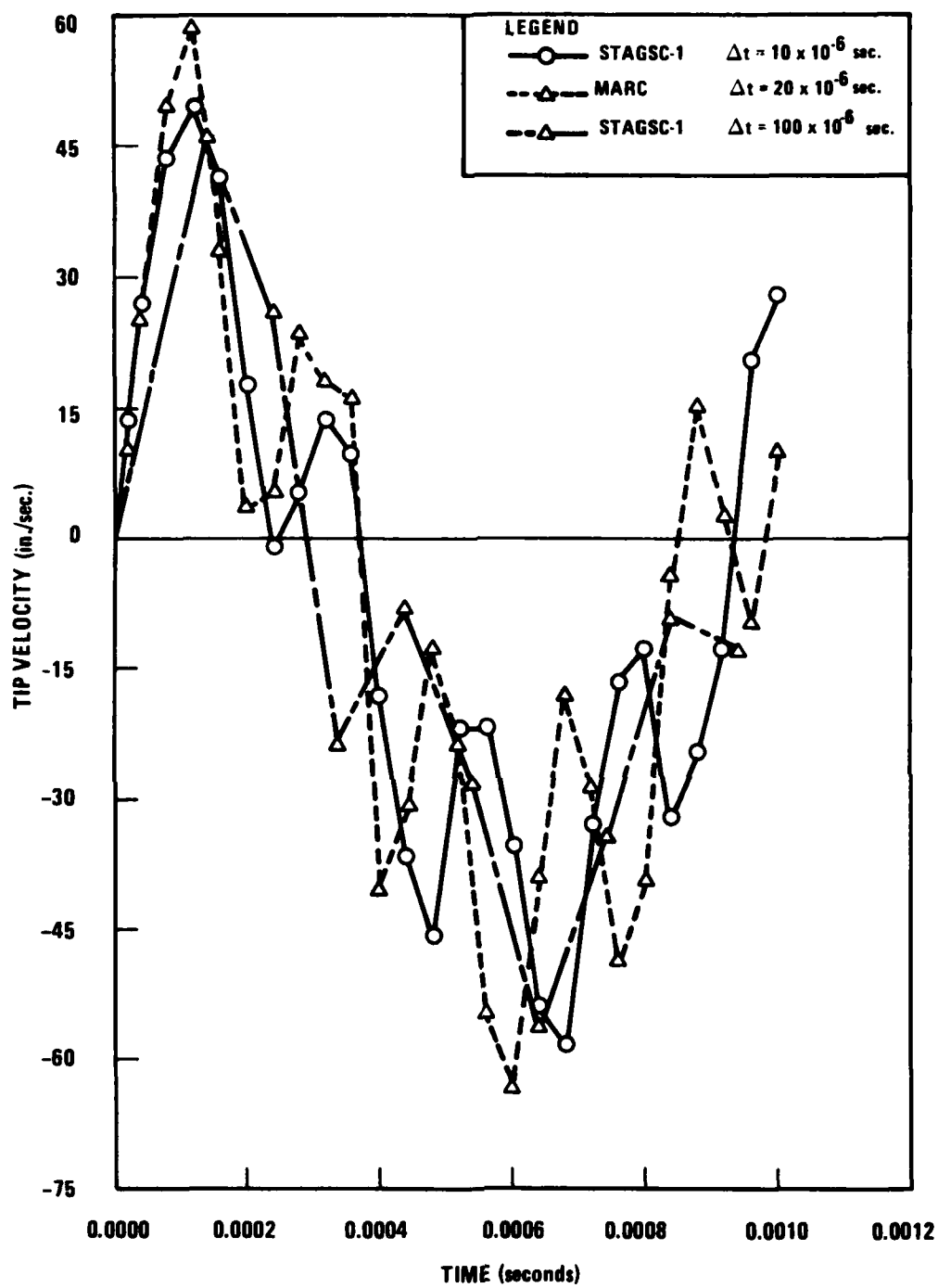


Figure 6.25 Cantilever Plate Under Transient Pressure Loading
— Tip Velocity History

5407-21

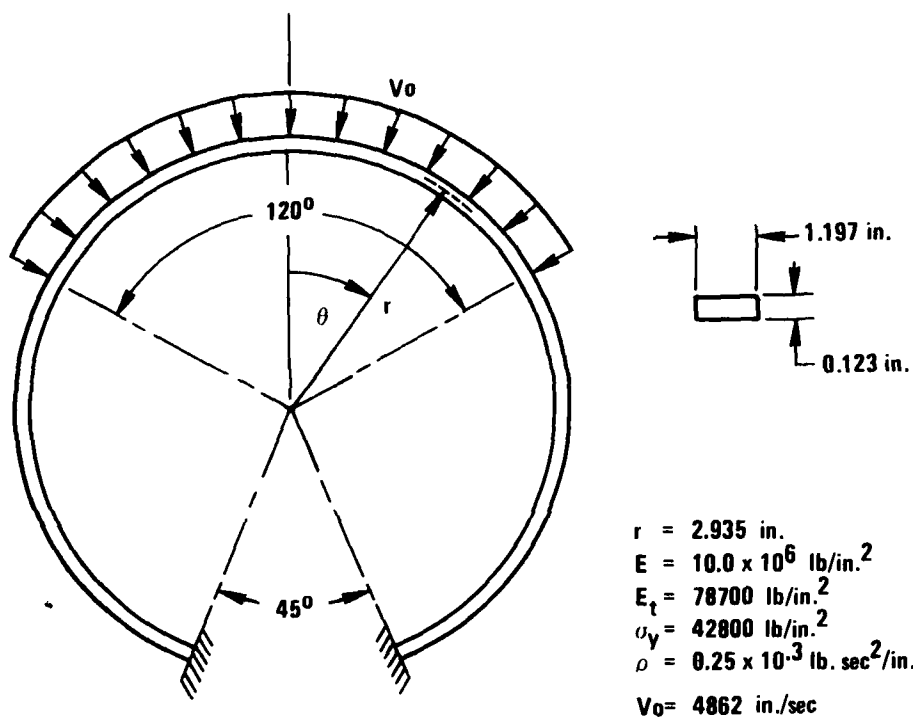


Figure 6.26 Impulsively Loaded Ring

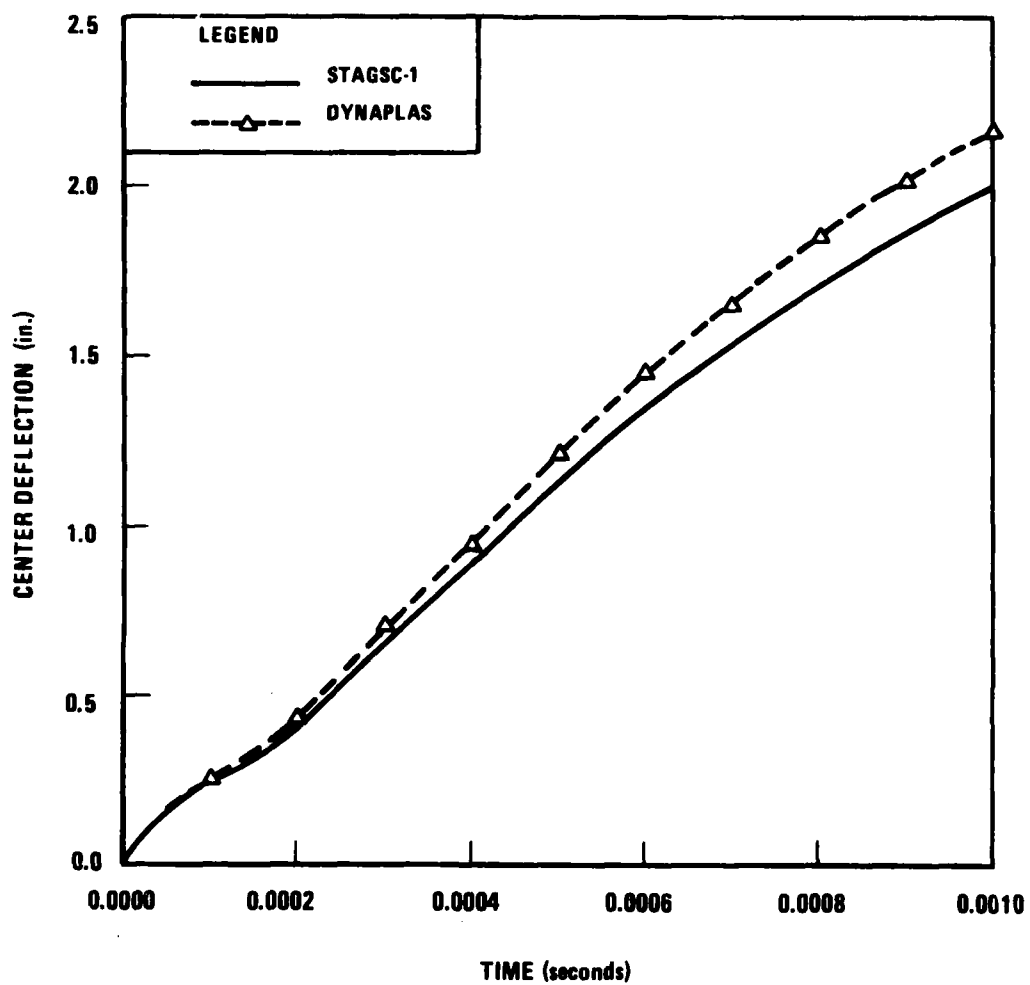


Figure 6.27 Impulsively Loaded Ring
-Nonlinear Elastic Plastic Response
-Deflection

5407-17

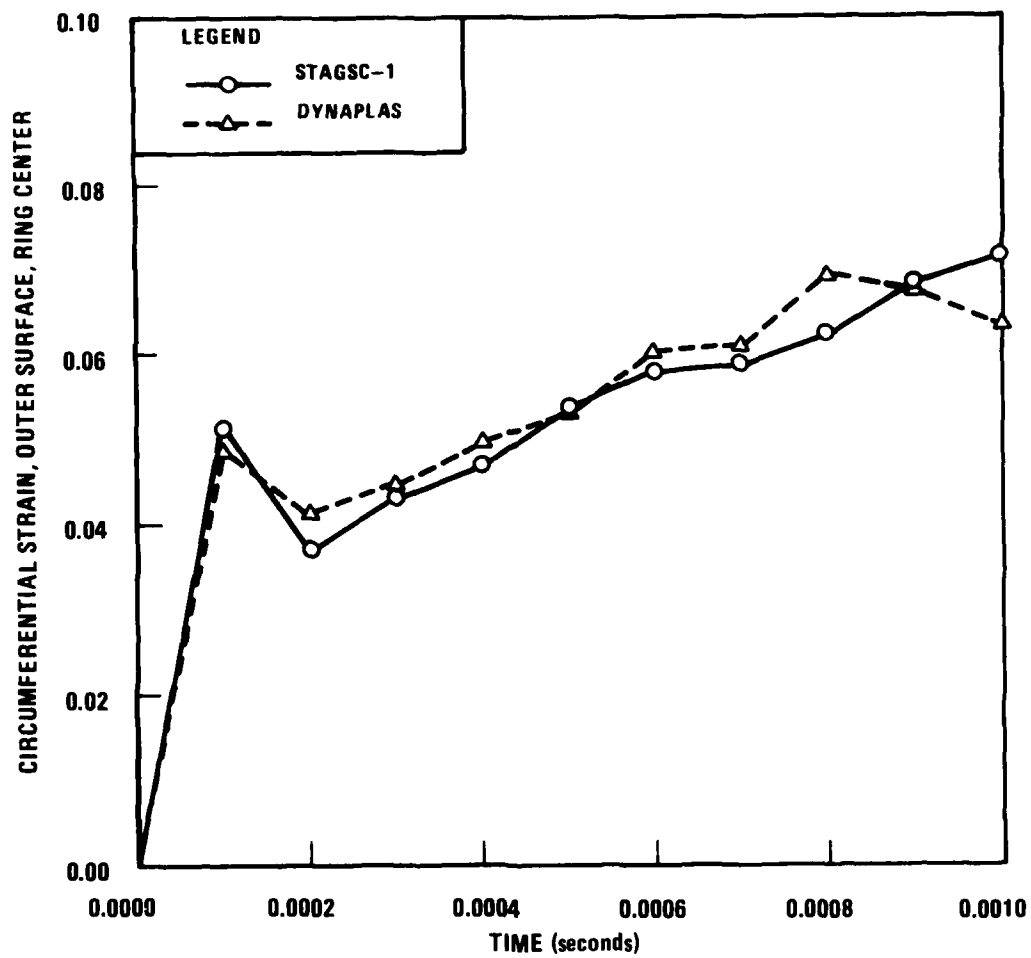


Figure 6.28 Impulsively Loaded Ring
-Nonlinear Elastic Plastic Response
-Circumferential Strain

5407-18

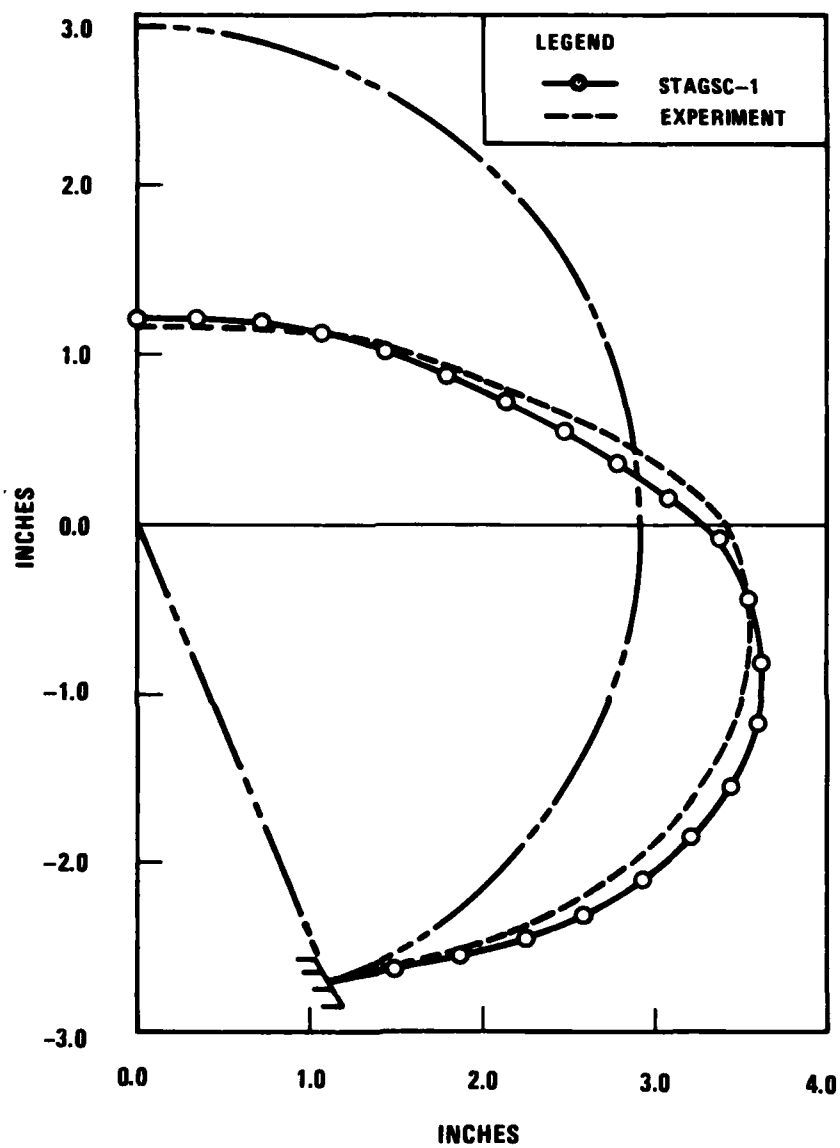


Figure 6.29. Impulsively Loaded Ring - Deformed Shape at About 0.0008 Seconds

5407-20

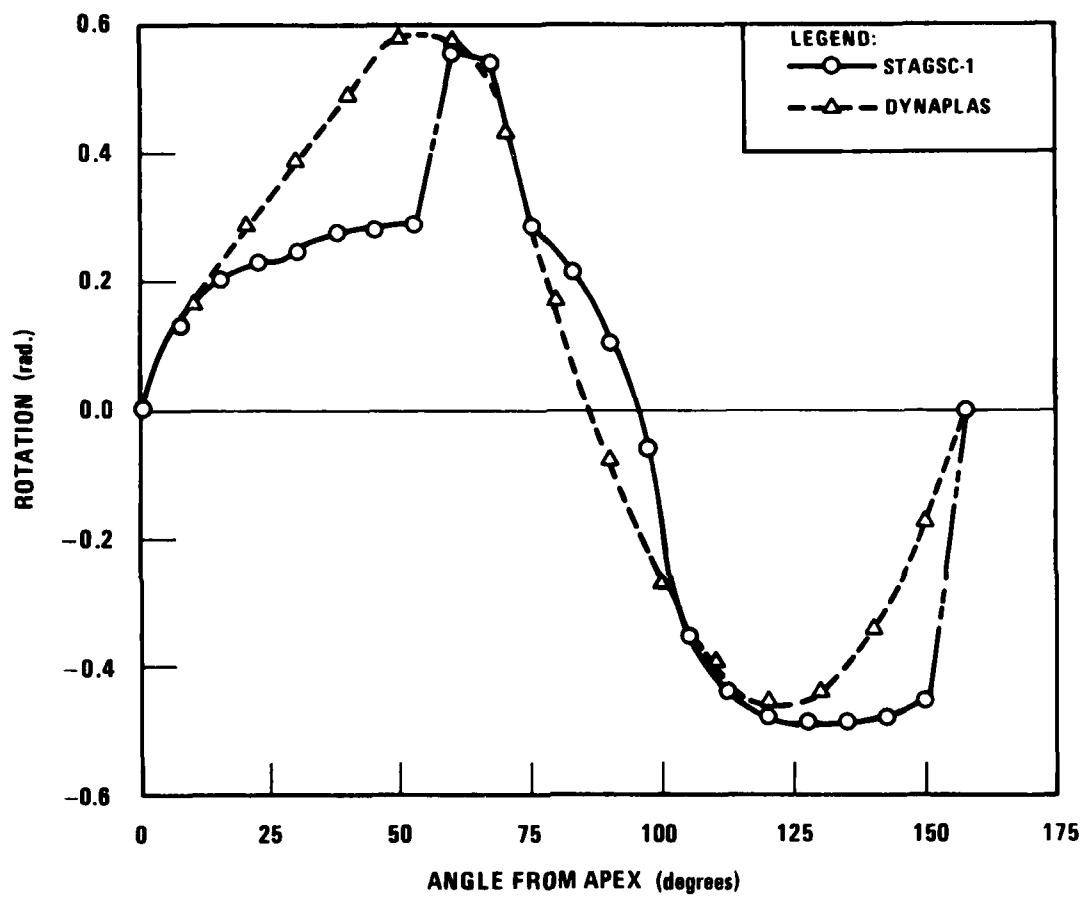


Figure 6.30 Impulsively Loaded Ring - Rotation at 0.0010 Seconds

5407-19

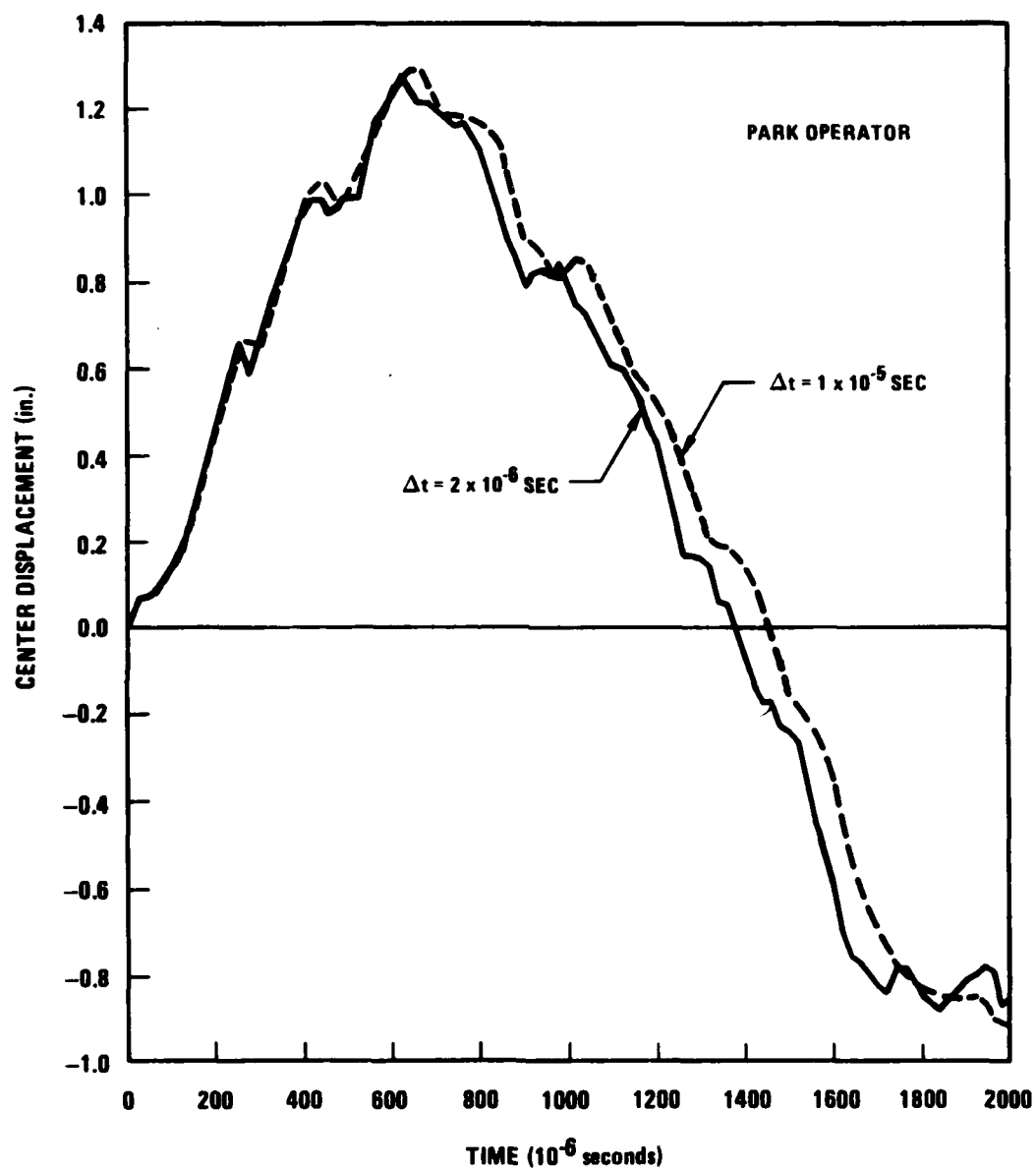


Figure 6.31 Impulsively Loaded Ring - Nonlinear Elastic Response
-- Park Operator

5407-81

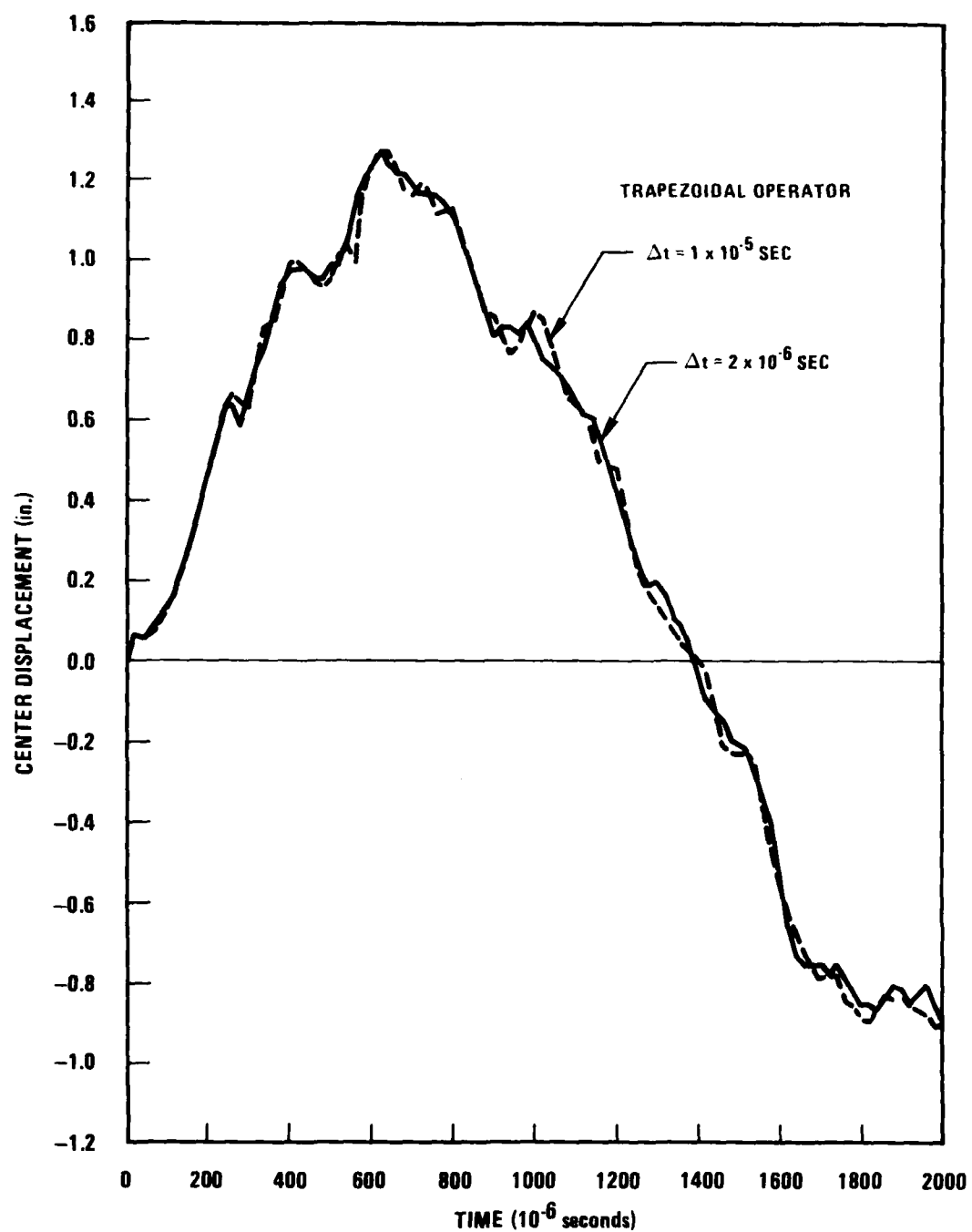


Figure 6.32 Impulsively Loaded Ring - Nonlinear Elastic Response
- Trapezoidal Operator

5407-82

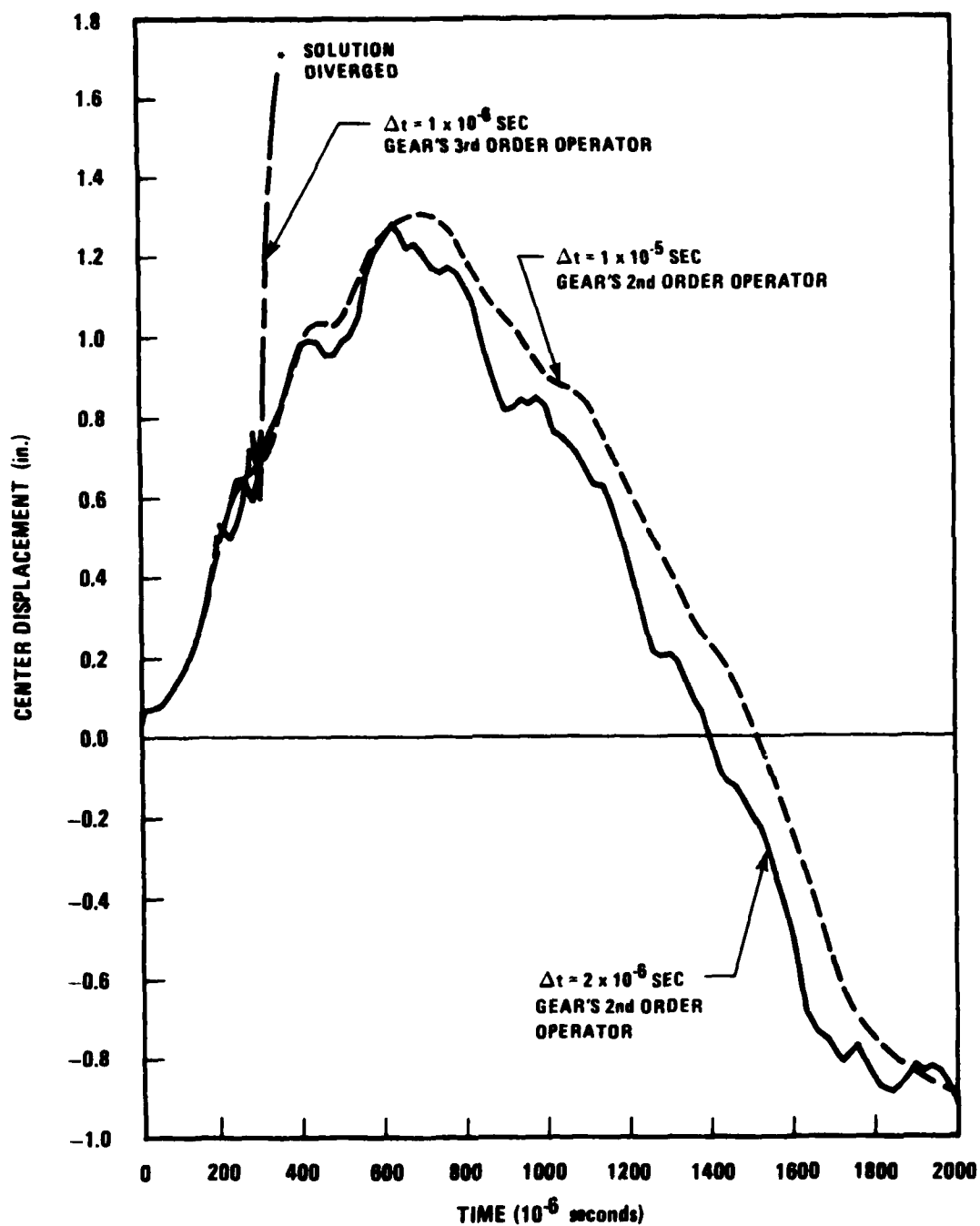


Figure 6.33 Impulsively Loaded Ring - Nonlinear Elastic Response
- Gear's Operator

5407-83

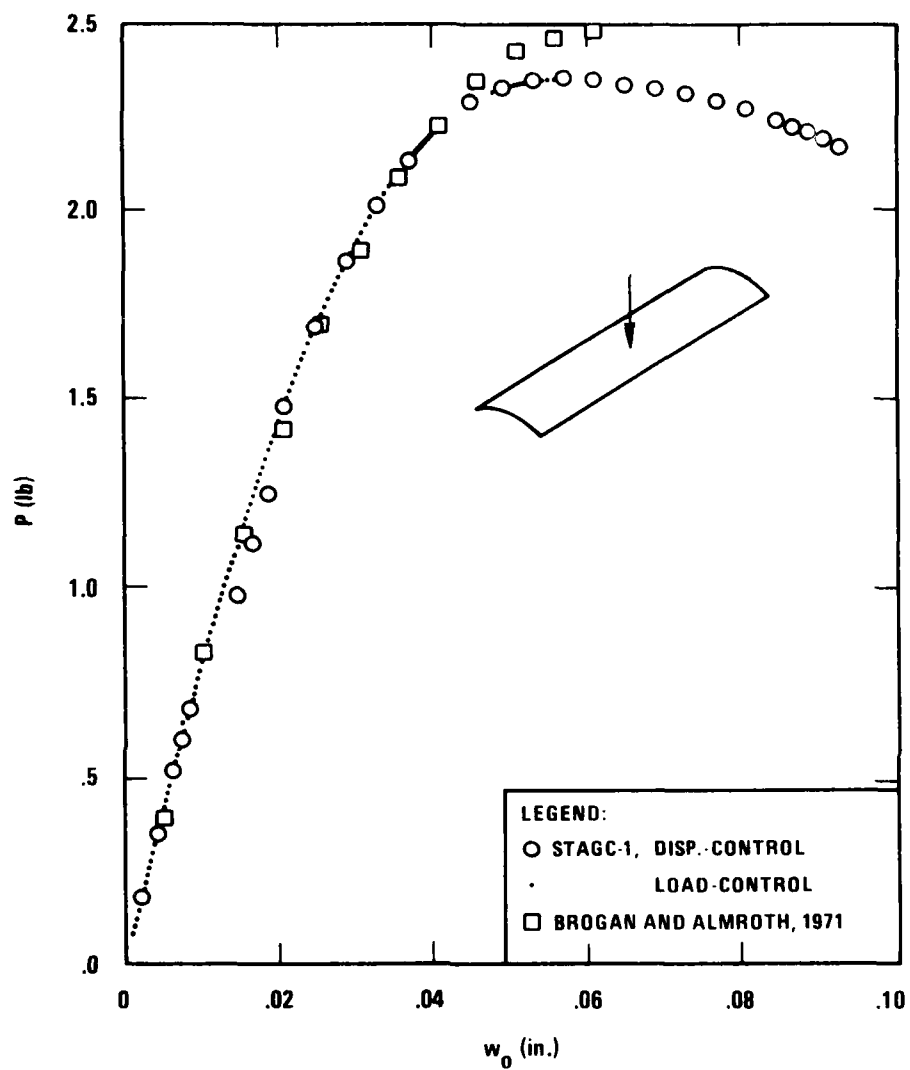


Figure 6.34 Comparison of Load-Displacement Results for the Venetian Blind

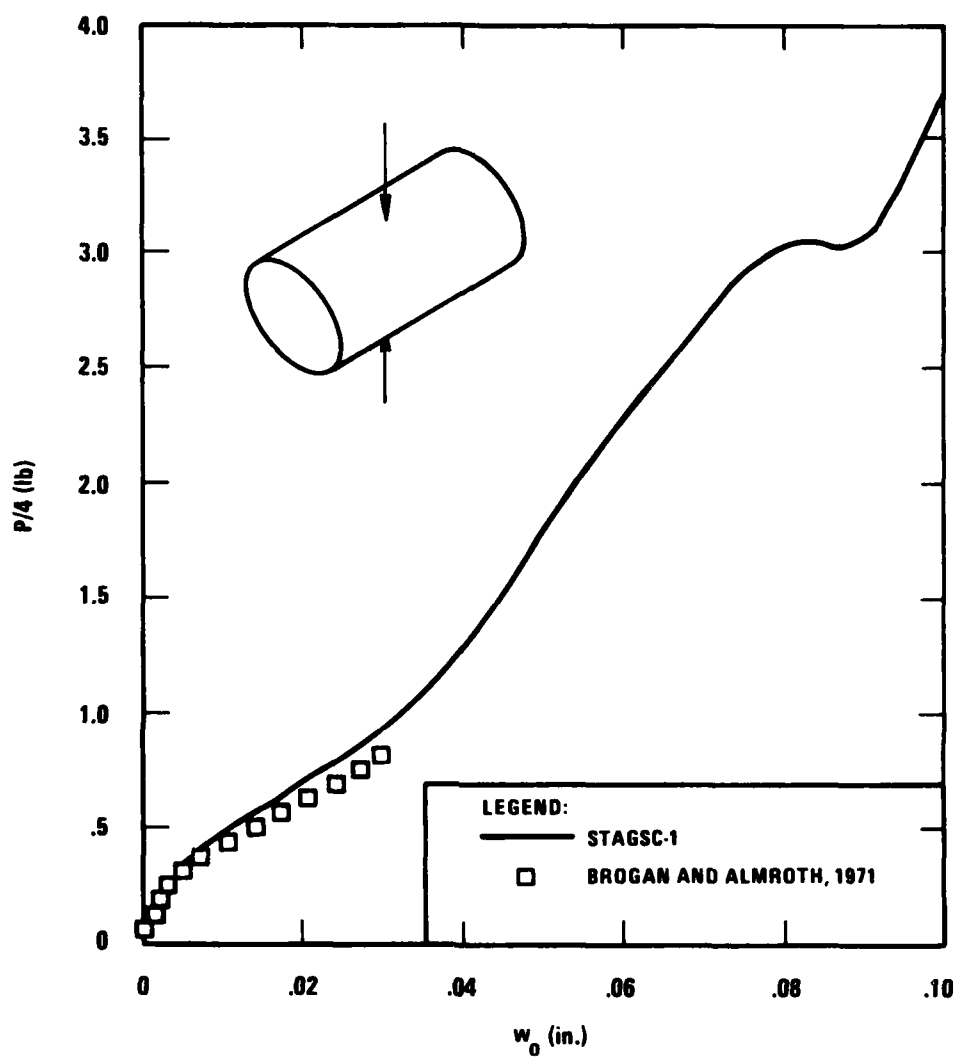


Figure 6.35 Comparison of Load-Displacement Results for the Pinched Cylinder

5407-64

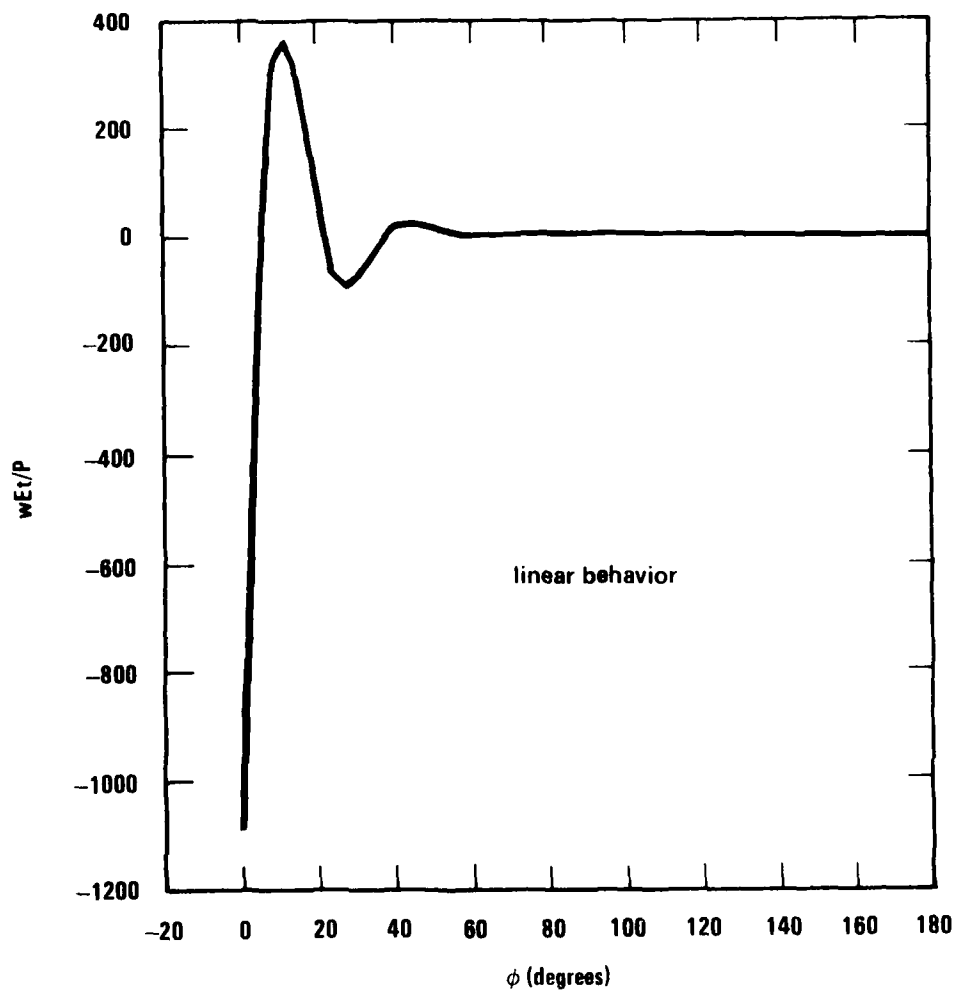


Figure 6.36 Hoop Variation of Radial Displacement at Midlength. Linear Results for Poked Cylinder. $R/t=638$, $L/R = .892$

5407-86

WESTINGHOUSE ELECTRIC CORP MADISON PA ADVANCED REACT--ETC F/8 13/13
EVALUATION OF THE STAGEC-1 SHELL ANALYSIS COMPUTER PROGRAM. (U)
AUG 81 K THOMAS, L M SOBEL N00014-79-C-0825
WARD-10881 NL

UNCLASSIFIED

3 of 3
2102794

1

END
DATE
FILMED
9-8-1
DTIC

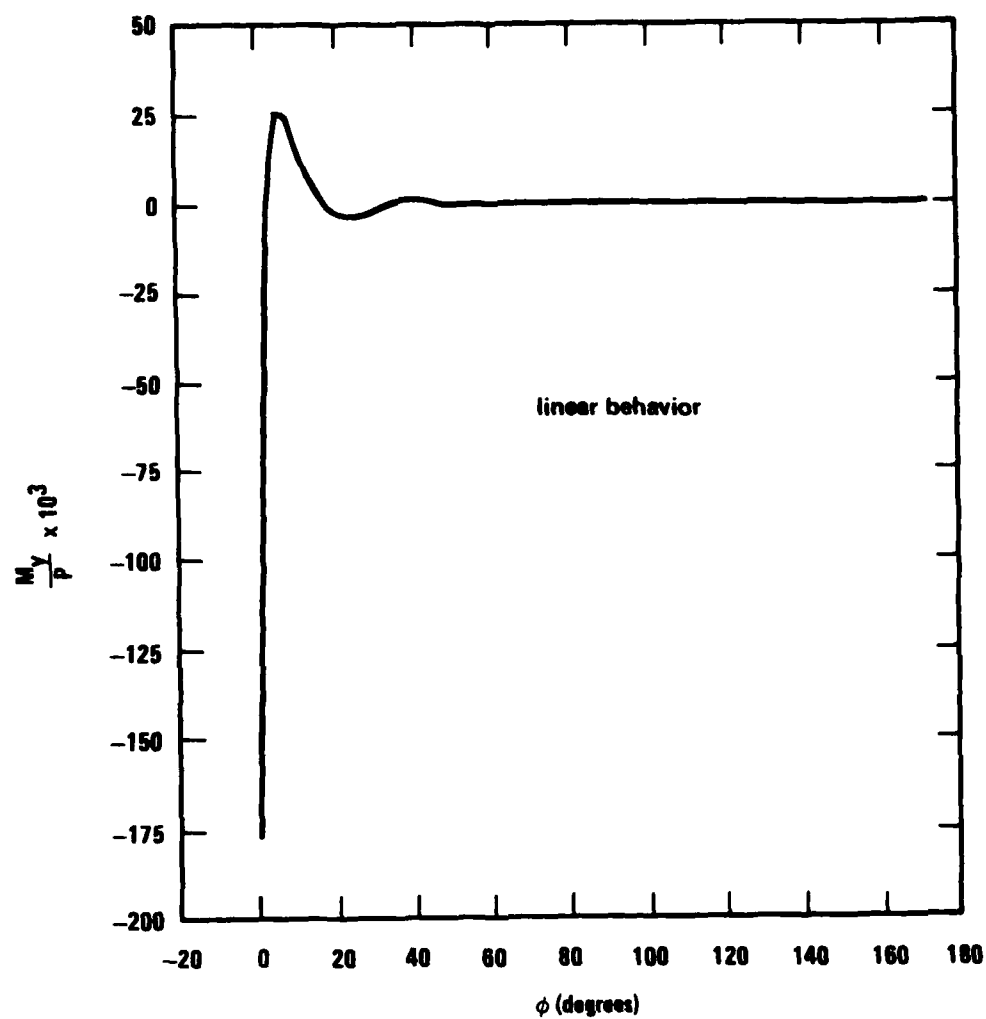


Figure 6.37 Hoop Variation of Hoop Bending Moment at $x = 3.5'' \approx (1/40)(L/2)$. Linear Results for Poked Cylinder. $R/t = 638$, $L/R = .892$

5407-87

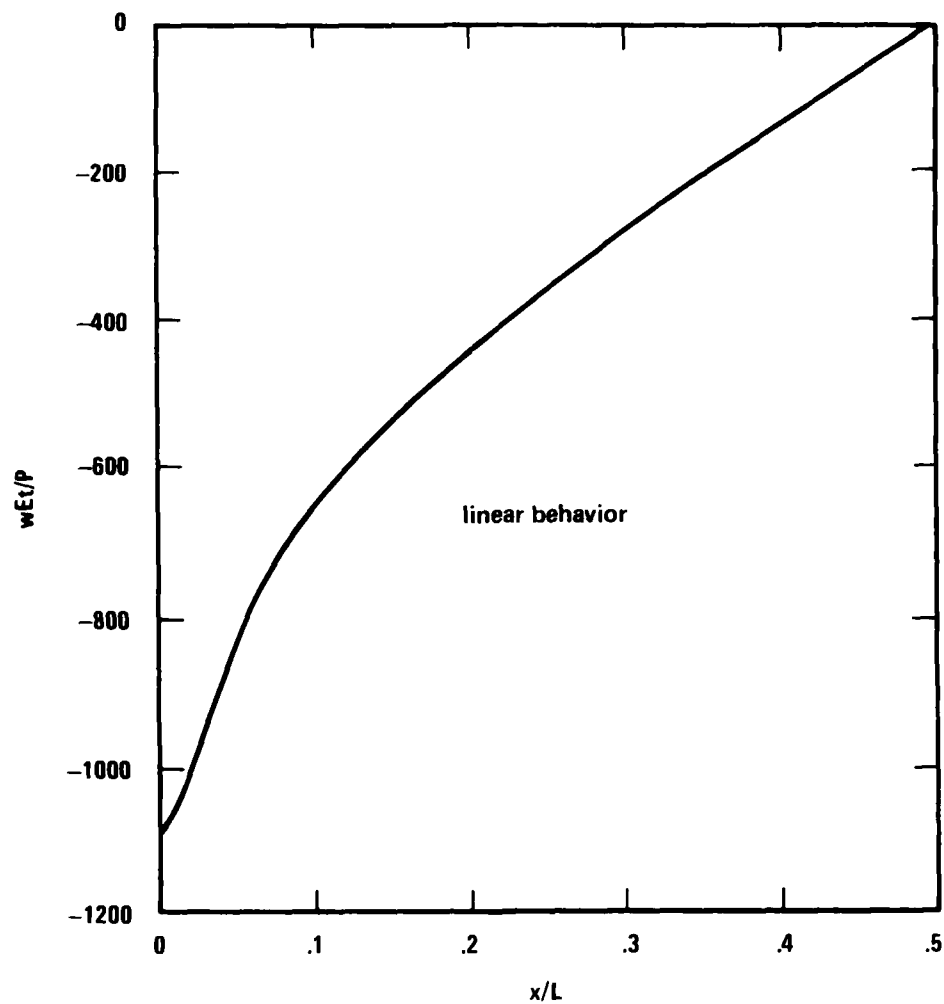


Figure 6.38 Axial Variation of Radial Displacement Along the Loaded Generator.
Linear Results for Poked Cylinder. $R/t = 638$, $L/R = .892$

5407-88

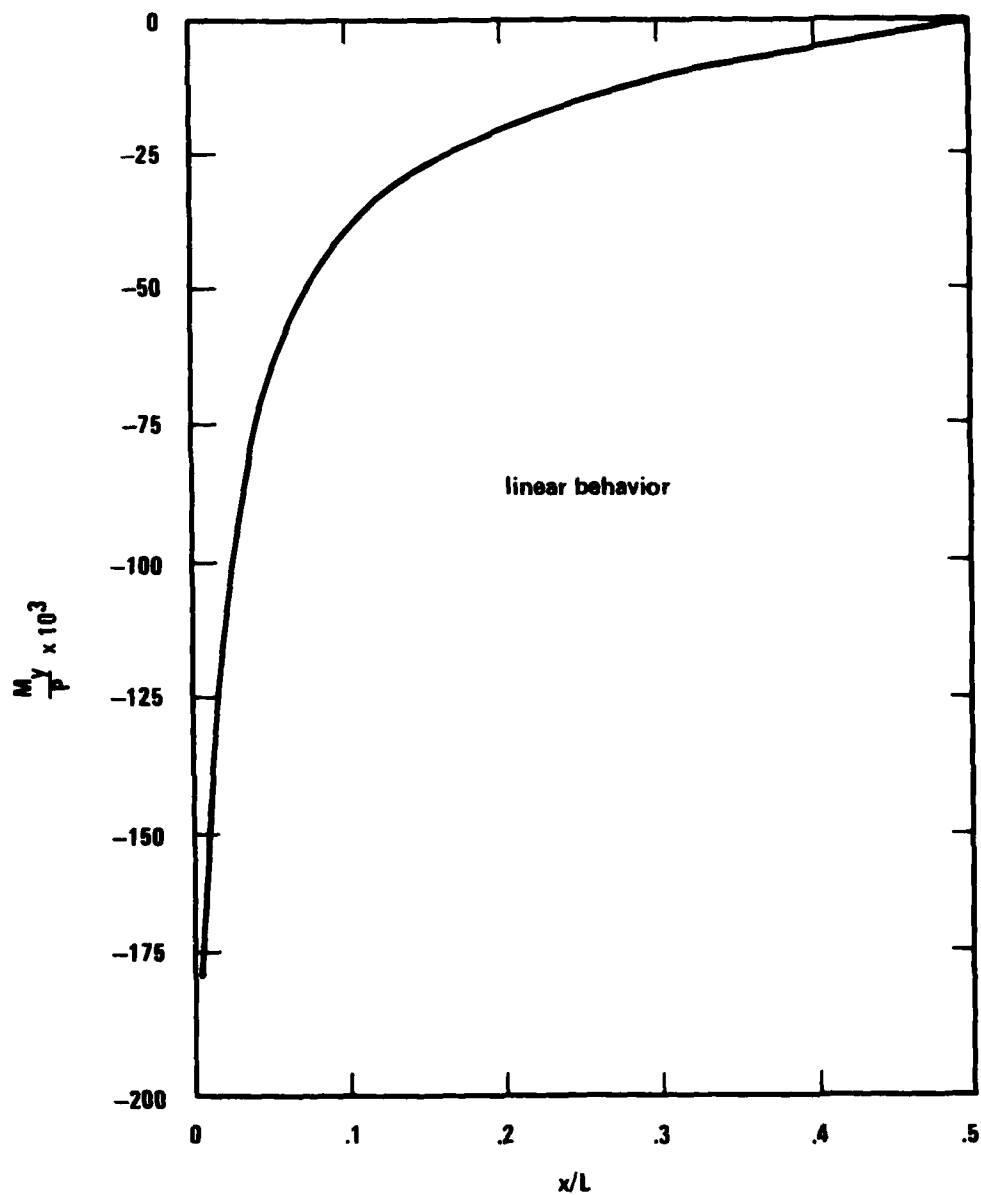


Figure 6.39 Axial Variation of Hoop Bending Moment Along $\phi = 1/2^\circ$. Linear Results for Poked Cylinder. $R/t = 638$, $L/R = .892$

5407-68

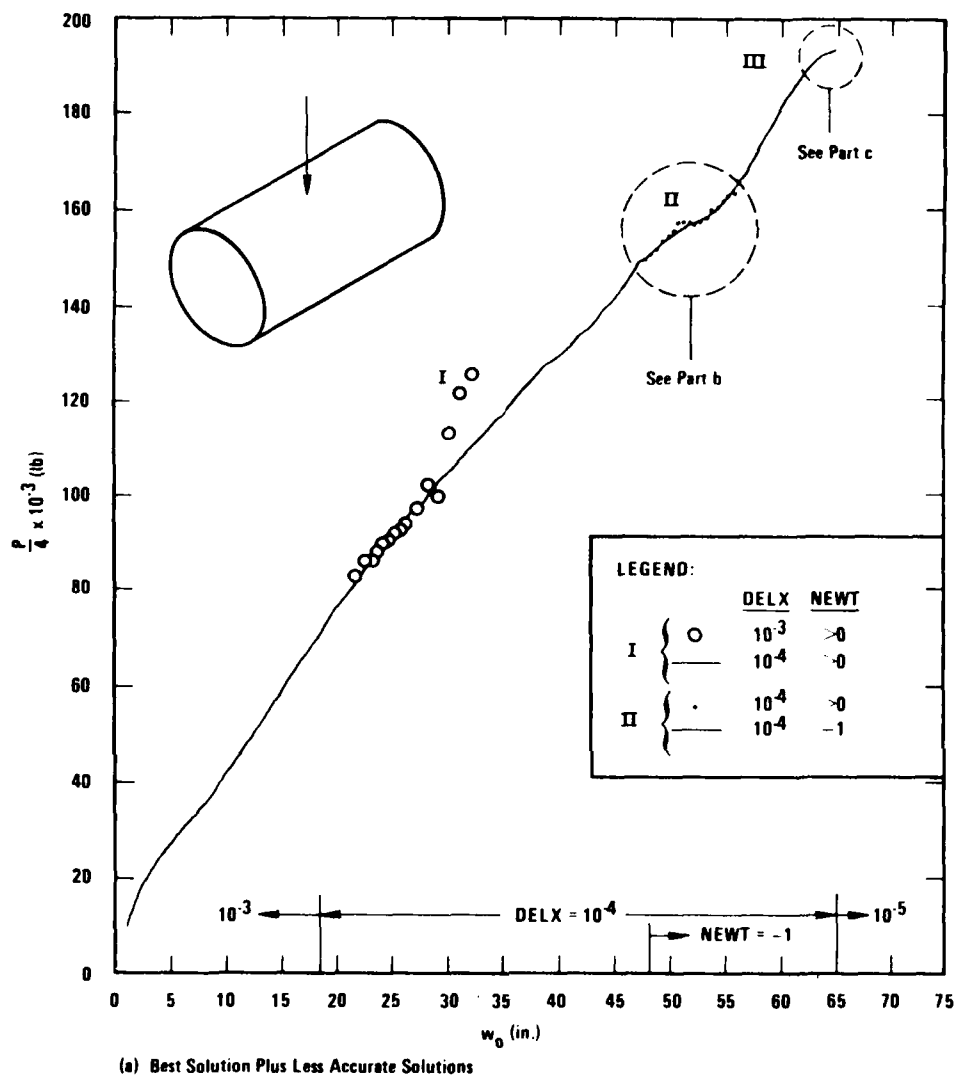
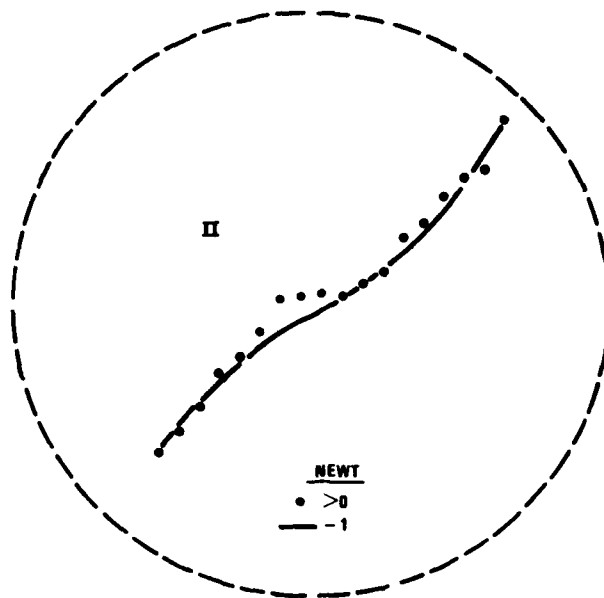
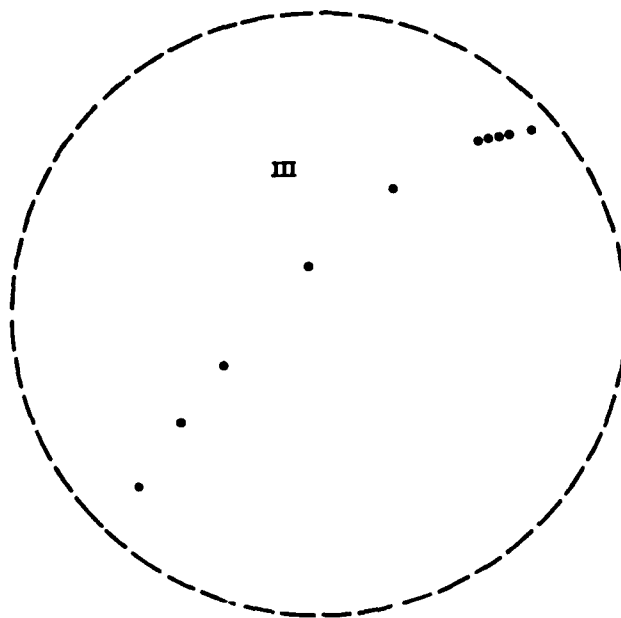


Figure 6.40 Load-Displacement Results for Poked Cylinder

5407-69



b) Region II, $\text{DELX} = 10^{-4}$



c) Region III

Figure 6.40 (Continued)

5407-77

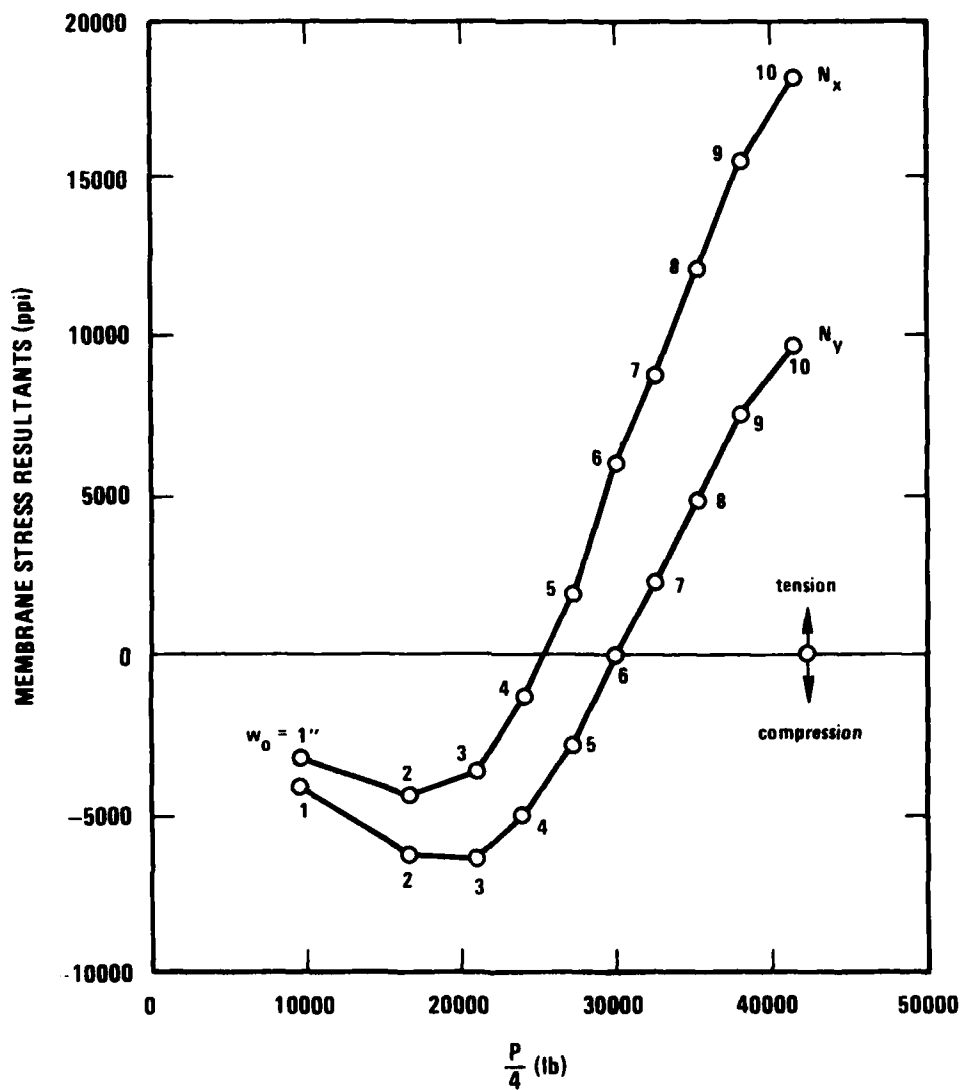


Figure 6.41 Initially Compressive Membrane Forces Near Load ($x = 3.5''$, $\phi = 1/2^\circ$) Become Tensile Due to Geometry Changes. Poked Cylinder

5407-91

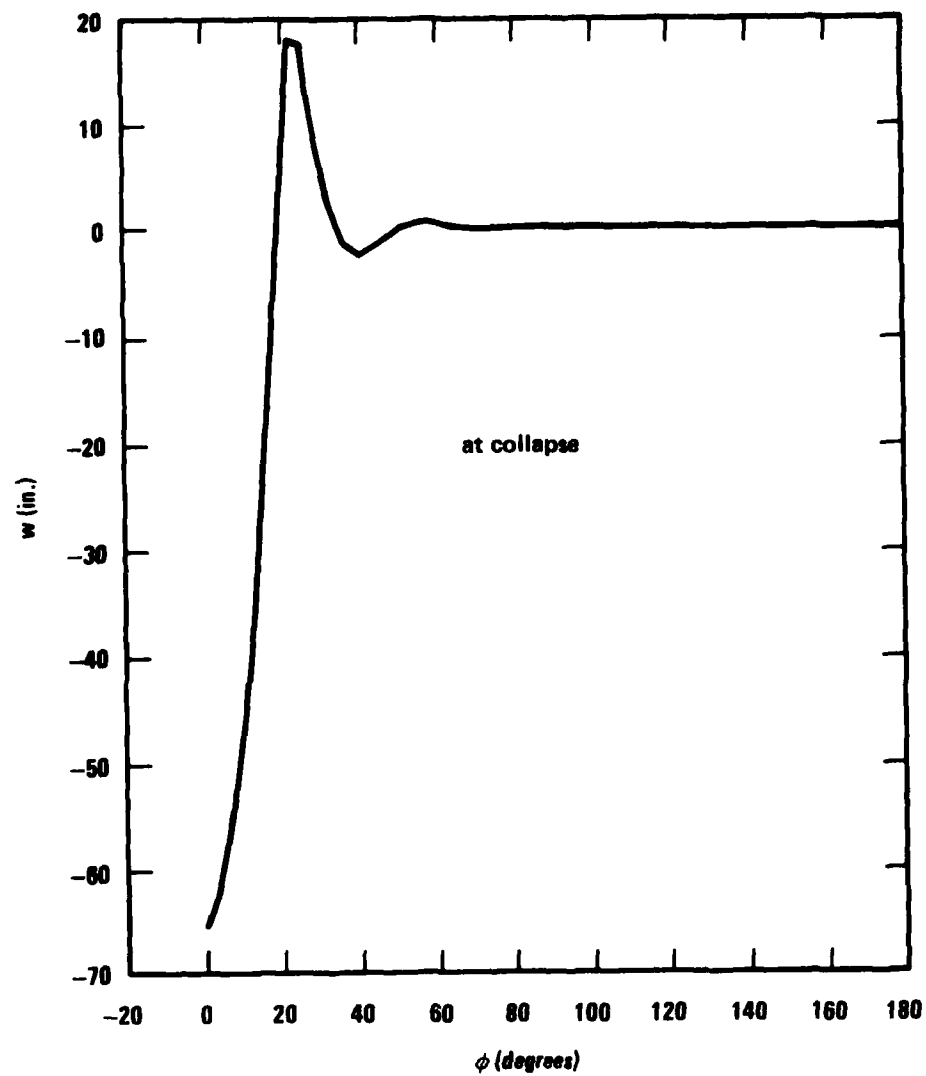


Figure 6.42 Hoop Variation at Midlength of Radial Displacement at Collapse.
Poked Cylinder

5407-71

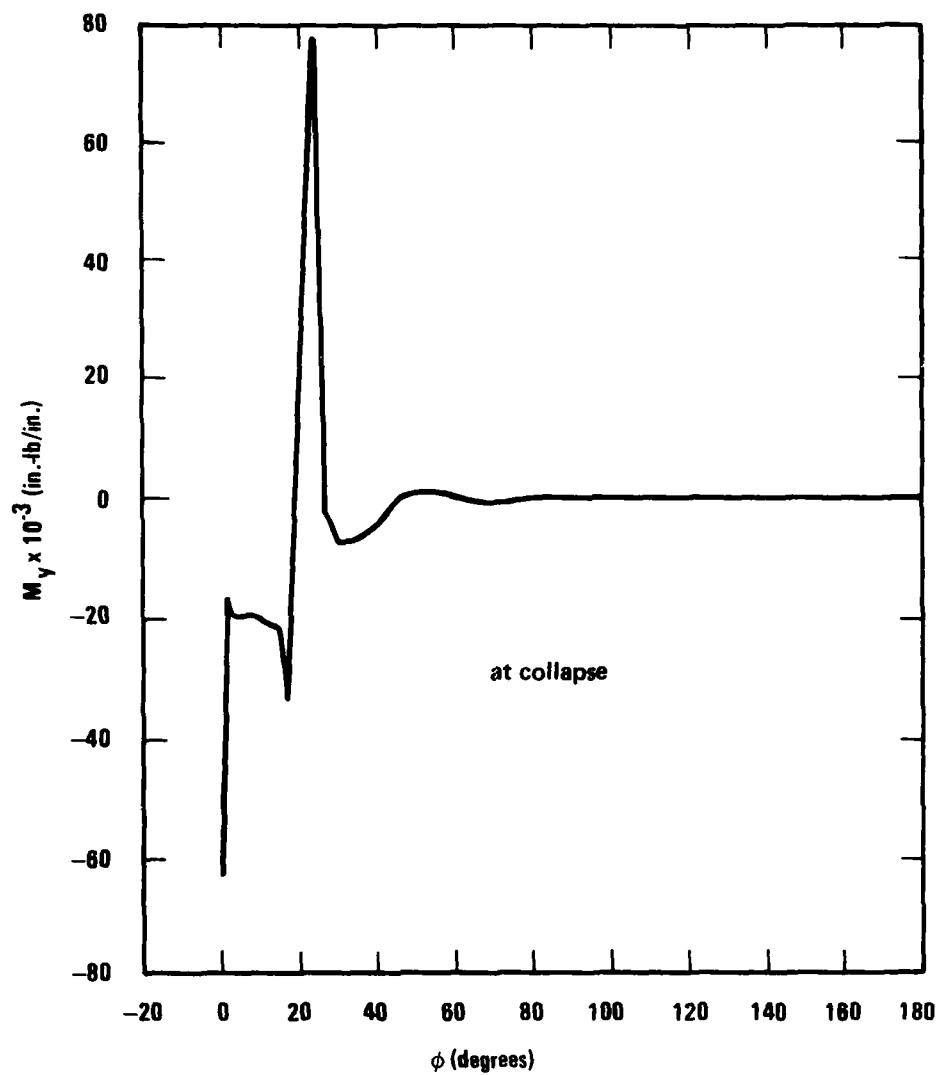


Figure 6.43 Hoop Variation Along $x = 3.5''$ of Hoop Bending Moment at Collapse, Poked Cylinder

5407-72

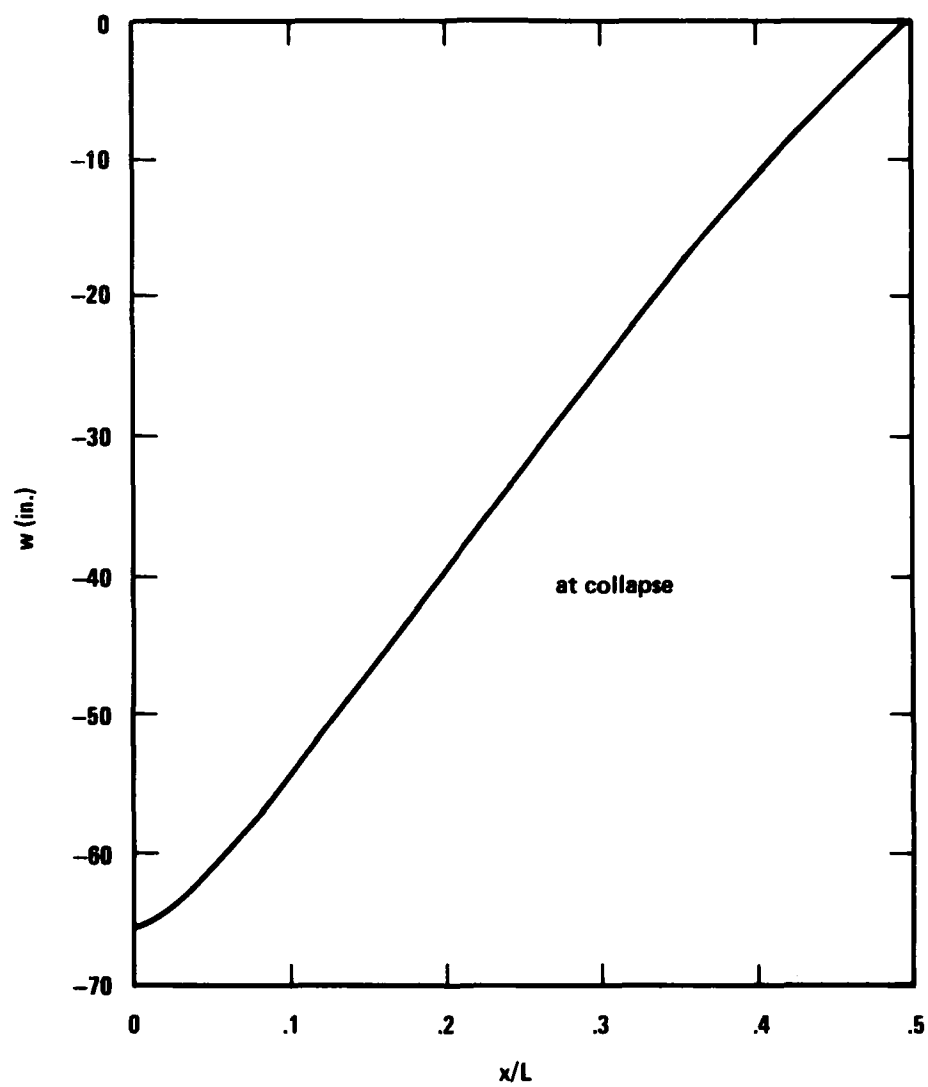


Figure 6.44 Axial Variation Along Loaded Generator of Radial Displacement at Collapse.
Poked Cylinder

S407-94

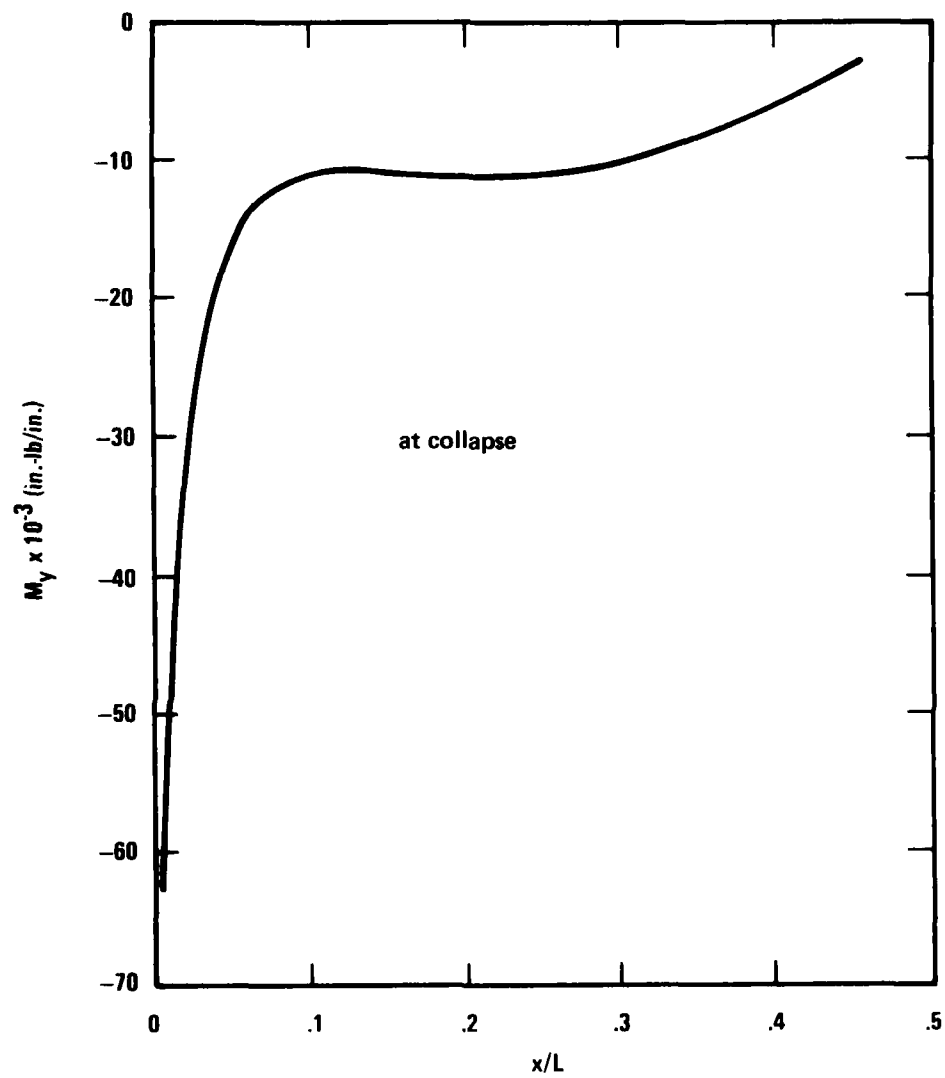


Figure 6.45 Axial Variation Along $\phi = 1/2^\circ$ of Hoop Bending Moment at Collapse. Poked Cylinder

5407-74

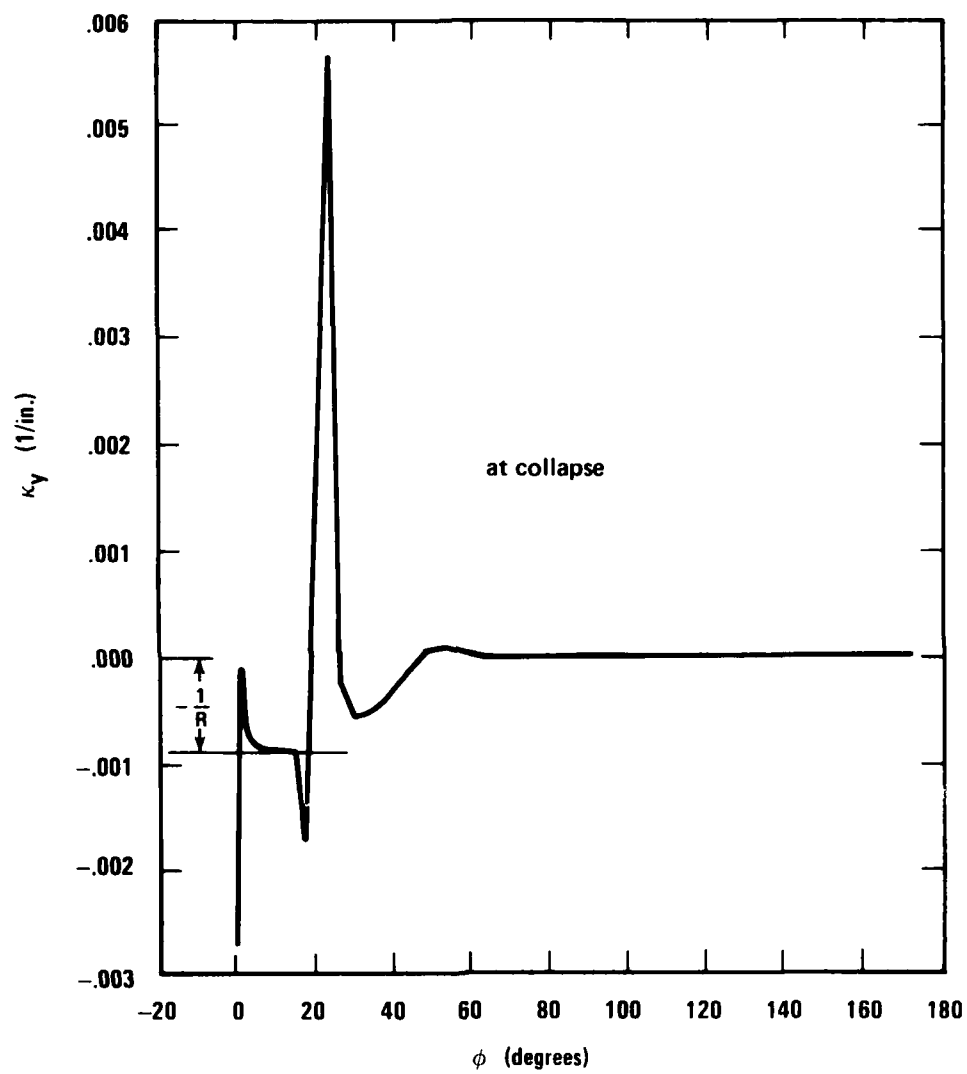


Figure 6.46. Hoop Variation Along $x = 3.5''$ of Change in Hoop Curvature at Collapse, Poked Cylinder

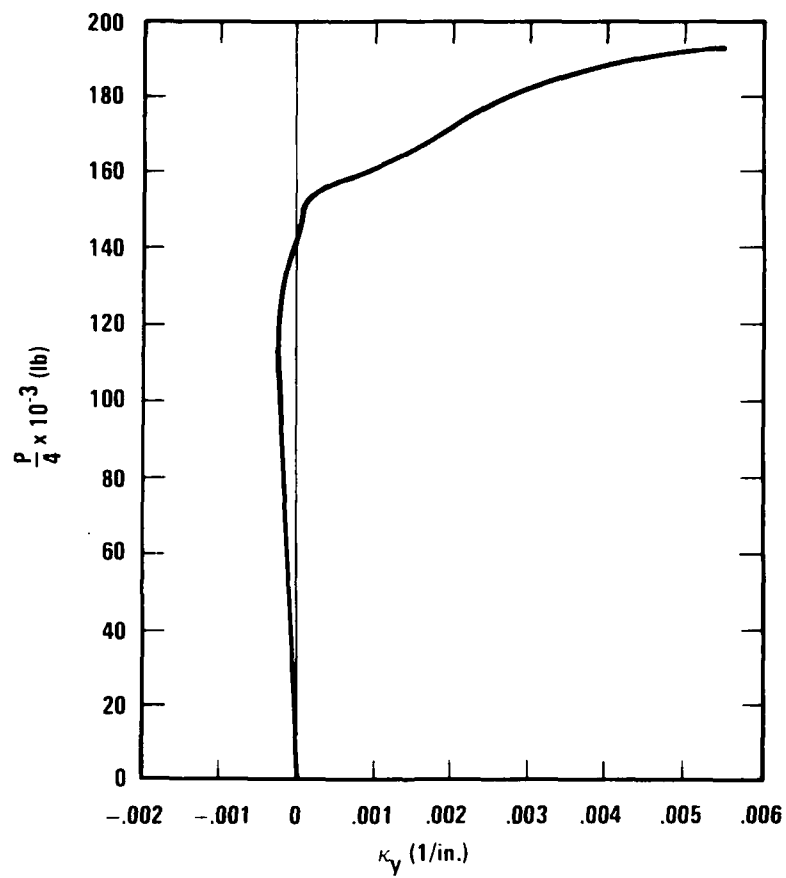
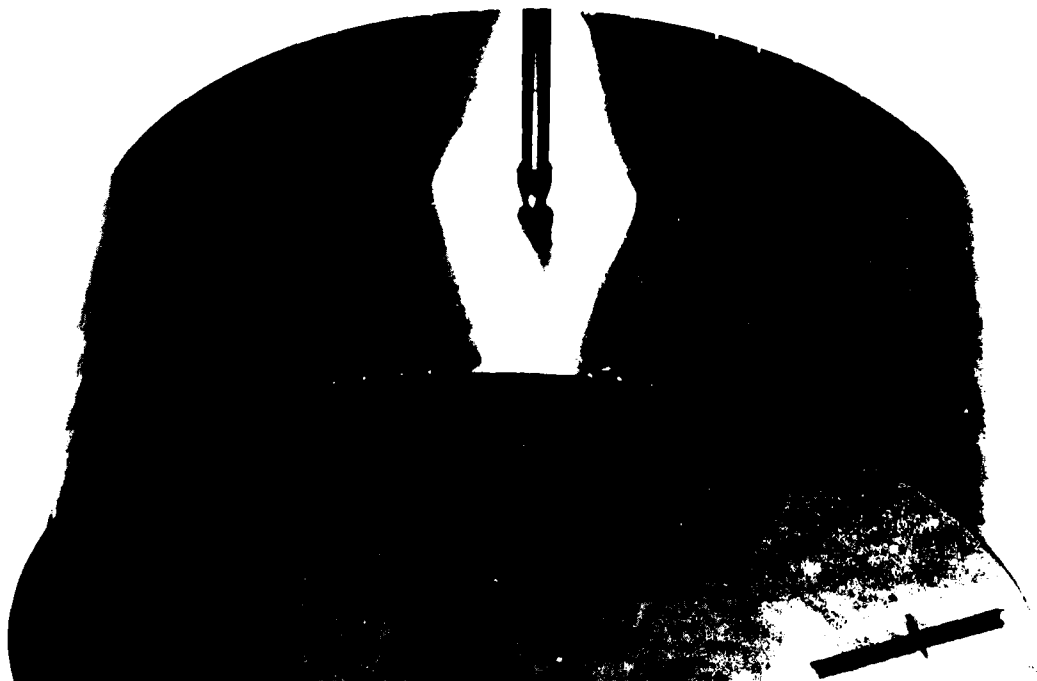


Figure 6.47. Load vs. Change in Hoop Curvature at $x = 3.5''$, $\phi = 22.95^\circ$. Poked Cylinder

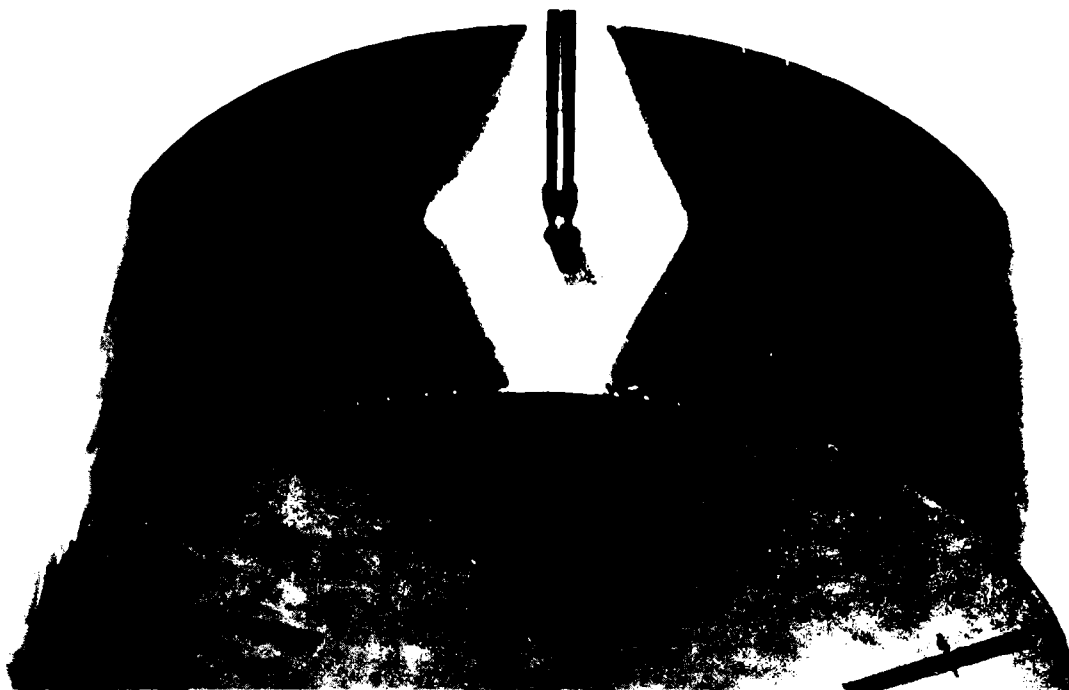


a) UNLOADED



b)

Figure 6.48. Progressive Deformation of Scaled Down Model Under Increasing Load
5407-B



c)



d) AFTER LOCAL SNAP AT RIGHT CORNER

Figure 6.48. (Continued)

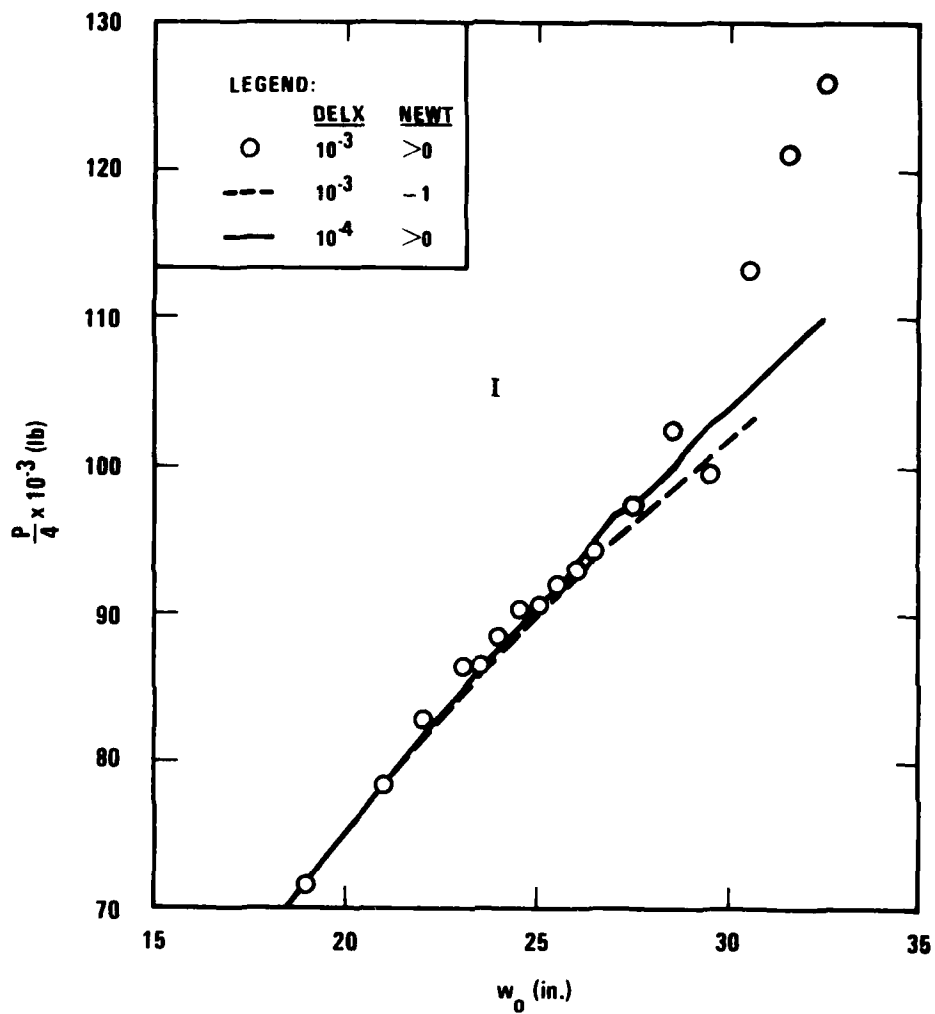


Figure 6.49 Comparison of Three Solutions for Region I of Figure 6.40. Poked Cylinder

5407-97

7.0 CONCLUSIONS AND RECOMMENDATIONS

In the Introduction, it was pointed out that the criteria for evaluating a structural analysis computer program should reflect both the nature of the program and the class of users most likely to require the program. Since STAGSC-1 is a nonlinear shell analysis program its nature is quite specialized and, by the same token, the majority of users will be relatively sophisticated. This places considerable weight on the technical excellence of the program, its flexibility in use and for post-processing and finally, on its documentation.

In order to obtain a systematic evaluation of the different aspects studied, a rating will be assigned to each aspect based on a scale of 0 to 4. Table 7.1 shows the interpretation of the rating method.

For the purposes of rating, five major aspects have been identified and given a relative weight as follows:

- | | |
|-------------------------|-----|
| o Program documentation | 20% |
| o Analysis capability | 20% |
| o Input and output | 20% |
| o Program performance | 25% |
| o User support | 15% |

These will each be discussed separately in the next sub-section, but at this point the overall conclusions can be stated; STAGSC-1 rates as about mid-way between "acceptable and "good" (i.e., an arithmetic result of 2.39).

This may seem to be a somewhat conservative evaluation considering the many unique capabilities of the program. In the opinion of the authors of this report, however, the lack of documentation of the program itself and the shortcomings in the area of post-processing justify this conclusion. If these two aspects were each upgraded to "excellent", then on the present system of rating the overall evaluation would than place STAGSC-1 in the "good-to-excellent" range.

7.1 PROGRAM DOCUMENTATION

The three types of documentation evaluated were the users' manual, theoretical manual and programmers' manual.

A. Users' Manual (Rating 3.5)

Highly rated because of logical organization and excellent user guidance. Negative features are lack of any index or cross-referencing and insufficiently clear indication of currently inoperational features.

B. Theoretical Manual (Rating 1.5)

The low rating is due to incompleteness and substantial obsolescence.

C. Programmers' Manual (Rating 0)

The programmers' manual does not exist. Equal weighting is given to each of these so that the overall rating for documentation is only 1.67, i.e., between "marginal" and "acceptable".

7.2 ANALYSIS CAPABILITY

Eleven areas were selected for the purposes of rating. Each will be briefly discussed and rated.

A. Static Linear (Rating 3.5)

STAGSC-1 is not specifically intended for linear analysis but such problems are nevertheless handled very well by the program.

B. Static Nonlinear (Rating 4.0)

The highest rating must be given to this capability by virtue of its speed and the way in which solution strategy is handled semi-automatically by the program while leaving the user significant control.

C. Vibration Modes (Rating 3.5)

This feature is also highly rated because of the use of a very effective eigenvalue solver, i.e., subspace iteration. This capability is current "state-of-the-art."

D. Bifurcation Buckling (Rating 3.5)

The same comments apply as in the case of vibration analysis.

E. Plasticity (Rating 2.0)

The plasticity capability is judged as "acceptable" for the reason that although a relatively modern hardening model (White-Besseling) is implemented, current practice requires that a variety of hardening models be available. Therefore, as a minimum, isotropic hardening should also be implemented (kinematic hardening is available as a degenerate form of White-Besseling).

F. Nonlinear Collapse (Rating 3.8)

This capability only falls short of the "excellent" category because such analysis will often require the use of plasticity with the consequent limitations as described above.

G. Transient Response (Rating 3.8)

The time integration procedures available in STAGSC-1 provide standard explicit (central difference) and implicit (trapezoidal) methods plus three other implicit schemes (Park and Gear's 2nd and 3rd order). There is therefore considerable scope for the analyst to select a procedure best suited to the problem in hand.

H. User Subroutines (Rating 4.0)

The wide variety of user-coded functions which can be specially provided for any given function is well suited to the sophisticated user. The range of capabilities available in this form is believed to be exceeded only by the MARC Program [26].

I. Element Library (Rating 1.5)

The heart of any finite element program is the library of elements. In the case of STAGSC-1, the library consists mostly of flat plate elements with membrane and bending capability. There are, however, no genuine shell elements with curvature and this must be considered a significant disadvantage in a shell analysis program.

J. Elastic Material Properties (Rating 3.0)

Both isotropic and orthotropic material behavior are provided for together with the ability to orient material axes in any given direction. Multilayer composite materials may be represented by specifying properties for each layer independently.

K. Temperature Effects (Rating 1.0)

Temperatures may be specified as a function of surface coordinates but not in the thickness direction (except for discrete stiffeners). Moreover, material properties cannot be expressed directly as a function of temperature.

The overall rating for analysis capability is 2.89 (i.e., "good") with the element library carrying a weighting of 3 and all other components weighted as 1 or less.

7.3 INPUT AND OUTPUT

A. General Input (Rating 3.5)

The free format style of input and the ability to intersperse comment statements make for ease of input and subsequent ease of reading. The volume of input required is not excessive, even for larger problems.

B. Shell Unit Input (Rating 3.5)

The ability to generate both regular and irregular meshes on standard shell surface geometries is an excellent feature. Shell connections are also easily specified if the shell units are joined at compatible boundaries (e.g., a cylinder to a torus at a cross-sectional boundary). More general intersections are not determined by the program (e.g., a cylinder/sphere intersection) and the intersecting boundaries must be calculated and input by the user. This also denies the use of the shell unit library and the intersecting shells must be defined by user subroutine or by a spline fit to specified points.

C. Element Unit Input (Rating 1.5)

Input for the element unit places a much greater burden on the user and the generation of a finite element mesh requires the use of user subroutines; otherwise, input must be provided node by node and element by element. However, the use of the element unit is normally expected to be confined to local regions of the shell where the geometry and/or the mesh may be very irregular.

D. User Subroutines (Rating 4.0)

As has been indicated, most of the input data may be specified by user subroutines and in many instances they provide the only means (e.g., shell geometries not included in the library or shell surface imperfections). The capability must be rated as excellent on account of the range of functions available.

E. General Output (Rating 2.0)

There is an acceptable degree of selective control over solution output, at least in terms of the frequency of the output. According to the manual, complete sets of displacements or stresses, stress resultants etc. can be printed at different intervals; this feature is currently defective in that all the various quantities must be output at every load or time step. A frequency specification for selected displacements etc. would be a considerable improvement.

The occurrence of yielding is noted in the stress and strain output but only the total strains are given. There should also be an option to obtain the elastic and plastic components of the total strain.

F. Post-Processing (Rating 0.5)

The currently available post-processing using the STAPL program is inadequate for many analysis tasks. The model and solution data are saved for restart and this should be made accessible to the user for post-processing in any desired manner. A minimum effort in this direction would be for the developer to provide a complete description of the model geometry and solution data files.

The overall rating for input and output is 2.50 with equal weighting given to each topic discussed.

7.4 PERFORMANCE

The evaluation of performance is based on the specific advanced evaluation studies described in Section 6. Since this examines only selected aspects of the performance of STAGSC-1 the results cannot be claimed to be comprehensive but are, at least, a reasonable indication of general performance.

A. Element Convergence (Rating 1.5)

The element convergence observed in the tests conducted is judged to be less than acceptable in comparison with "state-of-the-art" curved shell elements. This is regarded as a serious shortcoming not only because of the loss in accuracy but also because the full potential of STAGSC-1 as an efficient shell analysis program cannot be properly exploited. The promised implementation of the Ahmad isoparametric shell element will, it is hoped, greatly improve this crucial aspect of performance.

B. Eigenvalue Solutions (Rating 3.5)

The eigenvalue solver performed well in determining modes and frequencies in the often pathological situations of closely spaced or repeated eigenvalues. It was also seen to be effective in computing a mode closest to a specified frequency. Situations where the performance was less effective were seen to be a consequence of an unsatisfactory mesh or element aspect ratio and hence not attributable to the eigensolver.

C. Transient Integration (Rating 3.5)

Performance of the transient integration schemes for linear and highly nonlinear problems was generally good. The trapezoidal scheme appeared marginally the best based on the least amount of frequency distortion and damping for the nonlinear transient. The explicit method was unable to complete the nonlinear problem even with an

order of magnitude smaller time step than the estimated critical value. From the aspect of economy, the explicit method did not appear advantageous because the problem size was too small. However, for highly nonlinear problems, the implicit schemes are of greater utility since the stiffness matrix can be reformulated.

D. Nonlinear Collapse (Rating 3.5)

The most significant conclusion that may be drawn from the performance of the elastic nonlinear collapse analyses is that STAGSC-1 has a clearly demonstrated capability to trace out a load-displacement curve for a shell with somewhat subtle collapse behavior. In the case of the point loaded cylinder, the predicted deformation pattern up to collapse appears to be in qualitative agreement with that observed visually in a small scale model of the cylinder.

STAGSC-1 performed successfully both for controlled load and controlled displacement incrementation, largely because of the adaptive incrementation based on the convergence of the solution. This particular feature distinguishes STAGSC-1 from most other finite element programs with nonlinear capability. Sufficient control was found to be available to the user both for incrementation strategy (ICUT and NEWT) and convergence tolerance (DELX). In addition to effective control of solution accuracy, these strategic parameters provide the means to obtain the most economical solution.

E. Program Efficiency (Rating 3.0)

The overall efficiency of STAGSC-1 cannot be adequately assessed in relation to other programs based on the present study. However, given the available evidence it appears that:

- (1) STAGSC-1 is a factor of 2 to 3 times more economical in solving a small linear transient problem than the MARC program.

- (2) there appears to be scope for improvement in data management for the CDC 7600 system version. Based on the admittedly subjective and imprecise impressions of other users, STAGSC-1 is a relatively fast running program in its present form. It seems safe to conclude, therefore, that improvements in the element library and in data handling could bring improvements in overall efficiency which would make it a first choice for shell analysis.

Giving equal weighting to each of the performance aspects of yields an overall rating of 3.0.

7.5 USER SUPPORT (RATING 1.5)

The topic of developer support for users of STAGSC-1 has not been discussed elsewhere, but being a significant factor in the use of a large scale program it deserves some consideration. STAGSC-1 is a program in the public domain and the developers, Lockheed Palo Alto Research Laboratory, are not suppliers of structural software in a general commercial sense. Potential users can obtain the source file for a nominal fee and are then responsible for installation on their own systems. For an additional annual fee, updates and consulting services are available from Lockheed.

Developer expertise is available for solving problems and applying the program correctly. Program malfunctions can be reported but corrective action must be taken by the user based on program "fixes" supplied by the developer.

Since funding for STAGSC-1 development is principally from NASA, the individual user has little or no control over future development items. It is clear that much better user support could be obtained if the fees were adequate to support a group whose sole responsibility was consultation and program maintenance. The present arrangement fails to be satisfactory if a user requires a minor modification for his particular purpose. Generally speaking, the complexity of STAGSC-1 makes user written modifications to the program very difficult to achieve and there seem to be no proper channels through which he can obtain them from the developers.

As far as program updates are concerned, none have been received since the evaluation version was delivered in November 1979.

During the present evaluation, the staff at Lockheed were consulted on numerous occasions and excellent cooperation was obtained.

7.6 RECOMMENDATIONS

A. Documentation

There are four major recommendations;

- (1) An up-to-date theoretical manual with adequate coverage of element formulations should be provided.
- (2) A programmer's manual is required which describes the program flow in sufficient detail to enable the skilled user to identify the source of any program difficulties and to make changes with help from the developers.
- (3) The users' manual should be provided with a suitable index.
- (4) A problem demonstration manual should be written specifically for STAGSC-1.

B. Capabilities

- (1) A good curved shell element (e.g., the Ahmad isoparametric) is essential for the full potential of STAGSC-1 to be realized. The simpler elements should be retained (QUAF410, 411) but the value of the higher order (QUARC) series would then be less and they could probably be discarded.

- (2) The option for additional plastic hardening models should be provided. As a minimum, isotropic hardening should be implemented and consideration should be given to simulating cyclic hardening (or softening), e.g., the so-called ORNL 10th Cycle Hardening Rule [40].
- (3) Inelastic behavior should be extended to include creep. A simple creep law (e.g., the Norton formula) should be provided with user input coefficients and the option for time hardening or strain hardening. In addition, provision should be made for a user specified creep law to be input. Consideration should also be given to the eventual inclusion of cyclic creep strain hardening behavior, e.g., the so-called ORNL auxiliary creep hardening rules [40].
- (4) Temperature distributions should include variations through the shell wall thickness. In addition, material properties should be allowed to vary with temperature.
- (5) The input for the element unit could be improved. Simple pattern generation for nodal coordinates and element connectivity, in addition to the present node-by-node and user subroutine methods, would make this feature much more usable.
- (6) The selectivity of stress and strain printout should be extended to include the ability to print selected quantities at any desired load or time step intervals. Also, the option should be provided to obtain strain components decomposed into elastic, plastic and thermal contributions.
- (7) A user post-processing file should be created which contains all the necessary model geometry and solution data to permit solution processing according to the needs of the analyst. The file should be constructed so that the information retrieval is straightforward and it should be fully documented.

TABLE 7.1
EVALUATION RATINGS

Rating	Interpretation
4	Excellent
3	Good
2	Acceptable
1	Marginal
0	Poor

8.0 REFERENCES

1. Nickell, R. E., "The Interagency Software Evaluation Group: A Critical Structural Mechanics Software Evaluation Concept," Report PT-U78-0246, Pacifica Technology, P.O. Box 148, Del Mar, California 92014.
2. Almroth, B. O., Brogan, F. A., Stanley, G. M., "Structural Analysis of General Shells, Volume II, User Instructions for STAGSC-1," LMSC-D 633873, July 1979, Applied Mechanics Laboratory, Lockheed Palo Alto Research Laboratory.
3. Users Manual for STAGS, Volume 1, Theory, Structural Mechanics Laboratory, Lockheed Palo Alto Research Laboratory, March, 1978.
4. Bushnell, D., "A Strategy for the Solution of Problems Involving Large Deflections, Plasticity and Creep," International Journal for Numerical Methods in Engineering, Vol. II, 683-708 (1977).
5. Almroth, B. O., Brogan, F. A., "Bifurcation Buckling as an Approximation of the Collapse Load for General Shells," AIAA Journal, Volume 10, N.4, April, 1972.
6. Marlowe, M. B., Flugge, W., "Some New Developments in the Foundations of Shell Theory," LMSC 6-78-68-13, May, 1968, Lockheed Missiles and Space Company, Palo Alto, California.
7. Besseling, J. F., "A Theory of Elastic, Plastic and Creep Deformation of an Initially Isotropic Material Showing Strain Hardening, Creep Recovery and Secondary Creep," J. App. Mech., Volume 25, N.4, December, 1958.
8. Clough, R. W., Felippa, C. A., "A Refined Quadrilateral Element for Analysis of Plate Bending," Proceedings of the Second Conference on Matrix Methods in Structural Mechanics, AFFDL-TR-68-150, 1968.
9. Tillerson, J. R., Stricklin, J. A., Haisler, W. C., "Numerical Methods for the Solution of Nonlinear Problems in Structural Analysis," ASME Publication AMD-Volume 6, Numerical Solution of Nonlinear Structural Problems, 1973.
10. Bushnell, D., "Large Deflection Elastic-Plastic Creep Analysis of Axisymmetric Shells," ASME Publication AMD-Volume 6, Numerical Solution of Nonlinear Structural Problems, 1973.
11. Chang, T. Y., Padovan, J., "Evaluation of ADINA: Part I, Theory and Programming Description," University of Akron Technical Report, ONR Contract N00014-78-C-0691, June, 1980.
12. Padovan, J., Chang, T. Y., "Evaluation of ADINA: Part II, Operating Characteristics," University of Akron Technical Report, ONR Contract N00014-78-C-0691, June, 1980.

13. Bathe, K., Wilson, E. L., "Numerical Methods in Finite Element Analysis," Prentice-Hall Inc., Englewood Cliffs, N.J., 1976.
14. Jones, J. W., Fong, H. H., Blehm, D. A., "Evaluation of the NASTRAN General Purpose Computer Program," SSC Report No. 81980, Swanson Service Corporation, Huntington Beach, California, August, 1980.
15. Park, K. C., "Evaluating Time Integration Methods for Nonlinear Dynamics Analysis," ASME Publication AMD-Volume 14, 1975.
16. Park, K. C., "Practical Aspects of Numerical Time Integration," Computers and Structures, Volume 7, 1977.
17. Belytschko, T., Schoeberle, D. F., "On the Unconditional Stability of an Implicit Algorithm for Nonlinear Structural Dynamics," J. App. Mech., Vol. 24, N.4, December 1975.
18. Giles, G. L., "Digital Computer Programs for Generating Oblique Orthographic Projections and Contour Plots," NASA Technical Note, TN D-7797, January, 1975.
19. Gibson, W., "A Contour Plot Package for the STAGSC Computer Program," ASIAC Report, Anamet Laboratories, San Carlos, California, July, 1976.
20. Pilkey, W., Saczalski, K., Schaeffer, H., "Structural Mechanics Computer Programs: Surveys, Assessments and Availability," The University Press of Virginia, 1974.
21. Hunsaker, B., Vaughan, D. K., Stricklin, J. A., "A Comparison of the Capability of Four Hardening Rules to Predict a Material's Plastic Behavior," Texas Engineering Experiment Station, Proceedings of the Office of Naval Research Plasticity Workshop, June, 1976.
22. Forsberg, K., "An Evaluation of Finite Difference and Finite Element Techniques for Analysis of General Shells," IUTAM Conference, Liege, 1970.
23. Ashwell, D. G., "Strain Elements with Applications to Arches, Rings and Cylindrical Shells," Finite Elements for Thin Shells and Curved Members, Ashwell and Gallagher (Eds.), Wiley, 1976.
24. Cowper, G. R., Lindberg, G. M., Olson, M. D., "A Shallow Shell Finite Element of Triangular Shape," International Journal of Solids and Structures, Volume 6, 1970.
25. Hibbitt, H. D., Karlsson, B., "ABAQUS, Draft Manual," Hibbitt & Karlsson Inc., Providence, R.I., April, 1979.
26. Anon., "MARC General Purpose Finite Element Program: User Manual", MARC Analysis Research Corporation, Palo Alto, California, 1979.
27. Roark, R. J., Young, W. C., "Formulas for Stress and Strain," 5th edition, pages 386, 392, 1975.

28. Argyris, J. H., "Continua and Discontinua," Proceedings of the Conference on Matrix Methods in Structural Mechanics, AFFDL-TR-66-80, December, 1965.
29. Gallagher, R. H., "Finite Element Analysis-Fundamentals," pages 46-49, Prentice-Hall, 1975.
30. Thompson, W. T., "Mechanical Vibrations," 2nd Edition, Prentice Hall, 1958.
31. Zienkiewicz, O. C., "The Finite Element Method," page 550, McGraw-Hill Book Co. (UK), 3rd Edition, 1977.
32. Green, B. E., Jones, R. E., McClay, R. W., Strome, D. R., "Dynamic Analysis of Shells using Doubly Curved Finite Elements," Proceedings of the Second Conference on Matrix Methods in Structural Mechanics, AFFDL-TR-68-150, October, 1968.
33. Voss, H. M., "The Effect of External Supersonic Flow on the Vibration Characteristics of Thin Cylindrical Shells," Journal of the Aerospace Sciences, December 1961.
34. Baron, M. L., Bleich, H. H., "Tables for Frequencies and Modes of Free Vibration of Infinitely Long Thin Cylindrical Shells," Journal of Applied Mechanics, Volume 21, Number 2, pages 178-184, June, 1954.
35. Krieg, R. D., Key, S. W., "Transient Shell Response by Numerical Time Integration," Int. J. for Num. Meth. in Engineering, Vol. 7, pp. 273-286, (1973).
36. Stricklin, J. A., Martinez, J. E., Tillerson, J. R., Hong, J. H., Haisler, W. E., "Nonlinear Dynamic Analysis of Shells of Revolution by Matrix Displacement Method," AIAA Journal, V. 9, N.4, April, 1971.
37. Stricklin, J. A., Haisler, W. E., Von Rieseemann, W. A., "Large Deflection Elastic-Plastic Dynamic Response of Stiffened Shells of Revolution," Paper 74-PVP-3, Pressure Vessels and Piping Conference, Miami Beach, FL, 1974.
38. Wu, R. W. H., Witmer, E. A., "Finite-Element Analysis of Large Elastic-Plastic Transient Deformations of Simple Structures," AIAA Journal, V. 9, N.9, pp. 1719-1724, September, 1971.
39. Flugge, W. (Editor), "Handbook of Engineering Mechanics," First Edition, McGraw-Hill Book Company, 1962.
40. Anon., "Guidelines and Procedures for Design of Nuclear System Components at Elevated Temperature," RDT Standard, RDT F 9-5T, September, 1974.
41. Brogan, F. A., Almroth, B. O., "Practical Methods for Elastic Collapse Analysis of Shell Structures," AIAA J., Volume 9, No. 12, 1971.
42. Lindberg, G. M., Olson, M. D., Cowper, G. R., "New Developments in the Finite Element Analysis of Shells," DME/NAE Quarterly Bulletin, No. 1969 (4), Jan. 1970.

43. Bijlaard, P. P., "Additional Data on Stresses in Cylindrical Shells under Local Loadings," Welding Research Council Bulletin No. 50, May, 1959.
44. Lukasiewicz, S., "Local Loads in Plates and Shells," Noordhoff International Publishing, The Netherlands, 1979.
45. Seide, P., "Small Elastic Deformations of Thin Shells," Noordhoff International Publishing, The Netherlands, 1975.
46. Bijlaard, P. P., "Stresses from Local Loadings in Cylindrical Pressure Vessels," Trans. ASME., V. 77, 1955.
47. Bijlaard, P. P., "Stresses from Radial Loads in Cylindrical Pressure Vessels," Welding Journal, V. 33, N. 12, Research Supplement, 1954.
48. Mizoguchi, K., Shiota, H., Shirakawa, K., "Deformation and Stress in a Cylindrical Shell under Concentrated Loading," 1st report, Radial Loading Bulletin, J.S.M.E. 11.45, 1968.
49. Kempner, J., Sheng, J., Pohle, F. V., "Tables and Curves for Deformation and Stresses in Circular Cylindrical Shells under Localized Loadings," J. Aeronaut, Sci., V. 24, 1957.
50. Crisfield, M. A., "A Fast Incremental/Iterative Solution Procedure that Handles "Snap-Through,"" J. Computers and Structures, V. 13, 1981.

9.0 APPENDIX

9.1 STAGSC-1 SUBROUTINE LINKAGES

The overlay structure, as described in Section 3, Program Architecture, makes frequent reference to the various subroutine calls made in each overlay. The diagrams showing the subroutine linking within each overlay are contained in this section. They are not flow diagrams since there is no sequence implied in the way the diagrams are constructed. Some of the overlays are too large to fit all the subroutine calls within a single diagram. For example, Overlay (1,0) requires three diagrams (Figures 9.4, 9.5, and 9.6). Where there are links between subroutines in different figures, the connection to the calling subroutine is shown by a dashed line.

There are also two subroutines which make a considerable number of calls and are themselves basic modules. These are MACUP in STAGS1, and CVR1 and VRDATA in STAGS2. The details of the calls within these subroutines are given only once (Figure 9.11 for MACUP and Figure 9.27 for VRDATA).

9.2 ELEMENT STIFFNESS EIGENSOLUTION

The concept of stiffness matrix eigenmodes is discussed by Gallagher [29]. In order to obtain the distribution of strain energy with respect to the eigenmodes for a given loading case, it is only necessary to decompose the solution vector into modal components. The calculation of the strain energy is then straightforward and can be obtained mode by mode since the modes are orthogonal. The necessary equations will now be developed.

For an element stiffness matrix $[k]$, the characteristic polynomial may be obtained by expanding the determinant

$$|[k] - \lambda [I]| = 0 \quad 9.1$$

and the eigenvectors by solution of the equation

$$[k] \{d_i\} = \lambda_i \{d_i\} \quad 9.2$$

where $\{d_i\}$, λ_i are the i th eigenvector and eigenvalue.

Because of the orthogonality of the eigenvectors, we may write

$$\{d_i\}^t [k] \{d_i\} = \lambda_i \quad 9.3$$

provided that

$$\{d_i\}^t \{d_i\} = 1 \quad 9.4$$

Thus, the eigenvalues are the corresponding generalized stiffness coefficients.

A matrix of the eigenvectors $[r_d]$ may be defined as

$$[r_d] = [\{d_1\} \dots \{d_1\} \dots \{d_n\}] \quad 9.5$$

where n is the order of $[k]$.

Since the eigenvectors are linearly independent, any solution vector $\{\Delta\}$ may be expressed as a linear combination of the eigenvectors as follows:

$$\{\Delta\} = [r_d] \{\alpha\} \quad 9.6$$

where $\{\alpha\}$ is a vector of modal coefficients.

Thus,

$$\{\alpha\} = [r_d]^{-1} \{\Delta\} \quad 9.7$$

which, again because of orthogonality, may be written equivalently as

$$\{\alpha\} = [r_d]^t \{\Delta\} \quad 9.8$$

The strain energy associated with the displacement vector $\{\Delta\}$ is

$$U = \frac{1}{2} \{\Delta\}^t [k] \{\Delta\} \quad 9.9$$

Because of Equation 9.6, this may also be written as

$$U = \frac{1}{2} \{\alpha\}^t [r_d]^t [k] [r_d] \{\alpha\} \quad 9.10$$

Because of the orthogonality as expressed by Equation 9.3, this may be rewritten as

$$U = \frac{1}{2} \{\alpha\}^t \Lambda \{\alpha\} \quad 9.11$$

$$= \frac{1}{2} \sum_{i=1}^n \alpha_i^2 \lambda_i \quad 9.12$$

where Λ is the diagonal matrix of the eigenvalues.

The program ELMOD was therefore written to perform the eigensolution for the element stiffness matrix and also to determine the corresponding modal coefficients for a solution vector $\{\Delta\}$. The strain energy distribution is then obtained simply from Equation 9.12. Table 9.1 gives the listing for ELMOD.

Table 9.1 ELMOD Listing

```

PROGRAM ELMOD(INPUT,OUTPUT,TAPE5=INPUT,TAPE6=OUTPUT,TAPE10,TAPE11)
DIMENSION A(1400),AKE(50,50),EIV(50,50),EIG(50),D(50),ALP(50),
IU(50),FV1(50),FV2(50)
INTEGER EIGEN,ATRANB
EIGEN = 3
ATRANB = 23

C
C READS IN ORDER OF ELEMENT MATRIX (M), FLAG ITAP TO INDICATE WHETHER
C STIFFNESS DATA AND SOLUTION VECTOR ARE TO BE READ FROM TAPE OR
C CARDS.
C
C          ITAP = C    DATA FROM CARDS
C          ITAP = 1    DATA FROM TAPE
C NSKIP IS THE NO. OF WORDS TO BE SKIPPED AT THE START OF TAPE10
C
READ(5,1000) M,ITAP,NSKIP,MATZ
N = M*(M+1)/2
K1 = N + 1
K2 = N + M

C
C READS IN ELEMENT STIFFNESS MATRIX AS A LOWER TRIANGLE INTO ARRAY A
C READS IN SOLUTION VECTOR AND TACKS IT ON TO THE END OF ARRAY A.
C
IF(ITAP.EQ.1) GO TO 50
READ(5,1010) (A(I), I=1,N)
READ(5,1010) (A(I), I=K1,K2)
GO TO 60
50 READ(10) (SKIP,I=1,NSKIP),(A(I),I=1,K2)
60 CONTINUE

C
C CREATES SEPARATE ARRAYS AKE AND D FOR THE ELEMENT STIFFNESS MATRIX
C AND SOLUTION VECTOR.
C
DO 100 I=1,M
DO 100 J=1,I
K = J + I*(I-1)/2
AKE(I,J) = A(K)
AKE(J,I) = AKE(I,J)
100 CONTINUE
DO 110 I=1,M
J = M*(M+1)/2 + I
D(I) = A(J)
110 CONTINUE

C
C FINDS THE EIGENVALUES AND EIGENVECTORS OF STIFFNESS MATRIX AKE.
C
CALL RS(50,M,AKE,EIG,MATZ,EIV,FV1,FV2,IERR)
C FINDS SCALAR PRODUCT OF EACH EIGENVECTOR WITH ITSELF TO FIND THE
C NORMALIZATION FACTORS AND PLACES THEM IN ARRAY A.
C

```

Table 9.1 ELMOD Listing (Continued)

```

DO 130 J=1,M
FACT = 0.0
DO 140 I=1,M
FACT = FACT + EIV(I,J)*EIV(I,J)
140 CONTINUE
A(J) = SQRT(FACT)
130 CONTINUE
C
C   SCALES EIGENVECTOR MATRIX EIV TO MAKE IT ORTHONORMAL.
C
DO 150 J=1,M
DO 150 I=1,M
EIV(I,J) = EIV(I,J)*A(J)
150 CONTINUE
C
C   THE VECTOR OF MODAL COEFFICIENTS IS NOW FORMED AND PLACED IN ALP.
C
CALL MATRIX(ATRANB,M,M,1,EIV,50,D,50,ALP,50)
C
C   DETERMINES THE VECTOR OF MODAL STRAIN ENERGIES.
C
UE = 0.
DO 160 I=1,M
U(I) = 0.5*ALP(I)*ALP(I)*EIG(I)
UE = UE + U(I)
160 CONTINUE
C
C   PRINTS OUT THE RESULTS.
C
DO 170 J=1,M
WRITE(6,1020) J
WRITE(6,1030) (EIV(I,J),I=1,M)
WRITE(6,1040) EIG(J)
WRITE(6,1050) U(J)
170 CONTINUE
WRITE(6,1060) UE
STOP
C
1000 FORMAT(4I3)
1010 FORMAT(6E12.6)
1020 FORMAT(1H1,///,10X,11HEIGENVECTOR,1X,I3,/)
1030 FORMAT(10X,E12.6)
1040 FORMAT(//,10X,31HTHE CORRESPONDING EIGENVALUE IS,1X,E12.6)
1050 FORMAT(//,10X,26HTHE MODAL STRAIN ENERGY IS,1X,E12.6)
1060 FORMAT(//,10X,26HTHE TOTAL STRAIN ENERGY IS,1X,E12.6)
END

```

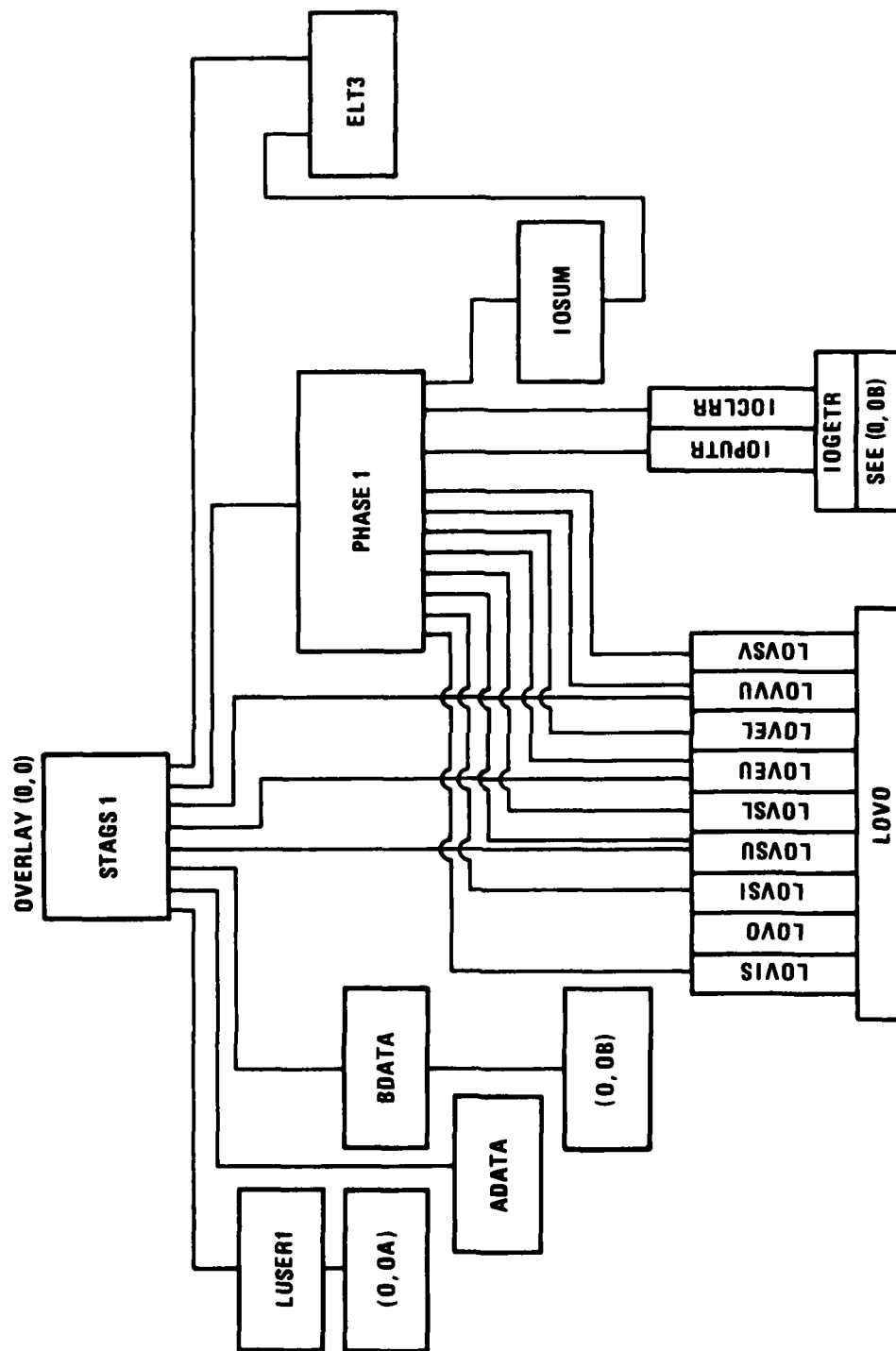


Figure 9.1 Main Pre-processing Program

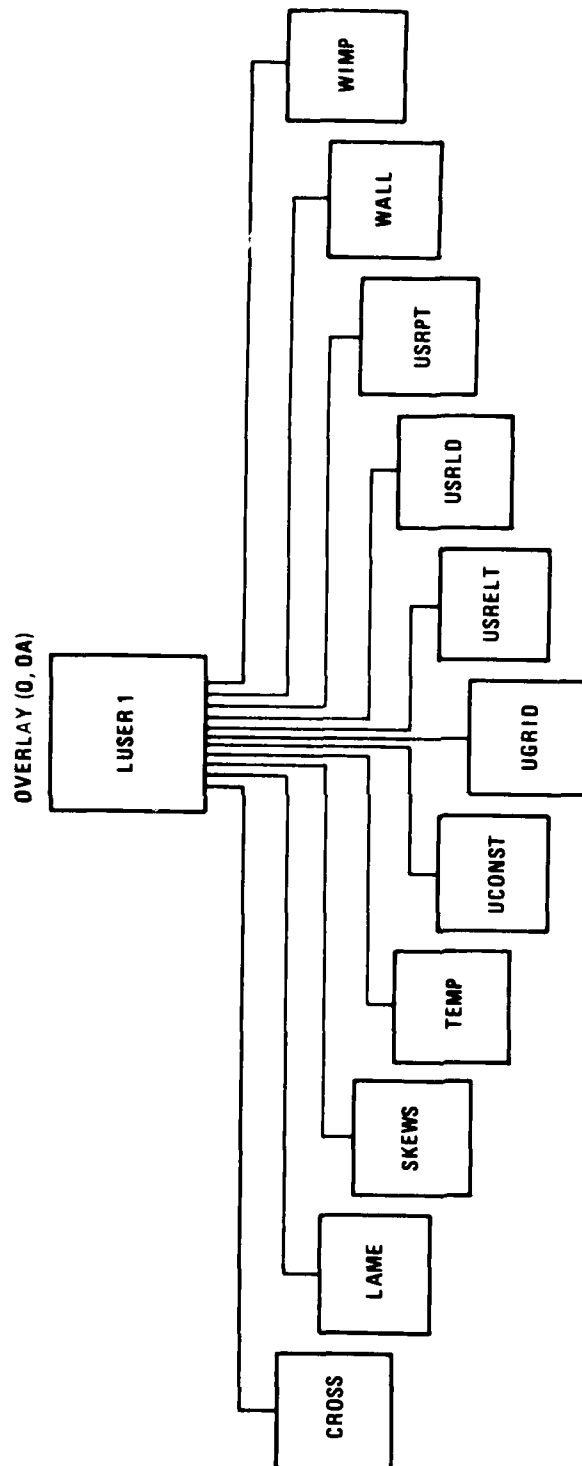


Figure 9.2 User Subroutine Loader (See Figure 9.1)

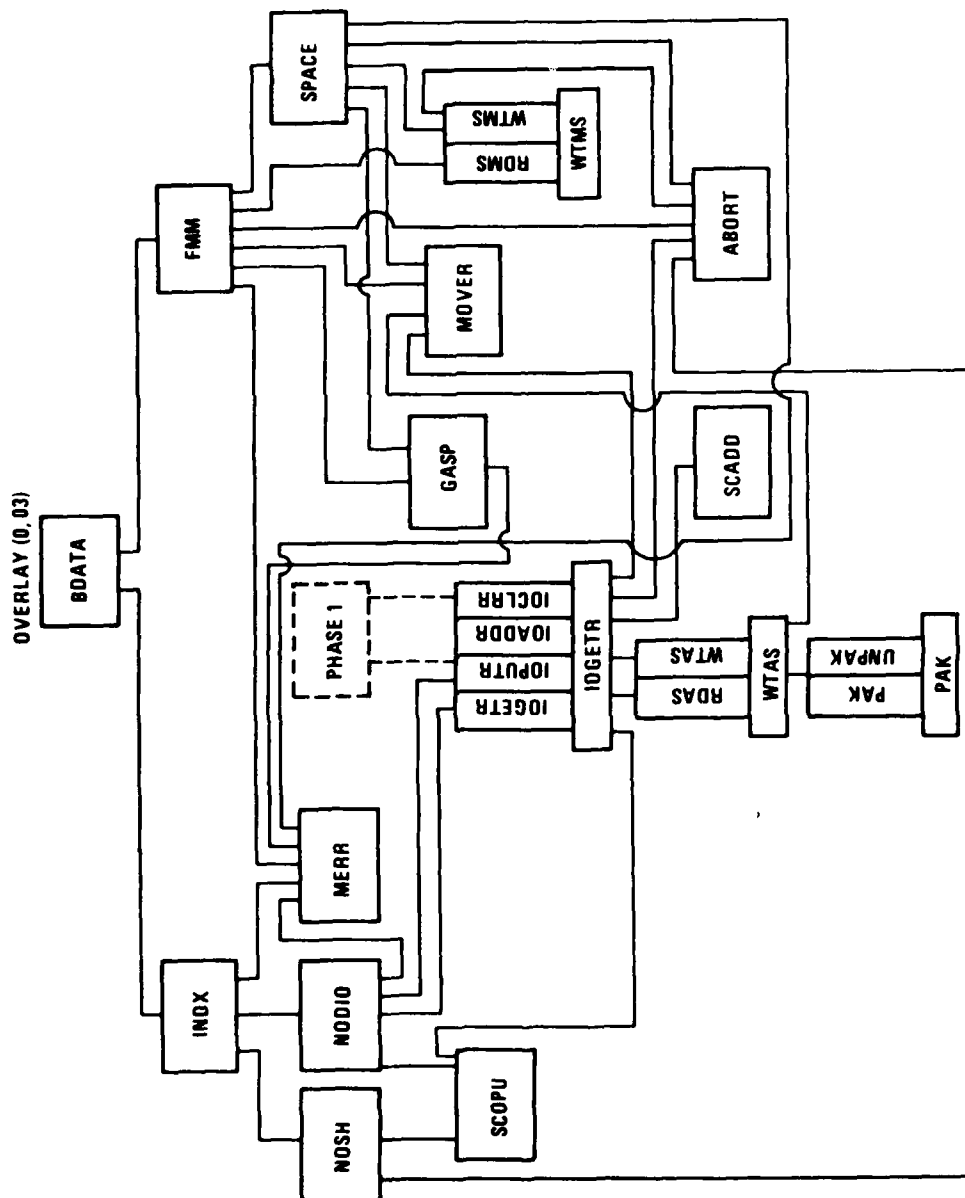


Figure 9.3 (See Figure 9.1)

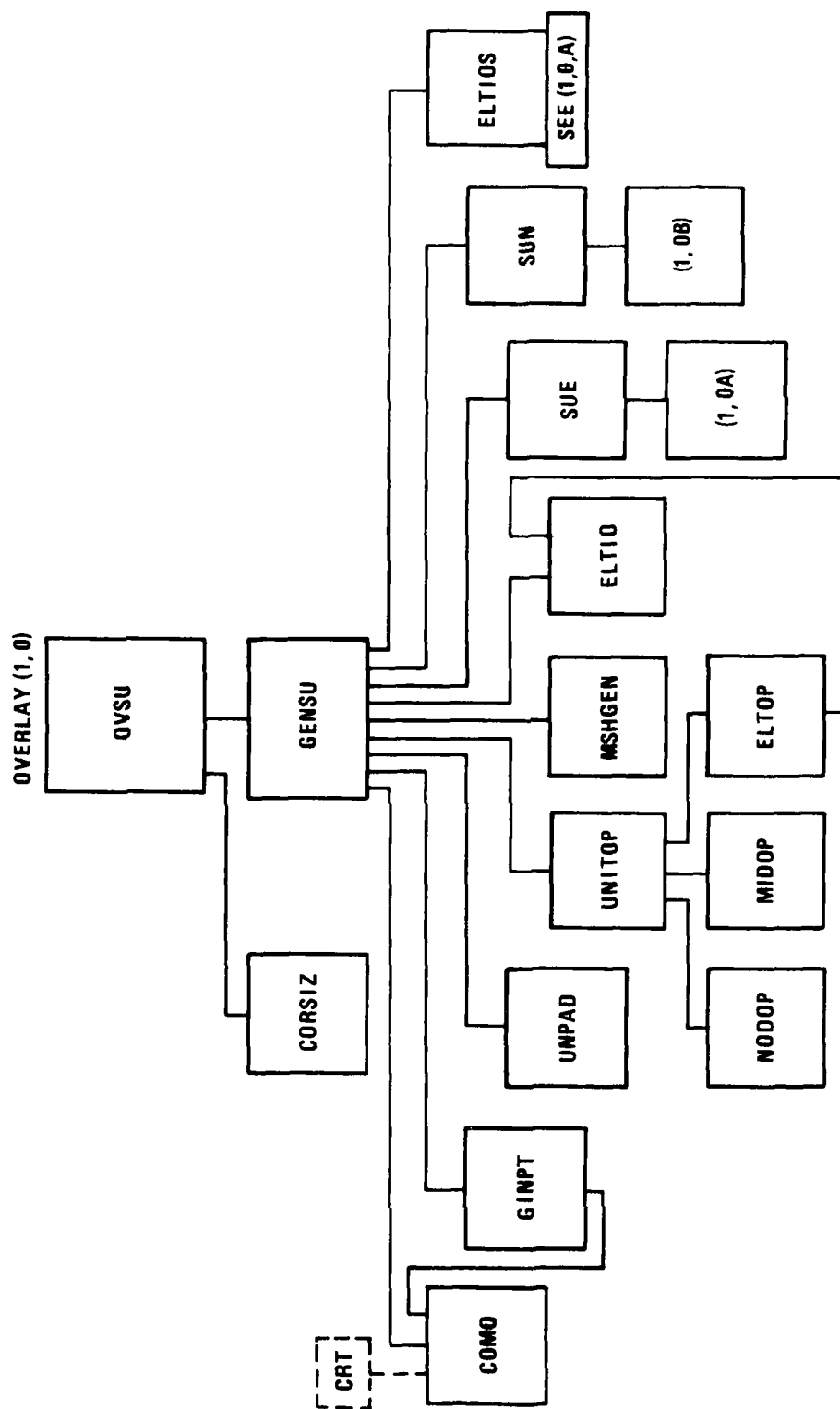


Figure 9.4 Shell Unit Generation Overlay

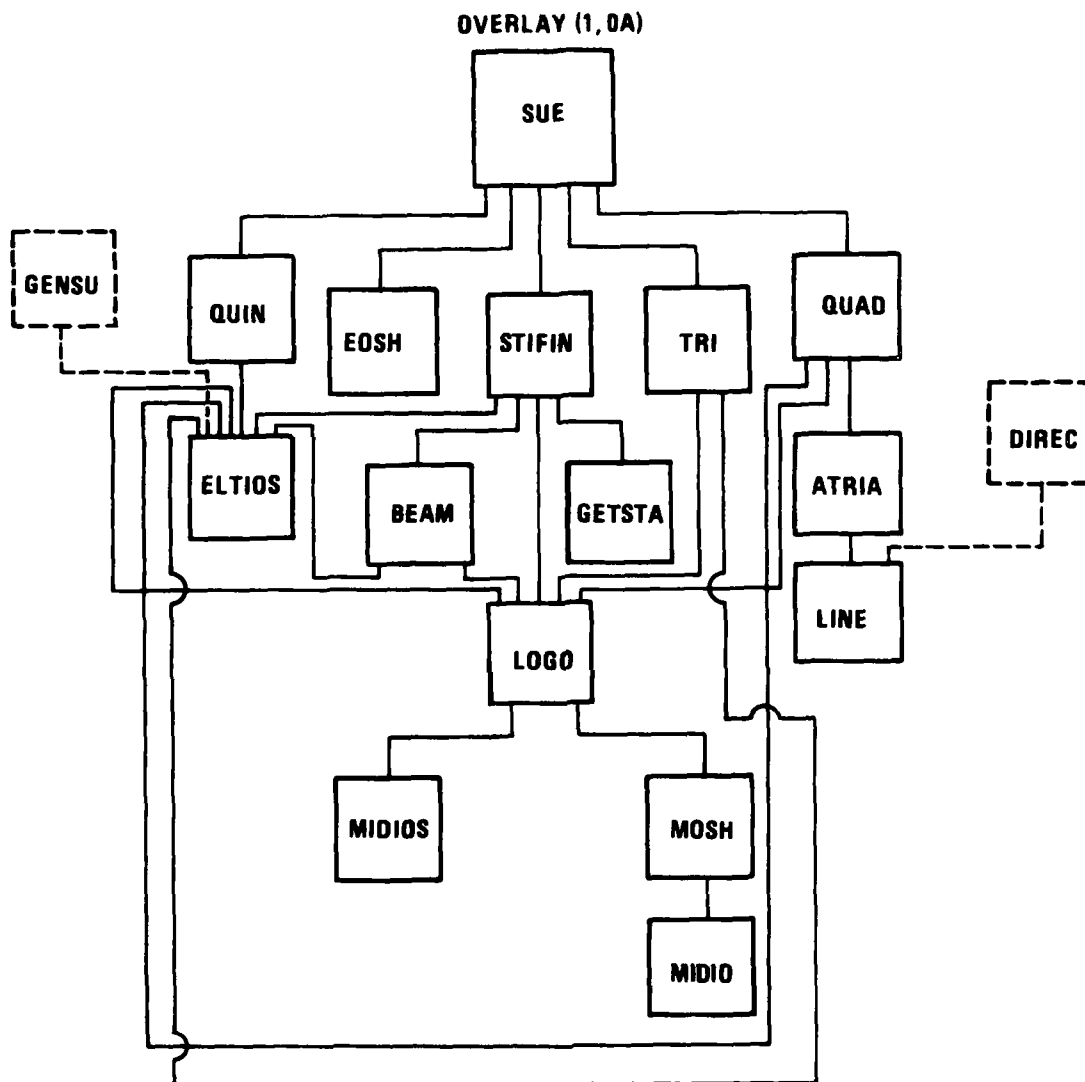


Figure 9.5 Element Table Generation (See Figure 9.4)

5407-67

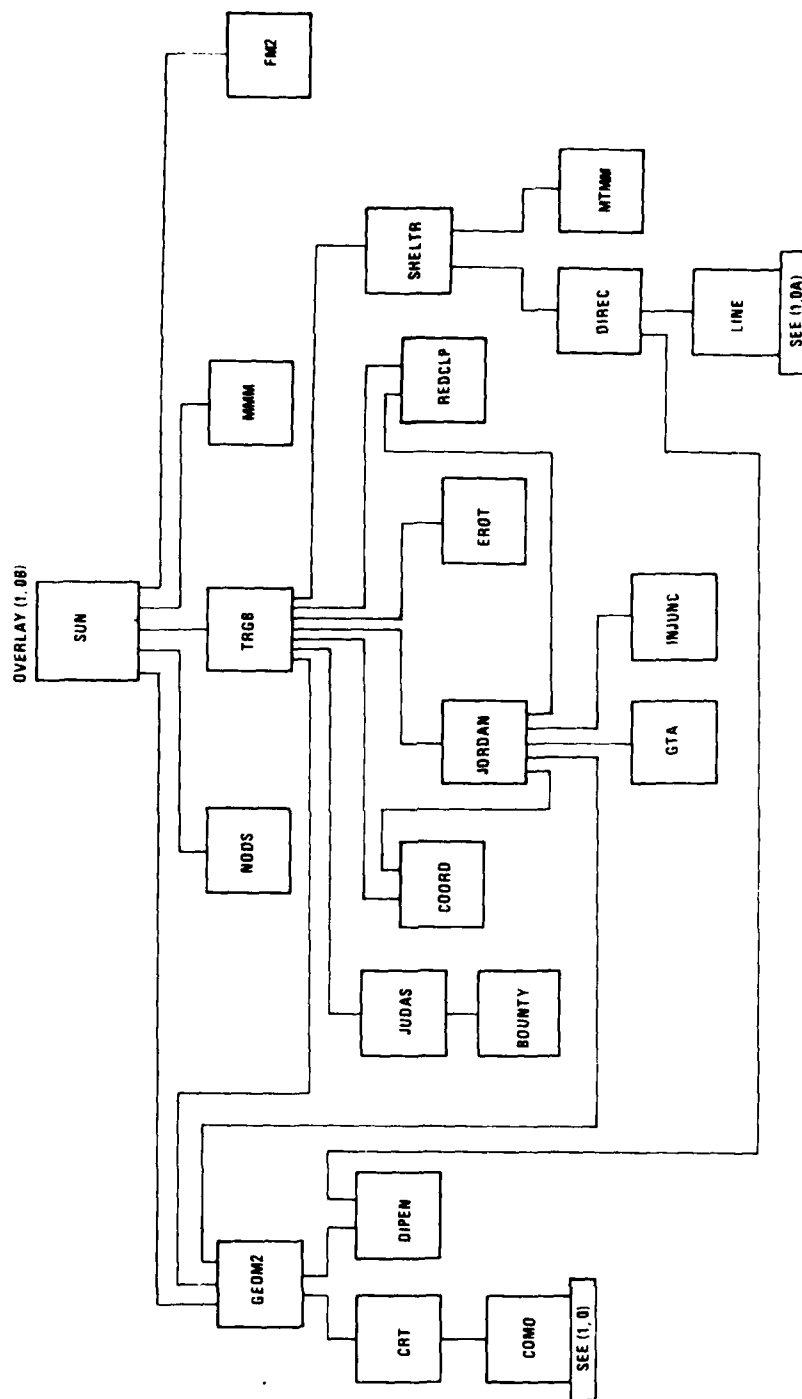


Figure 9.6 Node Table Generation (See Figure 9.4)

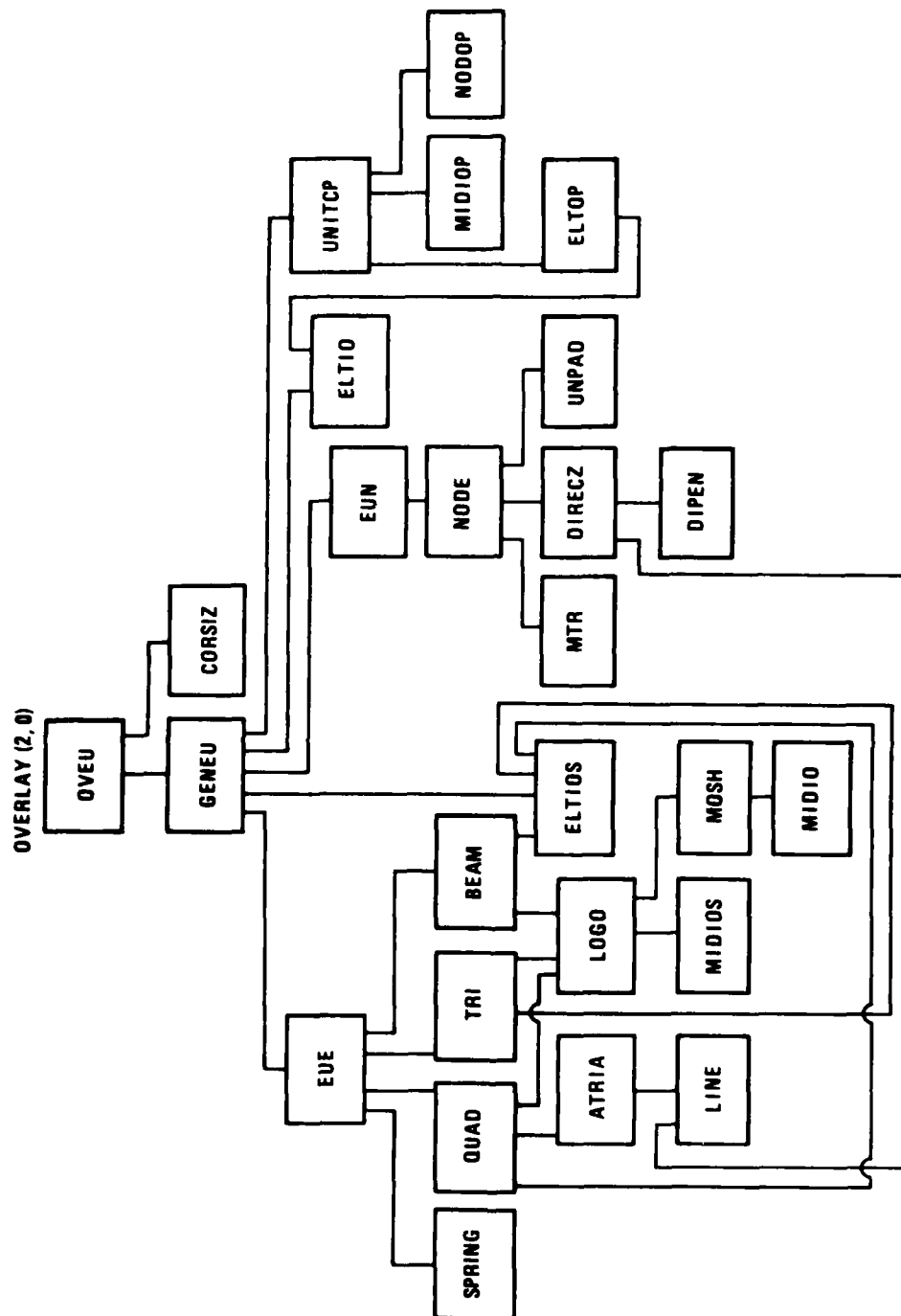


Figure 9.7 Element Unit Generation

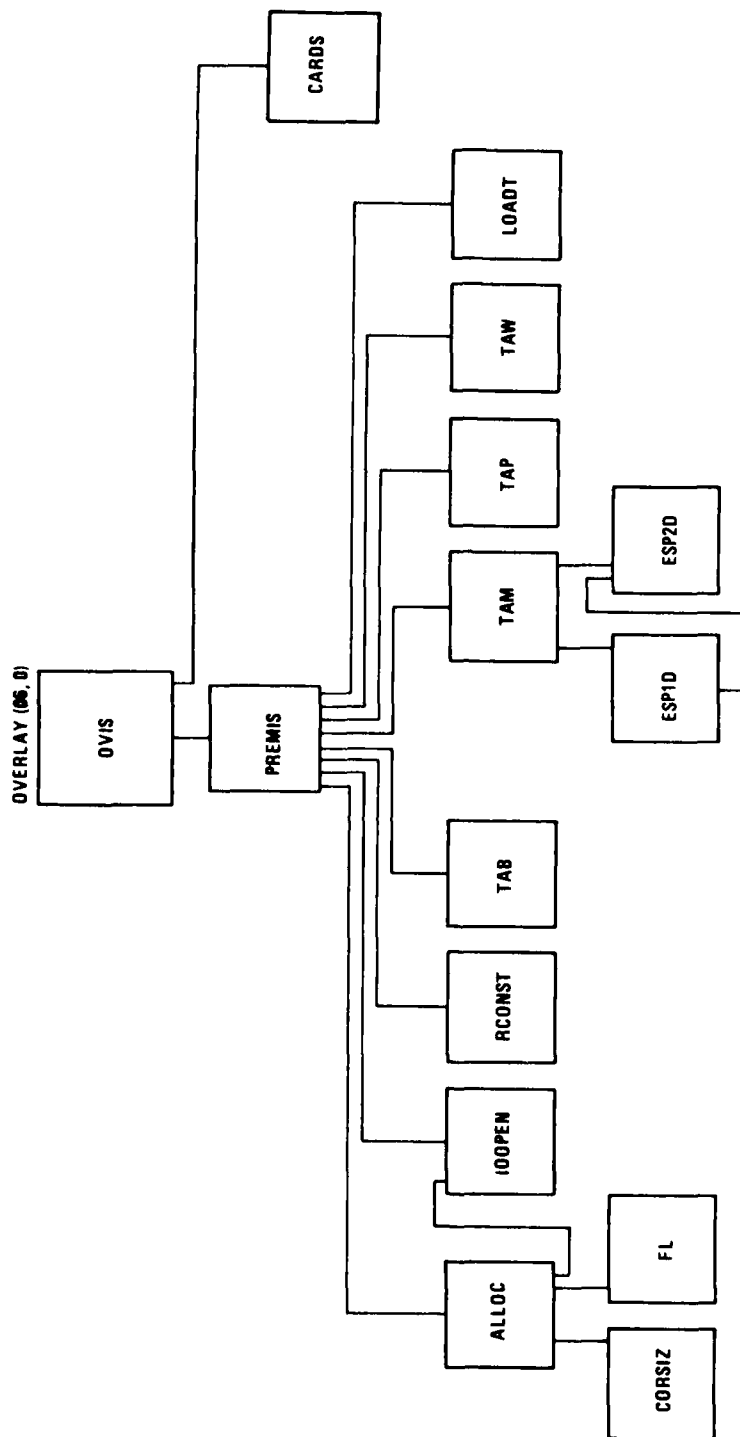


Figure 9.8 Model Input Summary

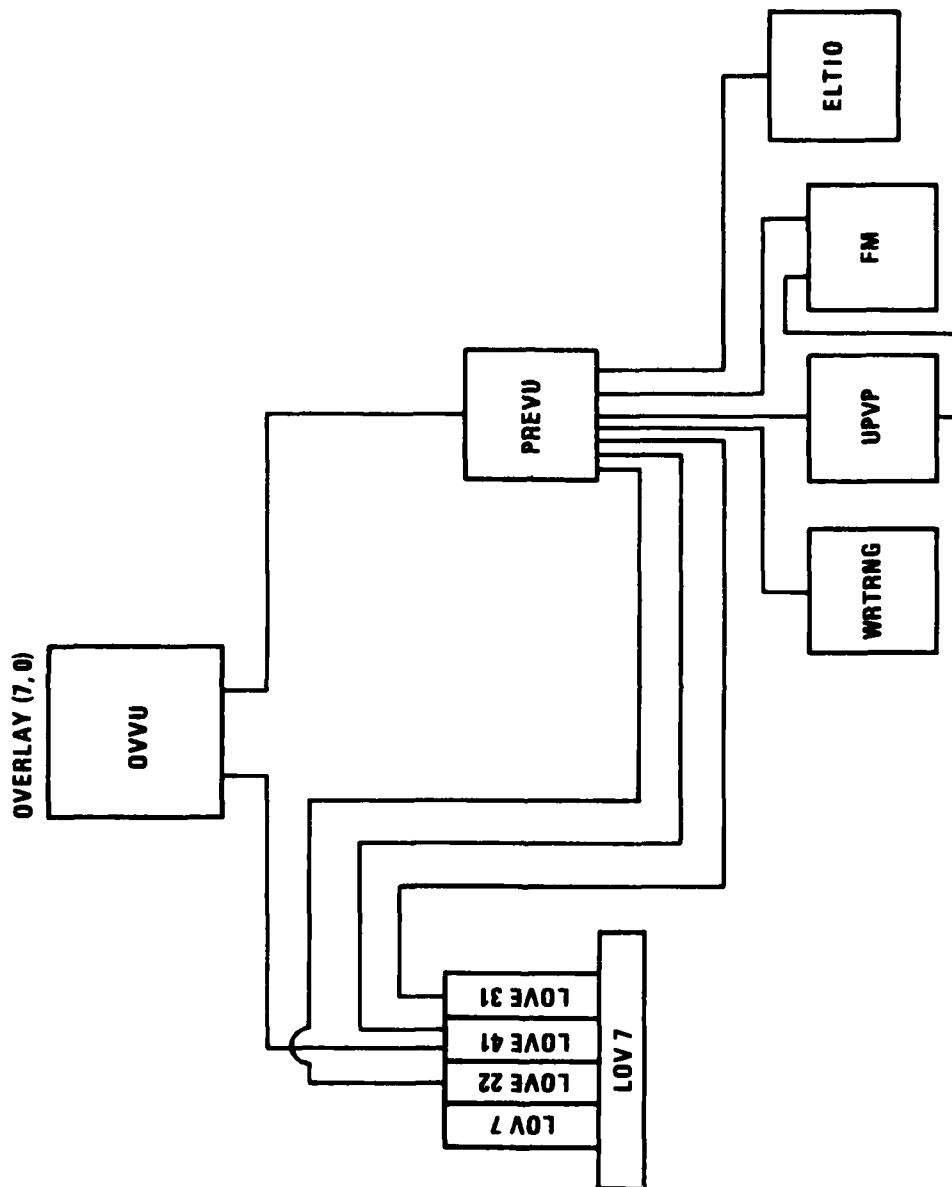


Figure 9.9 Element Stiffness Pre-processor

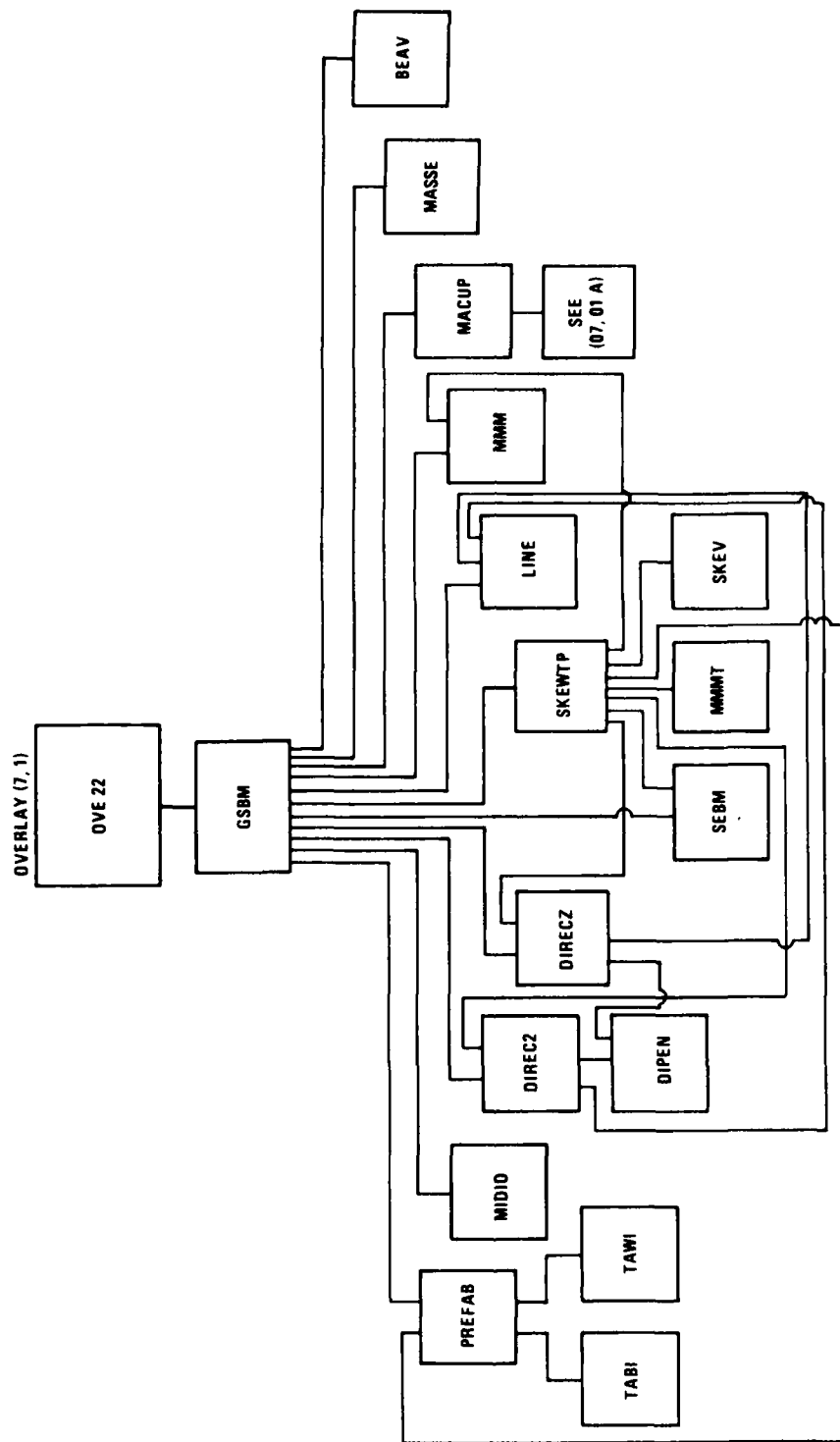


Figure 9.10 Beam Element Overlay

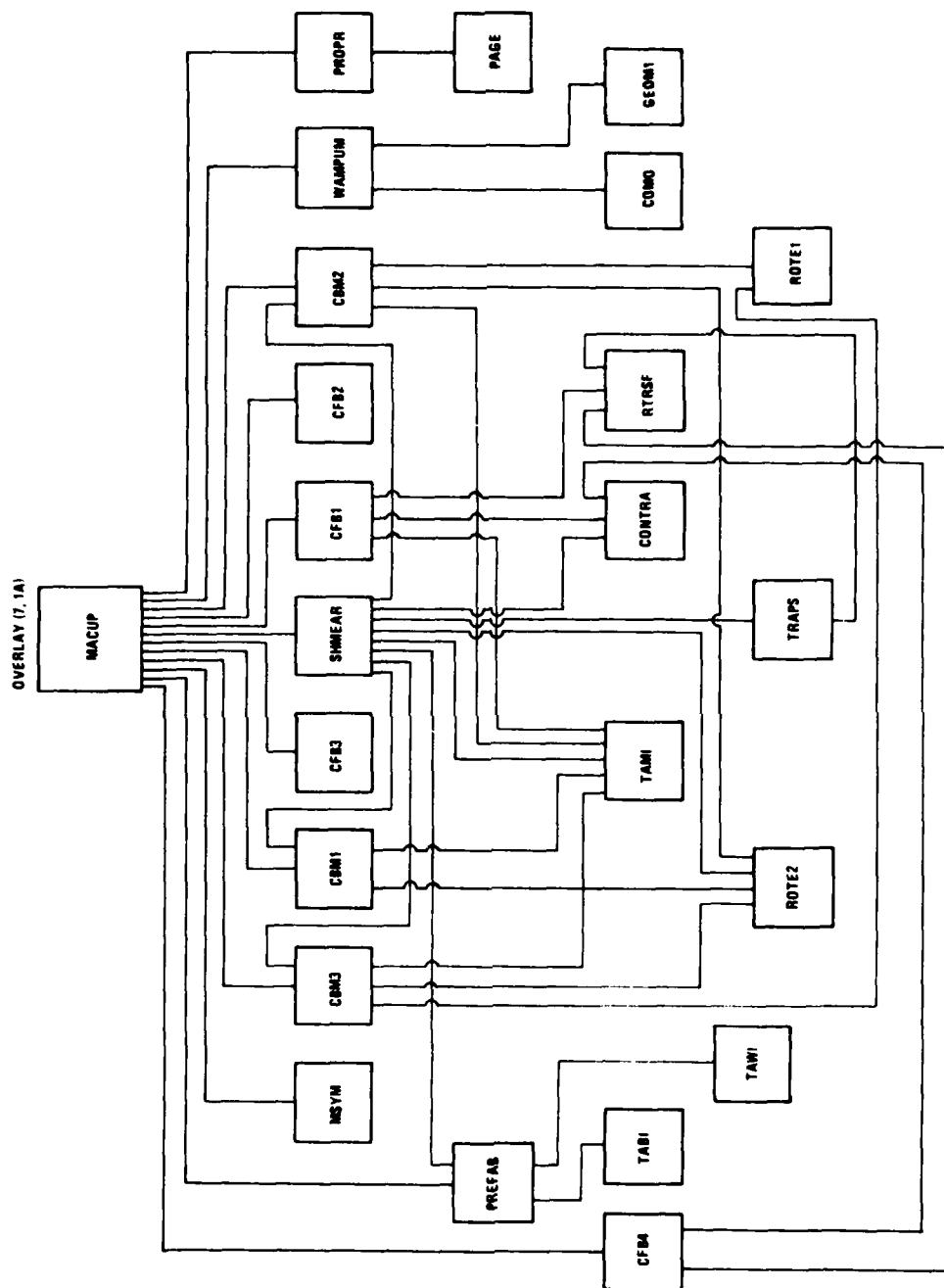


Figure 9.11 Formulation And Update Of Constitutive Matrices

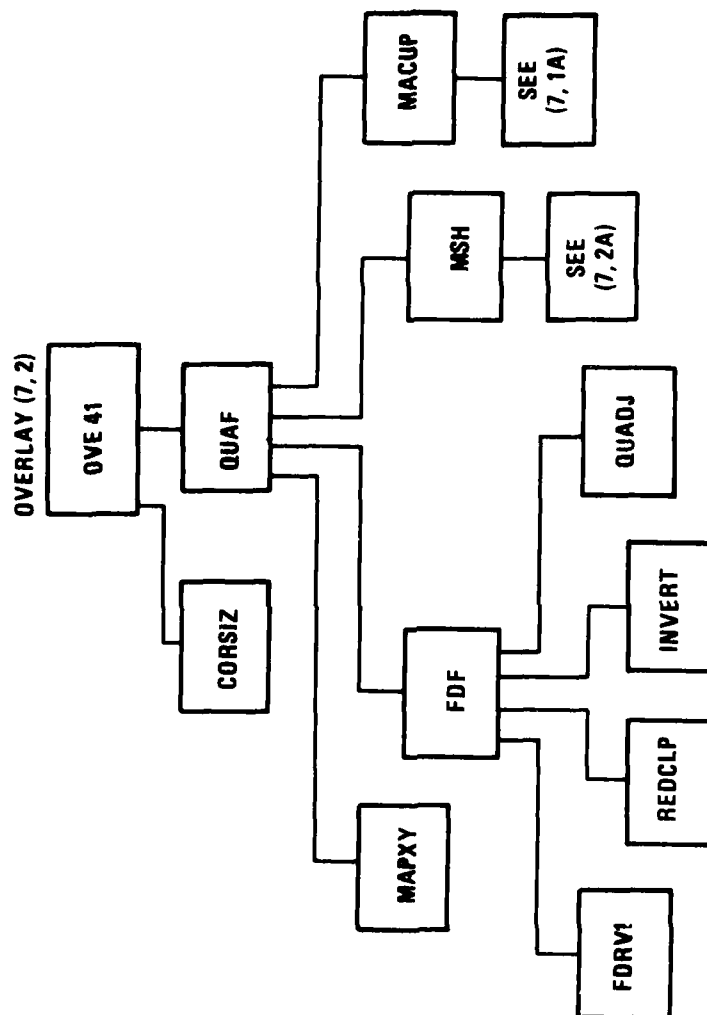


Figure 9.12 Quadrilateral Plate Element Generation

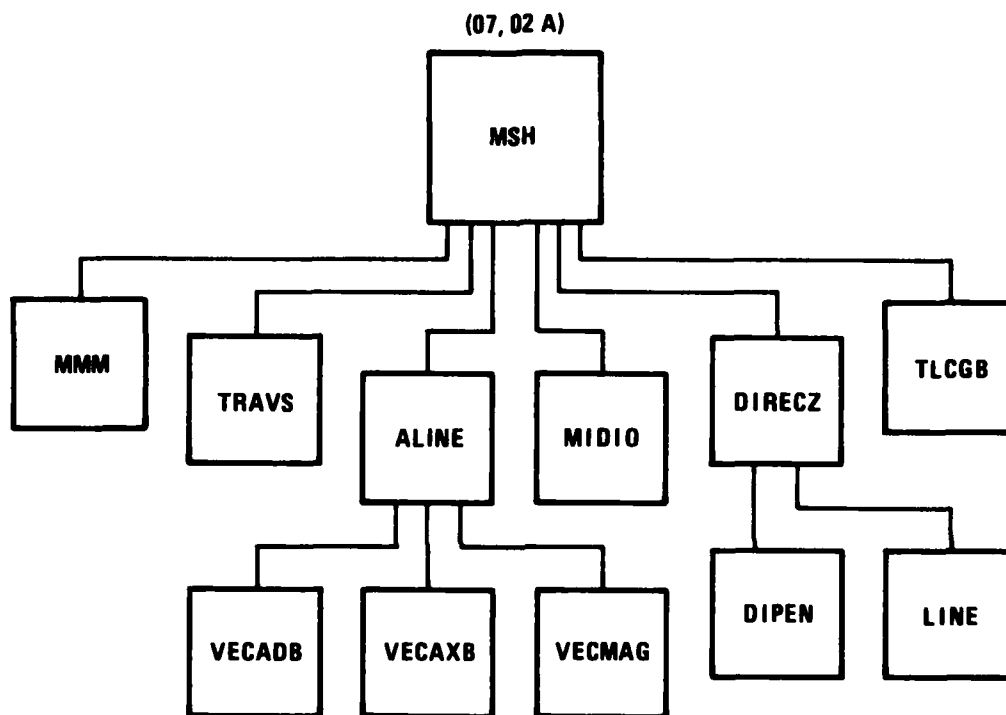


Figure 9.13 Nodal Coordinates and Integration Points

5407-75

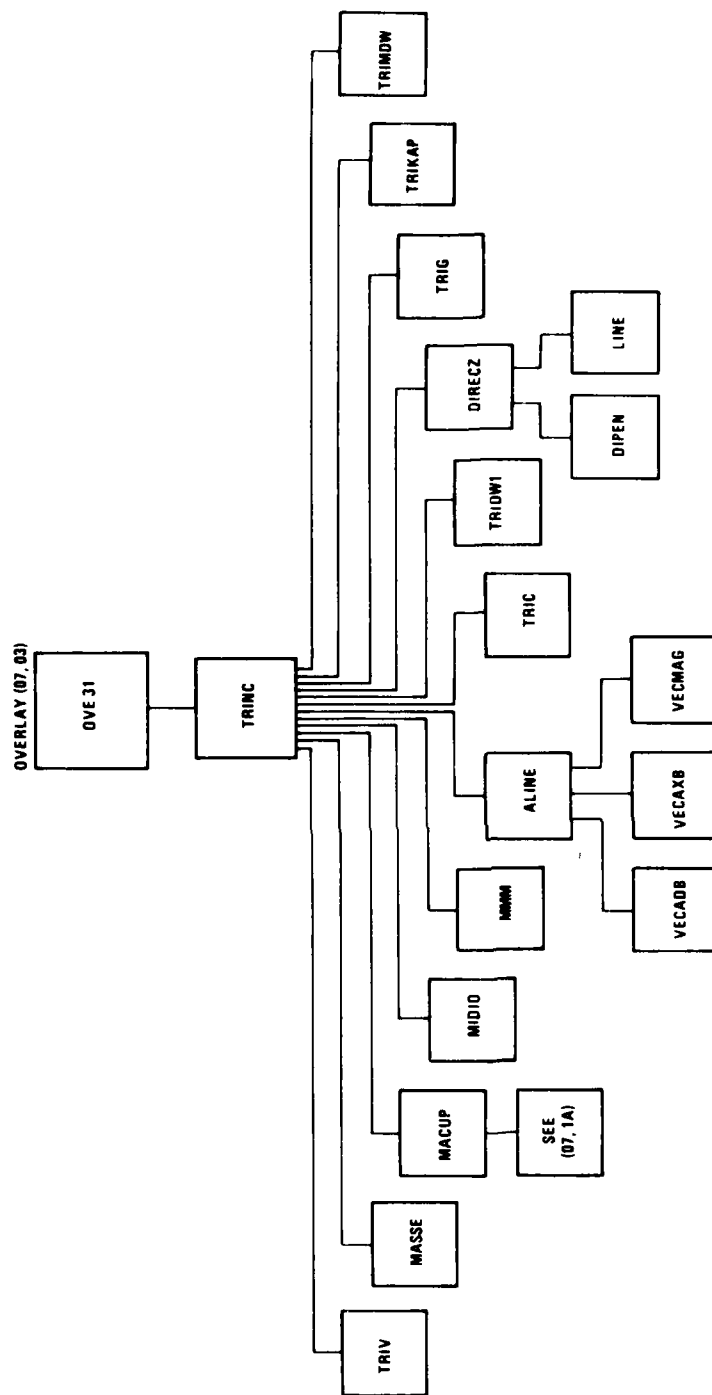


Figure 9.14 Triangular Plate Element Generation

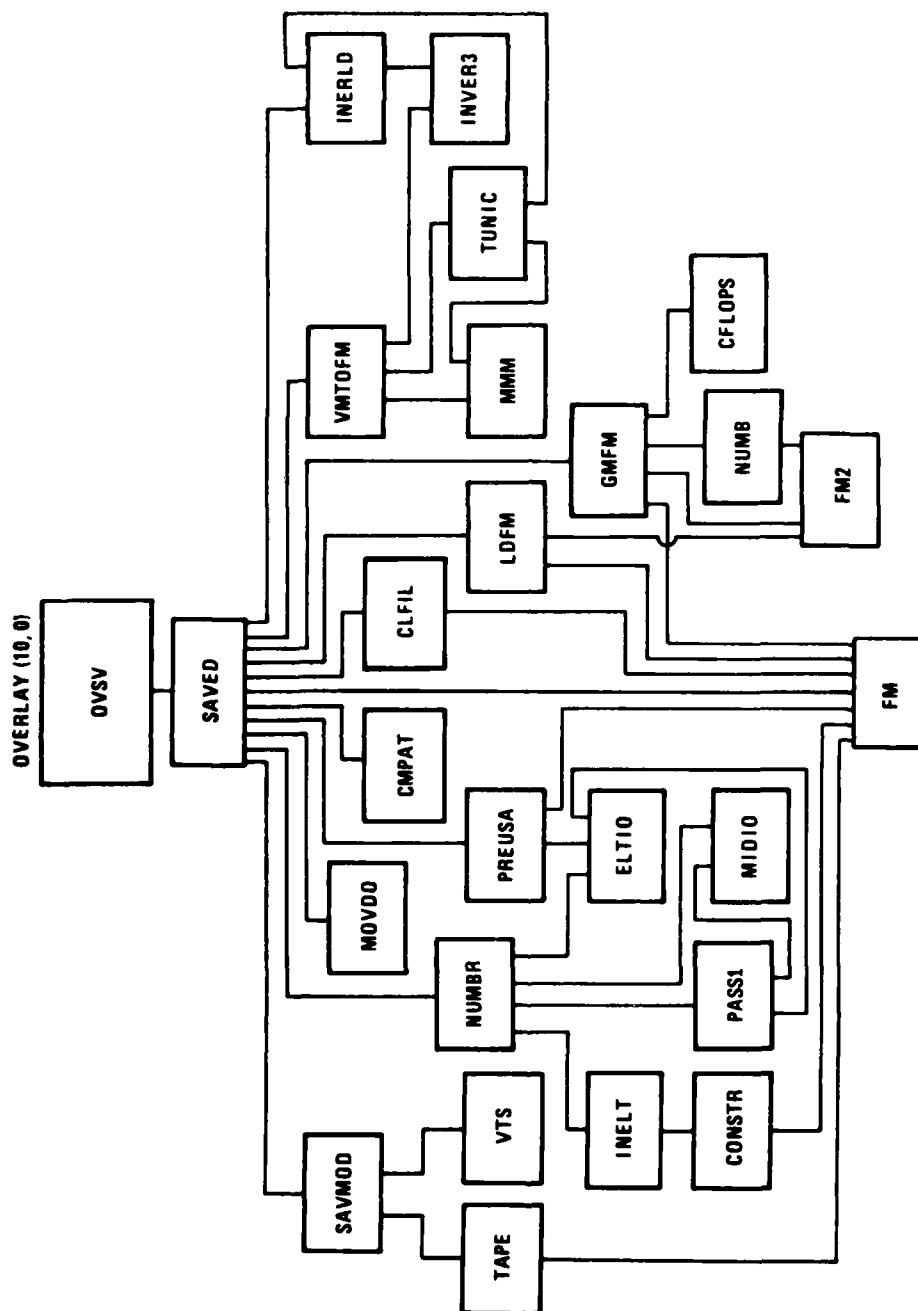


Figure 9.15 Data Base Preservation Overlay

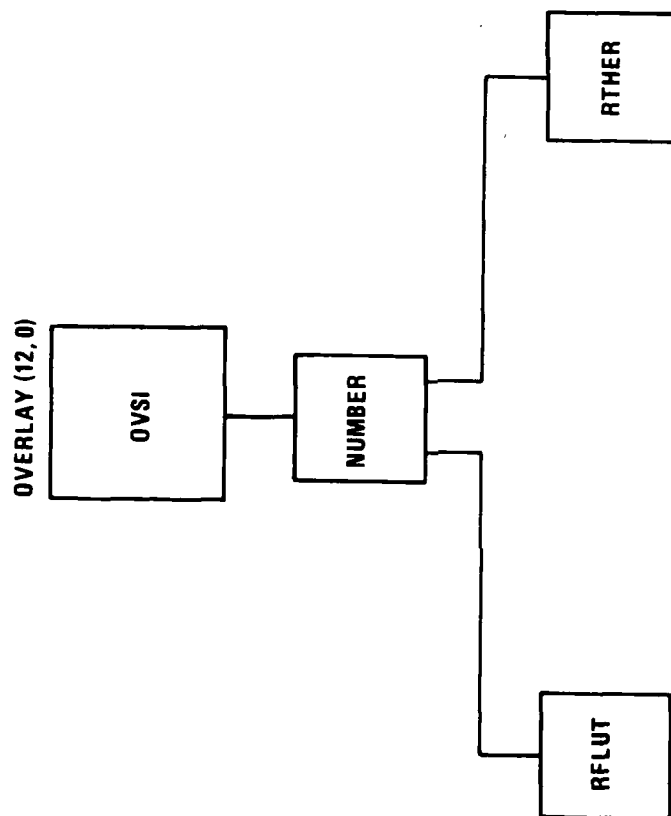


Figure 9.16 Shell Unit Intersection Overlay

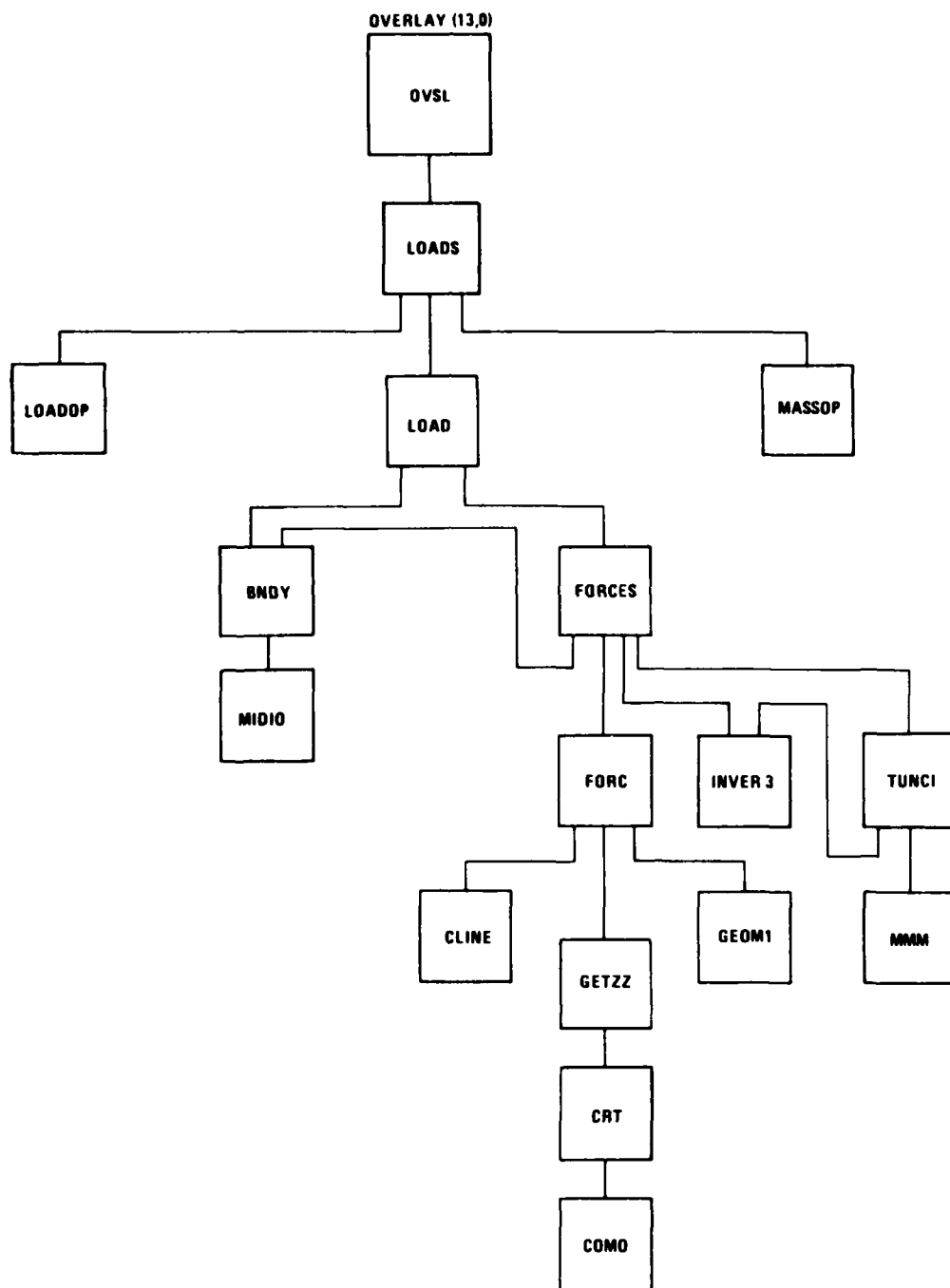


Figure 9.17 Shell Unit Loads Overlay

5407-79

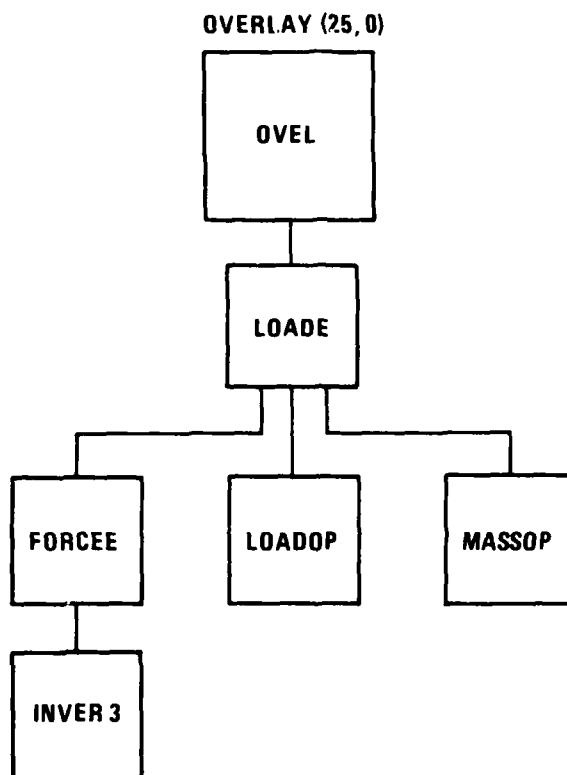


Figure 9.18 Element Unit Loads Overlay

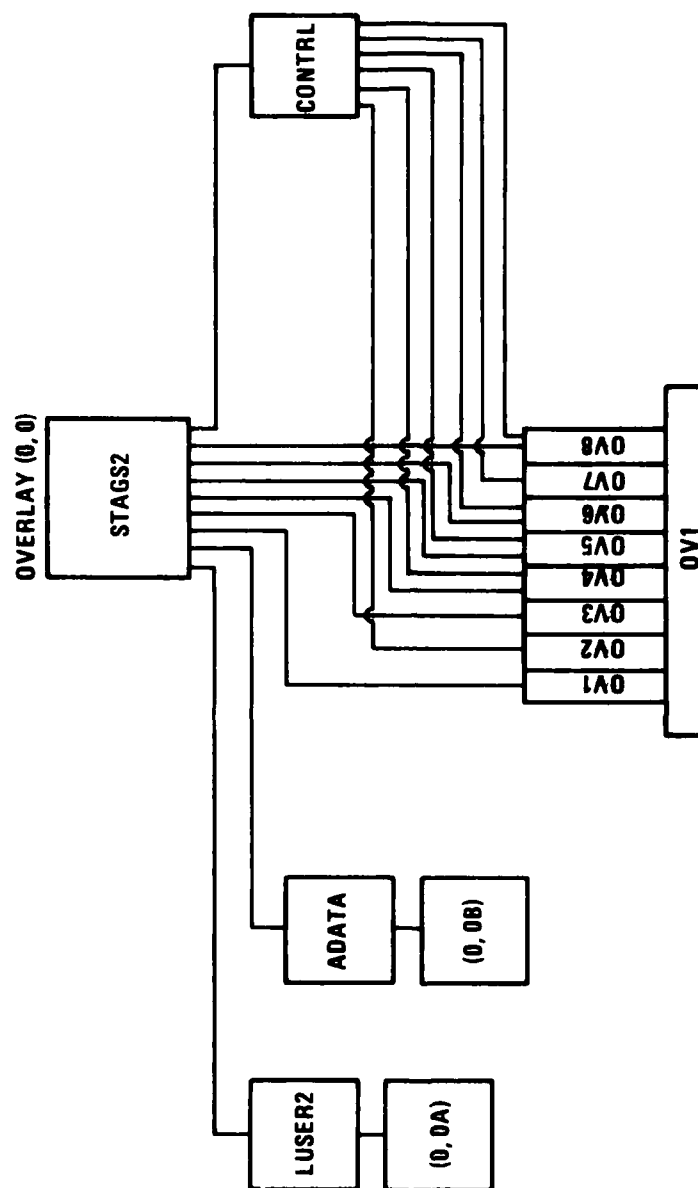


Figure 9.19 Main Execution Program

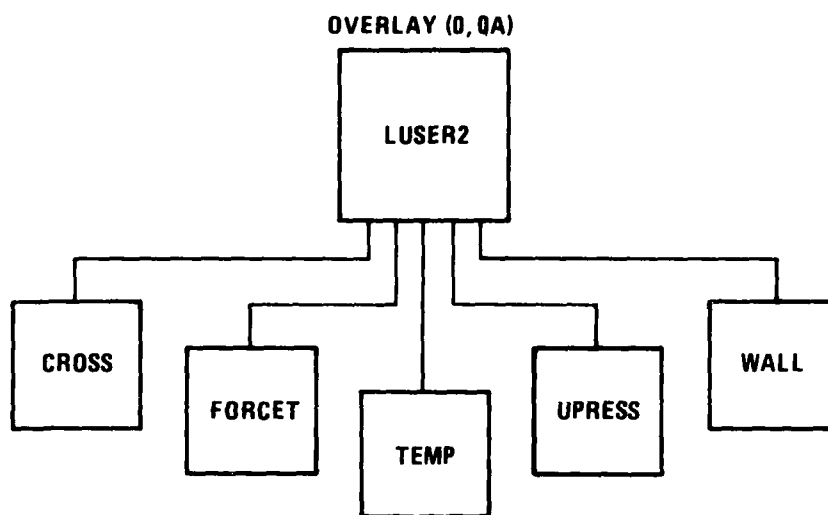


Figure 9.20 User Subroutine Loader

5407-43

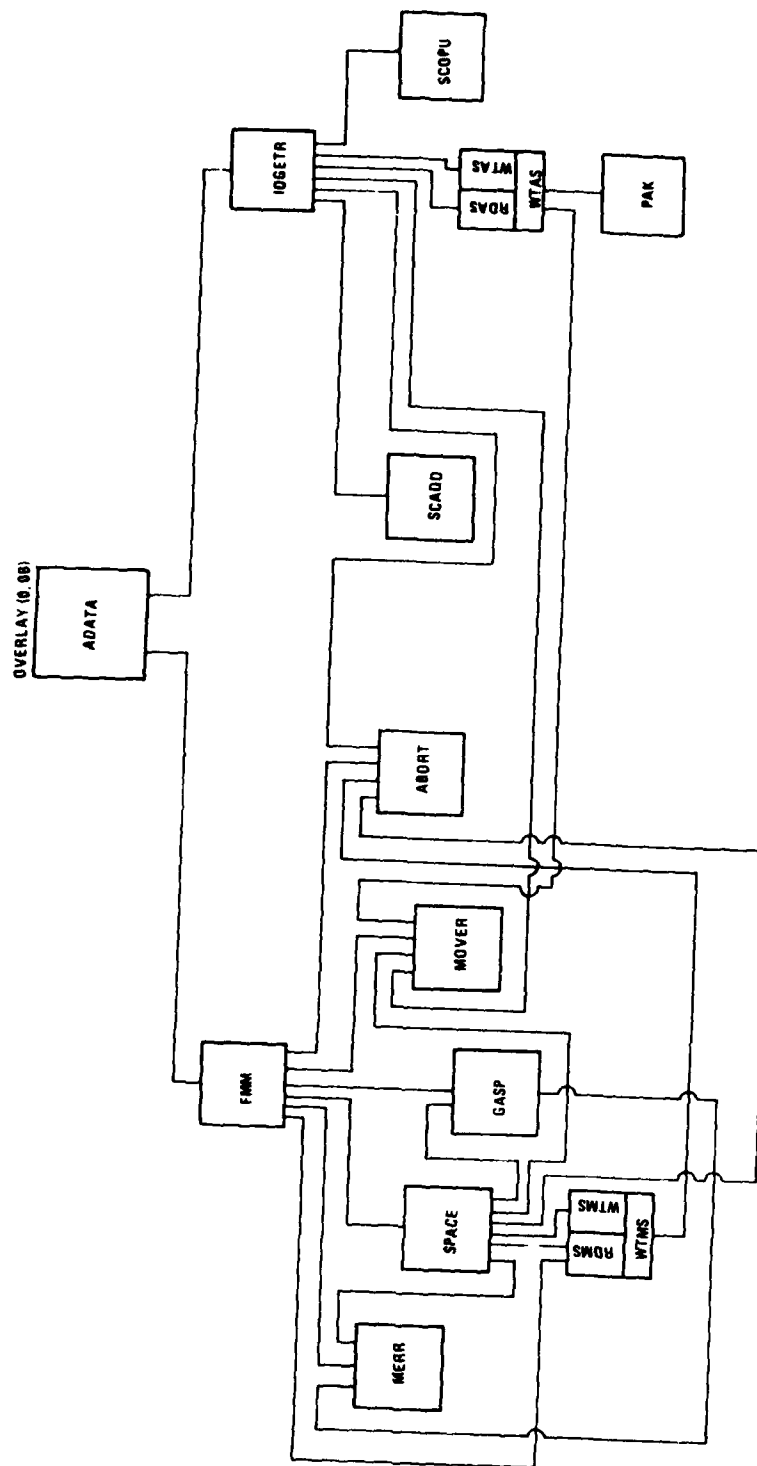


Figure 9.21 STAGS2 Data Statements

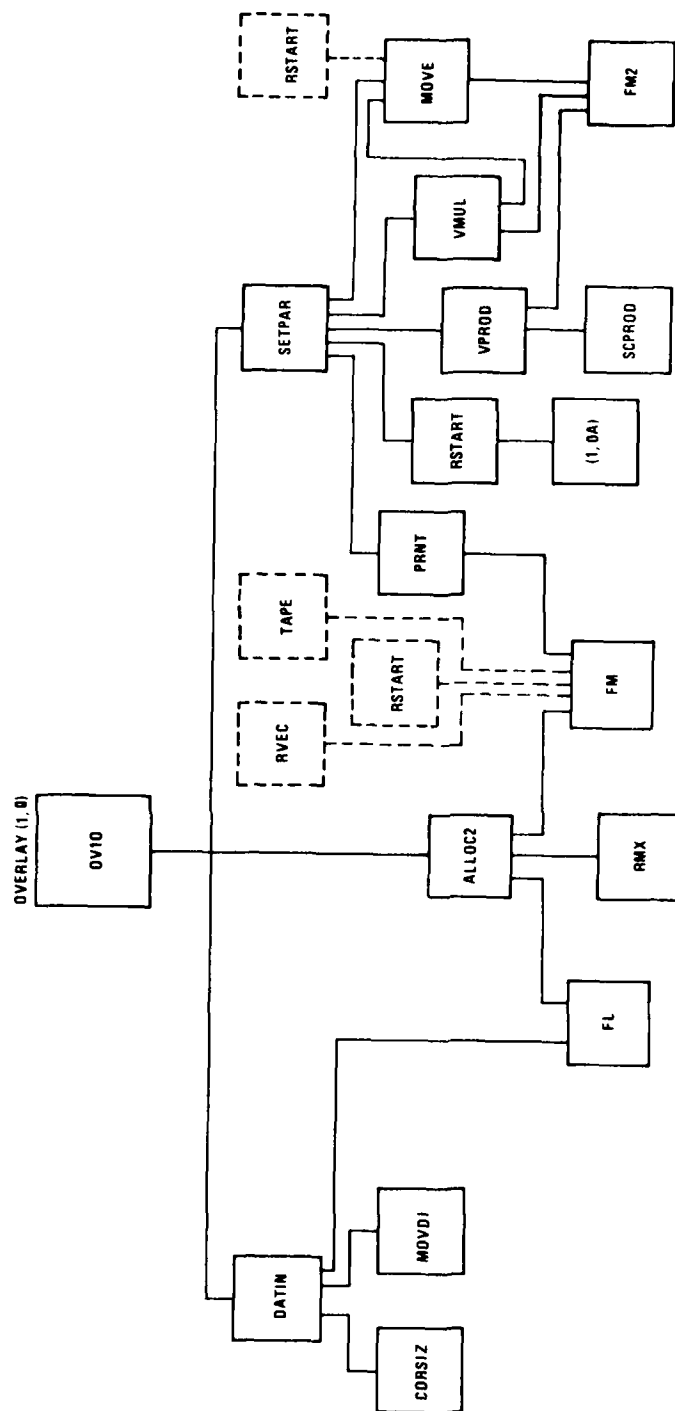


Figure 9.22 Data Transfer from STAGSI

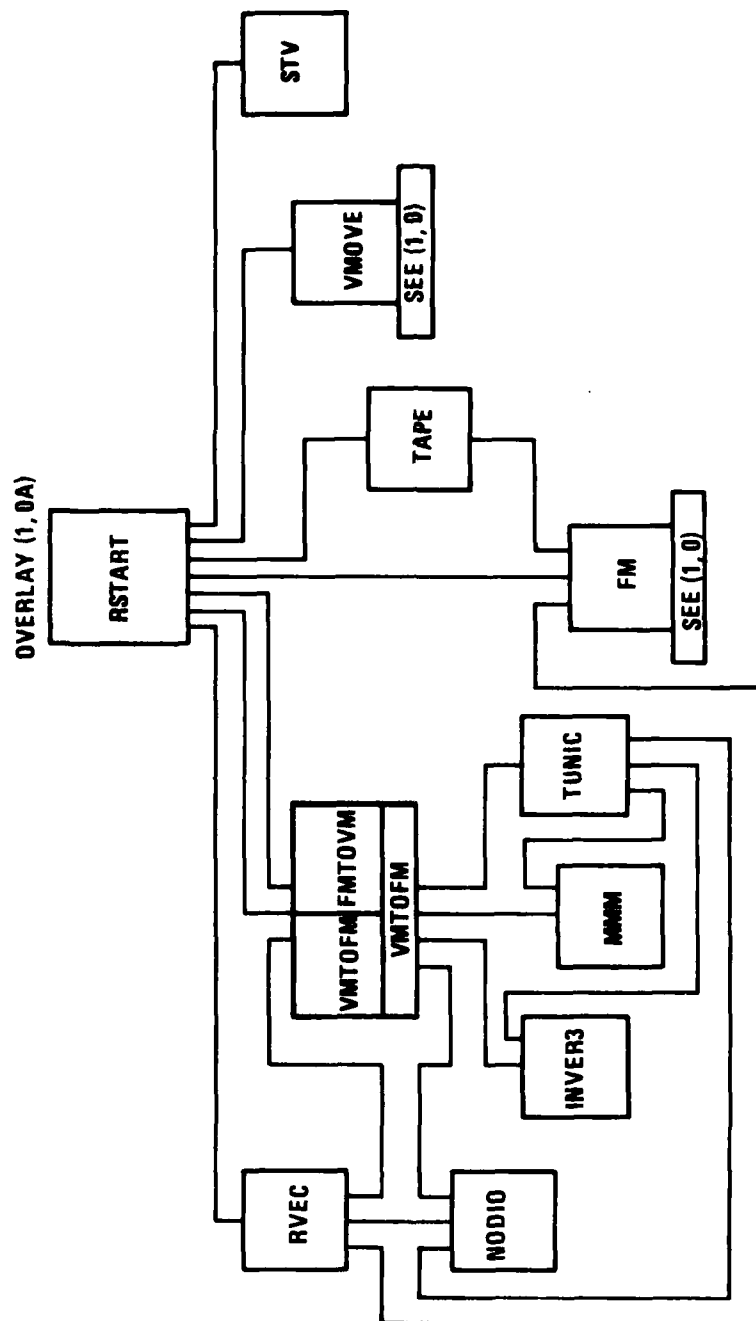


Figure 9.23 Analysis Restart Control

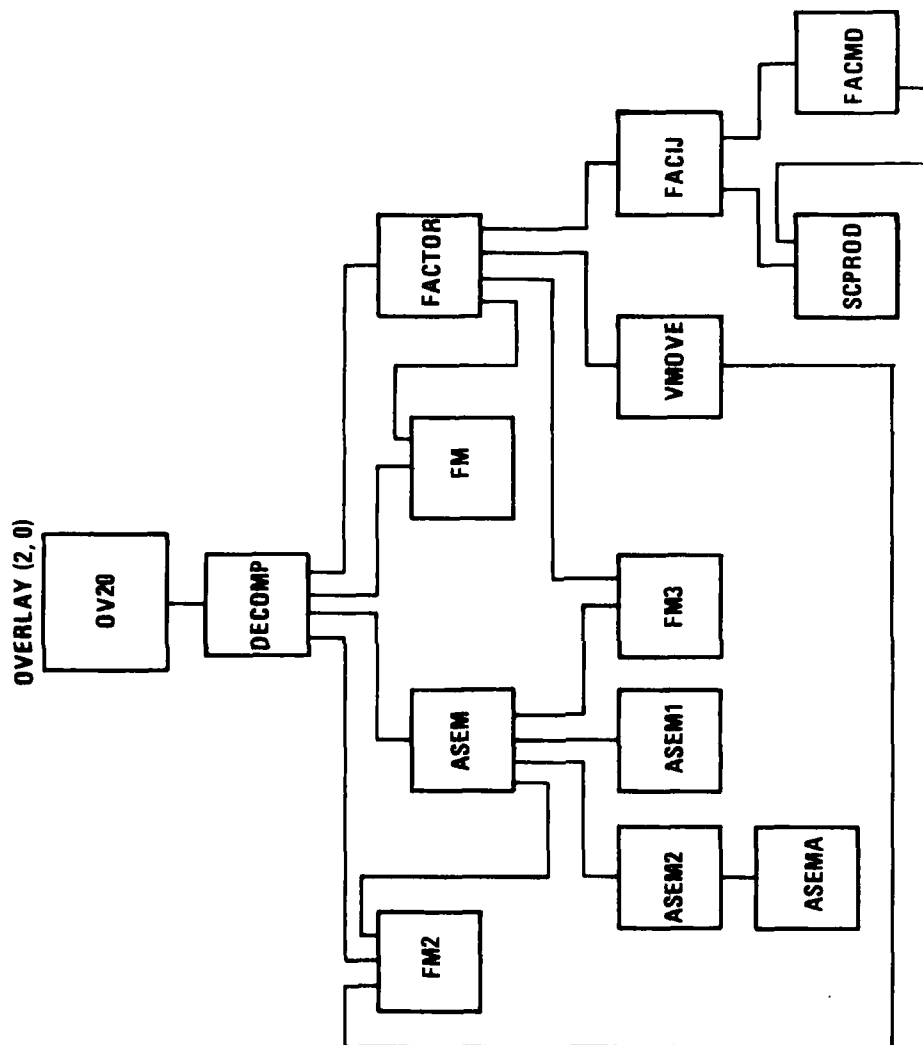


Figure 9.24 Stiffness Matrix Decomposition

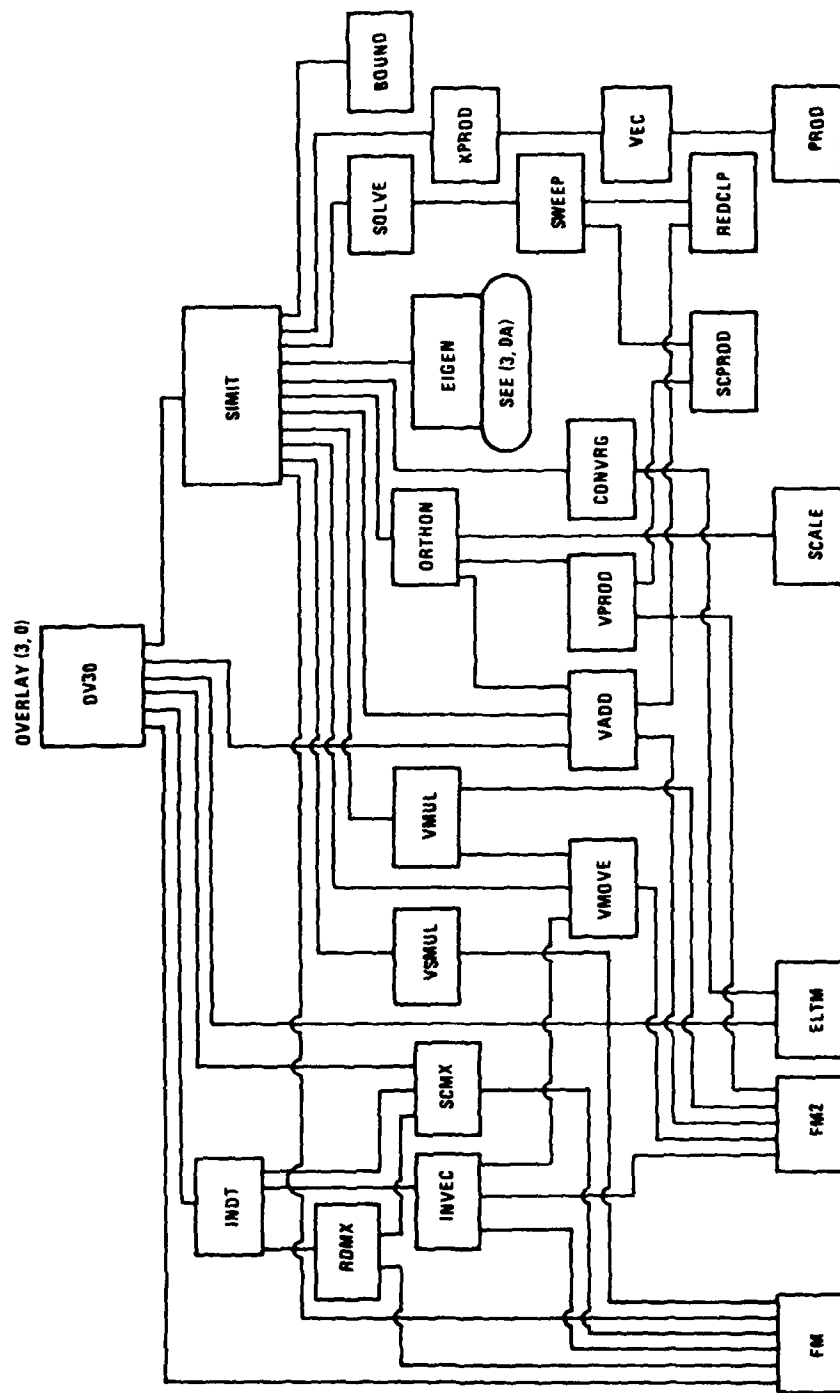


Figure 9.25 Eigenvalue Solver

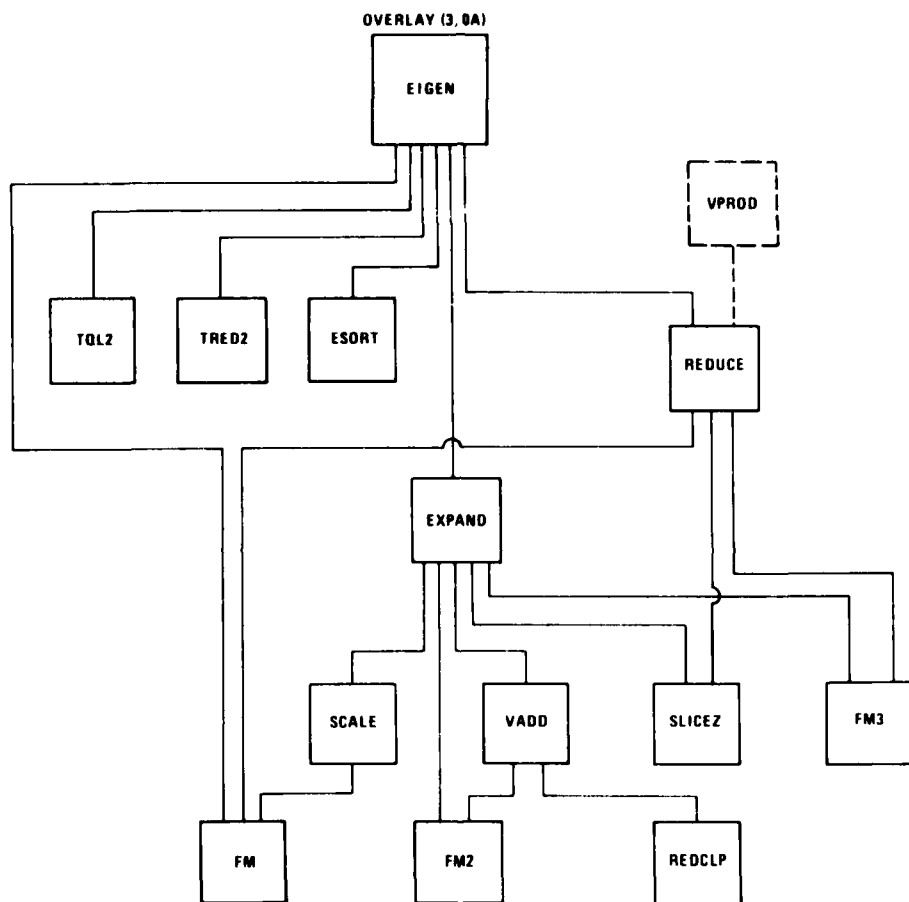


Figure 9.26 Eigensolution for Subspace

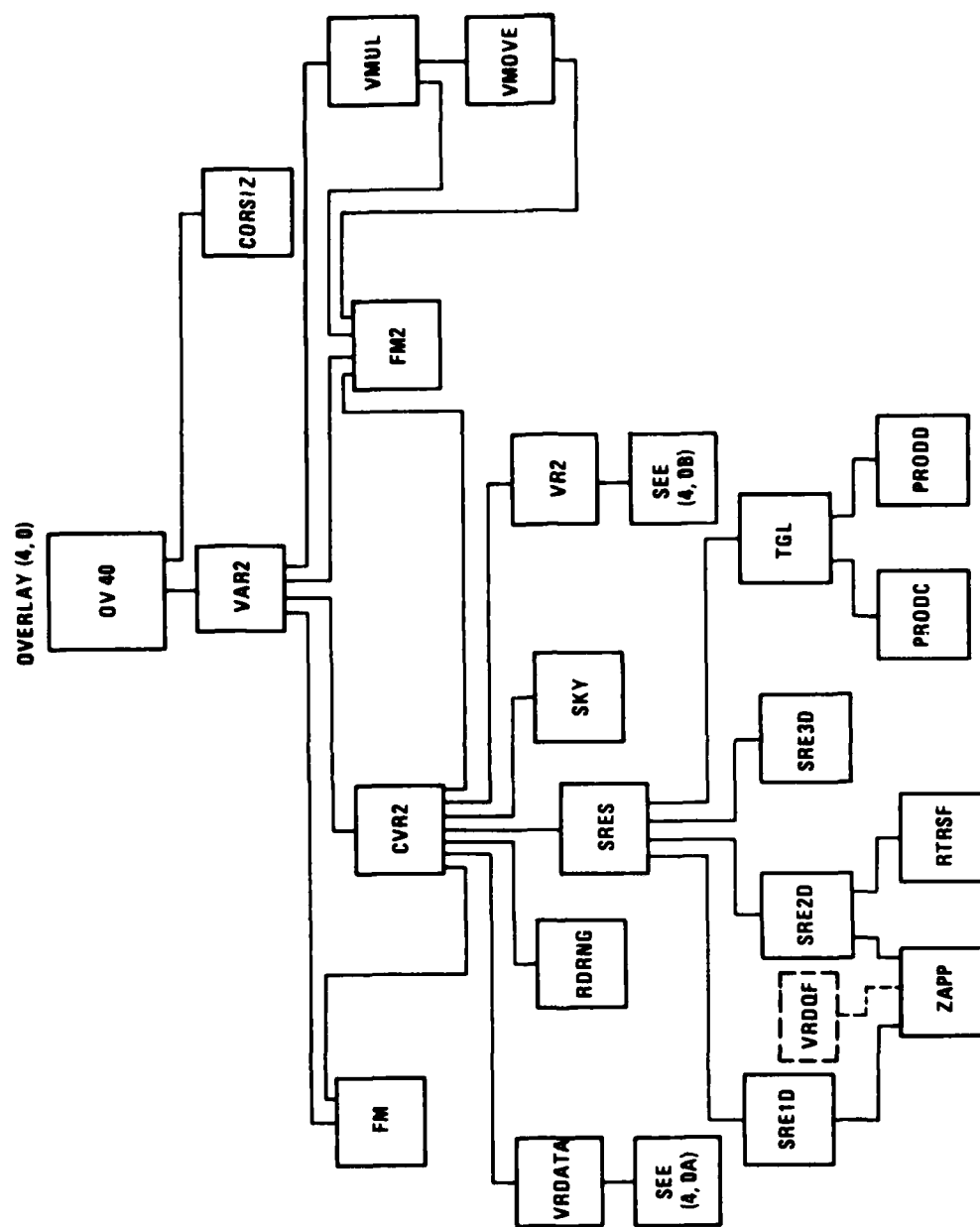


Figure 9.27 Stiffness Matrix Formulation

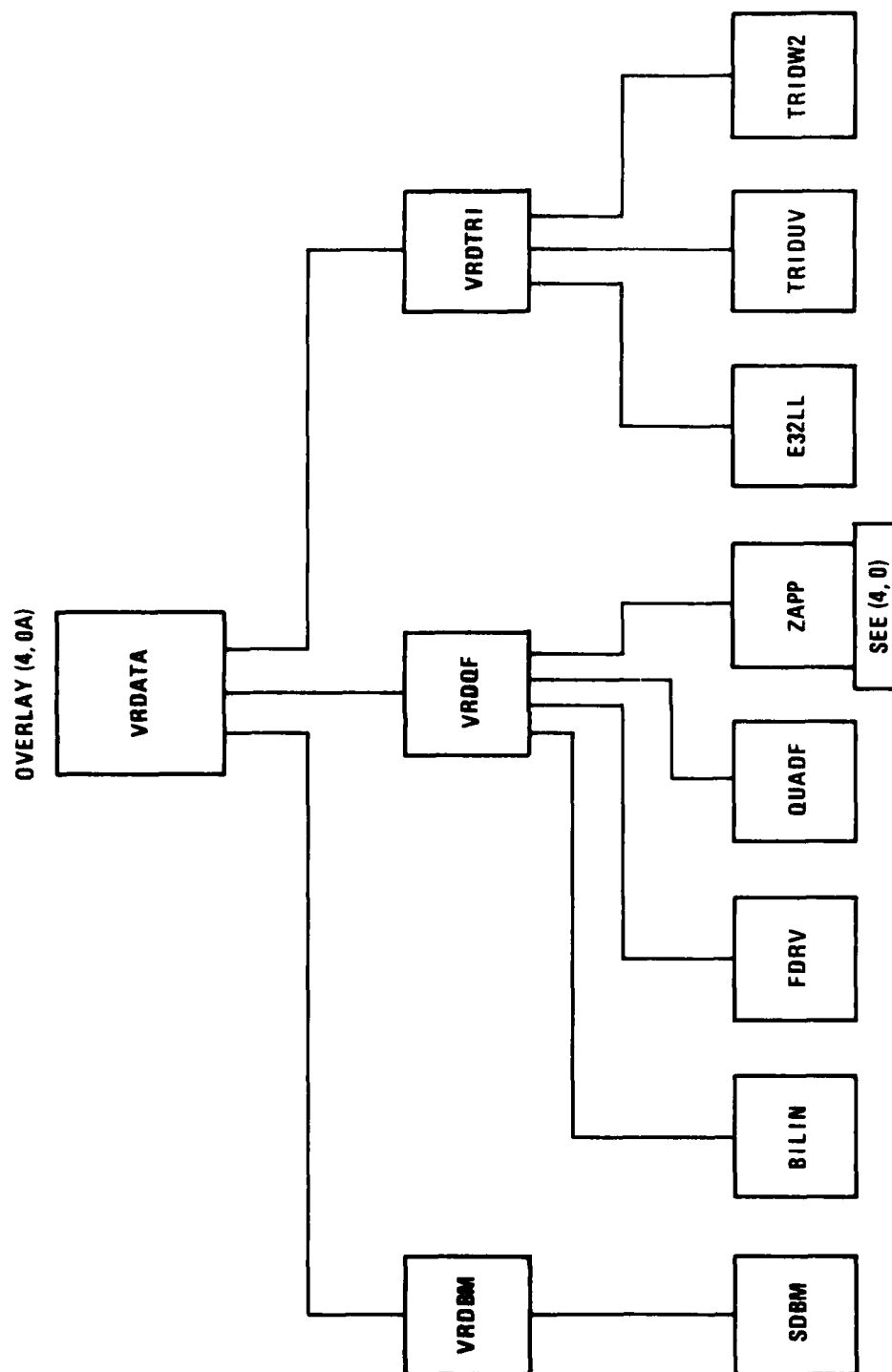


Figure 9.28 Element Stiffness Data

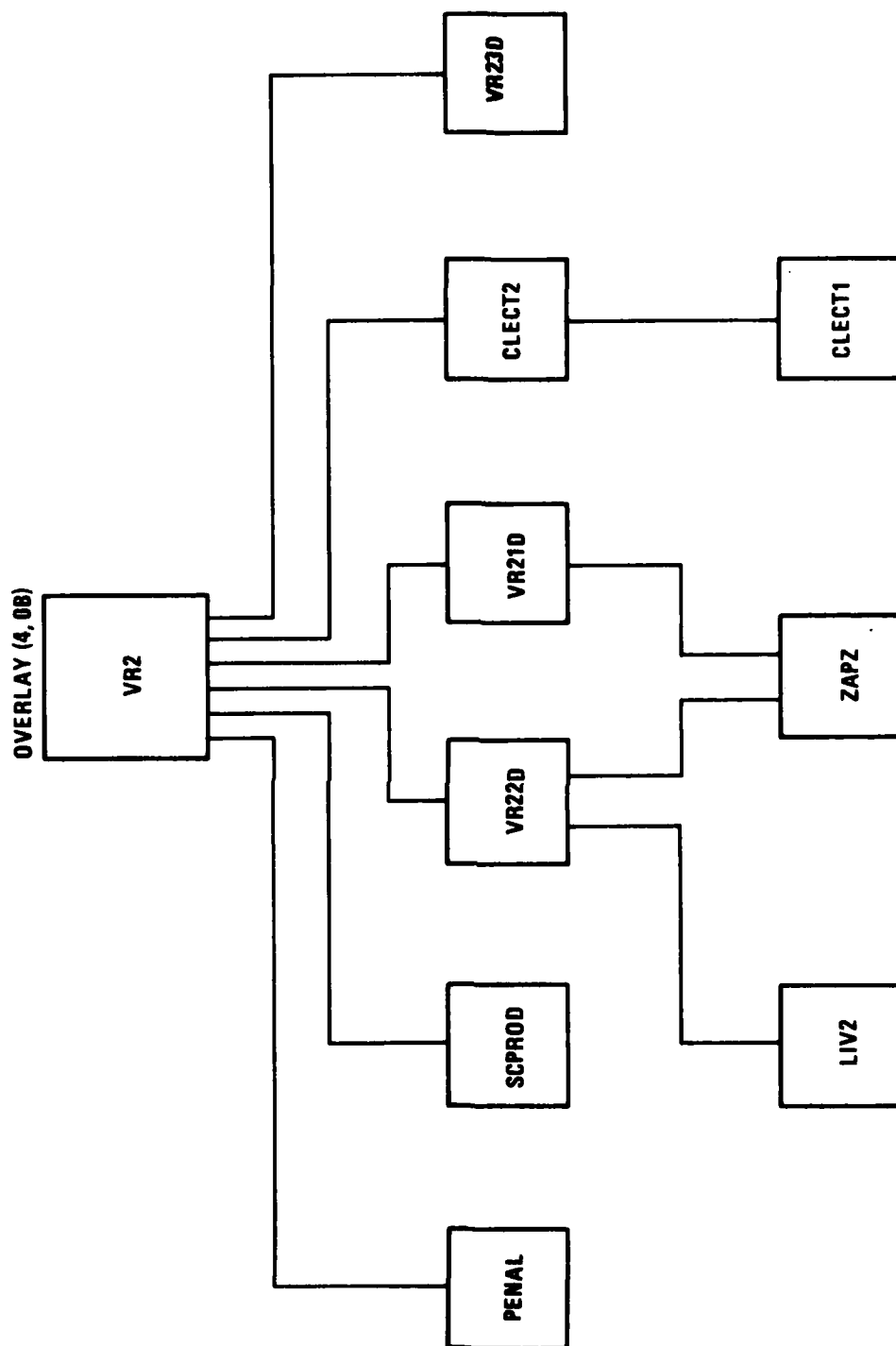


Figure 9.29 Element Stiffness Computation

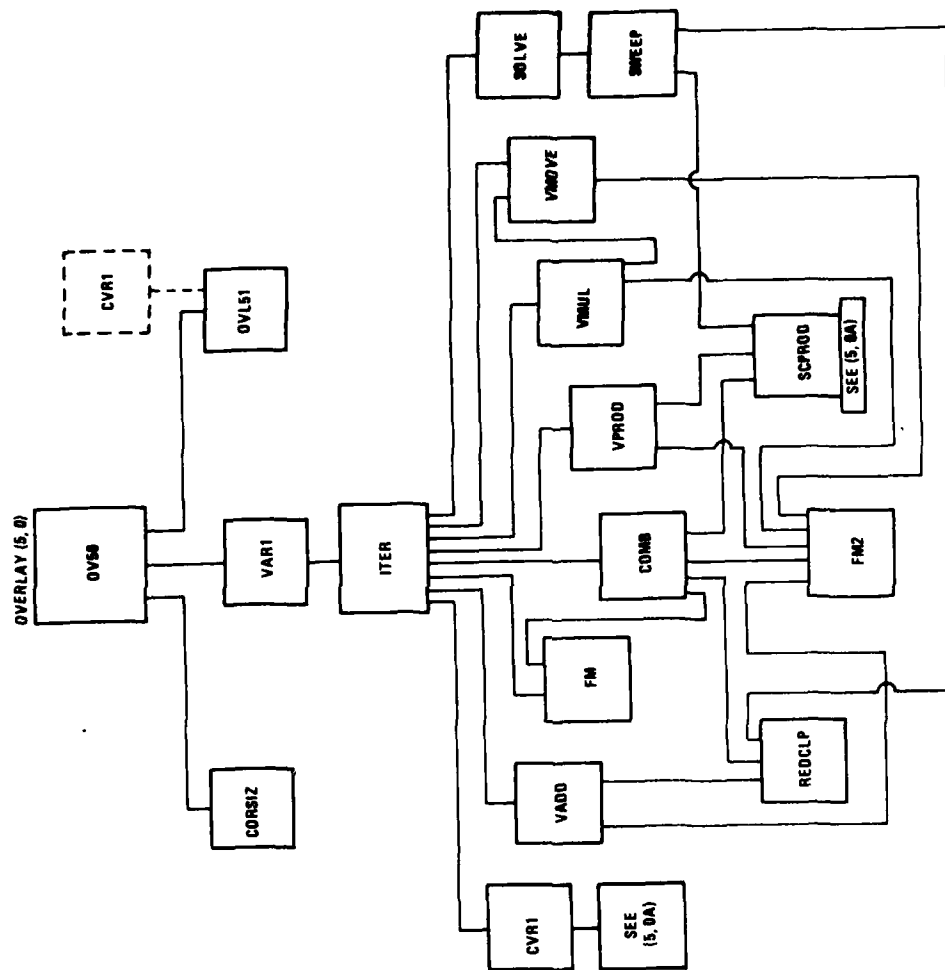


Figure 9.30 Overlay For 1st Variation of Strain Energy

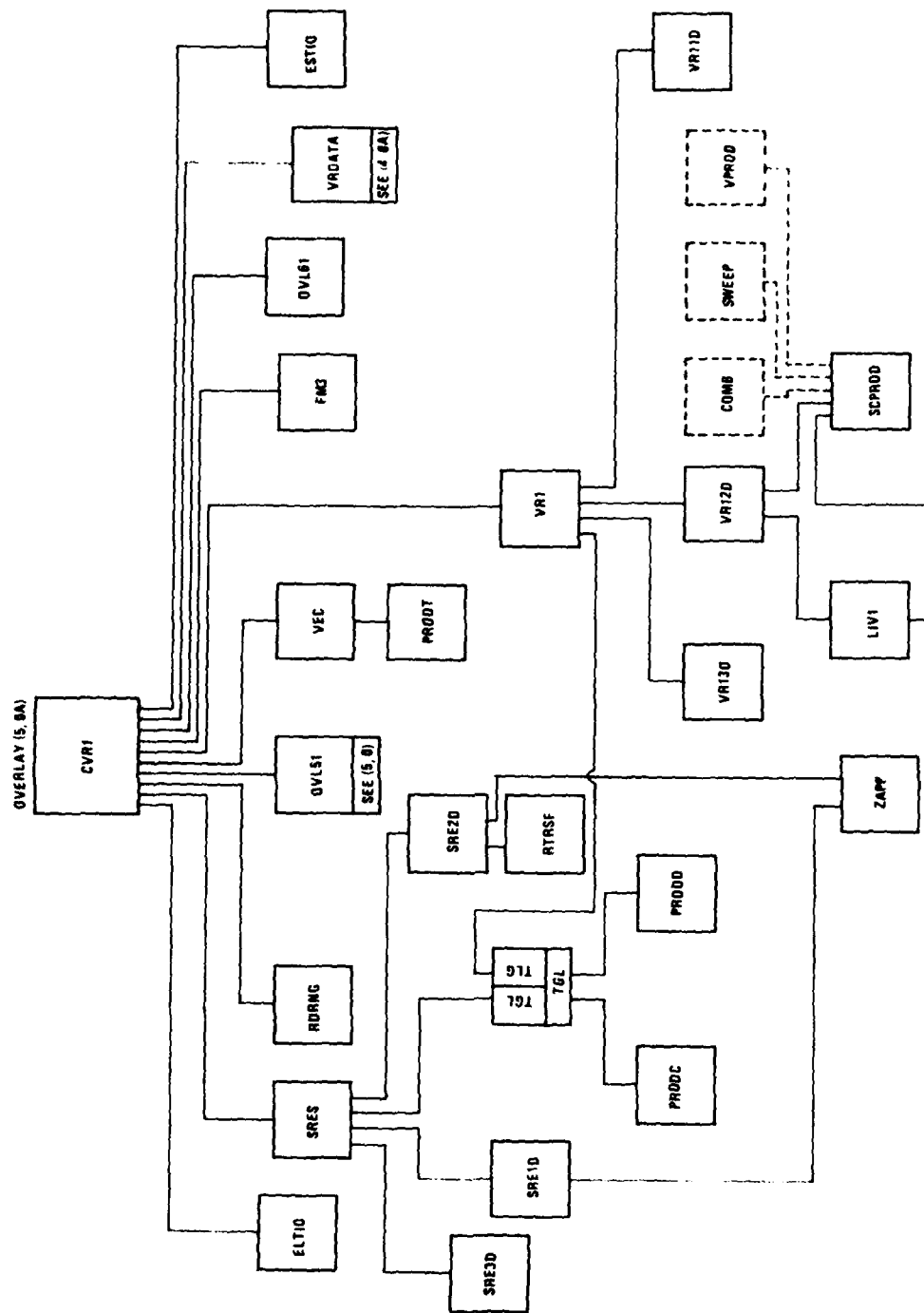


Figure 9.31 1st Variation of Strain Energy

OVERLAY (5, 1)

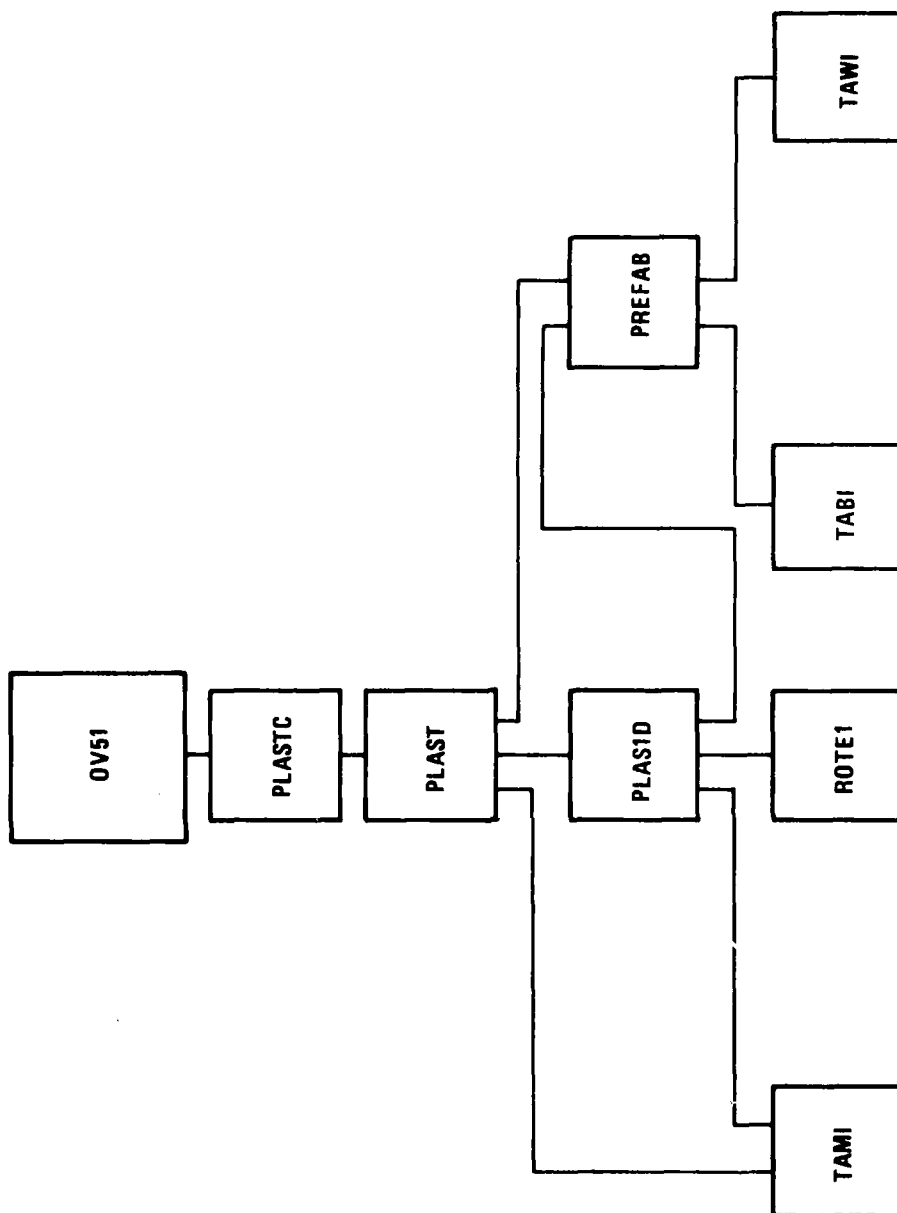


Figure 9.32 Plasticity Overlay

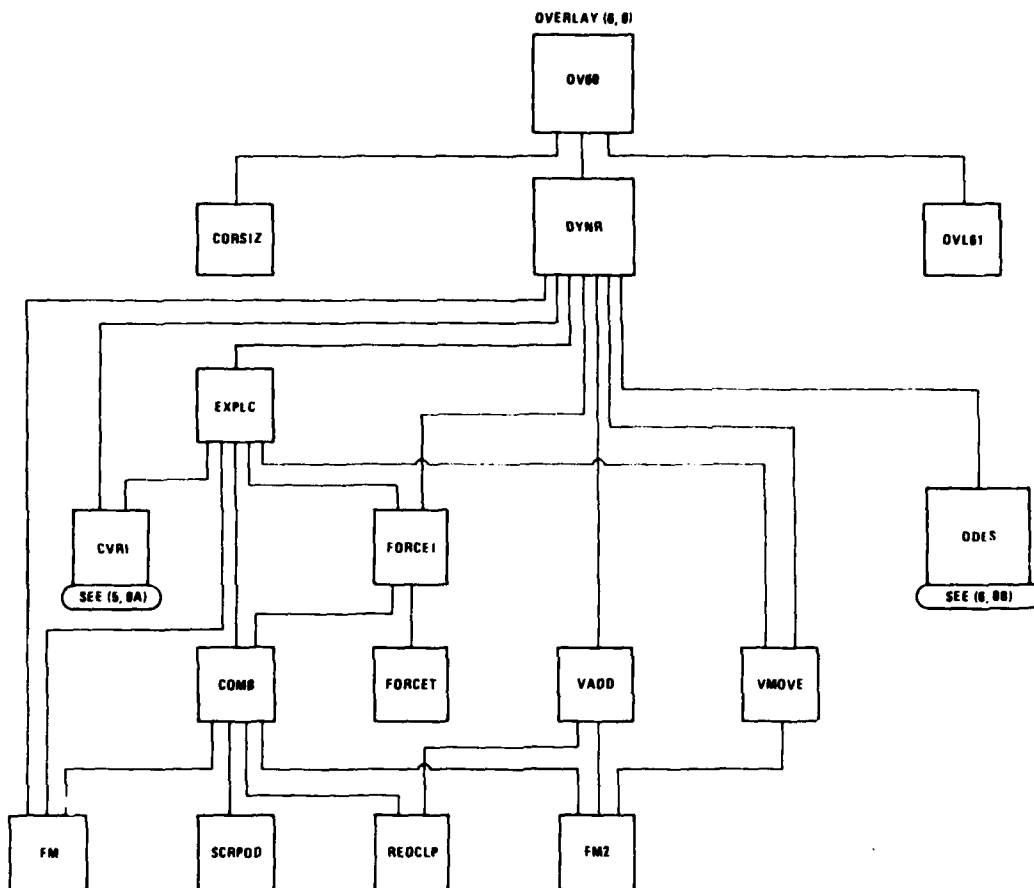


Figure 9.33 Dynamic Response Overlay

5407-56

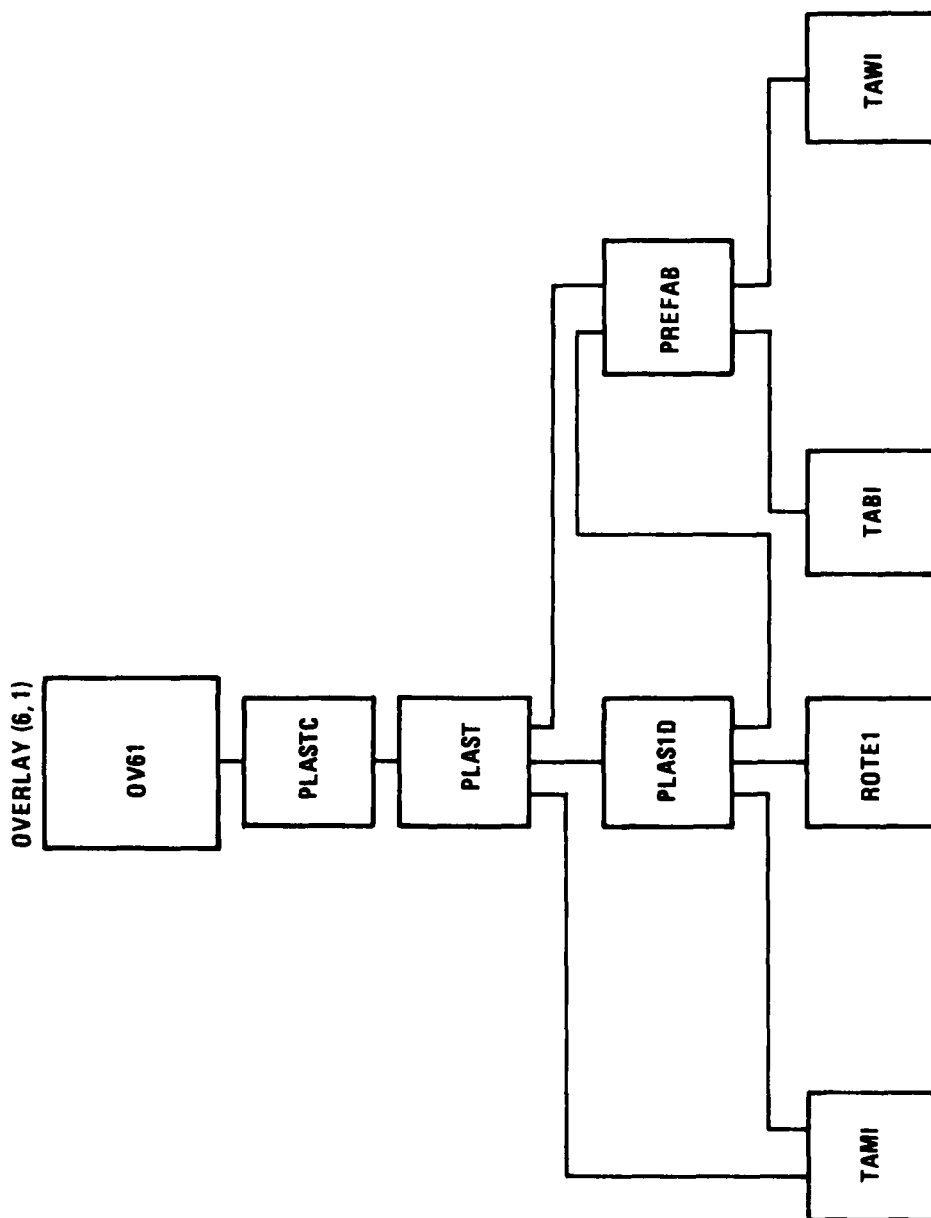


Figure 9.35 Plasticity Overlay (Dynamic)

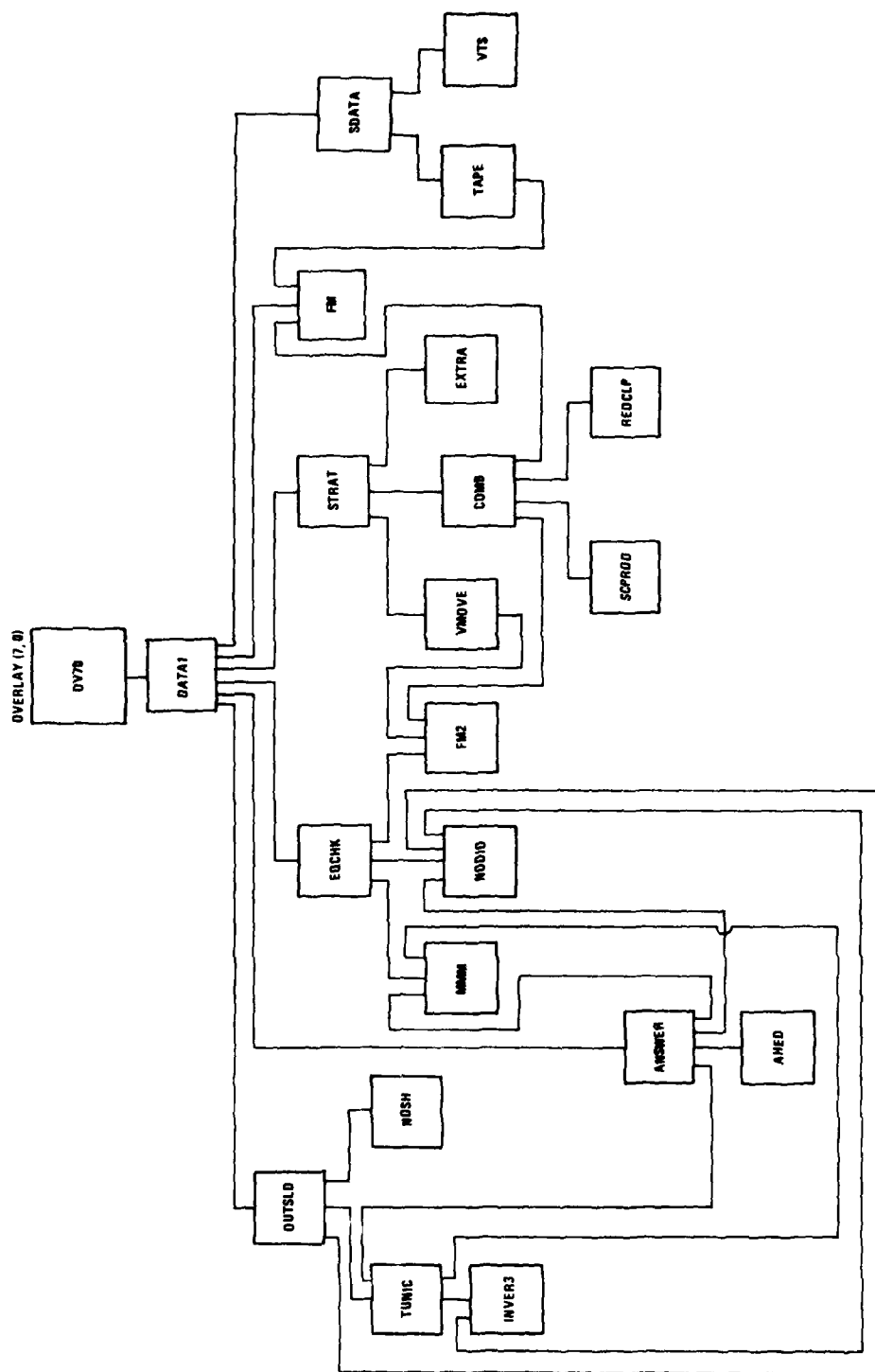


Figure 9.36 Overlay For Solution Strategy And Output Control

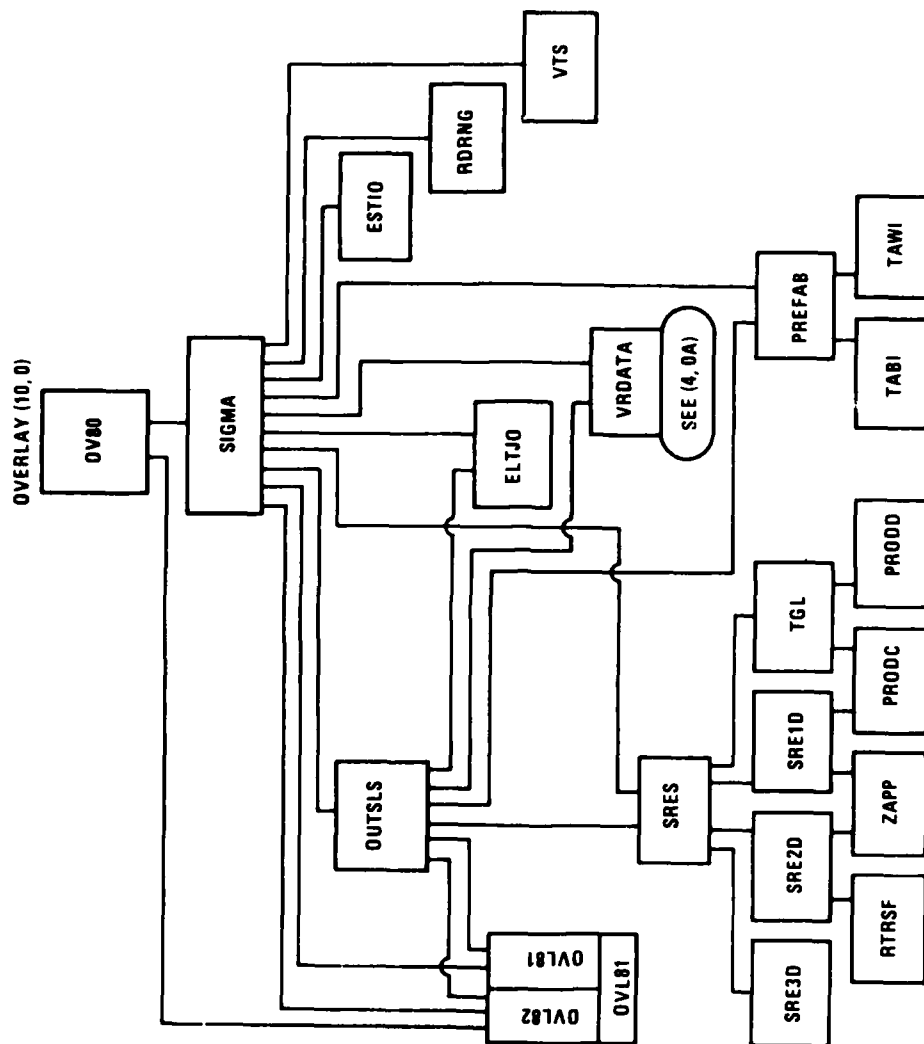


Figure 9.37 Overlay For Stress Computation And Output

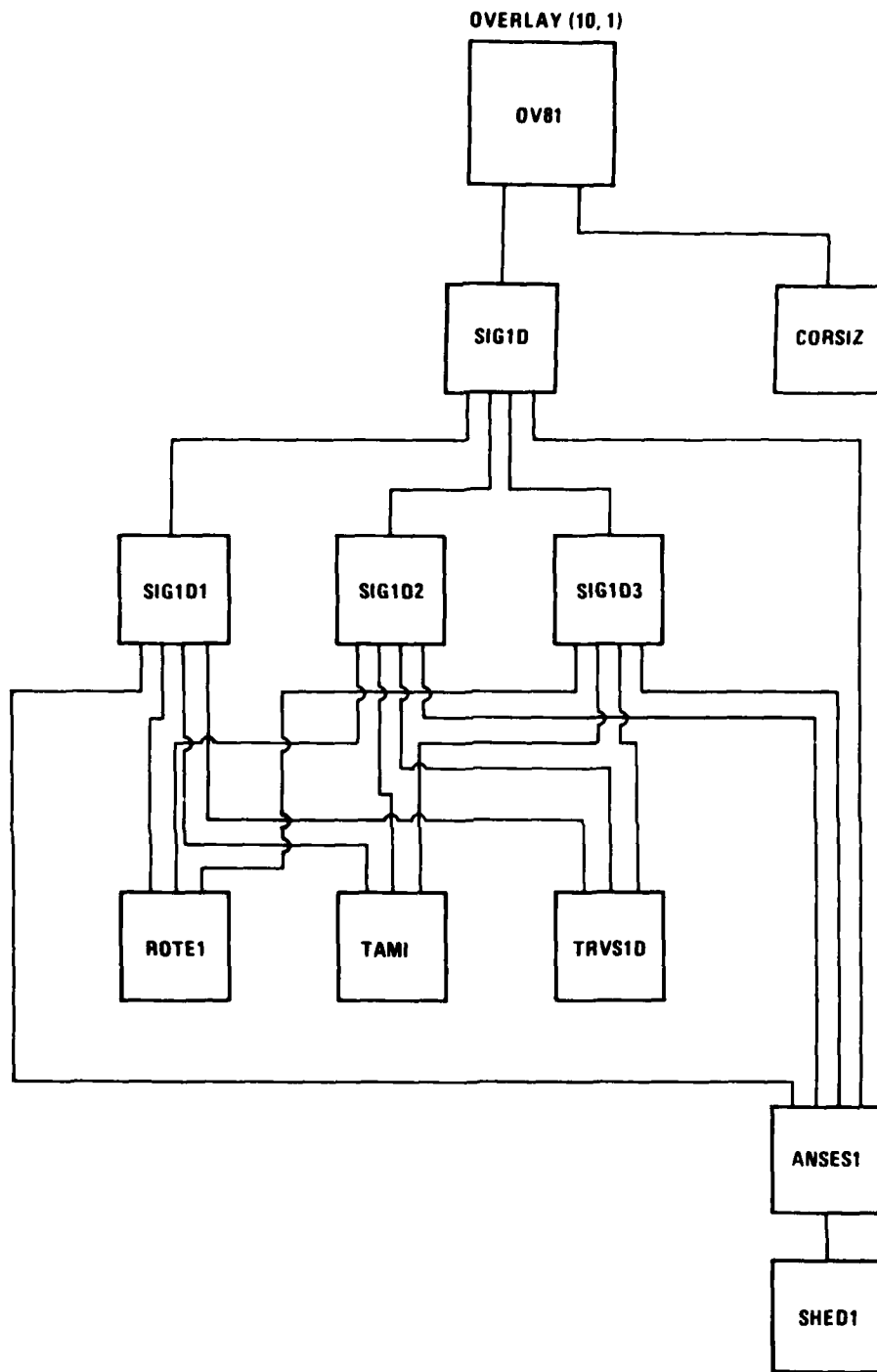


Figure 9.38 Overlay For Stress And Strain Computation - 1D Elements

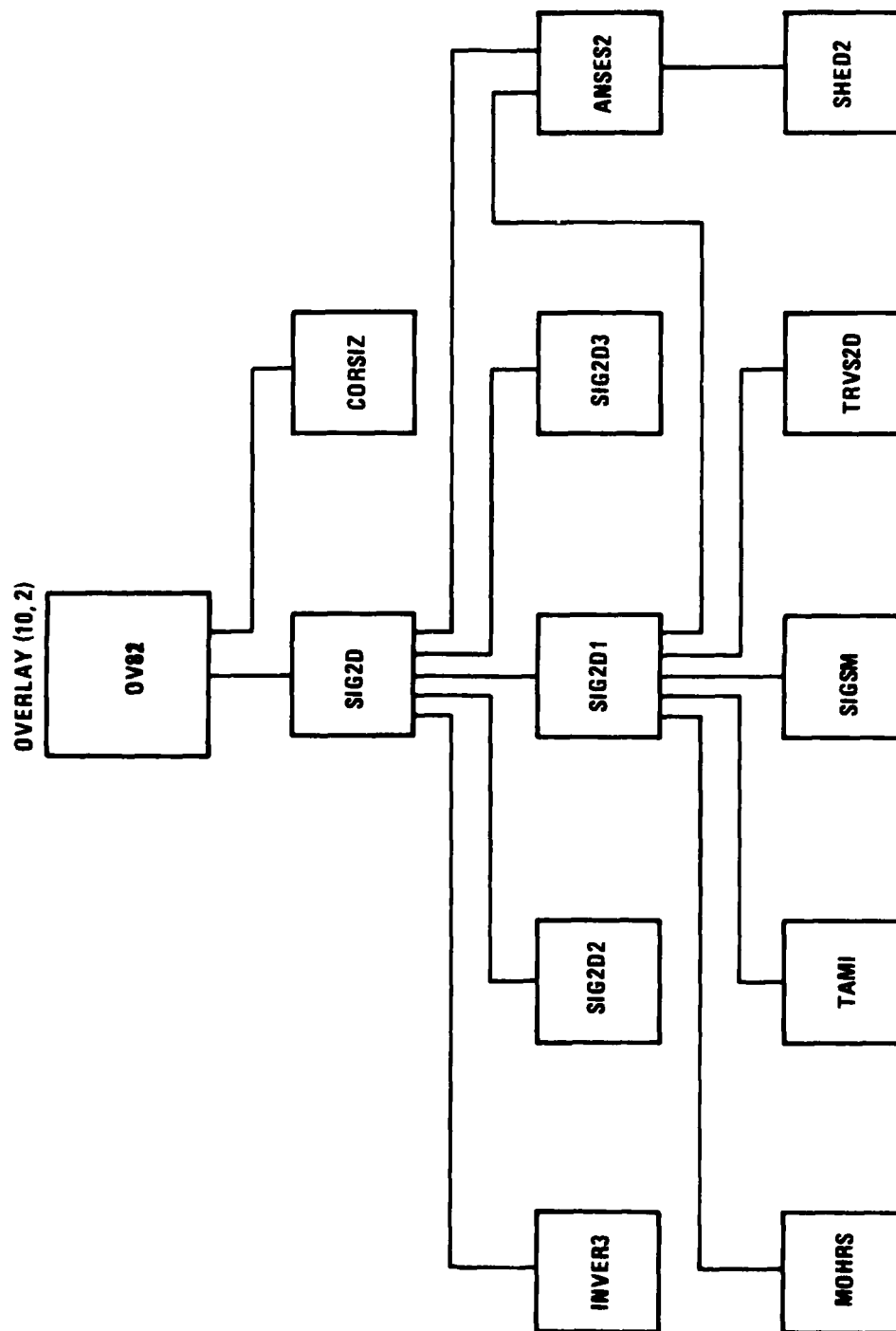


Figure 9.39 Overlay For Stress And Strain Computation - 2D Elements

5407-62

SECURITY CLASSIFICATION OF THIS PAGE (When Data Entered)

REPORT DOCUMENTATION PAGE		READ INSTRUCTIONS BEFORE COMPLETING FORM
1. REPORT NUMBER WARD-10881	2. GOVT ACCESSION NO. AD-102794	3. RECIPIENT'S CATALOG NUMBER
4. TITLE (and Subtitle) Evaluation of the STAGSC-1 Shell Analysis Computer Program		5. TYPE OF REPORT & PERIOD COVERED Final 9/28/79 to 1/12/81
		6. PERFORMING ORG. REPORT NUMBER
7. AUTHOR(s) Kevin Thomas L. H. Sobel		8. CONTRACT OR GRANT NUMBER(s) Office of Naval Research N00014-79-C0825
9. PERFORMING ORGANIZATION NAME AND ADDRESS Westinghouse Advanced Reactors Division Box 158 Madison, PA 15601		10. PROGRAM ELEMENT, PROJECT, TASK AREA & WORK UNIT NUMBERS NR064-429/6-22-79 (474)
11. CONTROLLING OFFICE NAME AND ADDRESS Office of Naval Research 800 N. Quincy St. Arlington, VA 22217		12. REPORT DATE August 1981
		13. NUMBER OF PAGES 265
14. MONITORING AGENCY NAME & ADDRESS (if different from Controlling Office)		15. SECURITY CLASS. (of this report) Unclassified
		15a. DECLASSIFICATION/DOWNGRADING SCHEDULE
16. DISTRIBUTION STATEMENT (of this Report) Distribution of this document is unlimited.		
17. DISTRIBUTION STATEMENT (of the abstract entered in Block 20, if different from Report)		
18. SUPPLEMENTARY NOTES		
19. KEY WORDS (Continue on reverse side if necessary and identify by block number) STAGSC-1, Finite Element, Shell analysis, Computer Program, Nonlinear analysis.		
20. ABSTRACT (Continue on reverse side if necessary and identify by block number) An evaluation of the STAGSC-1 finite element nonlinear shell analysis program was made. Detailed descriptions and critiques of the program capabilities, documentation, architecture and performance are provided. An in-depth technical evaluation of the element library performance is presented. Also studied were the eigensolver performance and performance of the transient integration operators for nonlinear problems. A detailed case study is presented for a nonlinear collapse problem.		

DD FORM 1473
1 JAN 73EDITION OF 1 NOV 68 IS OBSOLETE
S/N 0102-014-6601

SECURITY CLASSIFICATION OF THIS PAGE (When Data Entered)

